

AD-A070 528

INSTITUTE FOR DEFENSE ANALYSES ARLINGTON VA SCIENCE A--ETC F/G 21/7
TECHNOLOGY ASSESSMENT OF ADVANCED PROPULSION SYSTEMS FOR SOME C--ETC(U)
SEP 78 F R RIDDELL, D M DIX DAHC15-73-C-0200
IDA-P-1278-VOL-2 IDA/HQ-77-19843 NL

UNCLASSIFIED

1 OF 4
AD
A070528





NATIONAL BUREAU OF STANDARDS
MICROCOPY RESOLUTION TEST CHART

AD-E500 067

IDA PAPER P-1278

A070534 VOL I

TECHNOLOGY ASSESSMENT OF
ADVANCED PROPULSION SYSTEMS FOR SOME CLASSES
OF COMBAT VEHICLES

Volume II. Appendices A-F

Frederick R. Riddell
Donald M. Dix

LEVEL III

September 1978

DDC
RECEIVED
JUN 29 1979
B

Prepared for
DEFENSE ADVANCED RESEARCH PROJECTS AGENCY

DISTRIBUTION STATEMENT A

Approved for public release;
Distribution Unlimited



INSTITUTE FOR DEFENSE ANALYSES
SCIENCE AND TECHNOLOGY DIVISION

IDA Log No. HQ 77-19843

MA070528

DDC FILE COPY

The work reported in this document was conducted under contract DANC15 73 C 0200 for the Department of Defense. The publication of this IDA Paper does not indicate endorsement by the Department of Defense, nor should the contents be construed as reflecting the official position of that agency.

APPROVED FOR PUBLIC RELEASE; DISTRIBUTION UNLIMITED

UNCLASSIFIED

SECURITY CLASSIFICATION OF THIS PAGE (When Data Entered)

REPORT DOCUMENTATION PAGE		READ INSTRUCTIONS BEFORE COMPLETING FORM
1. REPORT NUMBER	2. GOVT ACCESSION NO.	3. RECIPIENT'S CATALOG NUMBER
4. TITLE (and Subtitle) Technology Assessment of Advanced Propulsion Systems for Some Classes of Combat Vehicles: Volume II, Appendices A-F		5. TYPE OF REPORT & PERIOD COVERED FINAL
7. AUTHOR(s) Frederick R. Riddell Donald M. Dix		6. PERFORMING ORG. REPORT NUMBER IDA PAPER P-1278
9. PERFORMING ORGANIZATION NAME AND ADDRESS INSTITUTE FOR DEFENSE ANALYSES 400 Army-Navy Drive Arlington, Virginia 22202		8. CONTRACT OR GRANT NUMBER(s) DAHC15 73 C 0200
11. CONTROLLING OFFICE NAME AND ADDRESS Defense Advanced Research Projects Agency 1400 Wilson Boulevard Arlington, Virginia 22209		10. PROGRAM ELEMENT PROJECT TASK AREA & WORK UNIT NUMBERS DARPA Assignment A-40
14. MONITORING AGENCY NAME & ADDRESS (if different from Controlling Office) N/A		12. REPORT DATE September 1978
		13. NUMBER OF PAGES 364
		15. SECURITY CLASS (of this report) UNCLASSIFIED
		15a. DECLASSIFICATION DOWNGRADING SCHEDULE N/A
16. DISTRIBUTION STATEMENT (of this Report) Approved for public release; distribution unlimited.		
17. DISTRIBUTION STATEMENT (of the abstract entered in Block 20, if different from Report) None		
18. SUPPLEMENTARY NOTES N/A		
19. KEY WORDS (Continue on reverse side if necessary and identify by block number) propulsion systems; scientific research; engineering development; tanks (combat vehicles); combat vehicles, ground level, mobility, warfare; ships, high velocity; engines, gas-turbine, Stirling cycle, Brayton cycle, Otto cycle; Diesel engines; transmissions (mechanical); transmissions (electrical); transmissions (hydrodynamic); thrusters; vehicle tracks;		
20. ABSTRACT (Continue on reverse side if necessary and identify by block number) This paper presents the results of a study of propulsion systems for surface combat vehicles which is intended to provide information useful to the Defense Advanced Research Projects Agency in identifying high-payoff R&D prospects. The primary purposes of the paper are to: (1) quantify the technological advances needed to make major improvements in appropriate military propulsion systems and indicate relative payoffs; and (2) provide criteria for evaluation of new propulsion system or		

DDC

RECEIVED
JUN 29 1979
B

UNCLASSIFIED

SECURITY CLASSIFICATION OF THIS PAGE (When Data Entered)

UNCLASSIFIED

SECURITY CLASSIFICATION OF THIS PAGE(When Data Entered)

19. vehicle wheels; propellers (marine); hydraulic jets

20.

subsystem concepts. The scope of the study is limited to an assessment of propulsion systems for four classes of surface combat vehicles: (1) main battle tanks; (2) light, tracked land combat vehicles; (3) high-mobility land combat vehicles; and (4) high-speed (more than 50 knots) ships. For propulsion subsystems, five engine types (Otto, Diesel, gas turbine, closed Brayton, Stirling), three transmission types (mechanical, hydrodynamic, electrical), and four thruster types (tracks, wheels, propellers, waterjets) are examined in some detail.

Results are presented in terms of technology goals which are within the bounds of what is judged to be physically possible and which together in relevant sets would have a major impact on the cost or performance of armored land combat vehicles or of high-speed ships. Relative payoffs within each set of goals are also estimated.

This report is in three volumes.

Accession For	
NTIS GRA&I	<input checked="checked" type="checkbox"/>
DDC TAB	<input type="checkbox"/>
Unannounced	<input type="checkbox"/>
Justification	
By	
Distribution/	
Availability Codes	
Dist	Avail and/or special
A	

UNCLASSIFIED

SECURITY CLASSIFICATION OF THIS PAGE(When Data Entered)

IDA PAPER P-1278

**TECHNOLOGY ASSESSMENT OF
ADVANCED PROPULSION SYSTEMS FOR SOME CLASSES
OF COMBAT VEHICLES**

Volume II. Appendices A-F

Frederick R. Riddell
Donald M. Dix

September 1978



INSTITUTE FOR DEFENSE ANALYSES
SCIENCE AND TECHNOLOGY DIVISION
400 Army-Navy Drive, Arlington, Virginia 22202

Contract DAHC15 73 C 0200
DARPA Assignment A-40

ACKNOWLEDGMENTS

The authors are indebted to a great number of experts in various aspects of propulsion system technology and its military applications for the contributions they made to this study.

First, there are the individuals who provided analyses of the performance characteristics of specific propulsion system elements and of specific vehicle classes. Their work is the backbone of the study, and their contributions, which are incorporated in the appendices in Volumes II and III, were invaluable. The individual contributors, the fields of their work, and where their contributions appear are as follows:

- E. William Beans, University of Toledo--Otto-cycle engines (Appendix C)
- M.G. Bekker, consultant--thrusters for ground combat vehicles (Appendix J)
- Peter C. Bertelson, consultant--mechanical and hydro-mechanical transmissions (Appendix H)
- A. Douglas Carmichael, MIT--closed Brayton-cycle engines (Appendix F) and thrusters for high-speed oceangoing ships (Appendix K)
- P.C.T. de Boer, Cornell University--Diesel engines (Appendix D)
- B.L. Fletcher, consultant--land combat vehicles (Appendix A)
- James E.A. John, University of Ohio--Otto-cycle engines (Appendix C)
- James L. Kirtley, MIT--electrical transmissions (Appendix I)
- Philip Mandel, MIT--high-speed ships (Appendix B)

- Joseph L. Smith, Jr., MIT--electrical transmissions (Appendix I)
- Graham Walker, University of Calgary--Stirling engines (Appendix G)
- David Gordon Wilson, MIT--open Brayton-cycle engines (Appendix E)

In addition to the specific contributions just cited, these individuals also provided greatly appreciated counsel to the authors throughout the study.

Another group participated in a Steering Committee that was most helpful in providing critical guidance throughout the study and in reviewing the initial draft of this report. Members of the Steering Committee were:

- Carl F. Bachle, consultant
- Arden L. Bement, Defense Advanced Research Projects Agency
- Austin W. Betts, Southwest Research Institute
- Charles H. Church, Headquarters, Department of the Army
- George J. Huebner, Jr. (Chairman), consultant
- E.L. Resler, Jr., Cornell University
- John A. Satkowski, Office of Naval Research
- Edward C. van Reuth, Defense Advanced Research Projects Agency
- Donald D. Weidhuner, consultant.

Thanks are also due to James J. Murray, U.S. Army Research Office, S.J. Deitchman, IDA, and Bernard Paiewonsky, consultant, for reviewing the initial draft of this report. Finally, the contribution of Reinald G. Finke and Nancy Fredman at IDA in preparing computer programs is gratefully acknowledged.

ABSTRACT

This paper presents the results of a study of propulsion systems for surface combat vehicles which is intended to provide information useful to the Defense Advanced Research Projects Agency in identifying high-payoff R&D prospects. The primary purposes of the paper are to: (1) quantify the technological advances needed to make major improvements in appropriate military propulsion systems and indicate relative payoffs; and (2) provide criteria for evaluation of new propulsion system or subsystem concepts. The scope of the study is limited to an assessment of propulsion systems for four classes of surface combat vehicles: (1) main battle tanks; (2) light, tracked land combat vehicles; (3) high-mobility land combat vehicles; and (4) high-speed (more than 50 knots) ships. For propulsion subsystems, five engine types (Otto, Diesel, gas turbine, closed Brayton, Stirling), three transmission types (mechanical, hydrodynamic, electrical), and four thruster types (tracks, wheels, propellers, waterjets) are examined in some detail.

Results are presented in terms of technology goals which are within the bounds of what is judged to be physically possible and which together in relevant sets would have a major impact on the cost or performance of armored land combat vehicles or of high-speed ships. Relative payoffs within each set of goals are also estimated.

CONTENTS

Acknowledgments	iii
Abstract	v
Appendix A--Relationship of Propulsion System Parameters to Land Combat Vehicle Characteristics;	A-1
Appendix B--Relationship of Propulsion System Parameters to the Characteristics of High-Speed Ships;	B-1
Appendix C--Size and Specific Fuel Consumption Relation- ships in Otto-Cycle Engines ;	C-1
Appendix D--Size and Specific Fuel Relationships for Diesel Engines ;	D-1
Appendix E--Size and Fuel Consumption Relationships for Open Brayton-Cycle Engines ; and	E-1
Appendix F--Size and Specific Fuel Consumption Relation- ships for Closed Brayton-Cycle Engines .	F-1

APPENDIX A

RELATIONSHIP OF PROPULSION SYSTEM PARAMETERS
TO LAND COMBAT VEHICLE CHARACTERISTICS

B. L. Fletcher, F. R. Riddell, and D. M. Dix

CONTENTS

A. Introduction	A-3
B. Relationship between Vehicle and Propulsion System Parameters	A-5
1. Performance	A-5
2. Costs	A-9
3. Sensitivity Factors	A-13
C. Results for Three Classes of LCVs	A-16
Glossary	A-22
References	A-24

APPENDIX A

RELATIONSHIP OF PROPULSION SYSTEM PARAMETERS TO LAND COMBAT VEHICLE CHARACTERISTICS

B. L. Fletcher, F. R. Riddell, and D. M. Dix

A. INTRODUCTION

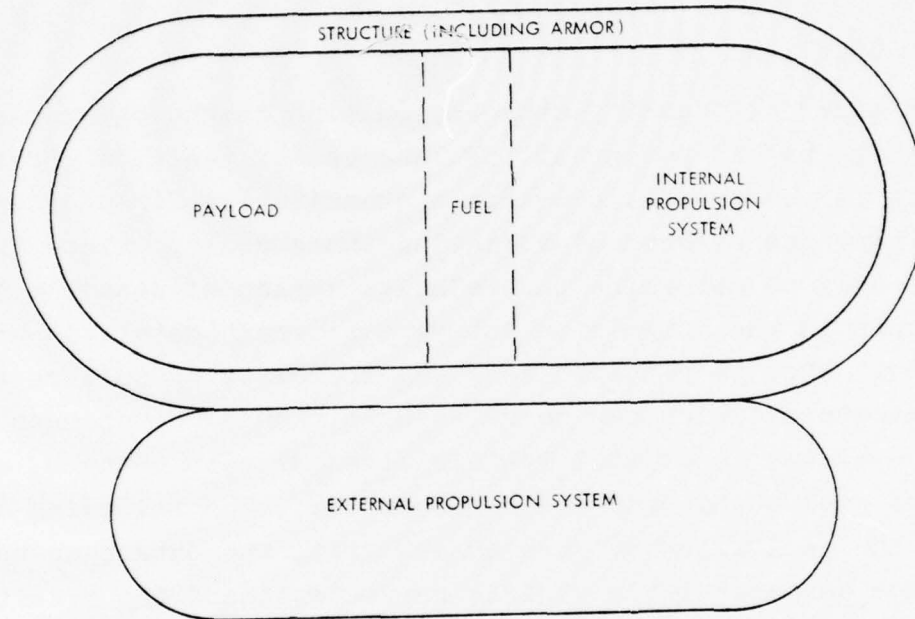
In order to identify those propulsion technology goals that have a high payoff potential for land combat vehicles (LCVs), an analysis is needed that provides a quantitative first-order view of the expected effects of achieving those goals. Since the intent is only to determine the relative impact of possible improvements in the propulsion subsystems, great detail is not required. What is required is a way to relate propulsion system parameters (which can be related to technology changes in the subsystems) to overall vehicle size and cost changes, as a means of evaluating proposed improvements. The following explains the derivation of such an analysis, the data base used to determine characteristic vehicle parameters, and the results obtained.

The LCV is characterized according to the following parameters:

- Weight (total, payload, fuel, structure, power train, suspension)
- Armored volume (total, payload, fuel, power train)
- Horsepower (gross, sprocket and thrust)
- Range
- Specific fuel consumption
- Annual hours of operation
- Costs (procurement, maintenance, and fuel).

Figure A-1 shows the conceptualization of the vehicle in terms of the weights and armored volumes of interest.

LCV CONCEPT



TOTAL ARMORED VOLUME = VOLUME OF (PAYLOAD + FUEL + INTERNAL PROPULSION SYSTEM)

TOTAL WEIGHT = WEIGHT OF (STRUCTURE + PAYLOAD + FUEL + TOTAL PROPULSION SYSTEM)

2.9.77-11

FIGURE A-1. Characteristics of land combat vehicles by weights and volumes of major subsystems of interest.

Through the use of data for current, past or developmental vehicles, and by using simple relationships between the above parameters, it is possible to determine the effect of improvements in the specific weight and volume of propulsion systems on the size and cost of the LCV. Implicit in the evaluation of weight and volume distribution is the determination of how the payload weight and volume will be affected by propulsion system changes. In this analysis the impact of changes is determined under the assumption that the payload is kept constant. Such changes may offer many types of performance improvements, such as improved range for a given fuel load, higher speed, improved agility, and better RAM-D characteristics. In order to make comparative evaluations between different parametric changes the method used here measures the impact of changes on vehicle size and cost. Thus increments in size and/or cost are used as a measure of value, though in an actual design they can be traded for any of the performance parameters noted above.

B. RELATIONSHIP BETWEEN VEHICLE AND PROPULSION SYSTEM PARAMETERS

1. Performance

The performance parameters of interest are (see Fig. A-1):

W_v = gross vehicle weight (combat loaded)

W_L = payload weight

V_L = payload volume

W_S = structural and armor weight

P_{max} = maximum thrust power

P_{cr} = thrust power for maximum range

P_{inst} = installed engine power

P_{spr} = sprocket power

W_{ps} = propulsion system weight

W_{psp} = propulsion system weight enclosed in the armored volume

W_{psw} = propulsion system weight exterior to the armored volume

V_{psp} = propulsion system volume enclosed in armor

W_F = fuel weight

V_F = fuel volume

SFC = specific fuel consumption based on engine output at cruise power

η_x = transmission efficiency

η_t = thruster efficiency.

Since we are interested in treating the propulsion system (engine, transmission and thruster) as a whole, it is convenient to define an overall specific fuel consumption based on thrust power, i.e.,

$$\overline{SFC} = \frac{SFC}{\eta_x \eta_t} \quad (A-1)$$

For example, for the M60A1 RISE, $SFC = 0.38$ while $\overline{SFC} = 0.61$ lb/hp-hr.

The relationships between these parameters are

$$W_V = W_S + W_{ps} + W_F + W_L \quad (A-2)$$

$$W_S = \alpha(W_L + W_{psp} + W_F) + \beta(V_L + V_{psp} + V_F) \quad (A-3)$$

$$W_{ps} = W_{psp} + W_{psw} \quad (A-4)$$

$$W_F = (HP-HRS)_{cr} \overline{SFC} \quad (A-5)$$

where α defines the fraction of W_S needed for structural support and β defines the additional ballistic armor protection. W_L and V_L are given quantities determined by the payload to be carried. $(HP-HRS)_{cr}$ defines the combination of thrust power and endurance needed to provide the desired range.*

The weight and volume of the propulsion system enclosed in the armored volume, W_{psp} and V_{psp} , are determined by the specific weight and volume of the engine and transmission and by the required thrust power, i.e.,

$$W_{psp} = w_e P_{inst} + w_x P_{spr} = w_e \frac{P_{max}}{\eta_x \eta_t} + w_x \frac{P_{max}}{\eta_t}, \quad (A-6)$$

where w_e = specific weight of engine
 w_x = specific weight of transmission } based on output power.

A similar relationship exists for V_{psp} , i.e.,

$$V_{psp} = \delta_e \frac{P_{max}}{\eta_x \eta_t} + \delta_x \frac{P_{max}}{\eta_t}, \quad (A-7)$$

where δ_e = specific volume of engine
 δ_x = specific volume of transmission } based on output power.

For our purposes here we can treat engine and transmission together. Hence we define a parameter

* Range R in miles and $(HP-HRS)_{cr}$ are related by
 $(HP-HRS)_{cr} = 0.00267RD,$

where D is the average drag in pounds for the endurance run specifications.

$$\frac{\overline{W}_{psp}}{P_{max}} = \frac{w_e}{\eta_x \eta_t} + \frac{w_x}{\eta_t} \quad (A-8)$$

= specific weight of W_{psp} based on thrust power.

Similarly

$$\frac{\overline{V}_{psp}}{P_{max}} = \frac{\delta_e}{\eta_x \eta_t} + \frac{\delta_x}{\eta_t} \quad (A-9)$$

= specific volume of V_{psp} based on thrust power.

The weight of the propulsion system external to the armored volume, W_{psw} (essentially the tracks and suspension), is determined by the weight it must support rather than the power it delivers (see Appendix K). Hence we define

$$W_{psw} = \left(\frac{W_{psw}}{W_v} \right)_o W_v, \quad (A-10)$$

where $\left(\frac{W_{psw}}{W_v} \right)_o$ is a parameter defining the fractional weight of the total vehicle required for the tracks and suspension. For tracked vehicles $\left(\frac{W_{psw}}{W_v} \right)_o$ can be taken as a constant = 0.22; for wheeled vehicles (nonarticulated) it is also nearly constant at a value of 0.10 (see Appendix K).

To show the relationship of propulsion system parameters to LCV characteristics explicitly it is convenient to combine Eqs. A-2 through A-5 to give

$$\begin{aligned} \frac{P_{max}}{W_v} \left(1 + \alpha + \frac{\beta}{\rho_{psp}} \right) \left(\frac{\overline{W}_{psp}}{P_{max}} \right) + \frac{(HP-HRS)_{cr}}{W_v} \left(1 + \alpha + \frac{\beta}{\rho_F} \right) \overline{SFC} \\ = 1 - \left(\frac{W_{psw}}{W_v} \right)_o - \frac{W_L}{W_v} \left(1 + \alpha + \frac{\beta}{\rho_L} \right), \end{aligned} \quad (A-11)$$

where ρ_i is the density (W_i/V_i) of the i component. Equation A-11 is plotted in Fig. A-2 with the propulsion system parameters ($\overline{W}_{ps}/P_{max}$) and \overline{SFC} as independent variables. If the parameters that characterize the vehicle are now defined for a given class of vehicle, Fig. A-2 can be made quantitative. It can then be used to interpret how changes in propulsion system parameters are related to vehicle characteristics. This is done in Section C below.

2. Costs

Costs have three elements of interest: initial unit procurement, annual maintenance, and fuel. Although fuel costs appear small compared with the overall O&M costs for existing LCVs, they are considered in the analysis because of their potential for assuming greater significance as fuel costs rise or higher fuel consumption results from the use of new technology, e.g., turbine-powered vehicles.

The unit procurement cost for the LCV is considered to be a function of the weights of the structure and propulsion system and the power of the engine. Analytically, this relationship may be described by the equation

$$\mathcal{Z}_p = (\mathcal{Z}/W)(W_S + W_{ps}) + P_{max} [(\mathcal{Z}/P)_S + (\mathcal{Z}/P)_{ps}] \quad , \quad (A-12)$$

where \mathcal{Z}_p is the unit procurement cost of the vehicle platform* (i.e., without payload) and (\mathcal{Z}/W) is a constant that is multiplied by the weights of the structure (W_S) and propulsion system (W_{ps}). To this cost is added the product of the thrust horsepower (P_{max}) times two constants, one, $(\mathcal{Z}/P)_S$, representing the structural cost that is power dependent and the other, $(\mathcal{Z}/P)_{ps}$, representing the propulsion system cost that is power dependent.

*Throughout this appendix, costs will refer to the vehicle without payload, sometimes referred to as "platform" costs.

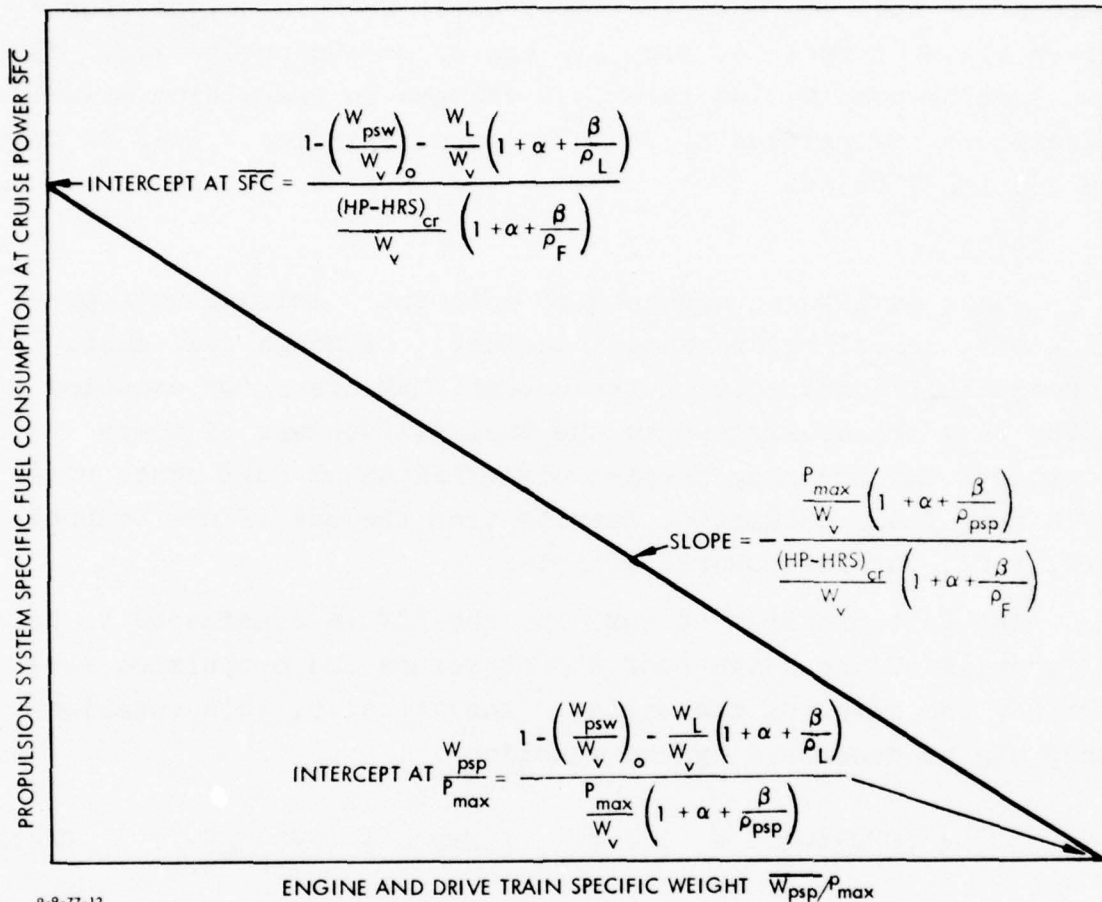


FIGURE A-2. Relationships between propulsion system parameters and LCV characteristics.

The total maintenance and fuel costs for the assumed 20-year life of the LCV is calculated from the following relationship:

$$\begin{aligned} \mathcal{Z}_M = & K_{MS} [(\mathcal{Z}/W)(W_S + W_{ps}) + P_{\max} (\mathcal{Z}/P)_S] \\ & + K_{MP} P_{\max} (\mathcal{Z}/P)_{ps} + P_{\max} \cdot \overline{SFC} \cdot DC (\mathcal{Z}_F/W_F) , \end{aligned} \quad (A-13)$$

where \mathcal{Z}_M is the total maintenance and fuel cost for 20 years of operation, and K_{MS} and K_{MP} are multipliers for the procurement cost elements defined for Eq. A-12. K_{MS} relates maintenance costs to the procurement costs of the structure, while K_{MP} relates maintenance costs to the propulsion system procurement cost. The third term of Eq. A-13 determines the fuel costs on the basis of specific fuel consumption (\overline{SFC}), hours of operation during the 20-year period (DC), and cost per pound of fuel (\mathcal{Z}_F/W_F).

Determination of Costing Constants. Cost, weight, and power data for the M60A1 RISE tank were used to establish values for the procurement and O&M cost parameters (\mathcal{Z}/W) , $(\mathcal{Z}/P)_S$, $(\mathcal{Z}/P)_{ps}$, K_{MS} , K_{MP} and DC . The following summarizes the derivation of these constants.

(1) Procurement Cost. The unit procurement cost for the M60A1 RISE is approximately \$494,000 (Ref. A-1).* A cost of about \$361,000 for the vehicle, engine, transmission, and track is included in this total (Ref. A-2), the other costs being for ordnance equipment and other items that are considered to be payload in this analysis.

Since procurement cost data is not given in the form required to solve Eq. A-12, it is necessary to interrelate (\mathcal{Z}/W) and $(\mathcal{Z}/P)_S$. This is done by assuming that $(\mathcal{Z}/P)_S$, which

*All costs are in FY 77 dollars.

is the structural cost that is linearly related to horsepower, is related to $(\$/W)$ in the same proportion as the internal propulsion system (power train) volume is to the total armored volume. Or, for the M60A1 RISE,

$$P_{\max} (\$/P)_S = 0.245 (\$/W)(W_S + W_{ps})$$

$(\$/P)_{ps}$ was determined by combining data from two sources: (1) the costs of the engine, transmission and track given in Ref. A-2; and (2) a cost breakout that does not provide actual costs for the rest of the propulsion system (final drive, suspension, etc.) but gives these in terms of percentage of the total vehicle cost (Ref. A-3). By combining data from these two sources the procurement cost of the propulsion system was estimated to equal \$133,000, or, with P_{\max} of 466 hp, $(\$/P)_{ps}$ equals \$285/hp. With these results substituted in Eq. A-12, $(\$/W)$ equals \$2.00/lb and $(\$/P)_S$ equals \$96/hp.

(2) Maintenance and Fuel Costs. The fuel costs are derived from the expression in Eq. A-13

$$P_{\max} \cdot \overline{SFC} \cdot DC \cdot (\$/W_F)$$

The hours of operation of the LCV for a 20-year period, DC, was estimated on the basis of information in Ref. A-4 and assumptions as to the equivalent hours of operation at P_{\max} for hours of operation at lower power settings. For all vehicles this value was set at 1440 hours. The cost of fuel $(\$/W_F)$ was assigned a value of \$0.07/lb for all types of fuel. \overline{SFC} , as defined in Eq. A-1, was set at 0.64 lb/hp-hr for diesel engines and 0.87 lb/hp-hr for turbine and gasoline engines.

The annual maintenance costs were developed from information provided in Ref. A-4. To do this it was necessary to separate operating and maintenance cost elements, this sometimes

requiring a judgment as to how these costs should be assigned. This led to an estimate of an annual maintenance cost of about \$48,000, excluding POL charges. This is 9.7 percent of the unit procurement cost of \$494,000. Other studies (Ref. A-5) indicate that about 10 percent of procurement cost is a good estimate of annual repair costs. On this basis both K_{MS} and K_{MP} are estimated to have values of 2 (i.e., 20×0.10).

3. Sensitivity Factors

Using the relationships discussed in Sections B-1 and B-2 above, weight and cost sensitivity factors, which relate changes in propulsion system weight, volume, and cost to changes in vehicle size (weight) and cost, can be derived. The weight sensitivity factor is defined by:

$$\frac{\Delta W_v}{W_v} = SW_i \frac{\Delta Q_i}{Q_i} ,$$

where SW_i = weight sensitivity factor

$\Delta Q_i/Q_i$ = fractional change in propulsion system parameter

$\Delta W_v/W_v$ = fractional change in gross vehicle weight.

Similarly the cost sensitivity coefficient is defined by

$$\frac{\Delta Z_T}{Z_T} = SC_i \frac{\Delta Q_i}{Q_i} ,$$

where SC_i = cost sensitivity factor

$\Delta Z_T/Z_T$ = fractional change in vehicle platform cost (i.e., ex-payload costs).

The weight sensitivity factors are given explicitly in Table A-1 in terms of the parameters defined above, and the cost sensitivity factors are given in Table A-2.

TABLE A-1. WEIGHT SENSITIVITY FACTORS

$$\frac{\Delta W_v}{W_v} = SW_i \frac{\Delta Q_i}{Q_i}$$

Parameter Q_i	Weight Sensitivity Factor SW_i
\overline{SFC}	$\frac{(1 + \alpha + \beta/\rho_F)W_F}{(1 + \alpha + \beta/\rho_L)W_L}$
$\frac{W_{psp}}{P_{max}}$	$\frac{(1 + \alpha)W_{psp}}{(1 + \alpha + \beta/\rho_L)W_L}$
$\frac{W_{psw}}{P_{max}}$	$\frac{W_{psw}}{(1 + \alpha + \beta/\rho_L)W_L}$
$\frac{\nabla_{psp}}{P_{max}}$	$\frac{(\beta/\rho_{psp})W_{psp}}{(1 + \alpha + \beta/\rho_L)W_L}$
ρ_F	$-\frac{(\beta/\rho_F)W_F}{(1 + \alpha + \beta/\rho_L)W_L}$

TABLE A-2. COST SENSITIVITY FACTORS

$$\frac{\Delta \$_T}{\$_T} = SC_i \frac{\Delta Q_i}{Q_i}$$

Parameter Q_i	Cost Sensitivity Factor SC_i
$\frac{W_{psp}}{P_{max}}$	$(1 + K_{MS}) \left(\frac{\$}{W} \right) \frac{W_L}{\$_T} \left[\frac{(1 + \alpha) W_{psp}}{(1 + \alpha + \beta/\rho_L) W_L} \right]$
$\frac{W_{psw}}{P_{max}}$	$(1 + K_{MS}) \left(\frac{\$}{W} \right) \frac{W_L}{\$_T} \left[\frac{W_{psw}}{(1 + \alpha + \beta/\rho_L) W_L} \right]$
$\frac{V_{psp}}{P_{max}}$	$(1 + K_{MS}) \left(\frac{\$}{W} \right) \frac{W_L}{\$_T} \left[\frac{(\beta/\rho_{psp}) W_{psp}}{(1 + \alpha + \beta/\rho_L) W_L} \right]$
\overline{SFC}	$(1 + K_{MS}) \left(\frac{\$}{W} \right) \left[\frac{(1 + \alpha + \beta/\rho_F) W_F}{(1 + \alpha + \beta/\rho_L) W_L} \right] + \left(\frac{\$_F}{W_F} \right) \frac{(DC) \overline{SFC} P_{max}}{\$_T}$ $- (1 + K_{MS}) \left(\frac{\$}{W} \right) \frac{W_F}{\$_T}$
ρ_F	$- (1 + K_{MS}) \left(\frac{\$}{W} \right) \frac{(\beta/\rho_F) W_F}{(1 + \alpha + \beta/\rho_L) W_L}$
$\$_{ps}$	$\left(\frac{\$}{P} \right)_{ps} \frac{P_{max}}{\$_T}$
$\$_F$	$\left(\frac{\$_F}{W_F} \right) \frac{(DC) \overline{SFC} P_{max}}{\$_T}$

C. RESULTS FOR THREE CLASSES OF LCVs

For this analysis, three classes of LCVs were used:

- Main battle tanks (40 to 60 tons)
- Light tracked LCVs (under 20 tons) .
- High-mobility LCVs (horsepower/weight ratios greater than 35).

Realistic values of the parameters which characterize the vehicle for each class of LCV were determined from available data for existing vehicles or, in the case of advanced main battle tanks, estimated as typical for 1500-hp tanks. Table A-3, Typical Land Combat Vehicle Characteristics, shows the weight, armored volume, and other physical or performance characteristics for LCVs typical of each class. The specific vehicles used are as follows:

<u>Main Battle Tanks</u>	<u>Typical Vehicle</u>
Current (Diesel)	M60A1 RISE
<u>Medium-Weight LCV</u>	
Tank (Diesel)	M551
APC (Diesel)	M113A1
<u>High-Mobility LCV</u>	
Articulated (Gasoline)	XM808

The data sources used are shown in the table. In addition to the current main battle tank, two additional sets of data were estimated to typify advanced main battle tanks with 1500-gross-hp diesel or turbine engines. The thrust power, P_{\max} , is derived from the sprocket horsepower, allowing for an estimated loss of about 3% in the thruster.* For those vehicles for which sprocket horsepower data were not available, the gross engine horsepower was corrected on the basis of available data or estimates of engine net and losses in the transmission and final drive.

*Due to slip; see Appendix K.

TABLE A-3. TYPICAL LAND COMBAT VEHICLE CHARACTERISTICS

	Main Battle Tanks			Medium Weight LCV		High-Mobility LCV: Articulated (Gasoline)
	Current (Diesel)	Advanced (Diesel)	Advanced (Turbine)	Tank (Diesel)	APC (Diesel)	
<u>Weight (lb)</u>						
Structure	53,492	51,497	50,610	12,589	9,040	5,792
Propulsion System	37,921	32,860	30,575	11,095	8,758	10,661
Internal	(13,551)	(10,011)	(8,195)	(3,772)	(3,351)	(5,322)
External	(24,370)	(22,849)	(22,380)	(7,323)	(5,407)	(5,339)
Payload	18,387	18,387	18,387	10,241	6,072	3,747
Fuel	2,800	3,030	4,034	1,019	724	1,008
Total	112,600	105,774	103,606	34,944	24,594	21,208
<u>Armored Volume (ft³)</u>						
Propulsion System	203	139	109	50	56	79
Payload	572	572	572	428	323	171
Fuel	53	58	78	19	14	22
Total	828	769	759	497	393	272
<u>Other</u>						
Gross Horsepower	750	1,500	1,500	300	220	300
Specific Fuel Consumption (lb/hp-hr)	0.61	0.64	0.87	0.61	0.61	0.87
Fuel Density (lb/ft ³)	52	52	52	52	52	44.9
Range (mi)	300	300	300	373	300	300
<u>References</u>	A-1	--	--	A-5 thru 7	A-5 & 8	A-9 & 10

Using the values of the vehicle and propulsion system parameters shown in Table A-3, the specific fuel consumption-specific weight relationship, as shown in Fig. A-2, were derived for each class of LCV. These are shown in Fig. A-3, which gives limiting values of acceptable propulsion system parameters for each class of LCV considered. That is to say, any combination of propulsion system parameters that does not fall on or below the lines indicated will not meet the demands for that class of vehicle without degrading its performance.

In addition, sensitivity factors were calculated for each class of vehicle. These are shown in Table A-4, Weight Sensitivity Factors for Land Combat Vehicles, and Table A-5, Cost Sensitivity Factors for Land Combat Vehicles. These tables include sensitivity factors for vehicle and payload parameters as well as those for propulsion system parameters, to provide reference comparisons. Since the vehicle size is scaled directly by payload size, the sensitivity factor for payload weight or volume at constant density is unity.

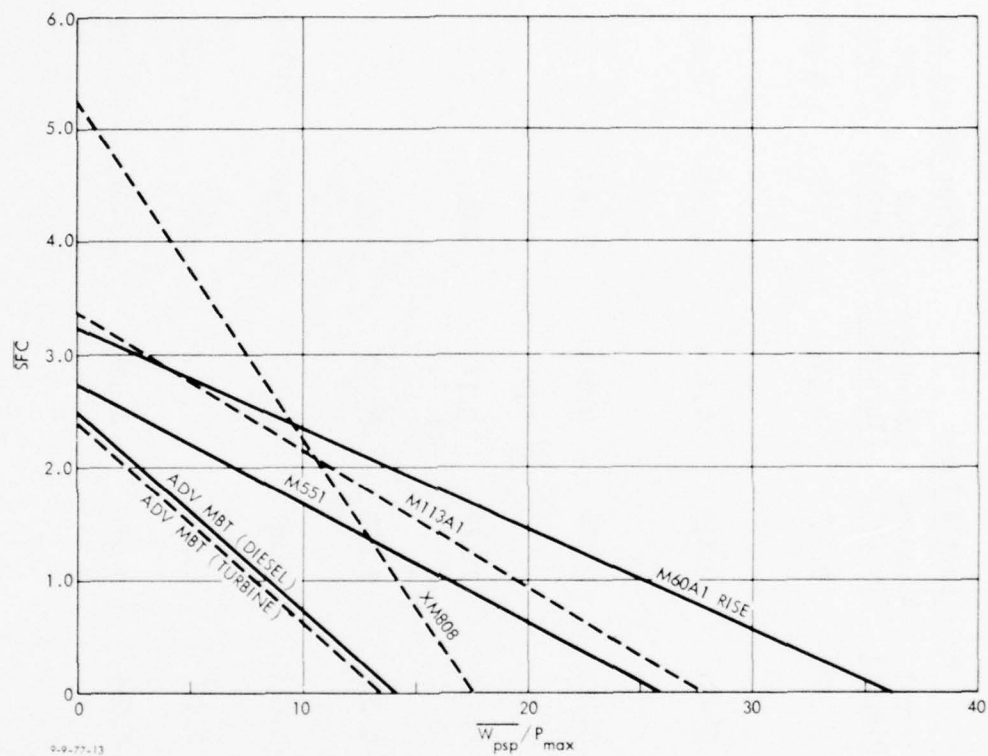


FIGURE A-3. Specific fuel consumption versus specific weight of power train for selected classes of vehicles.

TABLE A-4. WEIGHT SENSITIVITY FACTORS FOR LAND COMBAT VEHICLES

Parameter	Main Battle Tanks			Medium Weight LCV		High-Mobility LCV: Articulated (Gasoline)
	Current (Diesel)	Advanced (Diesel)	Advanced (Turbine)	Tank (Diesel)	APC (Diesel)	
Propulsion Power System Specific Weight w_{psp}/P_{max}	0.327	0.235	0.192	0.242	0.339	1.048
Propulsion Support System Specific Weight w_{psw}/P_{max}	0.452	0.413	0.404	0.363	0.422	0.810
Propulsion Power System Specific Volume v_{psp}/P_{max}	0.193	0.134	0.013	0.040	0.067	0.123
Propulsion System Specific Fuel Consumption \overline{SFC}	0.121	0.129	0.172	0.081	0.090	0.233
Fuel Density ρ_F	-0.052	-0.058	-0.077	-0.016	-0.017	-0.035
Vehicle Specific Weight w_v/P_{max}	-0.521	-0.369	-0.295	-0.283	-0.406	-0.171
Vehicle Range R	0.121	0.129	0.172	0.081	0.090	0.233
Payload Density w_L/v_L	-0.554	-0.568	-0.568	-0.354	-0.385	-0.262

TABLE A-5. COST SENSITIVITY FACTORS FOR LAND COMBAT VEHICLES

	Main Battle Tanks			Medium Weight LCV		High-Mobility LCV: Articulated (Gasoline)
	Current (Diesel)	Advanced (Diesel)	Advanced (Turbine)	Tank (Diesel)	APC (Diesel)	
Propulsion Power System Specific Weight, W_{psp}/P_{max}	0.360	0.318	0.268	0.282	0.383	1.090
Propulsion Support System Specific Weight, W_{psw}/P_{max}	0.497	0.468	0.458	0.422	0.475	0.842
Propulsion Power System Specific Volume, V_{psp}/P_{max}	0.213	0.173	0.138	0.047	0.075	0.128
Specific Fuel Consumption, SFC	0.144	0.173	0.231	0.110	0.118	0.290
Fuel Density, ρ_F	-0.058	-0.066	-0.087	-0.018	-0.019	-0.036
Propulsion System Procurement Cost (Power), $\$_{ps}$	0.121	0.166	0.164	0.146	0.149	0.191
Propulsion System Maintenance Cost (Power), $\$_{mps}$	0.243	0.331	0.329	0.292	0.299	0.383
Fuel Cost, $\$_F$	0.026	0.037	0.050	0.031	0.032	0.059
Vehicle Specific Weight, W_V/P_{max}	-1.082	-1.189	-1.112	-0.943	-1.085	-2.041
Vehicle Range, R	0.117	0.136	0.18	0.078	0.086	0.231
Payload Density, W_L/V_L	-0.609	-0.597	-0.598	-0.411	-0.434	-0.273

GLOSSARY, APPENDIX A

APC	Armored personnel carrier
DC	Hours of operation during 20-year period
$(HP-HRS)_{cr}$	Thrust power and endurance needed to provide desired range
LCV	Land combat vehicle
O&M	Operation and maintenance
P_{cr}	Thrust power for maximum range
P_{inst}	Installed engine power
P_{max}	Maximum thrust power
P_{spr}	Sprocket power
R	Vehicle range
RAM-D	Repairability, Availability, Maintainability, Dependability
SFC	Specific fuel consumption based on engine output at cruise power
\overline{SFC}	Specific fuel consumption based on delivered thrust at cruise power
w_e	Specific weight of engine based on output power
W_F	Fuel weight
W_L	Payload weight
W_{ps}	Propulsion system weight
W_{psp}	Propulsion system weight enclosed in the armored volume

W_{psw}	Propulsion system weight exterior to the armored volume
W_S	Structural and armor weight
W_V	Gross vehicle weight (combat loaded)
w_x	Specific weight of transmission based on output power
α	Fraction of W_S needed for structural support
β	Fraction of W_S for ballistic armor protection
δ_e	Specific volume of engine based on output power
δ_x	Specific volume of transmission based on output power
η_t	Thruster efficiency
η_x	Transmission efficiency
ρ	Density
V_F	Fuel volume
V_L	Payload volume
V_{psp}	Propulsion system volume enclosed in armor
$\$F$	Fuel cost
$\$_{mps}$	Propulsion system maintenance cost (power)
$\$_p$	Unit procurement cost of vehicle platform (i.e., without payload)
$\$_{ps}$	Propulsion system procurement cost (power)

REFERENCES, APPENDIX A

- A-1. Letter from Project Manager M60 Tank Development, Code DRCPM-M60TD, Warren, Michigan, dated 24 June 1977.
- A-2. Telephone communications with Mr. T. Haymend, Office of Project Manager M60 Tank Development, DRCPM-M60TD, Warren, Michigan, July 1977.
- A-3. Briefing Chart, "M60A1 Cost Distribution," Anonymous, 1977.
- A-4. M60 Tank Development and TACOM Cost Analysis Division, M60A1 Tank, Annual Operating and Support Cost Per Vehicle, FY 76 Constant Dollars, Project Manager, April 1976.
- A-5. Letter from Tracked Vehicle Function Chief, Code DRSTA-GBT, U.S. Army Tank-Automotive Materiel Readiness Command, Warren, Michigan, dated 5 July 1977.
- A-6. Weight Summary, Armored Reconnaissance Airborne Assault Vehicle, Full Tracked, 152MM, M551-8736408, Drawing No. 11679098, undated.
- A-7. Allison Division of General Motors, M551 Armored Reconnaissance Airborne Assault Vehicle (brochure), 1969.
- A-8. U.S. Army Tank-Automotive Materiel Readiness Command, Warren, Michigan, Weight and Center of Gravity Data, M113A1, computer printout from Code DRSTA-GBT, 10 April 1973.
- A-9. Lockheed Missiles and Space Co., Sunnyvale, California, Twister Vehicle Development Program, Technical Report Summary, LMSC-695933, April 1971.
- A-10. U.S. Army Tank-Automotive Command, Combat Vehicle, Wheeled, Articulated, 8x8 XM808 (TWISTER), Characteristic Data, 28 April 1971 (Revised).

APPENDIX B

RELATIONSHIP OF PROPULSION SYSTEM PARAMETERS
TO THE CHARACTERISTICS OF HIGH-SPEED SHIPS

Philip Mandel

CONTENTS

A. Approach	B-3
B. Sample Calculations	B-5
1. For the Special Case of $V_e = V_m$	B-5
2. For the General Case of $V_e < V_m$	B-15
C. Conclusion	B-20
Glossary	B-21
References	B-23

APPENDIX B

RELATIONSHIP OF PROPULSION SYSTEM PARAMETERS TO THE CHARACTERISTICS OF HIGH-SPEED SHIPS

Philip Mandel

A. APPROACH

The weight equation (Eq. B-1) and the speed-to-power relationships of Ref. B-1 are utilized in this study to show how a first-order approximation of the impact of advances in propulsion system technology on the performance of waterborne vehicles can be made. Twelve parameters are used to characterize the vehicle and its propulsion system, as follows:

Propulsion System Parameters

1. SPPW Specific power-plant weight, pounds per shaft horsepower
2. SFC Specific fuel consumption at endurance speed V_e , pounds per shaft horsepower-hour
3. P_i Installed shaft horsepower
4. η Overall propulsive coefficient at any speed V ;
 $\eta = \eta_e @ V = V_e$, $\eta = \eta_m @ V = V_m$

Vehicle Parameters

5. V Vehicle speed, knots; V_m = maximum speed, V_e = endurance speed
6. W Vehicle total weight, long tons; 1 long ton = 2240 lb
7. E Vehicle endurance time at V_e , hours
8. R Vehicle endurance distance at V_e , nmi; $R = V_e E$
9. W/D Vehicle lift/drag ratio at any speed
10. P_r Shaft horsepower required at a specified speed
11. W_p/W Payload weight fraction
12. W_o/W Other weight fraction

B-3

PRECEDING PAGE BLANK-NOT FILMED

The weight items used in the above parameters and in the weight equation are:

- W_p Weight of fixed and consumable payload items, tons
- W_f Weight of fuel, tons
- W_m Weight of power plant, tons
- W Total vehicle weight, tons
- W_o Other vehicle weight, tons ($W_o = W - W_m - W_f - W_p$)

The weight equation is

$$\frac{W_m}{W} + \frac{W_f}{W} + \frac{W_p}{W} + \frac{W_o}{W} = 1. \quad (B-1)$$

By definition we have

$$\frac{P_i}{W} = \frac{2240}{SPPW} \frac{W_m}{W} \quad (B-2)$$

and

$$\frac{W_f}{W} = \frac{(SFC) (E) (P_r @ V_e)}{2240 W} \quad (B-3)$$

Combining Eqs. B-1 through B-3, we obtain

$$\frac{P_i}{W} = \frac{2240}{SPPW} \left(1 - \frac{W_o}{W} - \frac{W_p}{W} - \frac{(SFC) (E) \frac{P_r}{W} @ V_e}{2240} \right). \quad (B-4)$$

In the special case of $V_m = V_e$, and noting from Eq. B-7 that $P_i/W = P_r/W$ at $V = V_m$, P_i/W of Eq. B-4 can be expressed in terms of only five of the parameters of this study, as follows:

$$\frac{P_i}{W} = \frac{2240}{SPPW} \frac{1 - (W_o/W) - (W_p/W)}{1 + [E(SFC)/SPPW]} \quad (B-5)$$

For the limiting case of $SPPW = 0$, Eq. B-5 reduces to

$$\frac{P_i}{W} = \frac{2240 [1 - (W_o/W) - (W_p/W)]}{E(SFC)} \quad (B-6)$$

The maximum speed a vehicle can achieve is determined by the condition that

$$\frac{P_i}{W} = \frac{P_r}{W} @ V = V_m, \quad (B-7)$$

where

$$\frac{P_r}{W} = \frac{6.87 V}{\eta W/D}.$$

Values of effective horsepower per tonne* as a function of speed for a wide variety of vehicle types are given in Figs. B-1 through B-4, taken from Ref. B-1. The vehicle types considered are given in Table B-1. The effective horsepower per tonne of these figures is related to P_r/W of Eq. B-7 by the expression:

$$\text{EHP/tonne} = \frac{2240}{2205} \eta \frac{P_r}{W}. \quad (B-8)$$

Equations B-7 and B-8 may be used with Figs. B-1 through B-4 to determine V_m for any value of P_i/W . These figures may also be used to determine P_r/W for any value of V , including V_m and V_e .

The approach outlined by Eqs. B-4 and B-8 is applied in the following section to the special case of $V_e = V_m$ and to the more general case of $V_e \leq V_m$.

B. SAMPLE CALCULATIONS

1. For the Special Case of $V_e = V_m$

Calculations using the outlined approach have been carried out for the special case of $V_e = V_m$ for a sample 2000-ton destroyer of conventional configuration, but employing high-technology subsystems (apart from the power plant). Results of the calculations for most of the values of the parameters given in Table B-2 are shown in Fig. B-5.

*One tonne = 2205 lb.

TABLE B-1. VEHICLE TYPES AND CONFIGUARTIONS
FOR FIGURES B-1 THROUGH B-4

Identifying Acronym	Vehicle Type	Brief Configuration Description
1. LTA	<u>L</u> ighter <u>t</u> han <u>a</u> ir	L/B* = 10
2. FWA	<u>F</u> ixed- <u>w</u> ing <u>a</u> ircraft	--
3. RWA	<u>R</u> otary- <u>w</u> ing <u>a</u> ircraft	--
4. WIG	<u>W</u> ing- <u>i</u> n- <u>g</u> round effect	--
5. SUR-1	<u>S</u> urface ship	L/B = 9.6
6. SUR-2	<u>S</u> urface ship	Series 64; L/B = 17.9
7. SUR-3	<u>S</u> urface ship	L/B = 2.4
8. PLA-1	<u>P</u> laning craft	Series 62; L/B = 4.1
9. PLA-2	<u>P</u> laning craft	Series 62; L/B = 5.5
10. PLA-3	<u>P</u> laning craft	Series 65; L/B = 6.6
11. HYD-1	<u>H</u> ydrofoil	Series 65; $(C_v)_h = 5.94 \times 10^{-3}$
12. HYD-2	<u>H</u> ydrofoil	Series 65; $(C_v)_h = 3.03 \times 10^{-3}$
13. HYD-3	<u>H</u> ydrofoil	Series 65; $(C_v)_h = 1.53 \times 10^{-3}$
14. ACV	<u>A</u> ir- <u>c</u> ushion <u>v</u> ehicle	$L_c/B_c = 2$
15. SES-1	<u>S</u> urface- <u>e</u> ffect <u>s</u> hip	$L_c/B_c = 2$
16. SES-2	<u>S</u> urface- <u>e</u> ffect <u>s</u> hip	$L_c/B_c = 6.5$
17. SUB	<u>S</u> ubmarine	L/B = 9

*L/B \equiv Length/Breadth.

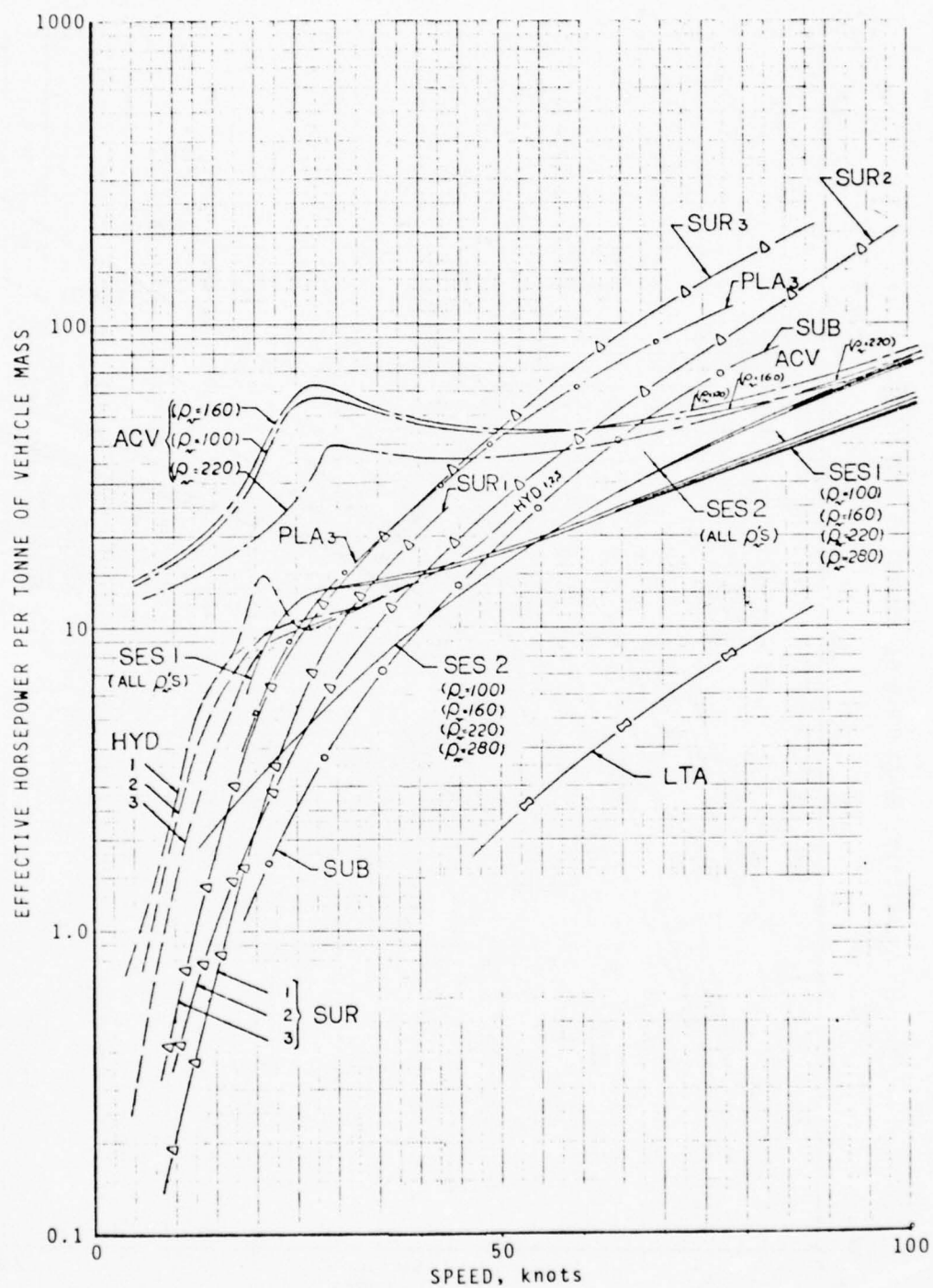


FIGURE B-1. Effective horsepower per tonne of vehicle mass versus speed for 1000-tonne LTA, SUR, PLA, HYD, ACV, SES, and SUB vehicles.

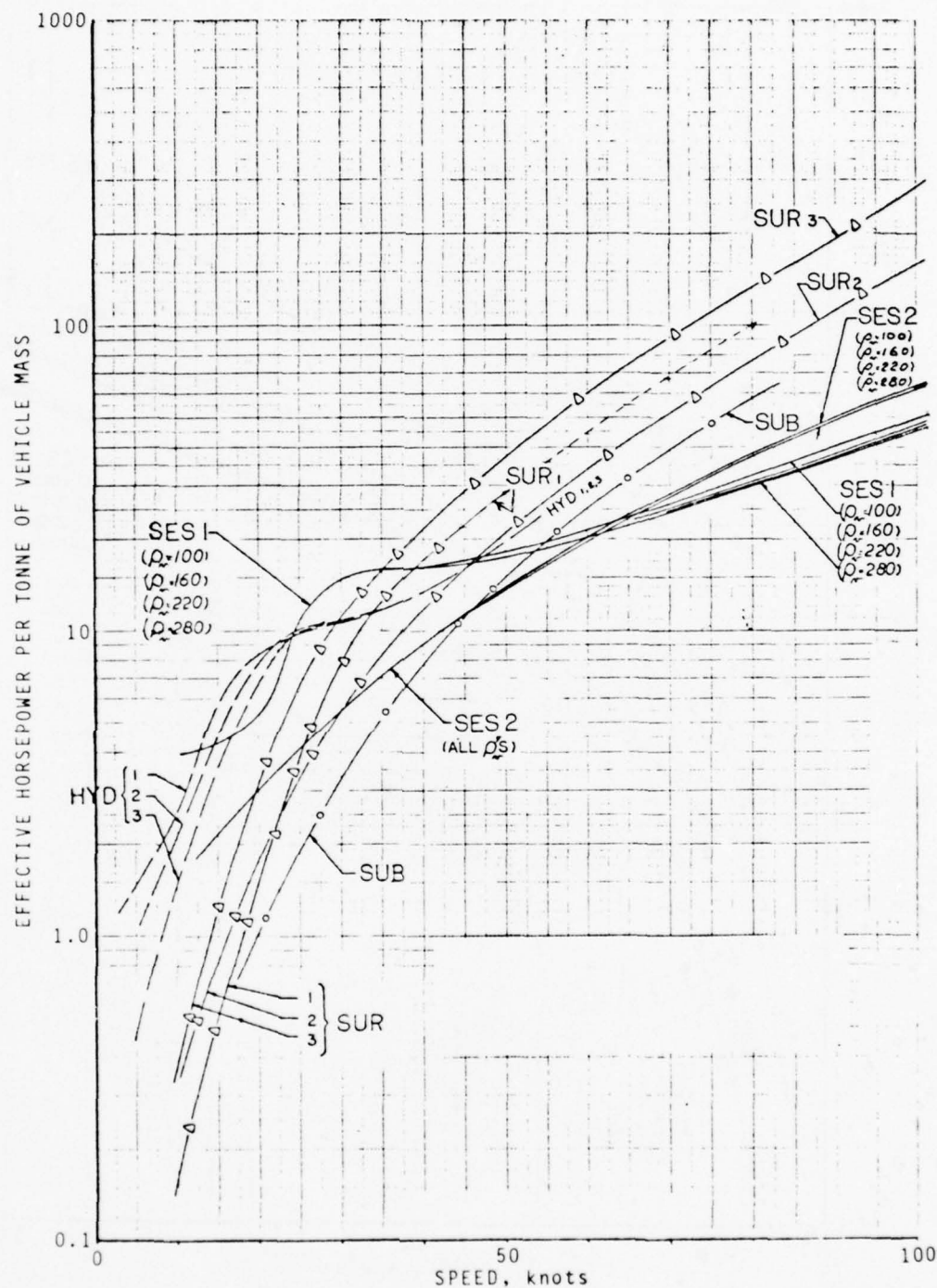


FIGURE B-2. Effective horsepower per tonne of vehicle mass versus speed for 2000-tonne SUR, HYD, SES, and SUB vehicles.

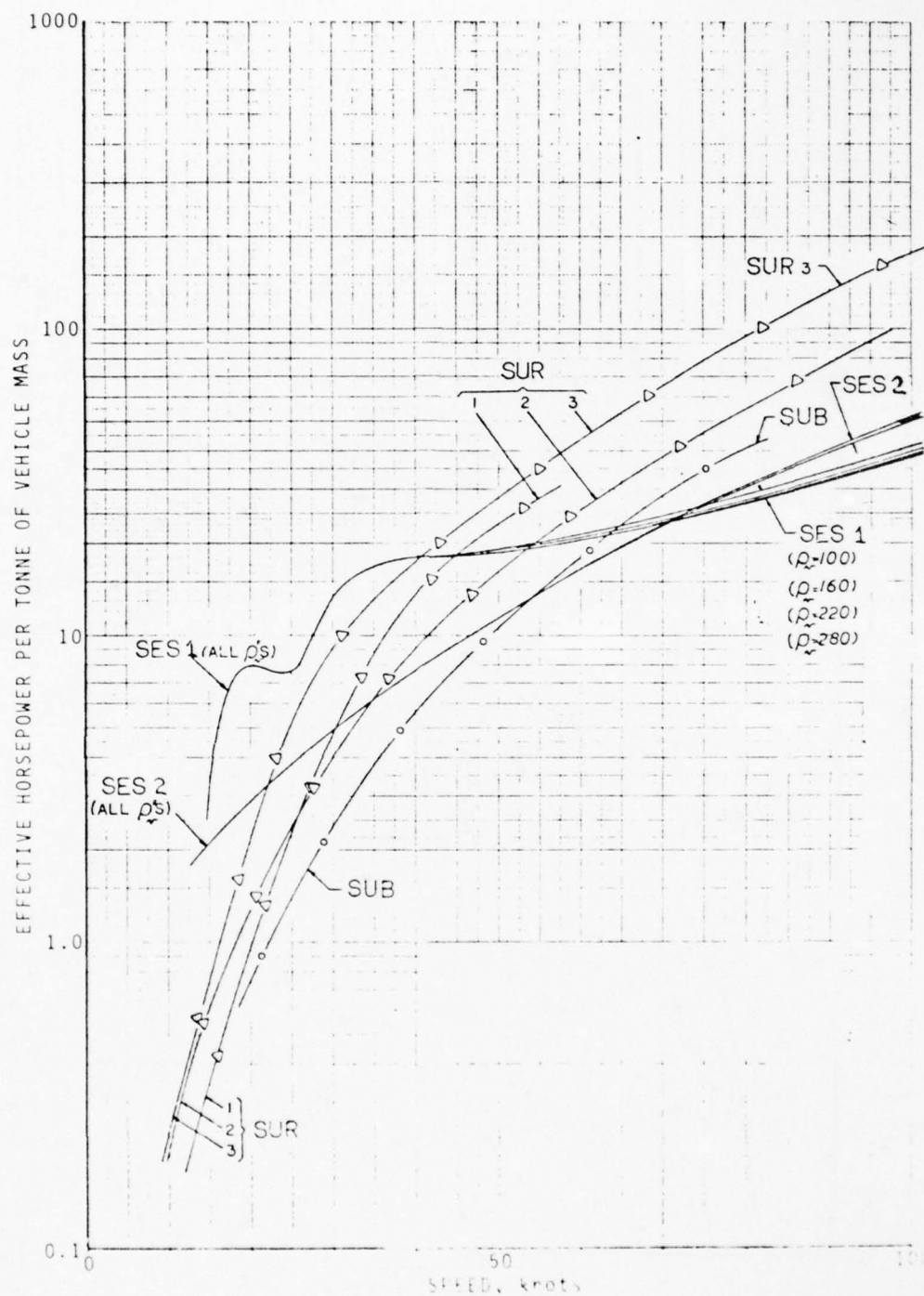


FIGURE B-3. Effective horsepower per tonne of vehicle mass versus speed for 5000-tonne SUR, SES, and SUB vehicles.

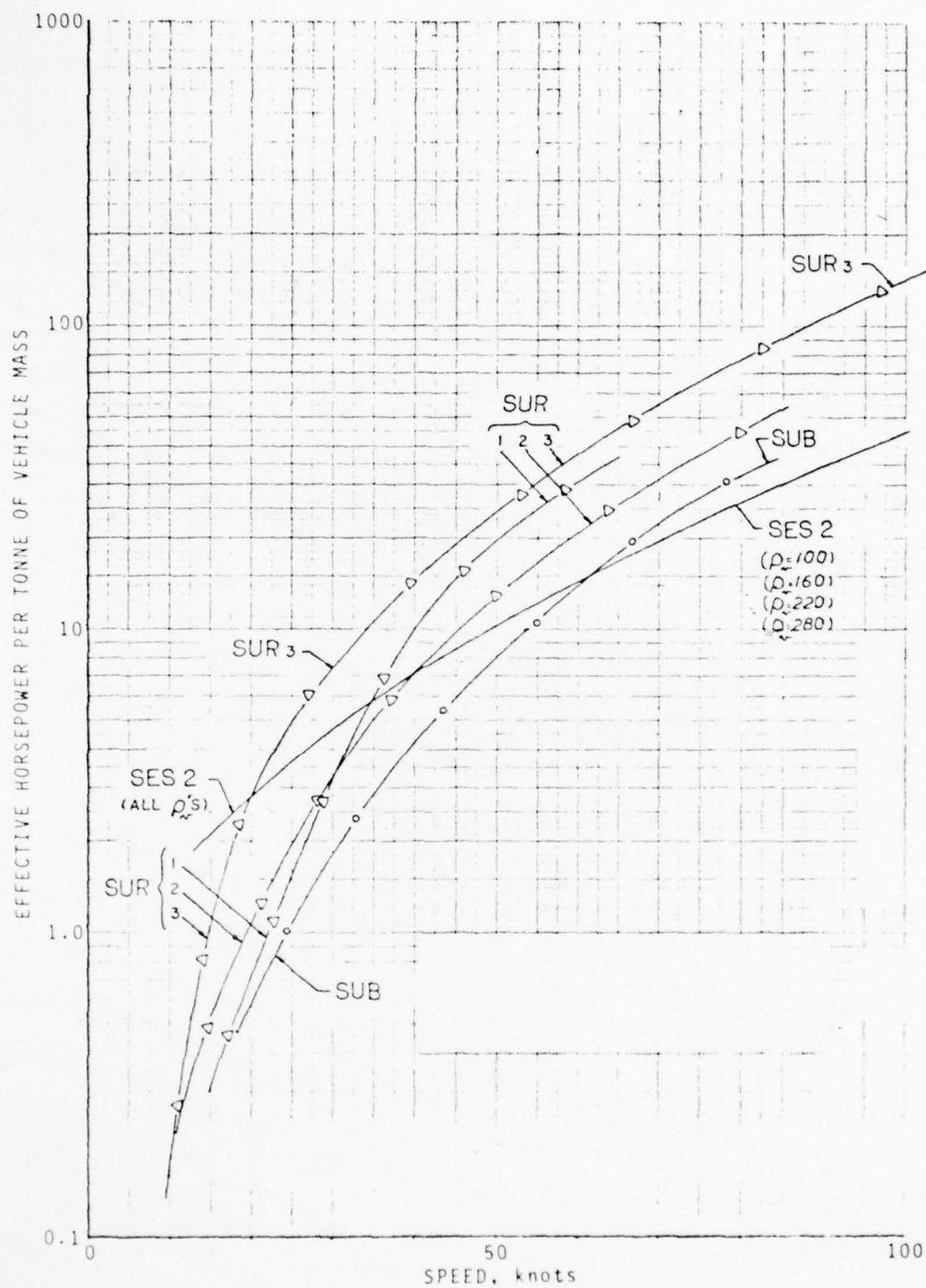


FIGURE B-4. Effective horsepower per tonne of vehicle mass versus speed for 10,000-tonne SUR, SES, and SUB vehicles.

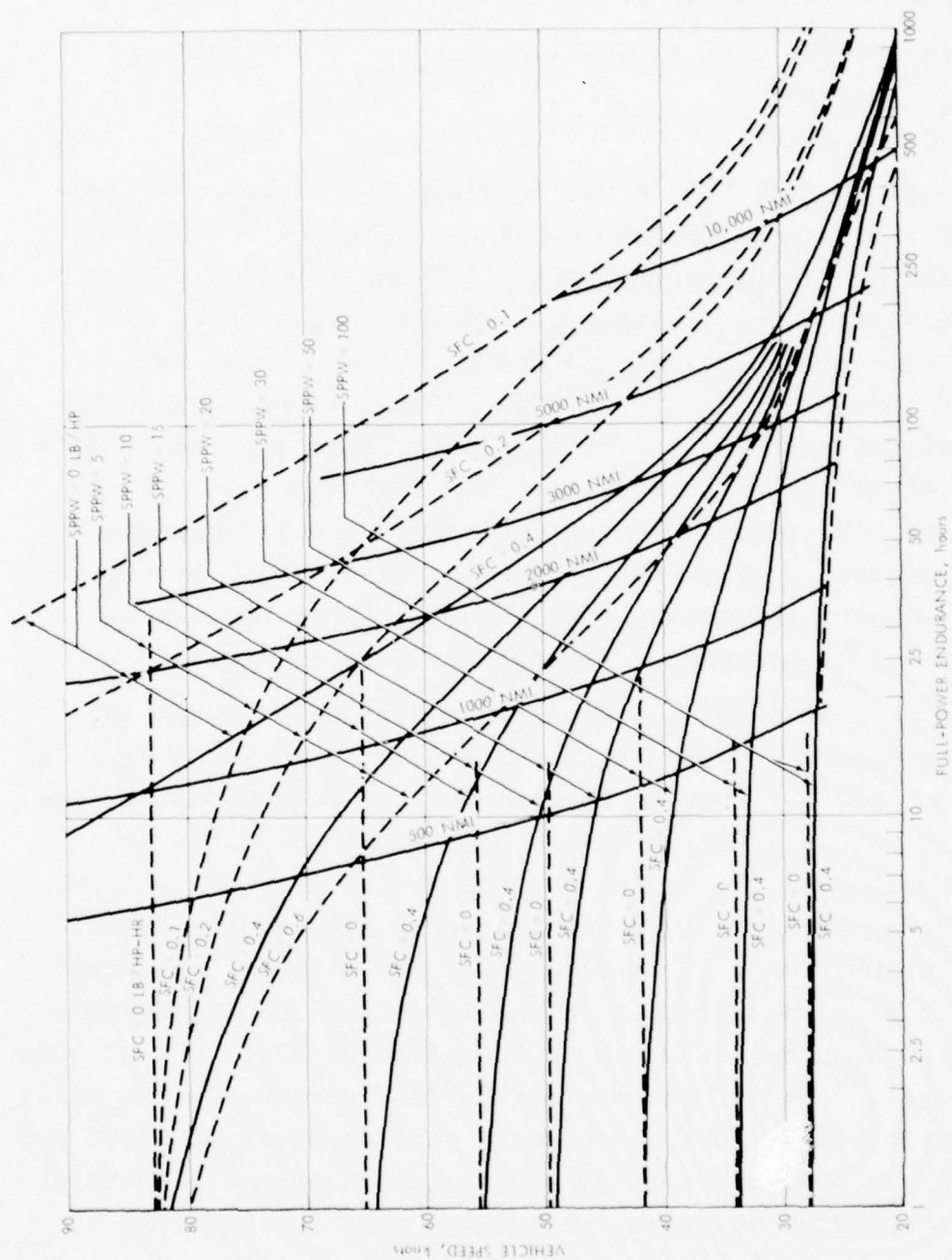


FIGURE B-5. Effect of propulsion system technology on speed and endurance of a 2000-ton high-performance surface ship.

TABLE B-2. VALUES OF PARAMETERS FOR SAMPLE 2000-TON DESTROYER

$$W_p/W = 0.10 \quad \text{SPPW} = 0, 5, 10, 15, 20, 30, 50, 100 \text{ lb/hp}$$

$$W_o/W = 0.40 \quad \text{SFC} = 0, 0.1, 0.2, 0.4, \text{ \& } 0.6 \text{ lb/hp-hr}$$

$$n = n_e = n_m = 0.50$$

The value $W_o/W = 0.40$ given in Table B-2 renders the subsystems of this sample vehicle as high-technology. Following conventional Navy surface-ship practice, the value of W_o (which includes all structural, electrical, auxiliary, outfit, and personnel weight) is between 55% and 65% of the total vehicle weight. With $W_p/W = 0.1$ (from Table B-2), this means that the total weight allocatable to fuel and propulsion systems in conventional naval combatant ships is between 25% and 35% of the total weight. Reference B-2 suggests that by using high-technology subsystems W_o/W can be reduced to 0.40, which increases the weight allocatable to $W_m + W_f$ to 0.50. This value was chosen for all of the sample vehicles of this appendix.

The effect of changes in the assumed values of W_o/W on P_i/W can be determined from Eqs. B-5 and B-6. At $\text{SFC} = 0$, it is evident from Eq. B-5 that an increase in the value of W_o/W from 0.40 to 0.55 (that is, from "high-technology" Navy standards to "conventional" Navy standards) results in a 30% decrease in the value of P_i/W , if one assumes no change in the value of SPPW. Similarly at $\text{SPPW} = 0$, it is clear from Eq. B-6 that the same increase in W_o/W would result in the identical 30% decrease in P_i/W , if one assumes no change in the value of SFC. For a 2000-ton destroyer, Fig. B-2 reveals that a 30% decrease in the value of P_i/W would result in a decrease in vehicle speed of about 1.8 knots at an initial speed of 20 knots and of about 8.5 knots at an initial speed of 80 knots. Extending this analysis, it is found that Fig. B-5 would apply to an ordinary rather than a high-technology 2000-ton destroyer if the values of the scale of the ordinate of Fig. B-5 were changed to read 18.2, 27.5, 34.5,

43, 52, 61.5, 71.5, and 81.5 knots rather than 20, 30, 40, 50, 60, 70, 80, and 90 knots. This analysis shows that the impact of changes in propulsion-system characteristics in a conventional-technology destroyer would be somewhat less than that shown in Fig. B-5 for a high-technology destroyer.

Table B-3, read directly from Fig. B-5, shows how high-technology destroyer speed increases with decreasing values of SPPW and SFC at a fixed value of full-power endurance distance R of 2000 nmi.

TABLE B-3. VALUES OF SPPW AND SFC FROM FIGURE B-5 FOR INCREASING VALUES OF SPEED FOR A FULL-POWER ENDURANCE OF 2000 NAUTICAL MILES

<u>SPPW, lb/hp</u>	<u>SFC, lb/hp-hr</u>	<u>V_m, knots</u>
100	0.6	25.1
100	0.4	25.8
100	0	27.7
50	0.4	30.0
30	0.4	32.5
50	0	33.9
20	0.4	35.7
15	0.4	38.5
5	0.6	38.5
30	0	41.8
10	0.4	42.3
5	0.4	48.2
20	0	49.5
15	0	55.5
0	0.4	57.6
5	0.2	62
10	0	65.2
5	0.1	71.1
5	0	83
0	0.2	83
0	0.1	>100

The limit lines shown in Fig. B-5 as $SFC = 0$ also apply to nuclear propulsion. One of the uses of data like that shown in Fig. B-5 is that it reveals directly the power-plant characteristics of nuclear and conventionally powered ships needed for the 2000-ton sample destroyer to achieve common performance goals. For example, Table B-4 shows the values of P_i/W and the combinations of values of SPPW and SFC that would be needed for the 2000-ton destroyer to achieve 40, 50, and 60 knots with 2000-nmi full-power endurance. The SFC and SPPW values given in Table B-4 can be read approximately from Fig. B-5 or derived precisely from Eqs. B-5 through B-8 and Fig. B-2.

TABLE B-4. VALUES OF SFC AND SPPW NEEDED TO ACHIEVE 40, 50, AND 60 KNOTS AND 2000-NMI ENDURANCE DISTANCE AT THOSE SPEEDS FOR THE SAMPLE DESTROYER

Speed = 40 knots $P_i/W = 34$ hp/ton		Speed = 50 knots $P_i/W = 59$ hp/ton		Speed = 60 knots $P_i/W = 90$ hp/ton	
SPPW, lb/hp	SFC lb/hp-hr	SPPW, lb/hp	SFC lb/hp-hr	SPPW, lb/hp	SFC lb/hp-hr
0	0.658	0	0.475	0	0.379
5	0.558	5	0.350	5	0.229
10	0.458	10	0.225	10	0.079
15	0.358	15	0.100	12.6	0*
20	0.258	19	0*		
30	0.058				
32.9	0*				

*The SPPW values associated with $SFC = 0$ correspond to the values for nuclear power. Clearly, at $SFC = 0$, infinite endurance rather than 2,000-nmi endurance can be obtained.

Table B-5 shows similar values needed to achieve 500-, 1000-, 2000-, 3000-, and 5000-nmi full-power endurance at a speed of 50 knots.

TABLE B-5. VALUES OF SFC AND SPPW NEEDED TO ACHIEVE 500-1000-, 2000-, 3000-, AND 5000-NMI ENDURANCE DISTANCE AT 50 KNOTS FOR THE SAMPLE DESTROYER

	500 nmi	1,000 nmi	2,000 nmi	3,000 nmi	5,000 nmi
SPPW, lb/hp	SFC, lb/hp-hr	SFC, lb/hp-hr	SFC, lb/hp-hr	SFC, lb/hp-hr	SFC, lb/hp-hr
0	1.9	0.95	0.475	0.317	0.19
5	1.4	0.7	0.350	0.233	0.14
10	0.9	0.45	0.225	0.150	0.09
15	0.4	0.20	0.100	0.067	0.04
19	0	0	0	0	0

The values of SFC and SPPW shown in Tables B-4 and B-5 are plotted in Fig. B-6. The results are straight lines that can be interpreted as giving the maximum values of SFC and SPPW that together will satisfy the given speed and range requirements. That is to say, any propulsion system that provides a combination of SFC and SPPW values that fall above the lines shown will not be adequate to provide the speed and range indicated. It can be seen that as either speed or range requirements are increased, acceptable values of both SFC and SPPW decrease quite rapidly.

2. For the General Case of $V_e \leq V_m$

Some vehicles achieve their largest possible endurance distance R at speeds much less than V_m . In fact, for ordinary conventional combatant surface ships, endurance distance increases significantly with reduced endurance speed V_e down to very low values of speed. Hence, since before World War I, the value $V_e = 20$ knots has been the established standard speed for quoting the endurance distance of combatant ships. For other vehicle types, such as hydrofoil and SES vehicles, V_e for maximum R is considerably greater than 20 knots but not necessarily as large as V_m . It is therefore very important to treat the general case of $V_e \leq V_m$ in addition to the special case of $V_e = V_m$.

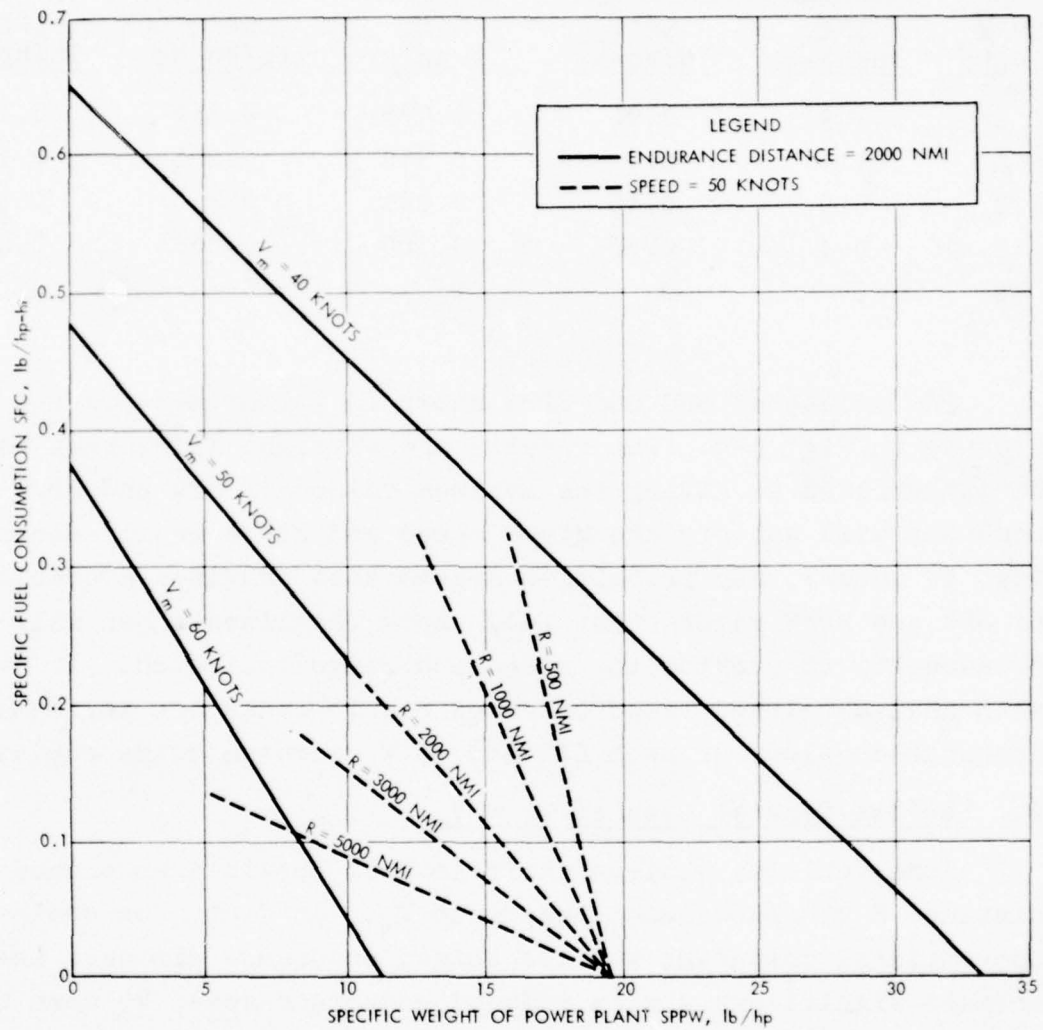


FIGURE B-6. Effect of changes in speed and endurance distance R on propulsion system parameters (SFC and SPPW) for a sample high-speed destroyer.

The fact that Fig. B-6 is in the form of straight lines renders the presentation of data for $V_e \leq V_m$ straightforward. Using Eq. B-4 and the assumptions of Table B-2 that $W_o/W = 0.40$ and $W_p/W = 0.10$, we find that the value of SPPW at SFC = 0 is

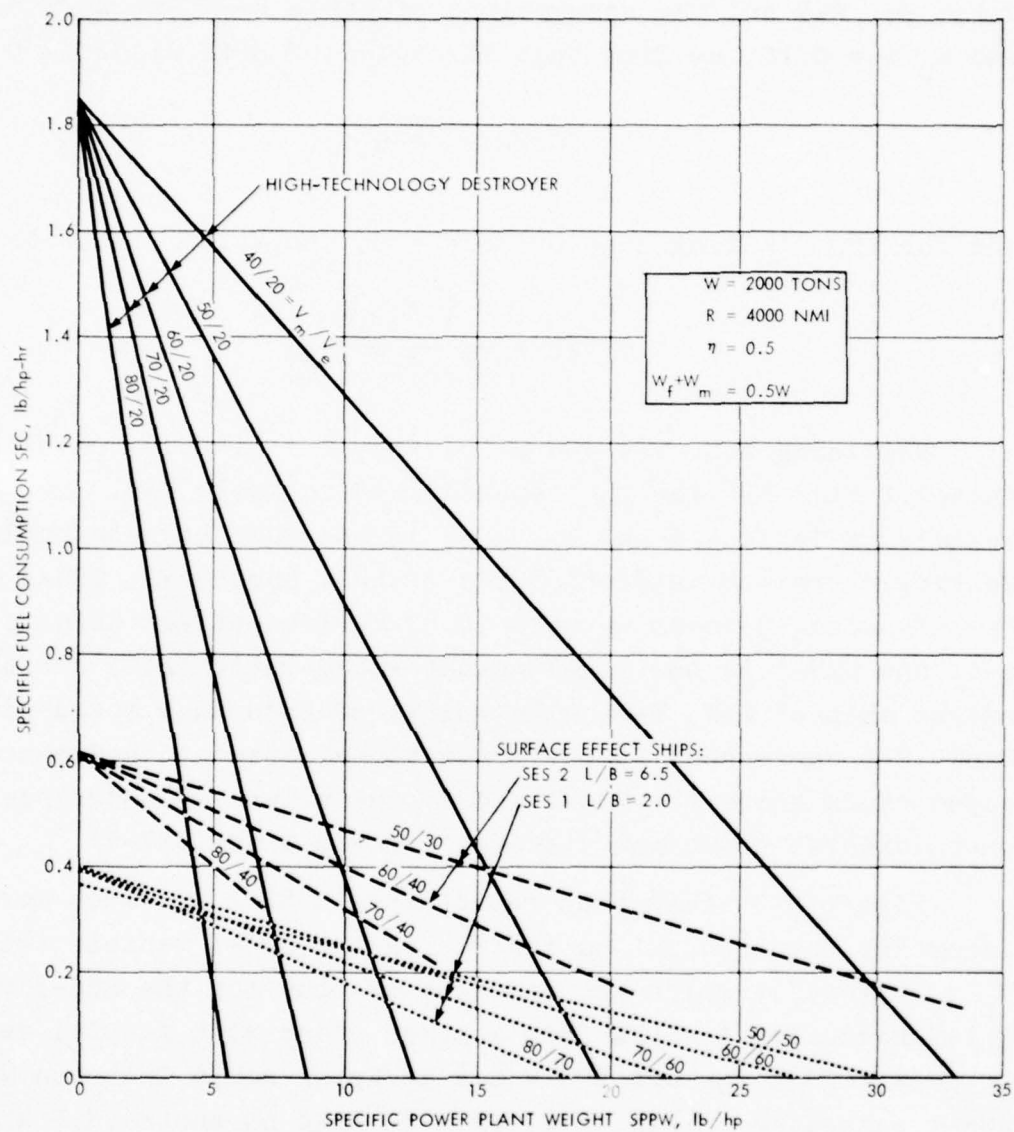
$$SPPW = \frac{1120W}{P_i}, \quad (B-9)$$

and for the limiting case of SPPW = 0, the value of SFC is

$$SFC = \frac{1120V_e W}{RP_r @ V = V_e} \quad (B-10)$$

Utilizing Eqs. B-9 and B-10, Fig. B-7 displays results like those of Fig. B-6 for the cases listed in Table B-6. The SUR-1 vehicle of Table B-6 and Fig. B-7 is the same high-technology destroyer treated in Section B-1 of this appendix. SES-2 is the high-length-to-beam-ratio (6.5) surface-effect ship of Ref. B-1, and SES-1 is the low-length-to-beam-ratio (2.0) surface-effect ship of Ref. B-1. The values of endurance speed given in Table B-6 correspond to the conventional standard endurance speed of 20 knots for SUR-1 and to the values of endurance speed that maximize endurance distance for SES-2 and SES-1.

Figure B-7 shows that reductions in SPPW are much more important than reductions in SFC for the SUR-1 vehicle (with $V_e = 20$ knots), while the opposite is true for the SES-2 vehicle. A 10% reduction in SPPW from a power plant with initial values of SPPW = 10 lb/hp and SFC = 0.4 lb/hp-hr would increase V_m for SUR-1 according to Fig. B-7, from 59.5 to 64 knots (3.5 knots), whereas a 10% reduction in SFC would increase V_m by only 0.5 knot. On the other hand, with SES-2, starting with the same power plant, Fig. B-7 shows that a 10% reduction in SPPW would only increase V_m from 60 to 63 knots (3 knots), whereas a 10% reduction in SFC would increase V_m from 60 to 66 knots (6 knots).



10-19-77-1

FIGURE B-7. Relationship between vehicle characteristics and propulsion system parameters for three types of high-speed ships.

TABLE B-6. CASES DISPLAYED IN FIGURE B-7

Vehicle Size W 2000 tons

Endurance Distance R = 4000 nmi

 $\eta \approx \eta_m \approx \eta_e \approx 0.50$ $W_o + W_p = 0.50W$

Vehicle	Maximum Velocity V_m , knots	Endurance Velocity V_e , knots	P_i ,* hp	P_r @ V_e ,* hp
SUR-1	40	20	68,000	6,080
SUR-1**	50	20	114,000	6,080
SUR-1**	60	20	178,000	6,080
SUR-1**	70	20	264,000	6,080
SUR-1	80	20	400,000	6,080
SES-2	50	30	54,800	27,400
SES-2	60	40	80,000	36,200
SES-2	70	40	110,800	36,200
SES-2	80	40	151,600	36,200
SES-1	50	50	75,200	75,200
SES-1	60	60	84,000	84,000
SES-1	70	60	100,000	84,000
SES-1	80	70	124,000	100,000

*From Eqs. B-7 and B-8 and Fig. B-2.

**Required an extrapolation of the SUR-1 effective horsepower per tonne data of Fig. B-2 to 60, 70, and 80 knots. This extrapolation is very likely valid.

C. CONCLUSION

Equations B-4 through B-10 and Figs. B-1 through B-7 can be used to assess the impact of propulsion-system advances on the performance characteristics of a wide variety of waterborne vehicles.

GLOSSARY, APPENDIX B

ACV	Air-cushion vehicle
B	Breadth
D	Drag
E	Vehicle endurance time at V_e , hours
FWA	Fixed-wing aircraft
HYD	Hydrofoil
L	Length
LTA	Lighter than air craft, airships
P_i	Installed shaft horsepower
PLA	Planing craft
P_r	Shaft horsepower required at specified speed
R	Vehicle endurance distance at V_e , nmi
RWA	Rotary-wing aircraft
SES	Surface-effect ship
SFC	Specific fuel consumption at endurance speed, V_e , lb/shp
SPPW	Specific power-plant weight, lb/shp
SUB	Submarine
SUR	Surface ship
V	Vehicle speed, knots
V_m	Maximum speed, knots
V_e	Endurance speed, knots

W	Total vehicle weight, long tons
W_f	Weight of fuel, tons
WIG	Wing-in-ground effect aircraft
W_m	Weight of power plant, tons
W_o	Other vehicle weight, tons ($W_o = W - W_m - W_f - W_p$)
W_p	Payload weight, fixed and consumable items, tons
η	Overall propulsive coefficient at any speed V
η_e	Overall propulsive coefficient at V_e
η_m	Overall propulsive coefficient at V_m

REFERENCES, APPENDIX B

- B-1. Department of Ocean Engineering, Massachusetts Institute of Technology, Report of MIT Vehicle Assessment Project, Report 77-14, P. Mandel, July 1977.
- B-2. C. Graham, J. L. Grostick, and T. E. Fahey, "A Comparative Analysis of Naval Hydrofoil and Displacement Ship Design," SNAME Transactions, Vol. 84, 1976.

APPENDIX C

SIZE AND SPECIFIC FUEL CONSUMPTION RELATIONSHIPS IN OTTO-CYCLE ENGINES

James E. A. John
E. William Beans

CONTENTS

A. Ideal Engine Performance	C-3
1. The Ideal Cycles	C-3
a. Otto Cycle	C-3
b. Other Ideal Cycles	C-4
2. Ideal Cycle Performance	C-6
3. Implications of Ideal Cycle Performance with Respect to Further Performance Improvements in Otto Engines	C-16
B. Relationships of Actual Performance to Ideal Performance	C-16
1. Real Gas Losses	C-18
2. Combustion Losses	C-21
3. Heat Transfer Losses	C-27
4. Exhaust Blowdown Losses	C-31
5. Friction Losses	C-35
6. Collective Impact of Losses of Performance	C-38
7. Part-Load Performance	C-40
8. Implications of Actual Performance with Respect to Further Improvements in Otto Engines	C-44
C. Weight, Size, and Performance Relationships	C-47
1. General Scaling Considerations	C-47
2. Current State of the Art	C-48
3. Component Loss-Weight Relationships	C-53
4. Overall Engine Weight and Size Scaling	C-55
5. Engine Specific Fuel Consumption Scaling	C-60
6. Current State of the Art in Specific Fuel Consumption-Weight Tradeoffs	C-62

D. Prospects for Improvements in Otto Engines	C-64
1. Utilization of Exhaust Energy	C-64
2. Stratified-Charge Engines	C-66
3. Rotary Engines	C-67
4. Adiabatic Engines	C-69
5. Potential Limits for Otto Engines	C-71
Glossary	C-74
References	C-78
Annex C1--Representative Gasoline Engines	C-79

APPENDIX C

SIZE AND SPECIFIC FUEL CONSUMPTION RELATIONSHIPS IN OTTO-CYCLE ENGINES

James E. A. John
E. William Beans

A. IDEAL ENGINE PERFORMANCE

1. The Ideal Cycles

a. Otto Cycle. The basic theoretical cycle for all spark-ignition engines is the Otto cycle. The ideal Otto cycle is shown in pressure-volume and temperature-entropy coordinates in Fig. C-1, and consists of four basic energy transfer processes:

1. Isentropic compression (1-2)
2. Heat addition at constant volume (2-3)
3. Isentropic expansion (3-4)
4. Cooling at constant volume (4-1).

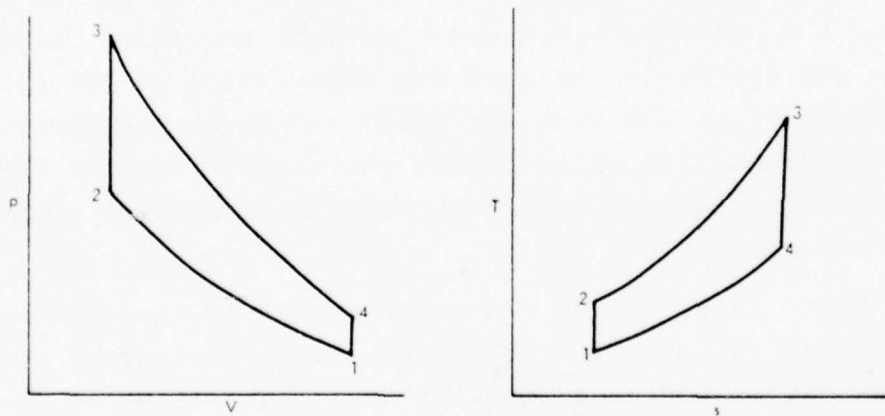


FIGURE C-1. The ideal Otto cycle.

The most common mechanization of this cycle is the carbureted, reciprocating, four-stroke, open-cycle engine in which a fuel-air mixture is inducted into a cylinder on the intake stroke of a piston, is compressed on the compression stroke, is ignited and burned at the end of the compression stroke, is expanded on the power stroke, and is expelled from the cylinder on the exhaust stroke. Other mechanizations include: the two-stroke engine, in which the combustion products are expelled from the cylinder and the fuel-air mixture is inducted into the cylinder between the power and compression strokes; the rotary engine, in which the intake, compression, expansion, and exhaust functions are accomplished by means of a geared, eccentric rotor; and the stratified-charge engine, in which nonhomogeneous fuel-air mixtures are introduced into the cylinder by means of either variable carburetion or direct fuel injection.

For a given fuel, the basic cycle parameters are the compression ratio--the ratio of the gas volume at the end of the compression stroke to that at the beginning--and the fuel-air ratio. In terms of power transfer parameters, in the context used in this report, the power required for compression is the internal power transfer; the rate of heat addition is the power added; and the difference between the power developed during expansion and the power required for compression is the power output. Typically, the fuel-air ratio can be stoichiometric with a consequent high rate of heat addition, since the intermittent operation of the engine permits the transient presence of high temperatures.

b. Other Ideal Cycles. A major source of inefficiency in the Otto cycle is the relatively high energy content of the exhaust gases, as suggested by Fig. C-1. Variations of the Otto cycle have been devised to utilize some of this exhaust energy, and three such ideal cycles are considered here: the turbo-charged Otto cycle, the regenerated Otto cycle, and the Lenoir cycle.

The ideal turbocharged Otto cycle is shown in temperature-entropy coordinates and pressure-volume coordinates in Fig. C-2. The cycle 1'-2-3-4 is identical to the conventional Otto cycle and is augmented by an isentropic expansion 4'-5, the work output of which is used for the isentropic compression 1-1'. The basic cycle parameters are the fuel-air ratio, the cycle compression ratio (v_0/v_2 , where v is the specific volume), and the turbocharging pressure ratio (p_1/p_1') or compression ratio (v_1/v_1'). The internal power transfer is the power required for the total compression process (0-2), and the power output is the total expansion power (3-4-4'-5) plus the net power developed by the intake and exhaust processes (4'-1'), less the internal power transfer.

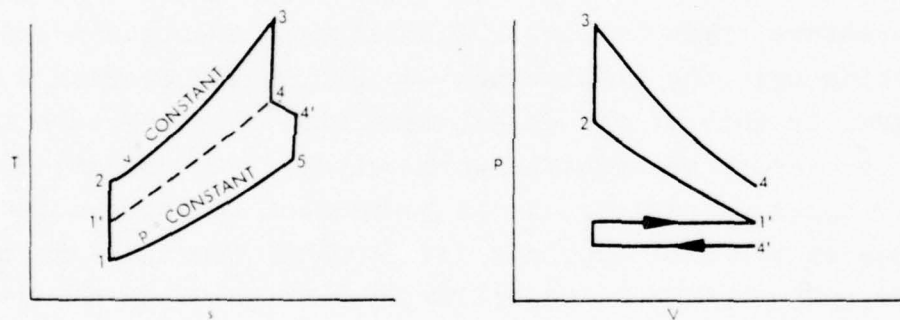


FIGURE C-2. The ideal turbocharged Otto cycle (four-stroke).

The ideal regenerated Otto cycle utilizes the energy in the exhaust at the end of the power stroke to preheat the gas at the end of the compression stroke; pressure-volume and temperature-entropy coordinates are shown in Fig. C-3. As with the ideal Otto cycle, the basic cycle parameters are the fuel/air ratio and the compression ratio. In terms of power transfer

parameters, the internal power transfer is the power required for compression (1-2) and the energy transfer rate by regeneration (2-2' or 4-4'), and the other power transfers are identical to those of the ideal Otto cycle.

In the Lenoir cycle, the expansion process is extended to the initial pressure rather than the initial volume, as shown in Fig. C-4. Again, the basic cycle parameters are identical to those of the Otto cycle--fuel/air ratio and compression ratio. The internal power transfer is that required for compression (1-2) and the energy transfer rate associated with the constant pressure process (1-4), and the other power transfers are identical to those of the ideal Otto cycle.

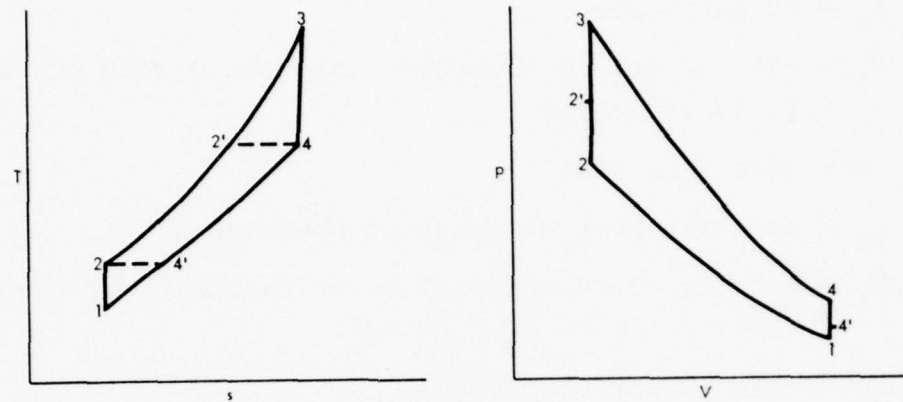
2. Ideal Cycle Performance

Conventionally, the performance of Otto engines is expressed in terms of the thermodynamic efficiency and the mean effective pressure. The latter is defined as a constant pressure which, acting over the displacement volume, would produce a work output equal to that of the cycle; mean effective pressure is therefore a measure of specific work output. For comparison with other types of engines, it is convenient to express the performance in terms of specific fuel consumption and a normalized power output per unit mass flow; for a fuel with a lower heating value of 18,400 Btu/lbm and a working fluid with constant specific heats, the interrelationships are

$$\text{sfc} = \frac{0.138}{\eta} \quad (\text{C-1})$$

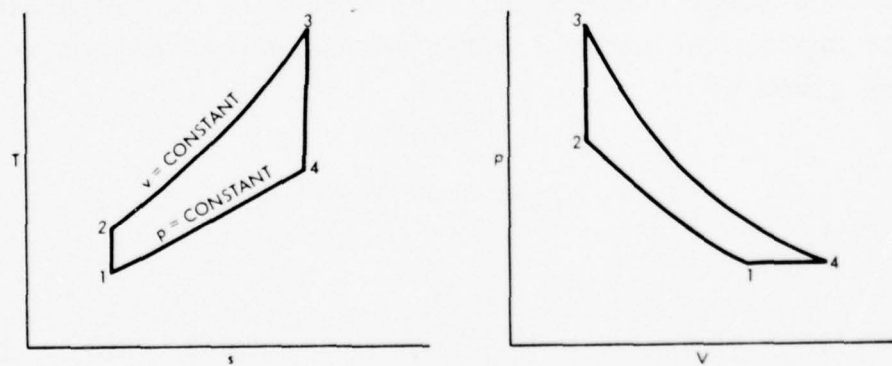
and

$$\frac{P_o}{P_i} \equiv \frac{P_o}{\dot{m} c_p T_1} = \frac{\text{mep}}{\rho_c c_p T_1} \left(\frac{r-1}{r} \right) = \frac{\text{mep}}{\left(\frac{\rho_c}{\rho_1} \right) P_1} \left(\frac{r-1}{r} \right) \left(\frac{\gamma-1}{\gamma} \right), \quad (\text{C-2})$$



9-6-77-16

FIGURE C-3. The ideal regenerated Otto cycle.



9-6-77-17

FIGURE C-4. The ideal Lenoir cycle.

where sfc = specific fuel consumption, lbm/hp-hr

η = thermodynamic efficiency

P_o = output power

P_i = rate of energy transport associated with the working fluid ($= \dot{m} c_p T_1$)

\dot{m} = mass flow rate

c_p = specific heat at constant pressure

T_1 = working fluid temperature at beginning of compression

mep = mean effective pressure

ρ_c = density of working fluid at beginning of compression in displacement volume

ρ_1 = density of working fluid at beginning of compression

r = compression ratio

p_1 = pressure of working fluid at beginning of compression

γ = ratio of specific heats.

For the ideal Otto cycle, with a working gas with constant specific heats, the thermal efficiency and mean effective pressure are given by

$$\eta_{id} = 1 - \frac{1}{r^{\gamma-1}} \quad (C-3)$$

and

$$mep = \eta_{id} \left(\frac{r}{r-1} \right) \left(\frac{f}{a} \right) \frac{p_1}{RT_1} \quad (C-4)$$

In terms of energy transfer parameters, the specific fuel consumption and normalized power output are given by

$$sfc = 0.138 \frac{\gamma(P_{add}/P_i)(P_{int}/P_o)}{\gamma(P_{add}/P_i)(P_{int}/P_o) - 1} \quad (C-5)$$

$$\frac{P_o}{P_i} = \frac{P_{add}}{P_i} - \frac{1}{\gamma(P_{int}/P_o)} \quad , \quad (C-6)$$

where HV = fuel heating value

f/a = fuel-air ratio

P_{add} = rate of heat addition = $\dot{m}(f/a)(HV)$

P_{int} = internal power transfer = $\dot{m}c_v(T_2 - T_1)$.

The performance of the ideal Otto cycle is shown in Fig. C-5, for a ratio of specific heats $\gamma = 1.4$, and for normalized heat addition rates P_{add}/P_i of 8 and 10, the latter value corresponding to stoichiometric operation. The well-known result that the specific fuel consumption of the ideal Otto cycle depends only upon compression ratio is evident in the figure. It is also apparent that the impact of higher heat addition rates is to increase the specific power output and decrease the ratio of internal power transfer to power output required to achieve a given level of specific fuel consumption.

The performance of the ideal turbocharged Otto cycle is shown in Fig. C-6. It can be observed that turbocharging reduces the specific power output and increases the specific fuel consumption for a fixed overall compression ratio (v_1/v_2 in Fig. C-2).

In terms of energy transfer parameters, the performance of the ideal regenerated Otto cycle is identical to that of the ideal Otto cycle shown in Fig. C-5. The major difference between the two cycles is of course in the mode of internal

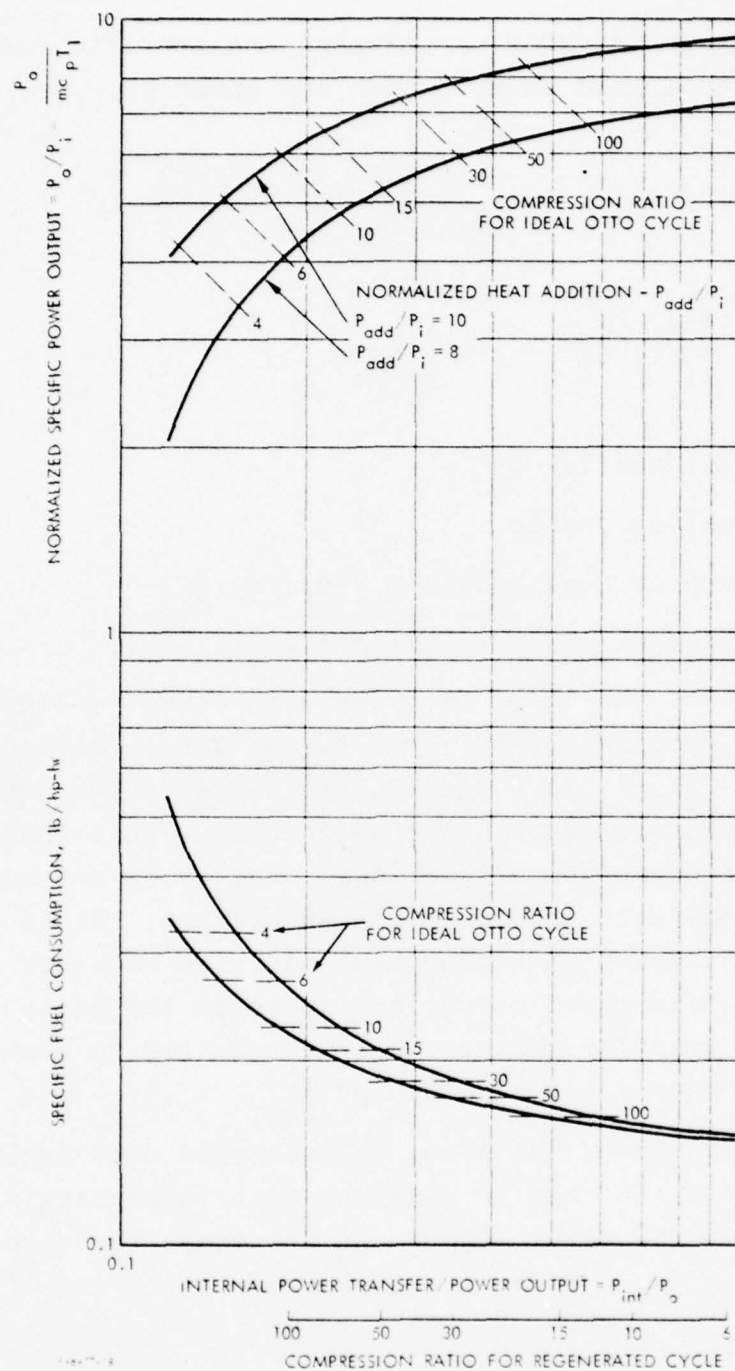


FIGURE C-5. Performance of ideal Otto cycle.

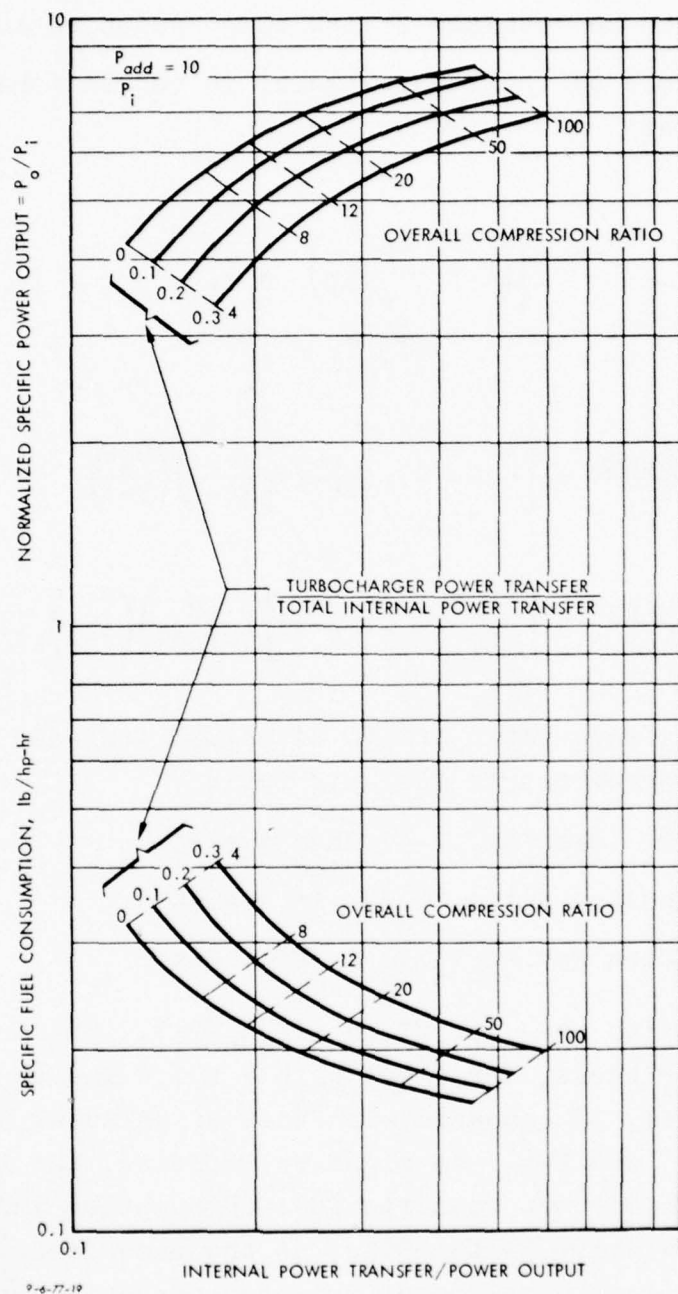


FIGURE C-6. Performance of ideal turbocharged Otto cycle.

power transfer; this is clearly indicated in Fig. C-5, wherein it can be observed that high ratios of internal power transfer to power output can be obtained at low compression ratios.

The performance of the Lenoir cycle, in conventional terms, can be expressed as

$$\eta = 1 - \frac{\gamma \left[\left(1 + \frac{\phi \Delta T_s}{T_1 r^{\gamma-1}} \right)^{\frac{1}{\gamma}} - 1 \right]}{\phi \Delta T_s / T_1} \quad (C-7)$$

$$\text{mep}_I = \frac{\text{Work Output}}{V_1 - V_2} = \left[\frac{\Delta T_s \phi}{T_1} - \gamma(r_t - 1) \right] \left(\frac{r}{r-1} \right) \left(\frac{p_1}{\gamma-1} \right) \quad (C-8)$$

$$\text{mep}_{II} = \frac{\text{Work Output}}{V_4 - V_2} = \left[\frac{\Delta T_s \phi}{T_1} - \gamma(r_t - 1) \right] \left(\frac{r}{r r_t - 1} \right) \left(\frac{p_1}{\gamma-1} \right) , \quad (C-9)$$

where ϕ = equivalence ratio, ratio of actual fuel-air ratio to stoichiometric fuel-air ratio

$\Delta T_s = T_3 - T_2$ (see Fig. C-4) when $\phi = 1$

r = compression ratio, V_1/V_2 in Fig. C-4

r_t = expansion ratio, V_4/V_2 in Fig. C-4.

and it is to be noted that $\phi \Delta T_s / T_1 = \gamma(P_{\text{add}}/P_1)$. The performance of the Lenoir cycle, for a gas with $\gamma = 1.4$ and an inlet pressure of 15 psia, is compared with that of an ideal Otto cycle in Figs. C-7 and C-8. As might be expected, the Lenoir cycle offers both improved specific fuel consumption and improved specific output relative to the Otto, at the same compression ratio. In terms of internal power transfer per unit output, however, the performances of the two cycles are not so different, as shown in Fig. C-9.

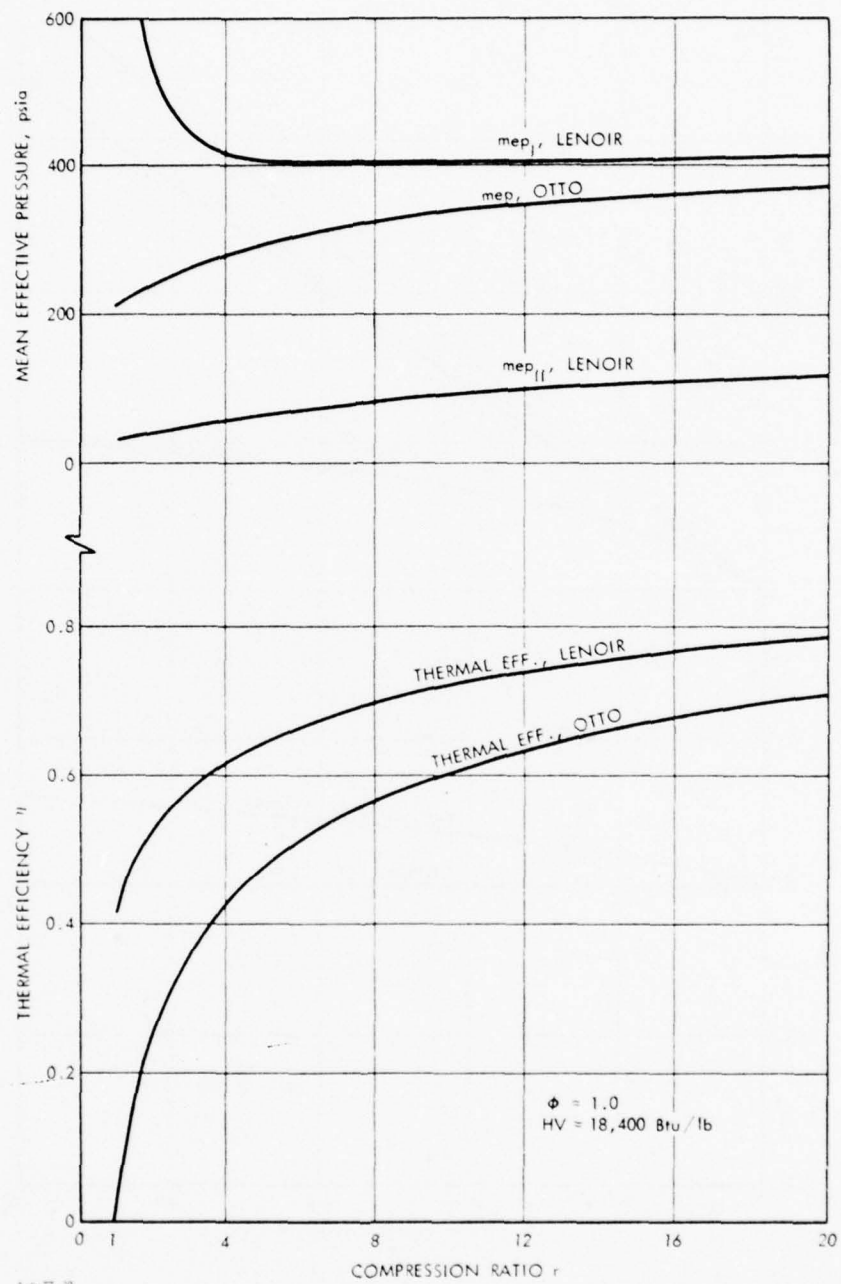


FIGURE C-7. Comparison of Otto and Lenoir cycles, effect of compression ratio.

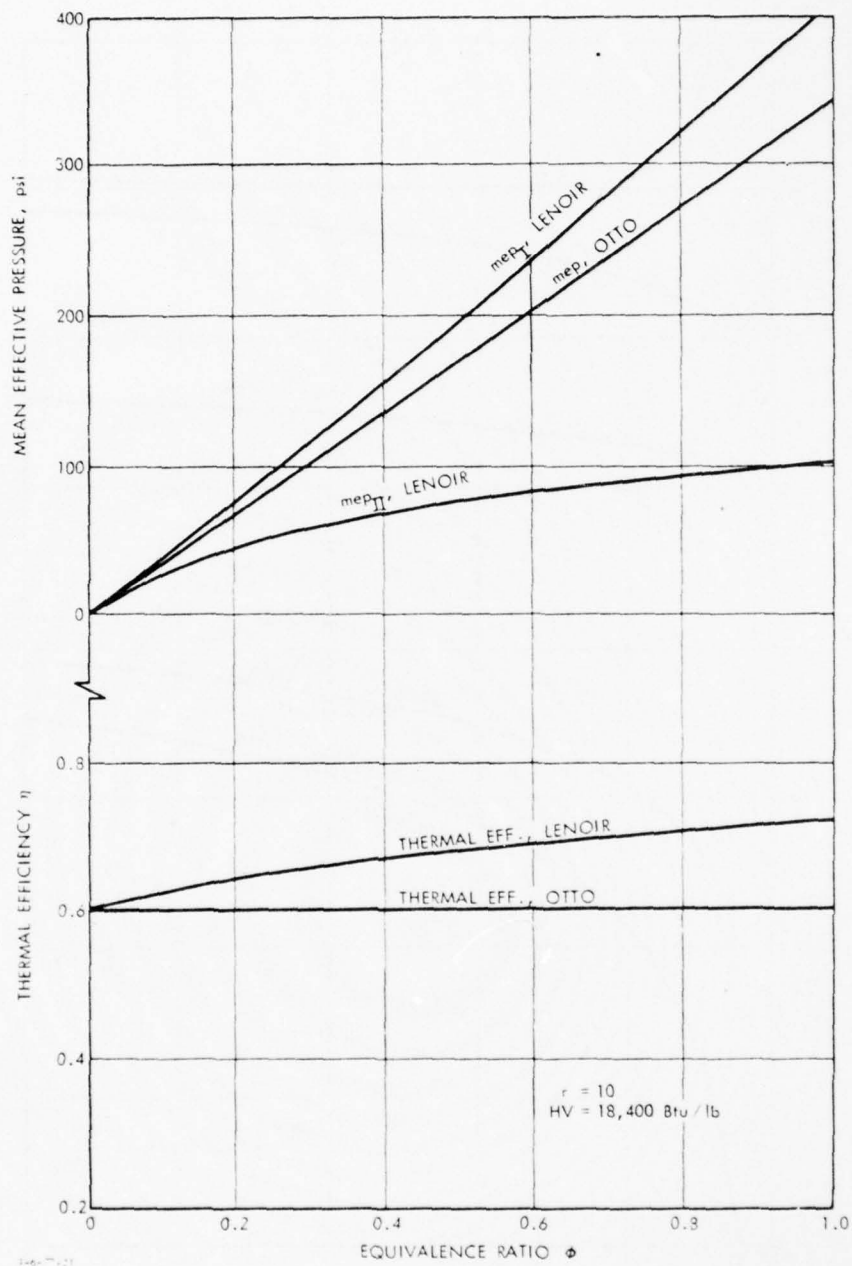


FIGURE C-8. Comparison of Otto and Lenoir cycles, effect of equivalence ratio.

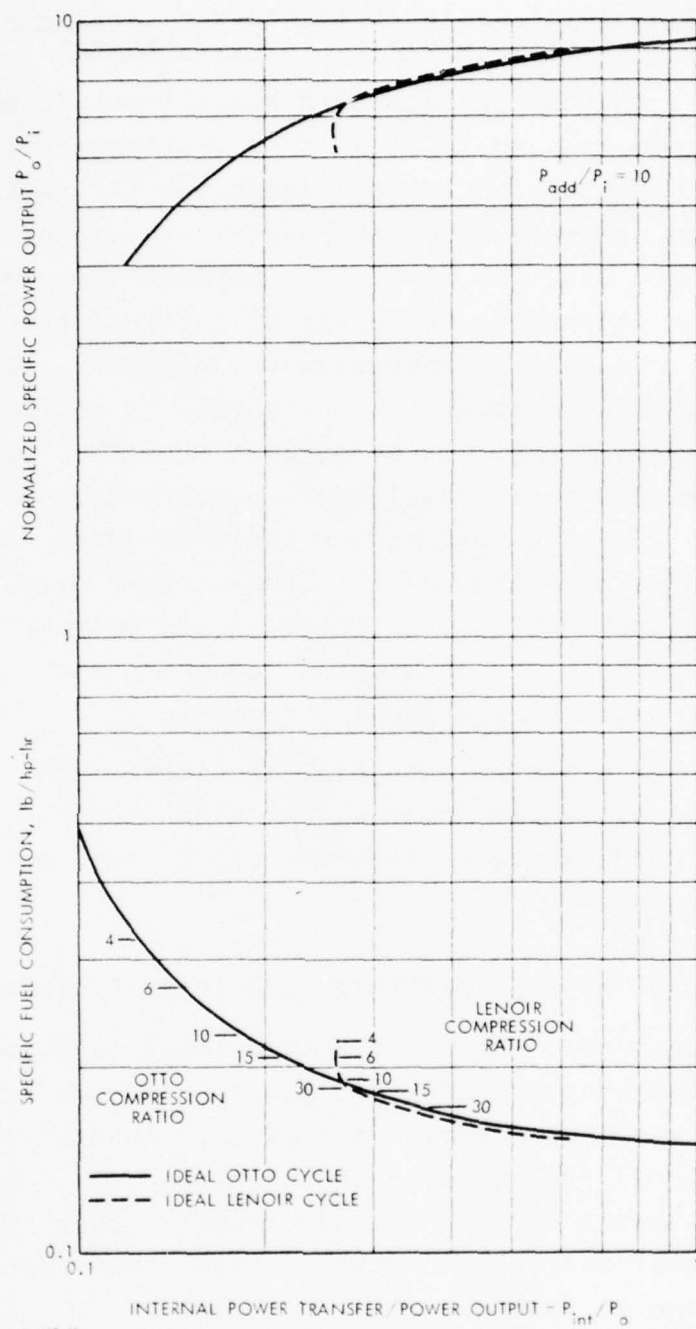


FIGURE C-9. Performance comparison of ideal Lenoir and Otto cycles.

3. Implications of Ideal Cycle Performance With Respect to Further Performance Improvements in Otto Engines

Present Otto engines operate with stoichiometric mixtures ($P_{add}/P_1 \approx 10$), and thus no further increases in specific heat addition can be expected for engines which use air as the working fluid. It can be observed from the performance of any of the ideal cycles (Figs. C-5, C-6, C-9) that further improvements must originate in increasing the ratio of internal power transfer to power output. As will be discussed subsequently, present Otto engines are limited by combustion considerations to compression ratios less than about ten. It is evident from Fig. C-5 that substantial improvements in ideal cycle performance could be achieved if this limiting compression ratio could be increased. The advantages of other ideal cycles (regenerated Otto, Lenoir) evidently lie in their ability to increase the ratio of internal power transfer to power output without requiring the increased pressure ratios needed by the ideal Otto cycle.

Obviously, the ultimate potential for improvement depends not only on ideal cycle performance, but also upon the efficacy with which the internal power transfers can be implemented in real cycles.

B. RELATIONSHIP OF ACTUAL PERFORMANCE TO IDEAL PERFORMANCE

As indicated above, the ideal cycles imply certain limitations on the efficiency and specific power which can be achieved from the Otto cycle and possible variations. Substantial deviations from the ideal cycles occur in actual engines, which cause losses in both thermal efficiency and specific power from those achievable in ideal cycles. In Otto engines, the major sources of such losses are as follows:

1. The working fluid is a mixture of air, fuel vapor, and combustion products at various points in the cycle, rather than a gas with constant specific heats, and

thermodynamic losses occur due to energy retained in internal degrees of freedom of the mixture.

2. The combustion process requires a finite time, and thus the combustion does not occur at constant volume, resulting in a loss of potential power output.
3. Heat is transferred to and from the gas at various points in the cycle.
4. A finite time is required for the "blowdown" process (3-4 in Fig. C-1), resulting in a further loss of potential power output.
5. Friction and valving losses as a result of fluid flow and the relative motion of solid surfaces necessary to implement the cycle.

In addition, the absolute and relative magnitudes of these losses vary with the operating point (fractional power and speed) of a given engine.

The impacts of these losses are analyzed in the following sections. In a general way, the impact of any loss can be viewed conceptually as a loss in potential output power; thus

$$P_o = P_{o,ideal} - \sum_i P_{loss,i} , \quad (C-10)$$

where P_o is the actual power output and $P_{loss,i}$ is the effective power loss associated with mechanism i . Dividing by the heat addition rate, which is the same for both ideal and actual cycles, produces

$$\eta = \eta_{id} - \sum_i \Delta\eta_i , \quad (C-11)$$

where

$$\Delta\eta_i = \frac{P_{loss,i}}{P_{add}} . \quad (C-12)$$

Hence the impact of losses can be expressed in terms of cycle efficiency decrements, and corresponding decrements in specific power. As a final point of terminology, the efficiency which would be obtained in the absence of friction losses is by convention called the indicated efficiency--that which would be deduced from a pressure-volume history of the enclosed mass.

1. Real Gas Losses

The impact of real gas effects--deviations of the working fluid from a gas with constant specific heats--can be displayed by using more refined models of the working fluid. For purposes of comparison, it is convenient to account for the residual fraction of gas left in the cylinder at the conclusion of the exhaust stroke. If the mass residual is included in the analysis, the cycle temperature will be increased due to the mixing of the incoming air with hotter exhaust air. This reduces the cycle mep because the mass charge of the engine is reduced; it has no effect on cycle efficiency. Inclusion of the effect of mass fraction residual will be termed Model 1.

Three more refined models of the working fluid will be examined: Model 2 will use gas tables to determine the properties of air, $c_p = c_p(T)$; Model 3 will use a hydrocarbon fuel, $(CH_2)_n$, with the properties after combustion and during expansion determined using an equilibrium thermochemical program; Model 4 will use the properties of the mixture of fuel vapor and air during compression, and equilibrium combustion properties after combustion, and is called the fuel-air cycle. Results using these various models are compared in Table C-1 for the following conditions:

Compression ratio $r = 9.0$

Fuel heating value $HV = 18,400 \text{ Btu/lb}$

Equivalence ratio $\phi = 1.1$

Atmospheric conditions $T_1 = 520^\circ R$, $P_1 = 1 \text{ atmosphere}$.

TABLE C-1. COMPARISON OF WORKING-FLUID MODELS FOR THERMAL EFFICIENCY, MEAN EFFECTIVE PRESSURE, AND SPECIFIC FUEL CONSUMPTION

<u>Model</u>	<u>Thermal Efficiency</u>	<u>mep (psi)</u>	<u>sfc (lb/hp-hr)</u>
Ideal ($\gamma = 1.4$)	0.58	340	0.26
1	0.58	300	0.26
2	0.50	250	0.30
3	0.37	190	0.37
4	0.42	230	0.33

Model 4 thus represents a limitation to the specific fuel consumption that can be obtained with an Otto engine operating with a premixed (carbureted) hydrocarbon fuel; Model 3, as compared to Model 4, serves to indicate the influence of mixture properties during the compression process. It is evident that real-gas effects have a large impact on the performance of Otto engines. As might be anticipated, these effects are a strong function of fuel-air ratio, as indicated in Fig. C-10 (from Ref. C-1). In general, operating leaner increases thermal efficiency (closer to the ideal cycle). A crude but useful approximation to the efficiency decrement due to real gas effects can be obtained by an empirical correlation with fuel-air cycle results presented in Ref. C-2:

$$\begin{aligned} \Delta\eta_{rg} &= 0.25(1.5\phi - 0.5)\eta_{id} & 0.8 \lesssim \phi \lesssim 1.1 \\ \Delta\eta_{rg} &= 0.21\phi\eta_{id} & \phi \lesssim 0.8 \end{aligned} \quad (C-13)$$

Although operation at decreased equivalence ratios increases efficiency, it also decreases specific power output, in accordance with Eqs. C-4 and C-6, as has been observed by others (Refs. C-3, C-4).

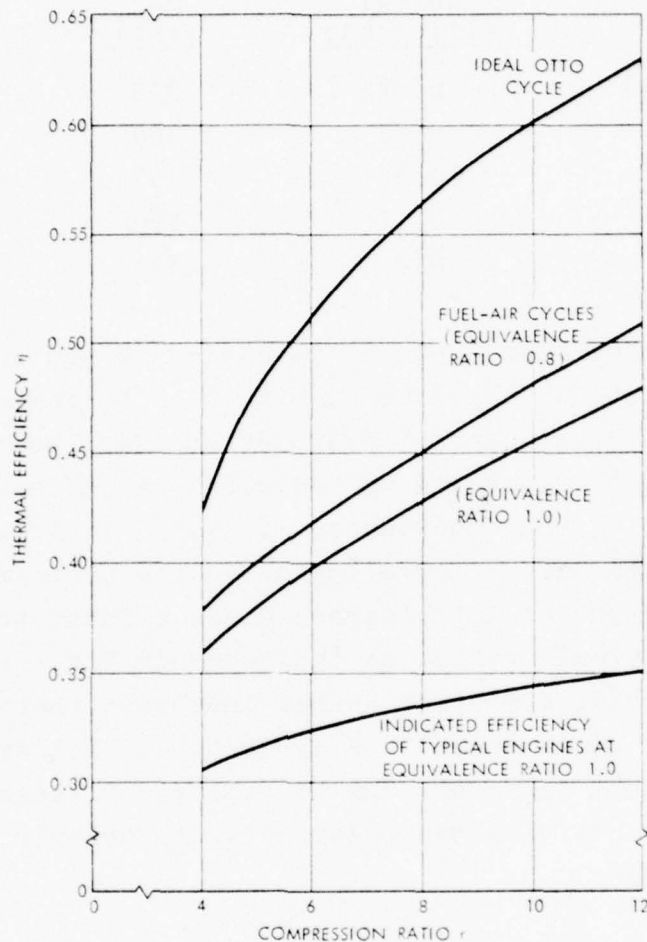


FIGURE C-10. Indicated thermal efficiency of ideal Otto cycle and of fuel-air Otto cycle at equivalence ratios 0.8 and 1.0; indicated efficiency of typical Otto engines at equivalence ratio 1.0. (Source: Ref. C-1)

2. Combustion Losses

The theoretical Otto cycle assumes constant-volume combustion. In the actual engine, the flame propagates through the fuel-air mixture at a finite speed, so that ignition must occur before the piston reaches the point of minimum volume, top dead center (TDC). Further, as the flame propagates through the mixture, the temperature of the unburnt portion increases. Under certain conditions, the unburnt portion may autoignite and produce knock. To avoid possible harm to the engine, knock must be avoided. This places a restriction on the cylinder size for a reciprocating homogeneous-charge Otto engine, since the entire charge must be burned with the flame starting from one point source (or, at most, a very limited number). It also places a restriction on engine compression ratio, since too high a temperature prior to combustion can lead to knock. Current automobile engines, operating on 90 RON* fuel, are limited to compression ratios of 8 to 8.5. Lead fuels, with RONs of 100 or more, could be used up to compression ratios of 10. The significance of compression ratio on specific fuel consumption or thermal efficiency can be seen in Fig. C-10.

To estimate the loss of efficiency due to nonconstant-volume combustion, assume a p-V diagram as shown in Fig. C-11 with

$$\frac{T_a}{T_i} = \left(\frac{V_i}{V_2} \right)^m = r_i^m = \left(\frac{V_e}{V_2} \right)^m = \frac{T_e}{T_a} ,$$

where m is an exponent to be determined. The work from i to a is:

*RON denotes Research Octane Number, with higher numbers indicating longer time delays before the onset of autoignition.

$$W_{ia} = \int p dV = RT_i \int_i^a \left(\frac{V_i}{V} \right)^m \frac{dV}{V} = RT_i \int_i^a \left(\frac{V_i}{V} \right)^{m+1} \frac{dV}{V_i}$$

$$W_{ia} = \frac{RT_i}{m} \left[\left(\frac{V_i}{V_a} \right)^m - 1 \right] = - \frac{RT_i}{m} (r_i^m - 1)$$

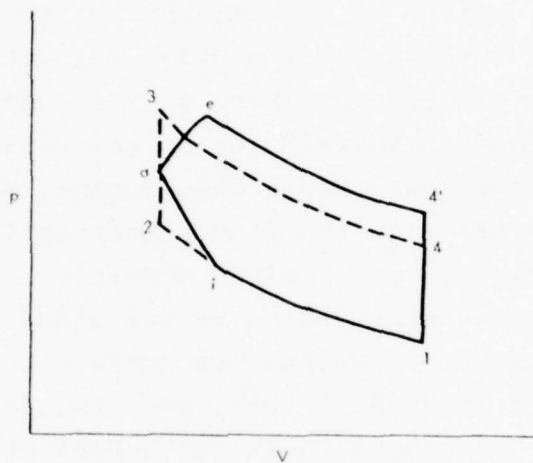


FIGURE C-11. Effect of combustion time on work output of an Otto engine.

Similarly, for the work term w_{ae} , we have

$$w_{ae} = RT_a \int_a^e \left(\frac{V}{V_2} \right)^m \frac{dV}{V} = \frac{RT_a}{m} (r_i^m - 1)$$

Since $T_a = T_i r_i^m$ and $T_e = T_a r_i^m$, we have

$$w_{ie} = w_{ia} + w_{ae} = - \frac{RT_i}{m} (r_i^m - 1) + \frac{RT_i}{m} r_i^m (r_i^m - 1)$$

or

$$w_{ie} = (RT_i/m)(r_i^m - 1)^2 .$$

The first law, therefore, becomes

$$Q_s = c_v T_i (r_i^{2m} - 1) + \frac{RT_i}{m} (r_i^m - 1)^2$$

or

$$\frac{Q_s}{c_v T_i} = (r_i^{2m} - 1) + \frac{k-1}{m} (r_i^m - 1)^2 , \quad (C-14)$$

where Q_s is the combustion heat release per unit mass of gas. If the compression ratio r and the energy released Q_s are known, Eq. C-14 can be used to determine the value of m as a function of r_i . The variation in the exponent m with the ignition compression ratio r_i is shown in the following table for $r = 9$, $\phi = 1.0$, and $HV = 18,400$ Btu/lb:

<u>Ignition Compression Ratio r_i</u>	<u>Combustion Exponent m</u>
1.0	∞
1.5	2.46
2.0	1.48
3.0	0.97
∞	0

The sum of the work from e to $4'$ and from 1 to i are, for isentropic processes with a compression ratio of r/r_i :

$$\begin{aligned}
w_{e4'} - w_{1i} &= c_v T_e \left[1 - \left(\frac{r_i}{r} \right)^{\gamma-1} \right] - c_v T_1 \left(\frac{r}{r_i} \right)^{\gamma-1} - 1 \\
&= c_v (T_e - T_1) \left[1 - \left(\frac{r_i}{r} \right)^{\gamma-1} \right].
\end{aligned}$$

Using the First Law, we obtain

$$c_v (T_e - T_i) = Q_s - w_{ie} ,$$

and the net cycle work is

$$w_c = Q_s [1 - (r_i/r)^{\gamma-1}] + (RT_1/m)(r_i^m - 1)^2 .$$

The net work for the ideal Otto cycle is

$$w_i = Q_s \left(1 - \frac{1}{r^{\gamma-1}} \right) .$$

Therefore, the net fractional work loss for the approximate solution for the combustion process is

$$\frac{\Delta w}{w_i} = 1 - \frac{w_c}{w_i} = 1 - \frac{\left[1 - \left(\frac{r_i}{r} \right)^{\gamma-1} \right] + \frac{(r_i^m - 1)^2}{m} \frac{RT_1}{Q_s}}{1 - \left(\frac{1}{r} \right)^{\gamma-1}} . \quad (C-15)$$

Fractional work loss due to finite combustion depends on compression ratio and combustion duration, as measured in crankangle degrees. For a sinusoidal piston motion, $r_i = 1 + \frac{r-1}{2} (1 - \cos \frac{\theta_c}{2})$, where θ_c = combustion duration. Results are shown in Fig. C-12. It can be seen that compression

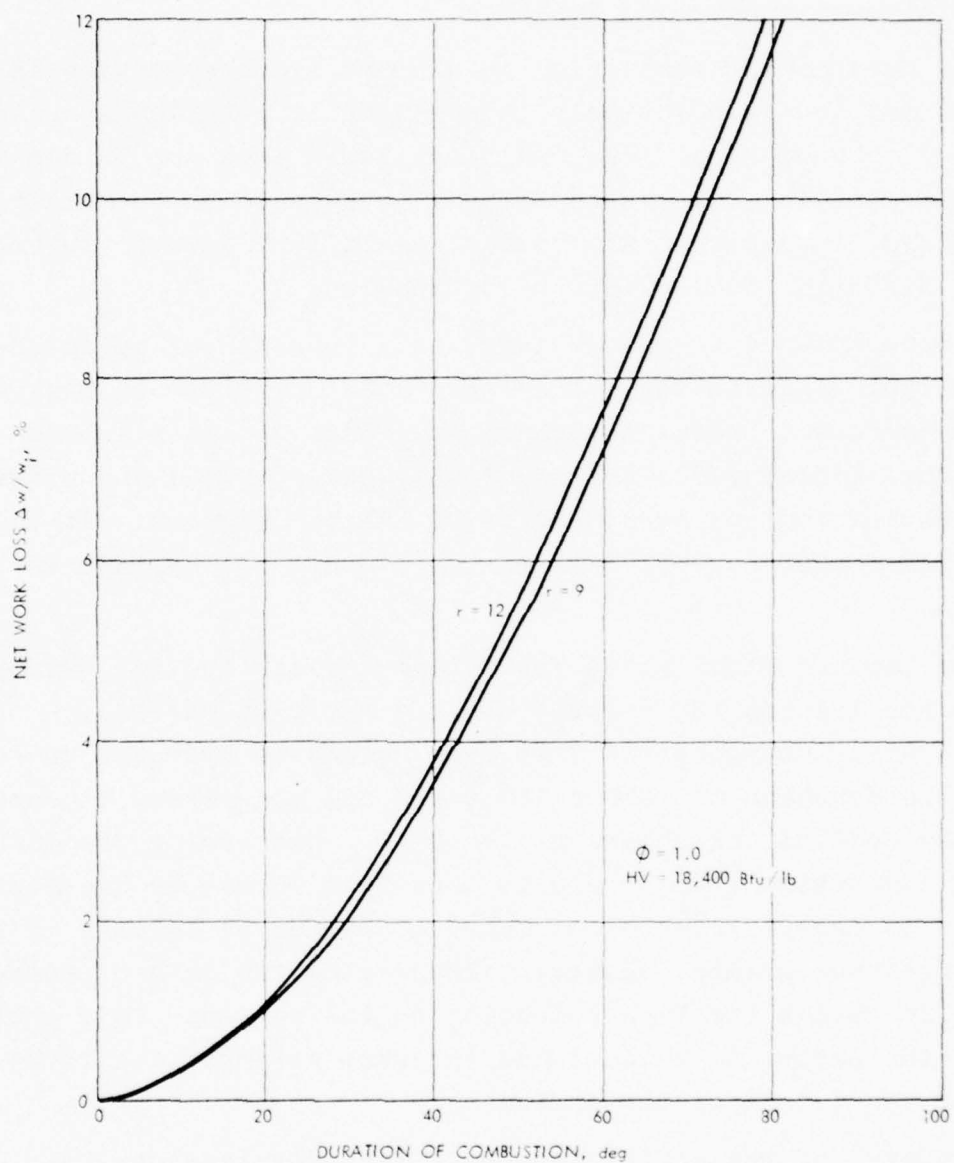


FIGURE C-12. Net work loss for finite combustion process.

ratio has only a small effect on work loss, but that work loss is sensitive to combustion duration.

The duration of combustion in a spark ignition engine is about 50 deg and is relatively independent of rotational speed (Ref. C-2). From Fig. C-12, fractional work loss for 50 deg is 6%. This loss in energy transfer can be reduced by increasing flame speed; increased flame speeds result from greater turbulence or from different fuel-oxidizer combinations.

The turbulence in the cylinder is a function of cylinder-head design. A great deal of cylinder-head development has been done to improve combustion turbulence. This includes I-head rather than L-head valve arrangements, hemispherical and wedge-shaped combustion chambers, and swirl chamber pistons. It is not believed that a great deal of improvement can be made in this area.

The laminar flame speed for octane and air and for hydrogen and air are 1.1 fps (35 cm/sec) and 6.4 fps (195 cm/sec), respectively. Changing the fuel from octane to hydrogen could reduce the duration of combustion to 10 deg and reduce the net work loss to 0.5%, as shown in Fig. C-12. Decreasing the duration of combustion from 50 deg to less than 10 deg by increasing the rate of energy release can improve thermal efficiency by 2 or 3 percentage points. However, increasing the rate of energy release increases the impact loading on the engine. This would require the engine to be designed for more strength, which would increase the weight of the engine.

A useful approximation for the efficiency loss due to combustion in current Otto engines is taken to be

$$\Delta\eta_c = 0.07(\eta_{id} - \Delta\eta_{rg}) \quad (C-16)$$

which, from Fig. C-12, corresponds to a combustion duration slightly greater than 50 deg. It is to be noted that no effect

of equivalence ratio is included here, and hence it can be expected that at low equivalence ratios efficiency losses due to combustion time will be greater than indicated by Eq. C-16.

3. Heat Transfer Losses

The heat transfer to and from the working fluid that occurs during the compression and expansion processes has a significant effect on the thermal efficiency of the Otto engine and is the subject of analysis here. This heat transfer is to be distinguished from that which occurs during the exhaust process, which is much larger in magnitude but which has no impact on thermal efficiency.

It is assumed that the piston motion is sinusoidal and that the surface temperature T_s of the cylinder is constant. The amount of heat transfer, Q , from the cylinder during each process will be represented by $Q = \bar{h} \bar{A} (\bar{T} - T_s)t$, where the barred terms are the average values for the stroke.

The usual form of the expression for the turbulent heat transfer coefficient applied to a cylinder is

$$\bar{h} = K R_e^{-0.8} Pr^{1/3} \bar{k}/D = K \bar{k} Pr^{1/3} (2SND\bar{\rho}/\bar{\mu})^{0.8}/D ,$$

where \bar{h} = heat transfer coefficient

K = an empirical constant

Re = cylinder Reynolds number

S = piston stroke

N = crankshaft rotational speed

D = cylinder diameter (bore)

ρ = gas density

μ = gas viscosity

Pr = Prandtl number

k = thermal conductivity of gas.

This permits the heat transfer to be written as

$$Q = K \pi Pr^{1/3} k_o \left(\frac{\rho_o D}{\mu_o} \right)^{0.8} \frac{S^{1.8}}{N^{0.2}} 2^\alpha \left[T_o a^{i(k-1)} - T_s \right],$$

where α and i are

$$\alpha = -0.4 + 0.2(\gamma - 1), \quad i = 1 \quad \text{for compression}$$

and

$$\alpha = -2 - 0.2(\gamma - 1), \quad i = -1 \quad \text{for expansion,}$$

and the reference state (subscript o) for compression and expansion processes is the initial state in either case. The different values for α and i result from the fact that temperature increases during compression and decreases during expansion.

Selecting the following numerical data as representative of Otto engines:

$$r = 10, \quad D = 3.75", \quad N = 3000 \text{ rpm}$$

$$T_s = 710^\circ R, \quad S = 3.25"$$

Process	T_o (°R)	p_o (atm)	ρ_o (lb/ft ³)	μ_o (lb/ft-sec)	k_o $\left(\frac{\text{BTU}}{\text{hrft}^\circ R} \right)$	Pr	c_{vo}	γ
Compression	600	1	0.0661	1.35×10^{-5}	0.0168	0.695	0.172	1.30
Expansion	4500	60	0.529	5.15×10^{-5}	0.0903	0.695	0.236	1.25

and selecting the value of $K = 0.061$, in agreement with data available from current engines (Ref. C-5), one finds that the resultant expressions for heat transfer per unit mass are

$$Q_c = -0.062 (750 - T_s)/N^{0.2} \text{ Btu/lb} = 0.5 \text{ Btu/lb at } N = 3000$$

$$Q_e = -0.192 (3800 - T_s)/N^{0.2} \text{ Btu/lb} = 120 \text{ Btu/lb at } N = 3000$$

It is evident that the heat transfer during the expansion process is much more significant than that during the compression process for current Otto engines.

To determine the impact of this heat transfer on engine performance, the compression and expansion processes are approximated by general polytropic processes:

$$pv^m = \text{constant}$$

The First Law for the compression process is

$$Q_c = u_2 - u_1 + w_c = c_v(T_2 - T_1) + w_c$$

For a general polytropic process, the temperature ratio and the work can be expressed as

$$\frac{T_2}{T_1} = r^{m-1}$$

$$w = \int p dv = \frac{p_2 v_2 - p_1 v_1}{1 - m} = - \frac{RT_1(r^{m-1} - 1)}{m - 1}$$

Substituting the above expressions into the First Law, one has for compression:

$$\begin{aligned} Q_c &= c_v T_1 (r^{m_c-1} - 1) - RT_1 (r^{m_c-1} - 1) / (m_c - 1) \\ &= c_v T_1 (r^{m_c-1} - 1) [1 - (\gamma_c - 1) / (m_c - 1)] \end{aligned} \quad (C-17)$$

or

$$m_c = 1 + \frac{\gamma_c - 1}{1 - E_c}, \quad (C-18)$$

where

$$E_c = \frac{Q_c}{[c_v T_1 (r^{m-1} - 1)]} \quad (C-19)$$

Similar relationships for the expansion process can be developed:

$$w_e = RT_3 \left(1 - \frac{1}{r^{m_e-1}} \right) / (m_e - 1)$$

$$m_e = 1 + \frac{\gamma_e - 1}{1 + E_e} \quad (C-20)$$

$$E_e = \frac{Q_e}{c_v T_3 \left(1 - \frac{1}{r^{m-1}} \right)} \quad (C-21)$$

It can be seen from Eqs. C-18 and C-21 that when $E = 0$ (adiabatic process), $m = \gamma$ for both processes. It can also be seen from Eq. C-18 that when E_c is positive (heat flow into the system), $m_c > \gamma_c$ and the work of compression is greater than the isentropic value. Similarly, from Eq. C-21 it can be seen that when E_e is negative (heat flow out of the system), $m_e < \gamma_e$ and the work of expansion is less than the isentropic value. The sign of the heat flow is controlled by the magnitude of the coolant or surface temperature T_s .

The loss in net work Δw , compared to the net isentropic work of the cycle w_1 , can be determined from the following relation:

$$\frac{\Delta w}{w_i} = 1 - \frac{w_e - w_c}{w_{e_i} - w_{c_i}}, \quad (C-22)$$

where the isentropic values are obtained by substituting $\gamma = m$ in the equations for work.

The variation in m_c and m_e as a function of engine speed n and coolant temperature T_s is presented in Fig. C-13. The percentage loss in net work as a function of the same two variables is presented in Fig. C-14. Both figures are for a constant compression ratio of $r = 9$. It can be seen from Fig. C-14 that for currently used coolant temperatures of 710°R (radiator pressure of 30 psia) the loss in net work is 10% at 4000 rpm. By raising the coolant temperature T_s , one would increase the work of compression and increase the work of expansion. The net effect is a reduction in net work loss. For a coolant temperature $T_s = 2000^\circ\text{R}$, the percentage loss in net work is 7%.*

Based on this analysis, a reasonable approximation to the efficiency loss associated with heat transfer in current Otto engines is

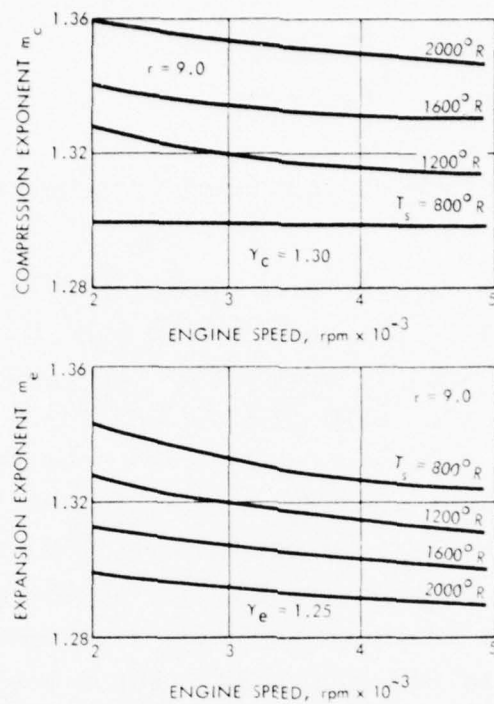
$$\Delta\eta_{\text{HX}} = 0.11(\eta_{\text{id}} - \Delta\eta_{\text{rg}}) \quad (C-23)$$

with somewhat higher losses at part-load conditions.

4. Exhaust Blowdown Losses

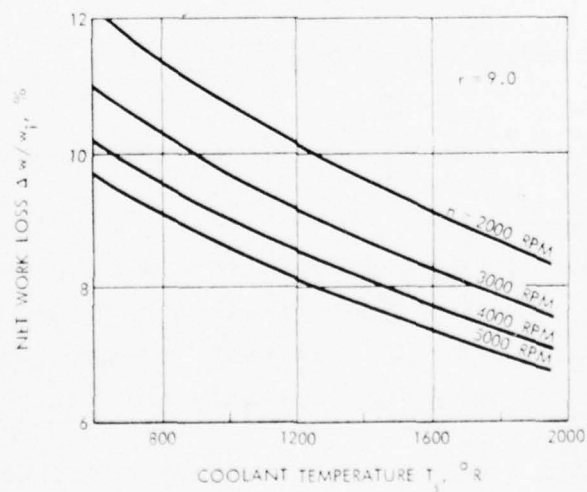
A sketch of the blowdown process for an Otto engine is shown in Fig. C-15. In the theoretical Otto cycle, it is assumed that exhaust blowdown occurs at constant volume. This requires that the exhaust valve be instantaneously and fully opened at 4.

*The present analysis assumes that the peak cycle temperature is unaffected by heat transfer during the compression process. This is an adequate assumption for current Otto engines but leads to an underestimate of the gain associated with higher coolant temperatures.



9 A-77-26

FIGURE C-13. Compression and expansion exponents.



9 A-77-27

FIGURE C-14. Net work loss due to heat transfer.

The gases continue to expand inside the cylinder along the isentrope 4 to 5. The mass fraction exhausted from the cylinder during this process is $f = 1 - v_1/v_5$, or typically about 75%. The remaining fraction of the exhaust gas is exhausted on the stroke from 1 to 6. Since it is impossible to open the exhaust valve instantaneously in a real engine, the valve must start to open before the maximum volume is reached (bottom dead center, BDC), as shown in Fig. C-15. This early opening modifies the p-V diagram, and the area b4l represents lost work.

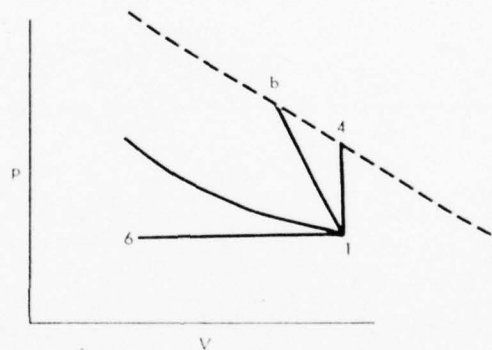


FIGURE C-15. Exhaust blowdown process.

In this approximate solution for the blowdown process, it is assumed (1) that the pressure varies linearly with volume from b to 1, (2) that the pressure p_1 is atmospheric pressure, and (3) that the piston motion is sinusoidal. These assumptions can be expressed functionally as

$$p = p_1 + \frac{p_b - p_1}{v_b - v_1} (v - v_1)$$

and

$$r_b = \frac{v_1}{v_b} = \frac{r}{1 + \frac{r-1}{2} [1 - \cos(180 - \theta_b)]} ,$$

where r_b is the blowdown compression ratio and θ_b is the valve opening angle in degrees of crankangle before bottom dead center.

The net work loss Δw during blowdown is

$$\Delta w = w_{b4} - w_{b1} ,$$

where

$$w_{b4} = \frac{p_b v_b - p_4 v_4}{\gamma - 1} = \frac{p_1 v_1 \left(\frac{p_4}{p_1} \right) (r_b^{\gamma-1} - 1)}{\gamma - 1}$$

and

$$w_{b1} = \frac{p_1 + p_b}{2} (v_1 - v_b) = \frac{p_1 v_1}{2} \left(1 + \frac{p_4}{p_1} r_b^{\gamma} \right) \left(\frac{r_b - 1}{r_b} \right) . \quad (C-24)$$

For an ideal Otto cycle, the pressure ratio p_4/p_1 and the isentropic work w_i are

$$\frac{p_4}{p_1} = \left(1 + \frac{\Delta T_s}{T_1 r^{\gamma-1}} \right)$$

$$w_i = Q_s \left(1 - \frac{1}{r^{\gamma-1}} \right) = c_v \Delta T_s \left(1 - \frac{1}{r^{\gamma-1}} \right) .$$

The percent loss in net work is, therefore,

$$\frac{\Delta w}{w_i} = \frac{w_{b4} - w_{b1}}{w_i} = \frac{\frac{p_4}{p_1} \left(r_b^{\gamma-1} - 1 \right) - \left(\frac{\gamma-1}{2} \right) \left(1 + \frac{p_4}{p_1} r_b^{\gamma} \right) \left(\frac{r_b^{-1}}{r_b} \right)}{\left(\frac{\Delta T_s}{T_1} \right) \left(1 - \frac{1}{r^{\gamma-1}} \right)} \quad (C-25)$$

The net work loss due to finite blowdown is given in Eq. C-25 as a function of crankangle BBDC and compression ratio r . It can be verified that the effect of compression ratio r is not great and that the net work loss is not large. For a typical valve opening angle of 45 deg BBDC, the percentage loss in net work is 2%, and a reasonable general approximation to the efficiency loss is

$$\Delta \eta_{bd} = 0.02(\eta_{id} - \eta_{rg}) \quad (C-26)$$

5. Friction Losses

In addition to the losses associated with the individual Otto reciprocating engine processes, there is a loss of available engine power output due to friction. Power is required to overcome mechanical friction of the bearings, valve train, crankshaft, piston and rings, cams, etc., as well as fluid friction as the air flows into the engine across the valves. These losses are usually represented by

$$bhp = ihp - fhp \quad ,$$

where bhp = brake horsepower

ihp = indicated horsepower

fhp = friction horsepower.

Friction horsepower increases at roughly the square of engine speed (Fig. C-16) for a reciprocating engine; it causes the maximum brake horsepower for a reciprocating Otto engine to peak at 4000-5000 rpm. The mechanical efficiency, defined as

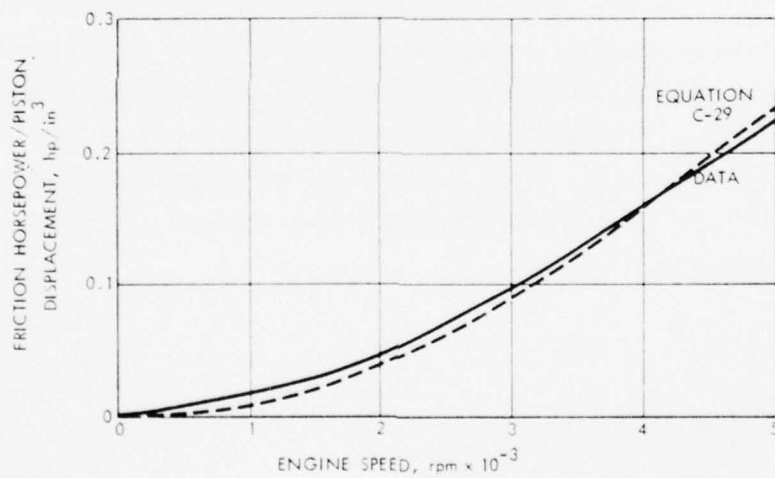
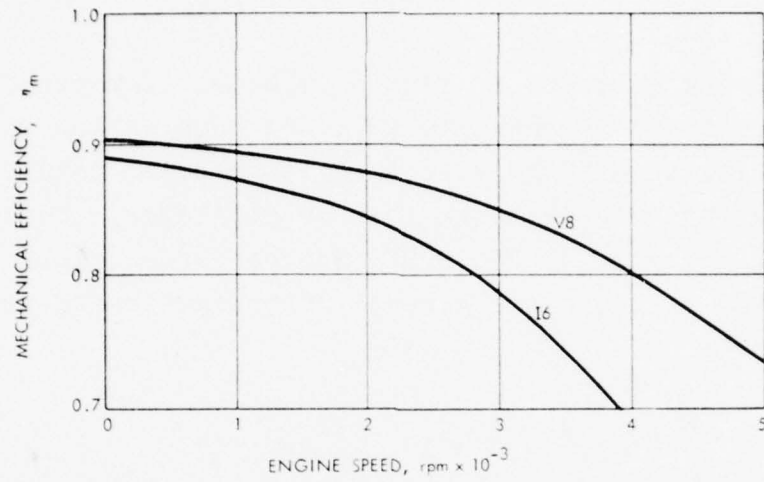


FIGURE C-16. Typical frictional losses in Otto engines.

$$\eta_m = \frac{bhp}{ihp} ,$$

generally lies between 85% and 90% at full load.

The frictional losses can also be characterized by the friction-mean-effective pressure (fmep), defined analogously to brake-mean-effective pressure, and the frictional power dissipation is given by

$$fhp = \frac{NV_D}{2} (fmep) , \quad (C-27)$$

where N is the rotational speed and V_D is the engine displacement volume. It has been empirically observed (Ref. C-2) that the fmep depends linearly on piston speed, defined as

$$V_p = \frac{2S}{N} , \quad (C-28)$$

where S is the piston stroke, and that the fmep appears to be relatively insensitive to other variables. Equations C-27 and C-28 can be combined to yield

$$\frac{fhp}{V_D} = \frac{1}{a_r} \left(\frac{fmep}{V_p} \right) \left(\frac{V_D}{N_{cyl}} \right)^{1/3} N^2 , \quad (C-29)$$

where a_r = cylinder form factor, $\pi D^2/4(V_D/N_{cyl})^{2/3}$
 N_{cyl} = number of cylinders

and $fmep/V_p \approx 0.013$ psi/ft/min.

Equation C-29 is shown in Fig. C-16 for a typical cylinder of 40-in.³ displacement and a form factor of 0.92; it is apparent that the approximation tends to underestimate the frictional horsepower at lower speeds.

Noting that the rate of energy addition can be written as

$$P_{add} = \rho_1 e_v \phi F_s (HV) \frac{NV_D}{2} ,$$

where F_s is the stoichiometric fuel-air ratio and e_v is the volumetric efficiency (the ratio of the mass inducted into the cylinder to that which would occupy the cylinder at gas inlet conditions), the efficiency decrement associated with friction can be written as

$$\Delta\eta_f = \frac{2N}{\rho_1 e_v \phi F_s (HV) a_r} \left(\frac{f_{mep}}{V_p} \right) \left(\frac{V_D}{N_{cyl}} \right)^{1/3} ,$$

which, for best performance conditions of current Otto engines, is approximately 0.06. Inasmuch as the quantity $2N/a_r (V_D/N_{cyl})^{1/3}$ is the piston speed, which is currently about 3000 fpm at maximum power, this equation can be written as

$$\Delta\eta_f = \frac{0.079}{e_v \phi} \left(\frac{\rho_o}{\rho_i} \right) \left(\frac{N}{N_{max}} \right) , \quad (C-30)$$

where N_{max} is the rotational speed corresponding to maximum power.

6. Collective Impact of Losses on Performance

The total impact of the previously discussed losses on the specific fuel consumption and specific power of Otto engines can be displayed as in Fig. C-17.* Current Otto engines, as will be discussed subsequently, operate with pressure ratios in

*Figure C-16 is obtained from Eqs. C-3, C-5, and C-6 for ideal performance, and from Eqs. C-13, C-16, C-23, C-26, and C-30 for the various losses. Any errors in the latter equations or in Fig. C-16 are attributable to one of the principal authors (DMD).

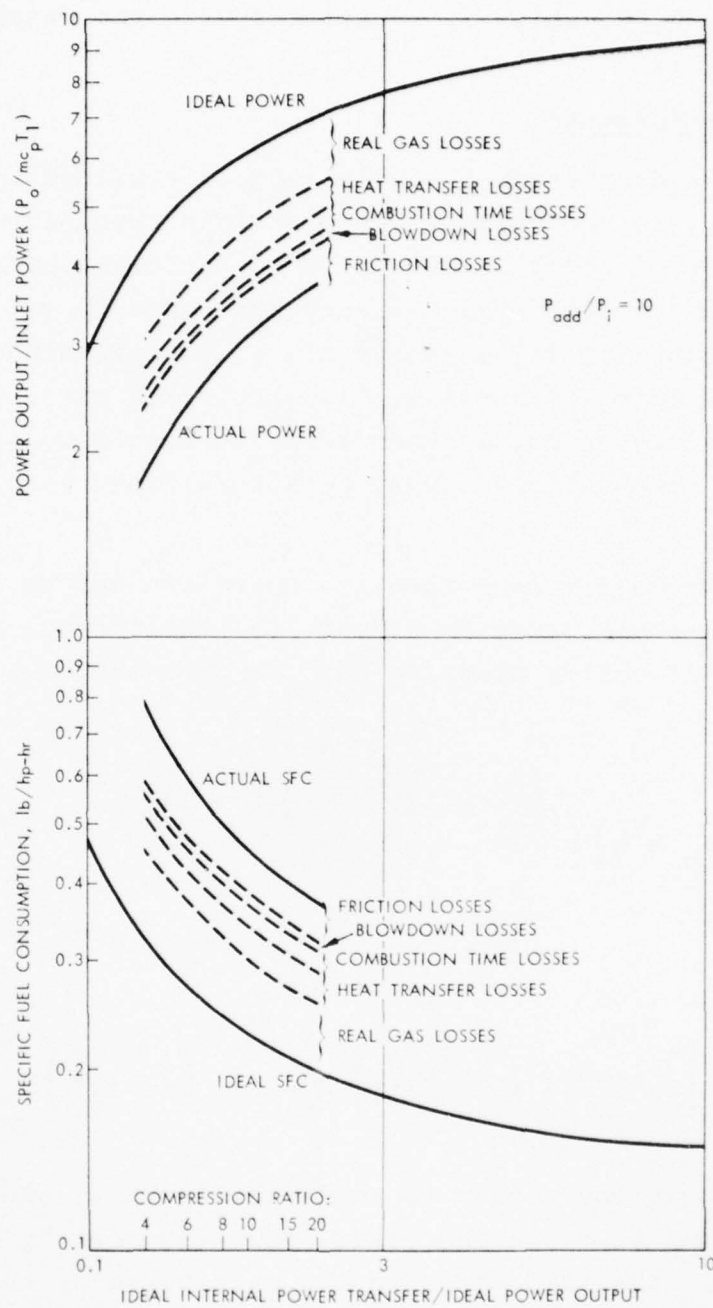


FIGURE C-17. Impact of losses on best performance of Otto engines.

the vicinity of 8-10 and achieve best specific fuel consumptions of approximately 0.49, which is consistent with the results shown in Fig. C-17.

7. Part-Load Performance

The previous discussion has been largely confined to full-load conditions. In conventional Otto engines, reducing power output at a constant speed is accomplished basically by reducing the inlet pressure to the engine--a process commonly called throttling. Throttling is necessary since, to maintain adequate combustion, the equivalence ratio of a carbureted mixture cannot be reduced below 0.8 or so, and hence any further reduction in power output at constant speed must be accomplished by reducing the air flow rate.

The performance for part-throttle operation can be determined from the part-throttle cycle in Fig. C-18. The thermal efficiency η_p and the mean effective pressure mep_p at part throttle are

$$\eta_p = \eta_o - \frac{\left(\frac{p_a}{p_1} - 1\right)\left(\frac{r-1}{r}\right)(\gamma-1)}{(\Delta T_s \phi_p / T_1)}$$

and

$$mep_p = \left[\eta_o \frac{r}{r-1} \frac{\Delta T_s \phi_p p_a}{T_1 (\gamma-1)} \right] \frac{p_1}{p_a} - p_a \left(1 - \frac{p_1}{p_a} \right).$$

Both of these equations reduce to the full-throttle condition when $p_1/p_a = 1$ and $\phi_p = \phi$. The first bracketed term in the above equation is the full-throttle mep multiplied by the ratio of equivalence ratios ϕ_p/ϕ . By defining the ratio of part-throttle load to full-throttle load

$$\psi = mep_p / mep \quad ,$$

the equation for part-throttle pressure ratio p_1/p_a becomes

$$\frac{p_1}{p_a} = \frac{\psi + p_a/\text{mep}}{\phi_p/\phi + p_a/\text{mep}}$$

and the part-throttle thermal efficiency is

$$\eta_p = \eta_o \left[1 - \frac{\phi_p/\phi \left(\frac{\phi_p}{\phi} - 4 \right)}{\psi(\text{mep}/p_a) + 1} \right].$$

The above equation shows that as the load of an Otto engine is decreased, the thermal efficiency also decreases and the specific fuel consumption ($1/\eta_o$) increases. For example, for an ideal cycle with $r = 10$, $\psi = 0.25$, and $\phi_p/\phi = 1$, one obtains $\text{sfc}_p/\text{sfc} = 1.123$.

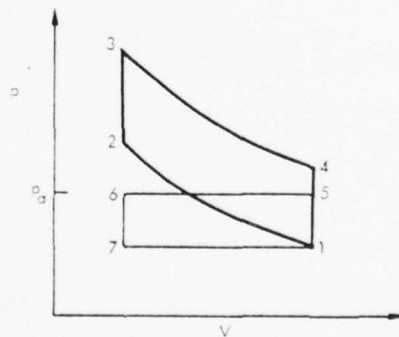


FIGURE C-18. Part-throttle operation.

The efficiency decrement due to throttling can be written in terms of power rather than mep by noting that

$$\Delta\eta_{th} = \frac{\text{work dissipated}}{\text{heat added}} = \frac{p_a - p_l}{\rho_a e_v \phi F_s (HV)} ,$$

which, for atmospheric ambient conditions and a typical hydrocarbon fuel, can be written as

$$\Delta\eta_{th} = 0.03 \left(\frac{\rho_a}{\rho_l} - 1 \right) \frac{1}{e_{vp} \phi_p} . \quad (C-31)$$

Since the power output is proportional to

$$P \sim \rho e_v N \phi \eta ,$$

then

$$\frac{\rho_l}{\rho_a} = \left(\frac{P_m}{P_p} \right) \left(\frac{e_{vp}}{e_{vm}} \right) \left(\frac{N_p}{N_m} \right) \left(\frac{\phi_p}{\phi_m} \right) \left(\frac{\eta_p}{\eta_m} \right) , \quad (C-32)$$

where the subscripts m and p refer to maximum-power and part-power conditions, respectively.

The throttling losses and other losses combine to produce a performance map of the form shown in Fig. C-19. The point of minimum fuel consumption (approximately full load and 40% speed) is determined largely by a balance between decreased friction losses (Eq. C-30) and increased heat transfer losses (Fig. C-14) as speed is reduced at constant load. As load is reduced at constant speed, both the throttling losses and friction losses increase, while real gas losses (Eq. C-13) decrease to the extent that the equivalence ratio can be decreased.

For the purpose of representing the part-load specific fuel consumption of an Otto engine by a single value, a point corresponding to 25% of maximum power and approximately 2/3 maximum

AD-A070 528

INSTITUTE FOR DEFENSE ANALYSES ARLINGTON VA SCIENCE A--ETC F/G 21/7
TECHNOLOGY ASSESSMENT OF ADVANCED PROPULSION SYSTEMS FOR SOME C--ETC(U)
SEP 78 F R RIDDELL, D M DIX DAHC15-73-C-0200

UNCLASSIFIED

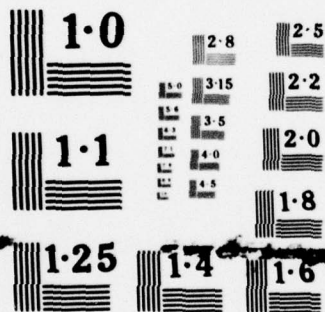
IDA-P-1278-VOL-2

IDA/HQ-77-19843

NL

2 of 4
AD
A070528





NATIONAL BUREAU OF STANDARDS
MICROCOPY RESOLUTION TEST CHART

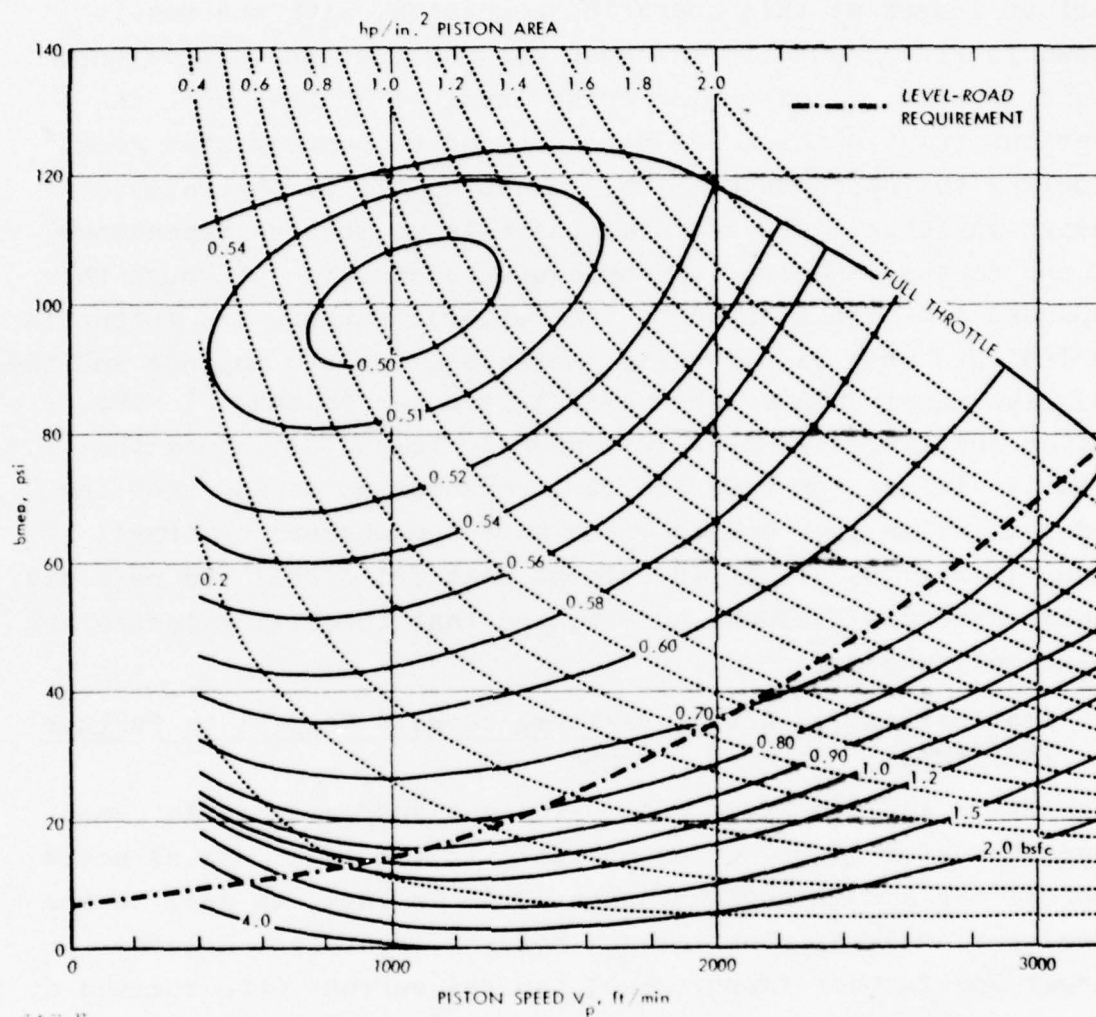


FIGURE C-19. Representative performance map of an Otto engine (from Ref. C-2).

speed is selected. From Fig. C-18, this corresponds to a point where the torque (which is proportional to bmep) being developed is about 25% of the maximum torque that can be developed at the same speed, and thus provides a reasonable acceleration capability. The previous relationships can be used to estimate the various losses at this operating condition, with the result shown in Fig. C-20* (it has been assumed that the equivalence ratio is 0.8). It is to be emphasized, of course, that the previous relationships are not intended to portray with great fidelity the dependence of the losses on all of the relevant design variables (for example, there is an obvious dependence of the combustion-time loss on equivalence ratio, through the dependence of flame speed on the latter); rather, the intent is to indicate what is currently achievable in Otto engines and the relative magnitudes of the various loss mechanisms. In the latter context, Fig. C-20 is somewhat misleading, since the relative impacts on specific fuel consumption depend upon the order in which they are shown; a more appropriate portrayal is shown in Fig. C-21. It is evident that frictional and real gas losses have the dominant effect, and that throttling losses are relatively modest.

8. Implications of Actual Performance With Respect to Further Improvements in Otto Engines

It is apparent from Fig. C-20 that increases in internal power transfer (or compression ratio in the ideal cycle) would improve the actual performance of Otto engines, as well as the ideal performance. The losses, however, represent a large target for further improvement; typical current Otto engines at compression ratios in the range of 8-10 operate with an ideal specific consumption of about 0.235 (58% thermal efficiency) and an actual specific fuel consumption of about 0.7 (20% thermal efficiency). Clearly, from Fig. C-21, losses associated with real gas effects and friction are the largest impediments to further improvement. Although it is conceivable that such

*Any errors in Fig. C-20 are attributable to one of the principal authors (DMD).

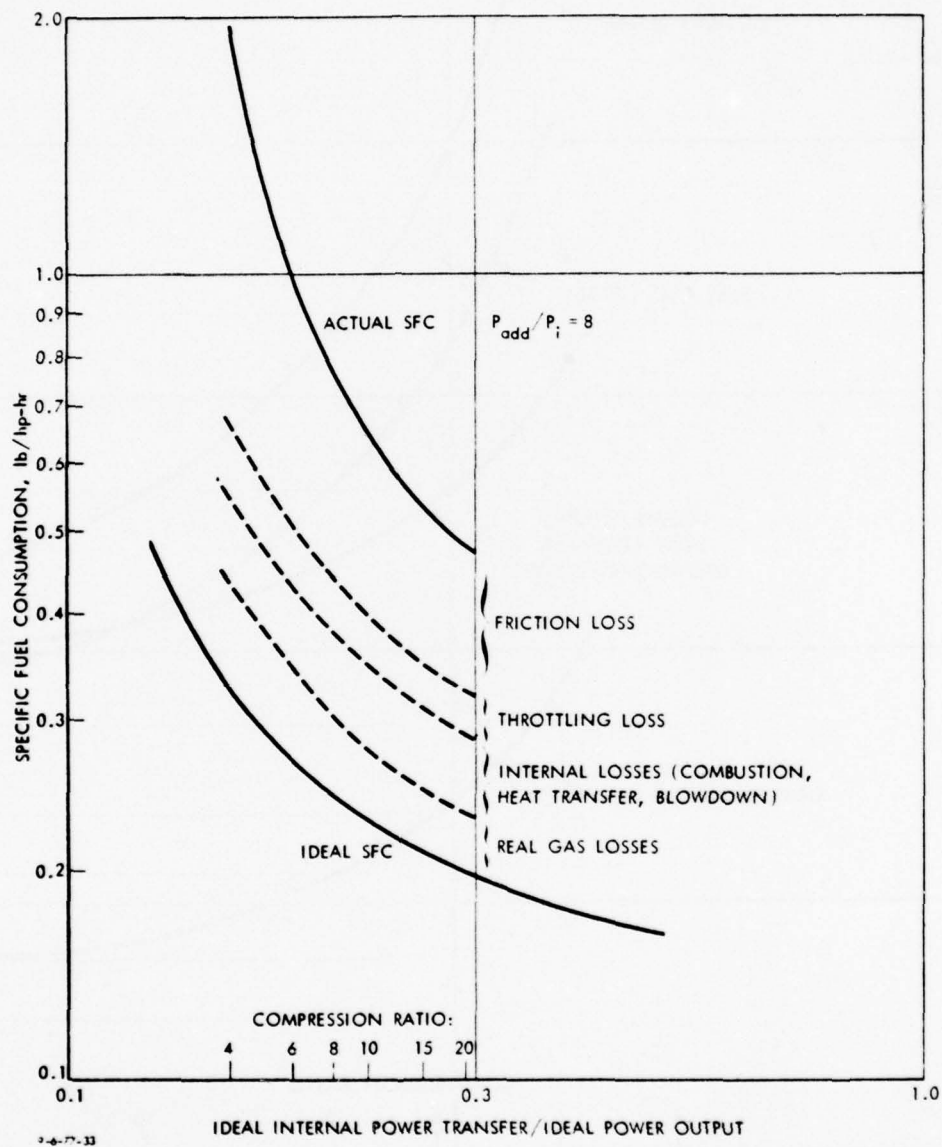


FIGURE C-20. Impact of losses on representative part-power performance of Otto engines.

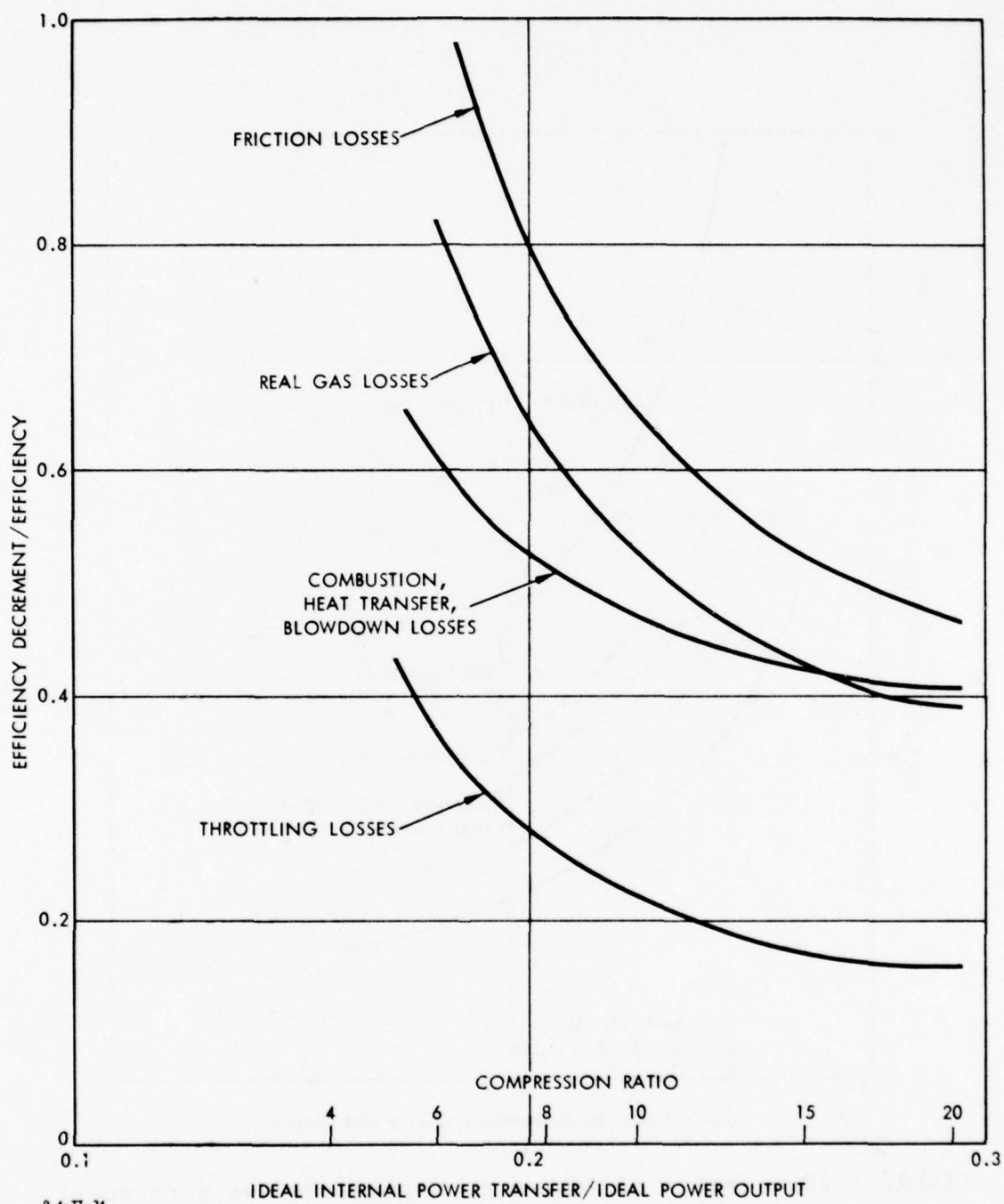


FIGURE C-21. Relative magnitudes of losses at representative part-power condition of an Otto engine.

improvements might be possible, as will be discussed subsequently, it is appropriate first to examine the relationship between performance, on the one hand, and weight and size, on the other.

C. WEIGHT, SIZE, AND PERFORMANCE RELATIONSHIPS

1. General Scaling Considerations

It is convenient to distinguish between two types of scaling: the scaling associated with increases in power level and the scaling associated with changes in design choice (e.g., compression ratio) at a constant power level. The latter scaling in fact defines the weight, size, and performance relationship available through design choice, a subject which will be dealt with in the following sections. The former scaling is inherent in the engine and, for any given state of technology and set of design choices, depends only upon power level.

For power scaling--fixed technology and design choices--the power output of an Otto engine is proportional to the displacement of the engine and the rotational speed:

$$P_o \sim V_D N .$$

To maintain the same relative velocities of both mechanical parts and gas flows, it is necessary to maintain the same piston speed, which is the product of the rotative speed and the characteristic cylinder dimension; thus,

$$N \sim \left(\frac{N_{cyl}}{V_D} \right)^{1/3} ,$$

where N_{cyl} is the number of cylinders. These two proportionalities imply that

$$\frac{V_D}{P_o} \sim \left(\frac{P_o}{N_{cyl}} \right)^{1/2} \sim \left(\frac{V_D}{N_{cyl}} \right)^{1/2} ;$$

that is, the displacement required per unit power increases as the square root of the power per cylinder or the cylinder displacement. Since the weight of an engine can be expected to be proportional to displacement

$$W \sim V_D ,$$

then the specific weight scales as

$$\frac{W}{P_o} \sim \left(\frac{P_o}{N_{cyl}} \right)^{1/2} \sim \left(\frac{V_D}{N_{cyl}} \right)^{1/2} .$$

Thus, for a constant number of cylinders, specific weight scales as the square root of power; for a constant cylinder size, specific weight is independent of power level.

2. Current State of the Art

A survey of current spark-ignition engines was made by contacting the major U.S. manufacturers of automotive, industrial, aircraft, reciprocating, and rotary engines. Data on approximately 80 different models were obtained. The data for 56 of these models are summarized in Annex C1. Piston displacements per cylinder were in the range of 15-90 in.³, 40-50 in.³ being most common; piston speeds were in the range of 1500-2800 fpm. The values in Table C-2 represent general trends of the data. Brake specific fuel consumption (BSFC) data at maximum power output were not obtained for all models. No appreciable data for quarter-load operation were obtained.

The average values for specific weight and specific volume are presented in Table C-2 for the various types of engines.

TABLE C-2. REPRESENTATIVE STATE OF THE ART OF OTTO ENGINES

TREND IN HORSEPOWER OF GASOLINE ENGINES OFFERED
(HP Ratings Shown in Percentages of Gasoline Engines Available Each Year)

Year	Number of Engine Models	Horsepower Ratings								Total Percent
		50 & Under %	51-100 %	101-150 %	151-200 %	201-300 %	301-400 %	401-500 %	Over 500 %	
1963	378	17.46	24.86	21.17	16.40	15.61	1.58	1.59	1.33	100.00
1964	389	16.96	26.48	19.28	17.22	15.43	1.28	1.29	2.06	100.00
1965	352	14.48	21.31	19.89	17.89	17.05	3.13	2.27	3.98	100.00
1966	308	13.20	20.50	21.63	23.60	16.29	1.97	.84	1.97	100.00
1967	329	11.85	21.88	22.50	20.97	16.72	2.43	.61	3.04	100.00
1968	301	12.62	24.59	18.96	21.93	15.94	1.99	.66	3.32	100.00
1969	285	14.74	23.16	18.25	20.35	15.09	3.86	1.75	2.80	100.00
1970	248	13.71	23.39	17.34	23.79	19.35	2.42	--	--	100.00
1971	277	15.53	22.74	17.33	23.46	18.41	2.53	--	--	100.00
1972	305	12.46	21.64	18.36	25.57	19.02	2.62	--	0.33	100.00

TREND IN DISPLACEMENT OF GASOLINE ENGINES OFFERED
(Displacement Groupings Shown in Percentages of Gasoline Engines Available Each Year)

Year	Number of Engine Models	Total Displacement, in. ³								Total Percent
		150 & Less %	151-200 %	201-300 %	301-400 %	401-500 %	501-800 %	801-1000 %	Over 1000 %	
1963	378	16.13	9.26	27.25	20.90	10.85	7.40	1.59	6.62	100.00
1964	389	15.93	10.29	28.27	18.77	10.80	7.19	1.80	6.95	100.00
1965	352	13.35	9.94	24.72	19.88	12.79	9.11	1.99	12.22	100.00
1966	308	10.95	9.55	26.69	24.43	14.89	6.46	1.97	5.06	100.00
1967	329	10.33	9.12	27.05	23.71	14.28	6.99	2.13	6.39	100.00
1968	301	10.95	9.97	26.25	24.26	12.96	6.61	2.33	6.64	100.00
1969	285	12.63	11.23	20.35	26.32	13.68	6.67	2.81	6.31	100.00
1970	248	13.31	11.29	18.15	31.85	16.53	7.66	.81	.40	100.00
1971	277	14.81	10.47	22.74	31.05	15.52	5.41	--	--	100.00
1972	305	11.15	10.82	21.97	33.44	17.38	5.24	--	--	100.00

Parameter	Units	Reciprocating				Turbo SC	Rotary*	2-Stroke
		Auto	Aircraft	Fuel Injection				
BSFC	lb/hp-hr	0.55	0.5	0.5		0.7	0.6	0.9
P/V _D	hp/in. ³	0.5	0.5	0.55		0.6	2.2	0.9
BMEP	psi	100	140	160		180	140	100
W/V _D	lb/in. ³	2.0	0.8	0.88		0.96	3.1	0.72
W/P	lb/hp	4.0	1.6	1.6		1.6	1.4	0.8
vol/P	in. ³ /hp	200	150	100		120	50	100

*The displacement of the rotary engine is that of one element of a three-element rotor.

It is interesting to note that aircraft, fuel-injected, and turbo-supercharged engines all appear to have the same specific weight--1.6 lb/hp. This indicates that the increase in power is the same as the weight of the equipment required to produce the power improvement. The specific weight for automotive engines, $W/P = 4.0$ lb/hr, is about twice the value for aircraft. The lower value for aircraft engines is a function of design for light weight, the large use of lightweight metals, and the absence of a water-cooling system. These differences in specific weights are, as expected, reflected in the differences in weight per unit displacement.

The two-stroke engine and the rotary engine have the lowest specific weight and the lowest specific volume, respectively. It should be pointed out that the data for these types of engines is rather limited. In particular, the data for two-stroke engines is limited to small cylinder sizes (25 in.³) and thus lower specific weights and higher specific fuel consumptions than would prevail at larger cylinder sizes. Nevertheless, the specific weight and specific volume of these two types of engines will always be less than those for four-stroke reciprocating engines because of the greater number of power strokes per revolution. The rotary will have the lowest specific volume because it is the most compact design. It is also evident that higher specific fuel consumption is associated with lower specific weight and volume.

Ideally, it would be desirable to associate component weights and sizes with the functions (compression, expansion, heat addition) that they perform and the efficiency with which the functions are performed. To this end, weight breakdowns of some automotive engines were obtained. Table C-3 contains the component weights of the Ford Model 351GP, a V-8 spark-ignition engine with a power rating of 180 hp and a piston displacement of 351 in.³ Table C-4 contains average percentage weight breakdowns for engines of three major U.S. manufacturers. Table C-5

TABLE C-3. WEIGHT BREAKDOWN FOR FORD MODEL 351GP

<u>Group</u>	<u>Weight</u>	
	<u>(lb)</u>	<u>%</u>
Block	175	29.1
Cylinder heads (2)	114	19.0
Rotating Mass	132	22.0
Crankshaft	83	
Pistons (8)	16	
Connecting rod (8)	12	
Valve lifter & push rods (16)	6	
Camshaft	10	
Timing chain & sprockets	5	
Induction system	91	15.1
Carburetor	8	
Intake manifold	45	
Exhaust manifold (2)	38	
Accessories	61	10.1
Oil pump	5	
Fuel pump	2	
Water pump	15	
Starter & solenoid	20	
Alternator & voltage regulator	12	
Ignition sys. (coil, distrib. & plugs)	7	
Miscellaneous	28	4.7
Oil pan	7	
Valve covers (2)	6	
Miscellaneous	15	
TOTAL	601	100.0

TABLE C-4. PARTIAL WEIGHT BREAKDOWN OF SELECTED U.S. AUTOMOTIVE ENGINES, AVERAGE VALUES

<u>Weight Group</u>	<u>Percentage of Total Weight</u>	
	<u>ATT Engines</u>	<u>Model 351GP</u>
Block	33.4	36.3
Cylinder head	29.1	23.7
Rotating mass	25.7	27.4
Accessories	11.8	12.7
Total for 4 Groups	100	100

TABLE C-5. PARTIAL WEIGHT BREAKDOWN OF U.S.
AUTOMOBILE ENGINES

No. of Cyl.	Weight Group	Chrysler		Ford		G.M.	
		(lb)	(%)	(lb)	(%)	(lb)	(%)
4	Engine			279	100	276	100
	Rotating mass			66	24	73	26
	Block			89	32	67	24
	Cyl. head			80	29	90	33
6-250	Engine	444	100	420		392	
	Rotating mass	122	27	129	31	122	31
	Block	188	42	111	26	93	24
	Cyl. head	85	19	135	32	125	32
8-350	Engine	484	100	506	100	484	100
	Rotating mass	134	28	134	26	111	23
	Block	149	31	171	34	164	34
	Cyl. head	152	31	135	27	153	32
8-400	Engine	561	100	513	100	558	100
	Rotating mass	134	24	136	27	121	22
	Block	226	40	174	34	179	32
	Cyl. head	150	27	147	29	200	36
8-450	Engine	571	100	540	100	550	100
	Rotating mass	134	23	136	25	126	23
	Block	226	40	204	38	204	37
	Cyl. head	158	28	140	26	160	29

contains data for individual manufacturers for 4-, 6-, and three sizes of 8-cylinder engines. In all cases, the weight of radiator, coolant, and oil is not included; other data indicate that the weight of the radiator is 0.2 lb per cubic inch of piston displacement.

3. Component Loss-Weight Relationships*

As mentioned previously, it would in principle be desirable to associate functions and losses with specific engine components, in order to assess potential limits somewhat more accurately. Unfortunately, the nature of an Otto engine does not lend itself to a convenient breakdown of this sort. It is clear, however, that a major element of both weight and loss in an Otto engine is associated with the compression and expansion processes, and with some effort, a descriptive loss-weight relationship can be obtained which relates to these processes.

It is assumed here that the losses associated with the compression and expansion processes are those previously denoted as frictional losses, and that some weight per unit displacement can be separately associated with the compression and expansion processes. Thus, for a four-stroke engine, the power loss associated with compression and expansion is

$$P_{\text{loss, cx}} = \frac{NV_D}{2} \left(\frac{f_{\text{mep}}}{V_p} \right) \frac{2N}{a_r} \left(\frac{V_D}{N_{\text{cyl}}} \right)^{1/3} \quad (\text{C-33})$$

and the weight is

$$W_{\text{cx}} = w_{\text{cx}} V_D, \quad (\text{C-34})$$

where w_{cx} is the weight per unit displacement associated with compression and expansion only. The ideal power transfer between expansion and compression is

*Misinterpretations or errors in this discussion are attributable to one of the principal authors (DMD).

$$P_{cx} = \dot{m} c_v T_1 (r^{\gamma-1} - 1) , \quad (C-35)$$

where \dot{m} is the mass flow rate, which is in turn related to displacement by

$$\dot{m} = \rho_1 e_v \frac{N}{2} V_D . \quad (C-36)$$

Equations C-33 through C-36 can be combined to give relationships for speed and specific weight as a function of loss:

$$N = \frac{a r^{3/2}}{4} \left(\frac{N_{cyl}}{P_{cx}} \right)^{1/2} \frac{[\rho_1 e_v c_v T_1 (r^{\gamma-1} - 1)]^2}{(f_{mep}/V_p)^{3/2}} \left(\frac{P_{loss, cx}}{P_{cx}} \right)^{3/2} \quad (C-37)$$

$$\frac{W_{cx}}{P_{cx}} = w_{cx} \frac{8(f_{mep}/V_p)^{3/2}}{[\rho_1 e_v c_v T_1 (r^{\gamma-1} - 1)]^3} \left(\frac{P_{cx}}{N_{cyl}} \right)^{1/2} \frac{1}{(P_{loss, cx}/P_{cx})^{3/2}} . \quad (C-38)$$

Taking the data in Table C-3 as representative, the weight per unit displacement of those items more directly associated with the compression-expansion processes (i.e., block, cylinder heads, rotating mass, induction system) is approximately 1.5 lb/in.³. Obviously, not all of this weight can be attributed to the compression and expansion processes alone--the increased strength required by peak combustion pressures are more attributable to heat addition. If it is assumed that 50% of the weight is associated with pressure loading, and further that the compression pressure is one-third the peak pressure (which are typical values), then the weight per unit displacement associated with compression and expansion is approximately 1 lb/in.³. Using this value for w_{cx} , and the following other representative values:

$$\rho_1 = 0.076 \text{ lb/ft}^3$$

$$e_v = 0.9$$

$$c_v = 0.171 \text{ Btu/lbm-}^\circ\text{R}$$

$$T_1 = 520^\circ\text{R}$$

$$r = 10$$

$$\gamma = 1.4$$

$$f_{mep} = 40 \text{ psi}$$

$$V_p = 3000 \text{ fpm}$$

$$a_r = 0.92$$

$$P_{cx}/N_{cyl} = 12.5 \text{ hp,}$$

the loss-weight relationship defined by Eqs. C-37 and C-38 can be portrayed graphically, as shown in Fig. C-22. The tradeoff between specific weight and loss is apparent. Considering the magnitude of the weight and loss associated with only the compression and expansion processes in Otto engines, the relationship serves as a useful benchmark for comparison of future proposed improvements in these processes.

4. Overall Engine Weight and Size Scaling

Although it is not practical to associate all specific components with specific functions in Otto engines, it is possible to determine some overall scaling relationships which indicate the dependence of engine size, weight, and specific fuel consumption on more basic properties of engines. In particular, the dependence of engine weight and size, at constant power level, on three variables will be examined here:

1. Compression ratio
2. Inlet density changes by means of turbocharging
3. Material properties.

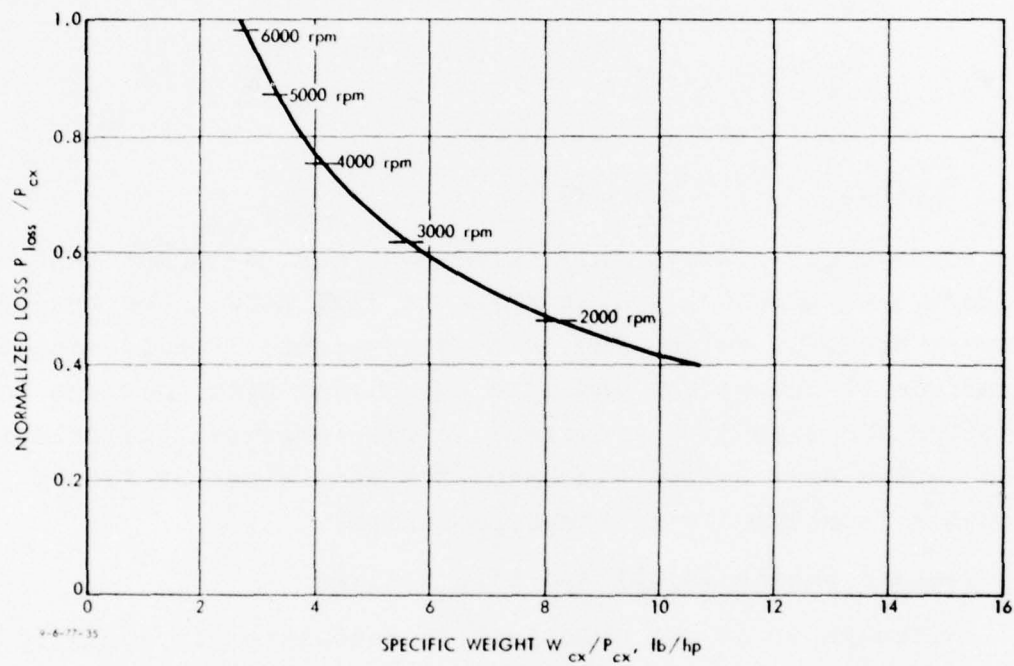


FIGURE C-22. Loss-specific weight relationship for compression-expansion processes in four-stroke Otto engines.

The compression ratio influences both the peak cylinder pressure and the displacement required to produce a given power level. Obviously, the weights of all components of an engine are not affected equally. At least three different groups of components can be identified: (1) those components which are unaffected by compression ratio at constant power output (e.g., the accessories and the cooling system); (2) those components which are affected only through changes in displacement required to produce a given power (e.g., the induction system); and (3) those components which are affected by both changes in displacement and peak cylinder pressure (e.g., pistons, cylinder heads, cylinder walls). The peak cylinder pressure varies ideally as r^{γ} and varies empirically as $r^{1.25}$, due primarily to real gas effects. If it is assumed that the weight per unit displacement of those components which depend upon both displacement and peak cylinder pressure vary linearly with the latter, and if it is noted that the displacement required per unit power varies linearly with the specific fuel consumption, the specific weights of two engines at different compression ratios can be written as:

$$\frac{(W/P)_2}{(W/P)_1} = 1 - Z_{r_1} - Z_{d_1} + Z_{d_1} \left(\frac{sfc_2}{sfc_1} \right) + Z_{r_1} \left(\frac{r_2}{r_1} \right)^{1.25} \left(\frac{sfc_2}{sfc_1} \right), \quad (C-39)$$

where Z_{r_1} and Z_{d_1} are the weight fractions of the components which depend upon cylinder pressure and displacement, respectively. From the previous weight data, it is difficult to deduce the appropriate weight fractions. From Table C-3, and with the addition of 70 lb for the radiator, a rough estimate might be that the power group consists of the accessories, radiator, miscellaneous fittings, and one-third of the block (217 lb, $1 - Z_{r_1} - Z_{d_1} \approx 0.32$); that the displacement group consists of the induction system and one-third of the block (159 lb, $Z_{d_1} \approx 0.24$) and that the cylinder pressure group consists of the cylinder heads, the rotating mass, and one-third of the block (305 lb,

$Z_{r_1} \approx 0.45$). Obviously such estimates are rather crude, and for simplicity here, Eq. C-39 is approximated by considering the engine to consist of only two groups--a power group and a cylinder pressure group:

$$\frac{(W/P)_2}{(W/P)_1} = 1 - Z_{r_1} + Z_{r_1} \left(\frac{r_2}{r_1} \right)^{1.25} \left(\frac{sfc_2}{sfc_1} \right) . \quad (C-40)$$

On the basis of the previously cited data in Table C-3, an assumption that $Z_{r_1} = 0.5$ (when $r = 9$) seems reasonable.

For turbocharging, at constant power level and constant overall compression ratio, similar consideration of an engine consisting of a power group and a displacement group yields the following scaling relationship:

$$\frac{(W/P)_2}{(W/P)_1} = 1 - Z_{d_1} + Z_{d_1} \left(\frac{\rho_1}{\rho_2} \right) \left(\frac{sfc_2}{sfc_1} \right) , \quad (C-41)$$

where ρ_1 and ρ_2 are the inlet manifold densities and Z_{d_1} is the fraction of engine weight which is proportional to displacement. Again, an assumption of $Z_{d_1} \approx 0.5$ at $r = 9$ seems reasonable.

With respect to the influence of material properties, the engine is considered to be composed of two groups: (1) a high-stress group whose weight is a function of load and (2) a low-stress group whose weight is not a function of load. It is assumed that the high-stress group is composed of the rotating mass and one-third of the weight of the block and cylinder heads. From the previous weight data, it is estimated that the weight breakdown for these two groups in an all-steel automotive engine are:

High-stress group	40%
Low-stress group	60%.

This weight breakdown is for a nominal 9:1 compression ratio. Increasing the compression will shift the weight breakdown in

the direction of the high-stress group. For different materials, the weight breakdown for the two groups will shift. The high-stress group is dependent upon the strength-to-density ratio S/ρ of the material, while the low-stress group is dependent only upon the density. Using these assumptions, one obtains for a scaling equation for different materials at the same power output

$$\frac{(W/P)}{(W/P)_s} = 0.4 \frac{S}{S_s} \frac{\rho}{\rho_s} + 0.6 \frac{\rho}{\rho_s} , \quad (C-42)$$

where S is the yield strength of the material and the subscript s stands for steel. Unlike the other scaling relationships, Eq. C-42 does not involve specific fuel consumption changes, and its implications can be examined directly.

The engine specific weights resulting from the use of various materials are presented in Table C-6, using an engine specific weight of 4.0 lbm/hp as representative of steel construction. The nominal yield strengths for steel and aluminum are 30 kpsi and 15 kpsi, respectively. Aluminum has a S/ρ ratio that is 1.5 that of steel. Steels with yield strengths up to 90 kpsi and aluminum with strengths of 30 kpsi are available with reasonable ductility. Table C-6 indicates that with high-strength aluminum in the high-stress group and lightweight metal such as magnesium or ceramics in the low-stress group specific weight ratios of 1 lb/hp may be possible for reciprocating engines. It is interesting to note that for medium-strength steel and aluminum one obtains a specific weight of 1.6, which is the nominal value for aircraft engines. The weight breakdown for these materials is 50% high, 50% low. One aircraft engine manufacturer has stated that it designs its engines with 45% steel and 55% aluminum.

TABLE C-6. EFFECT OF MATERIALS UPON ENGINE SPECIFIC WEIGHT

<u>High-Stress Group</u>		<u>Low-Stress Group</u>		
	<u>Yield Strength</u>		<u>Density</u>	$\frac{W}{P}$
<u>Material</u>	$\begin{matrix} S \\ \text{(kpsi)} \end{matrix}$	<u>Material</u>	$\begin{matrix} \rho \\ \text{(lb/ft}^3\text{)} \end{matrix}$	<u>(lb/hp)</u>
Steel	30	Steel	490	4.0
Steel	60	Steel	490	3.2
Steel	90	Steel	490	2.93
Steel	60	Aluminum	165	1.61
Steel	90	Aluminum	165	1.34
Steel	90	Ceramics	109	1.07
Aluminum	30	Ceramics	109	1.07

The previous scaling relationships are all concerned with engine specific weight. With respect to engine specific volume, it seems reasonable to assume that in all cases it is proportional to engine displacement, recognizing that this is somewhat of an overestimate of the sensitivity of engine specific volume to displacement. For the cases considered here, an appropriate scaling relationship is then

$$\frac{(\nabla/P)_2}{(\nabla/P)_1} = \frac{sfc_2}{sfc_1} \frac{\rho_1}{\rho_2}, \quad (C-43)$$

where ρ_1 and ρ_2 are the respective inlet manifold densities.

5. Engine Specific Fuel Consumption Scaling

Empirical data suggests that the minimum specific fuel consumption of Otto engines scales with compression ratio as

$$\frac{sfc_2}{sfc_1} = \frac{1 - \frac{1}{r_1^{1.25}}}{1 - \frac{1}{r_2^{1.25}}} \quad (C-44)$$

Inasmuch as the weight-size scaling relationships of the previous section require specific fuel consumption scaling at maximum power, rather than best sfc, and that the representative sfc is at part power, it is convenient to develop relative sfc scaling relationships based on the previous development of ideal cycle performance and the various loss contributions. Reasonable approximations to these relationships yield the following sfc scaling equations:

$$\frac{sfc_2}{sfc_1} = \frac{\eta_{id,1} - 0.16 - 0.20(\eta_{id,1} - 0.16)}{\eta_{id,2} - 0.16 - 0.20(\eta_{id,2} - 0.16)} \quad (C-45)$$

for both best sfc and maximum power, and

$$\frac{sfc_2}{sfc_1} = \frac{\eta_{id,1} - 0.16 - 0.20(\eta_{id,1} - 0.16) - 0.14}{\eta_{id,2} - 0.16 - 0.20(\eta_{id,2} - 0.16) - 0.14} \quad (C-46)$$

at 25% power, where η_{id} is the ideal cycle efficiency $\left(1 - \frac{1}{r^{\gamma-1}}\right)$. The origin of the various terms is simply that, in all cases, the first term is the ideal efficiency, the second term accounts for real gas losses, and the third term accounts for internal losses--heat transfer, combustion time, and exhaust blowdown; the fourth term, which appears in Eq. C-46, accounts for friction and throttling losses at part power.

With respect to turbocharging, similar scaling relationships are:

$$\frac{sfc_2}{sfc_1} = \frac{\eta_{id,1} - 0.184 - 0.20(\eta_{id,1} - 0.184) - 0.091/(\rho_1/\rho_o)}{\eta_{id,2} - 0.184 - 0.20(\eta_{id,2} - 0.184) - 0.091/(\rho_2/\rho_o)} \quad (C-47)$$

at maximum power,

$$\frac{sfc_2}{sfc_1} = \frac{\eta_{id,1}^{-0.16-0.20(\eta_{id,1}-0.16)} - 0.06/(\rho_1/\rho_o)}{\eta_{id,2}^{-0.16-0.20(\eta_{id,2}-0.16)} - 0.06/(\rho_2/\rho_o)} \quad (C-48)$$

at minimum sfc, and

$$\frac{sfc_2}{sfc_1} = \frac{\eta_{id,1}^{-0.16-0.20(\eta_{id,1}-0.16)} - 0.14/(\rho_1/\rho_o)}{\eta_{id,2}^{-0.16-0.20(\eta_{id,2}-0.16)} - 0.14/(\rho_1/\rho_o)} \quad (C-49)$$

at 25% power, where ρ_o is the density of air at standard conditions, and η_{id} is the ideal efficiency of the turbocharged cycle. The origin of the first three terms in all of these cases is identical to those in the compression ratio scaling relationships, while the last term accounts for throttling and friction losses. It should be noted that these relationships imply that the frictional loss contribution decreases with increasing density, which is undoubtedly an overestimate of the sensitivity; that the internal loss contribution in effect decreases with increased turbocharging due to the reduction in ideal efficiency, which may also be an overestimate of the sensitivity; and that the real-gas-loss contribution is independent of turbocharging, which is an overestimate of these losses. Obviously, the relationships are rather crude, but one hopes they are of sufficient accuracy for the present purposes.

6. Current State of the Art in Specific Fuel Consumption-Weight Tradeoffs

The previously developed scaling relationships, in conjunction with baseline state-of-the-art values, can be used to estimate the range of specific fuel consumption-specific weight values currently attainable in Otto engines as compression ratio and degree of turbocharging are varied. The results of such scaling are shown in Fig. C-23, where the baseline values are:

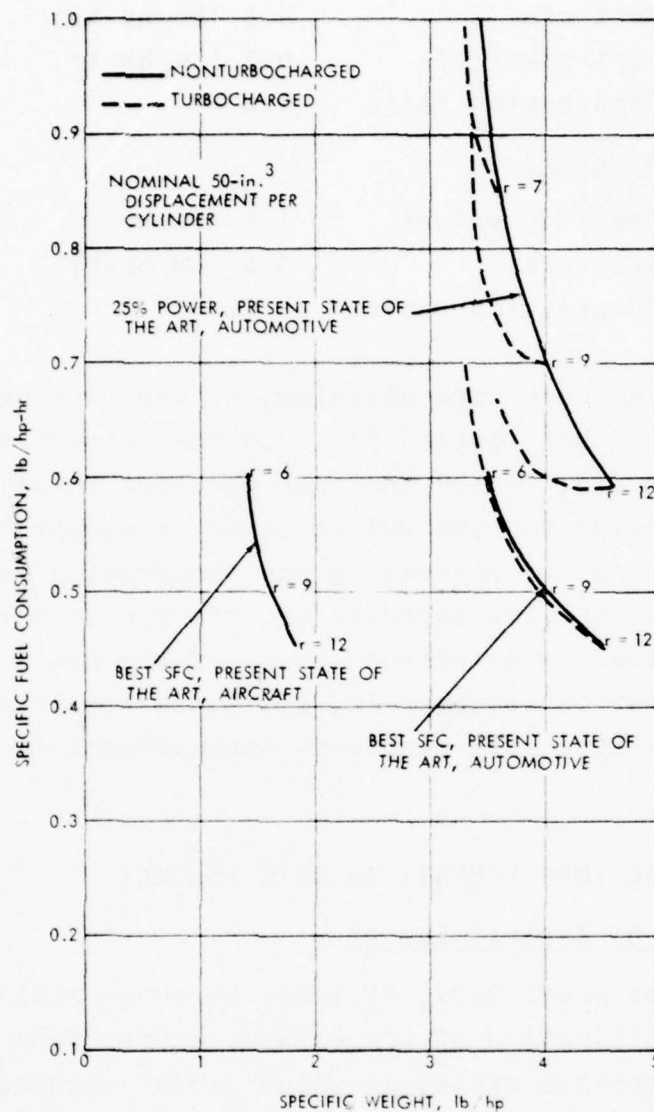


FIGURE C-23. Specific fuel consumption--specific weight relationships for four-stroke Otto engines.

Automotive

Specific weight	4.0 lbm/hp
Best sfc	0.5 lbm/hp-hr
Part-power sfc	0.7 lbm/hp-hr
Compression ratio	9.0

Aircraft

Specific weight	1.6 lbm/hp
Best sfc	0.5 lbm/hp-hr
Compression ratio	9.0.

It can be observed that turbocharging, at constant overall compression ratio, has little effect on the automotive relationship for minimum sfc, indicating that the loss in efficiency due to turbocharging for the weight saved is essentially identical to that obtained by decreasing the compression ratio. At part power, turbocharging improves the sfc due to a reduction in throttling required. The present state of the art is limited to compression ratios of about 10, and hence the lower portions of the curves in actuality represent improvements in the state of the art.

D. PROSPECTS FOR IMPROVEMENTS IN OTTO ENGINES

1. Utilization of Exhaust Energy

As mentioned previously, at least three possibilities exist for the utilization of the exhaust energy from the Otto cycle: a regenerative cycle, in which a heat exchanger would be used to transfer heat from the exhaust to preheat the fuel-air mixture prior to combustion; a turbocharger, where the exhaust would drive a turbine, the power output used in turn to operate a compressor which would increase cylinder pressure prior to combustion; and a Lenoir cycle, in which the combustion gases would be fully expanded to inlet pressure. In each case, gains in cycle thermal efficiency are possible.

The performance characteristics of an Otto regenerative air standard cycle (i.e., using $\gamma = 1.4$) are shown in Fig. C-24. Calculations were made for a stoichiometric air-fuel ratio, a fuel heating value of 18,400 Btu/lb, a cycle inlet temperature of 520°R, and heat transfer from the exhaust to the working fluid after the compression stroke. Several values of heat exchanger effectiveness were used in the analysis. Two major difficulties are inherent in the regenerative cycle. First, the time and area available for heat transfer to cylinder gases are very small, and it is doubtful that a suitable arrangement can ever be found. Second, even if the heat transfer to the fluid could be accomplished, this greater heat transfer prior to ignition would greatly increase the likelihood of knock. For example, to provide the same temperature prior to combustion as the Otto cycle without regenerator, at a compression ratio of 10, it would be necessary to reduce the compression ratio to a value below 2.0 with an effectiveness less than 0.2. From Fig. C-23, this would yield a large loss of efficiency. It seems that the regenerative Otto cycle is not a promising avenue of approach.

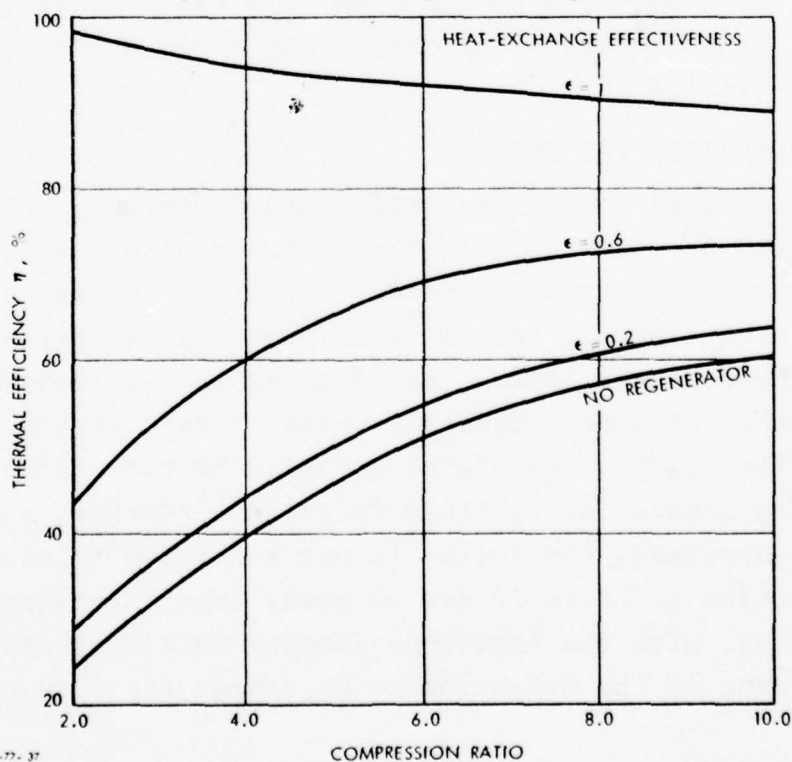


FIGURE C-24. Influence of heat-exchange effectiveness on regenerated Otto cycle ($\gamma = 1.4$).

As demonstrated earlier, the turbocharger provides some benefits in part-power fuel consumption (at a given specific weight and overall compression ratio), due to the reduction in throttling and friction losses. These gains are presently restricted by the necessity to decrease the cylinder compression ratio--and ideal efficiency--as the degree of turbocharging is increased. It seems plausible that this restriction could be overcome by employing a variable-compression-ratio piston, as in diesels, which would enable fuel turbocharging at reduced cylinder compression ratio at maximum power, thus taking advantage of the smaller size offered, and which would also enable operation at low turbocharging and high cylinder compression ratios at part power, thus improving part-power performance.

The Lenoir cycle offers improved ideal efficiency at lower compression ratios. However, the increased frictional losses which seem inherent in the cycle would appear to negate this potential improvement in specific fuel consumption; simultaneously, the increased size required to implement the cycle would be disadvantageous. The prospects for the Lenoir cycle are accordingly judged to be slim indeed.

2. Stratified-Charge Engines

With a direct-injected, stratified-charge engine, only air is compressed in the compression stroke, the fuel being injected directly into the cylinder just before ignition. Unlike the homogeneous-charge engine, here fuel is used only as needed, thus minimizing real gas losses, and economy is near optimum over a wide range of load. Typical curves of bsfc versus bmep are shown in Fig. C-25. The engine can also be run unthrottled, thus minimizing losses due to fluid friction. Further, since only air is compressed, the engine is not sensitive to knock. Compression ratios of 10 to 12 can be used, thus improving the ideal efficiency, with the engine possessing multifuel capability. To ensure burning of the non-homogeneous charge (that is,

to control combustion time losses), engine speed must be restricted to about 3000 rpm, with air-fuel ratios less than stoichiometric at full load. It would seem that the full potential of this engine requires an extremely fast combustion process at low loads, to take advantage of the reduced real gas losses, and a carbureted mixture at maximum power to increase fuel utilization.

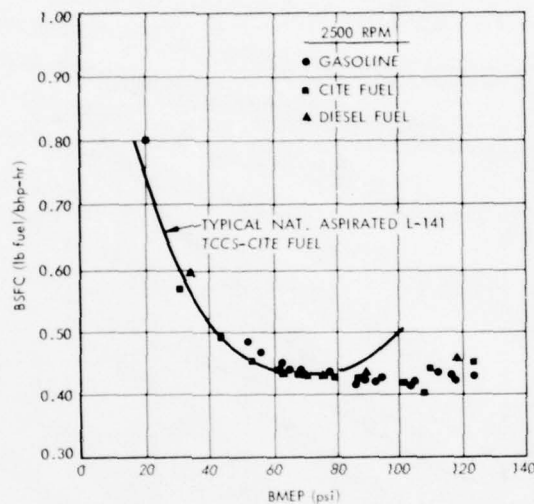


FIGURE C-25. Performance characteristics of a stratified-charge engine. (Source: Ref. C-6)

3. Rotary Engines

The rotary engine has the advantages of possessing fewer parts and being more compact and lighter than the reciprocating engine. The engine is ported, thus removing the need for the valve train of the reciprocating engine. With its rotary motion, many of the connecting rods and mechanisms of the reciprocating engine are no longer required. Further, the rotor is geared to rotate at one-third the crankshaft revolutions, so there is one power stroke per crankshaft revolution, as with a two-cycle

engine. The above contributes to a lower specific weight than the conventional reciprocating engine. Since there are fewer moving parts, the friction horsepower of the rotary is less than that of the reciprocating engine, and the rate of increase of friction losses with engine speed is less (Fig. C-26). The net result of these effects is that the rotary engine produces a much improved compression-expansion function, in the sense of Fig. C-22.

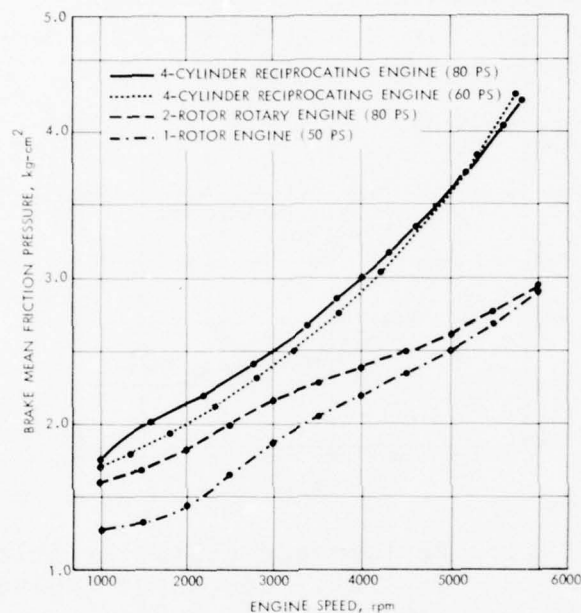


FIGURE C-26. Comparison of brake mean friction pressure of reciprocating and rotary engines (from Ref. C-7).

The rotary engine lends itself to stratified-charge operation, with the air moved past the injector and spark plug at high velocities by the rotor. Considerable testing has been done on rotary engines, both carbureted and stratified, by Curtiss-Wright. Results with a 60-in.³ rotary indicate that the brake horsepower curve does not peak until about 7000 rpm, unlike the curve for the reciprocating engine, which peaks at 4000-5000 rpm.

A comparison of rotary and reciprocating engines is shown in Fig. C-27. Operation at 2000 rpm for the stratified-charge rotary is shown in Fig. C-28. It can be seen that the performance of the rotary engine, as measured by bsfc, at least approaches that of the reciprocating engine (although the nature of the geometry dictates that heat transfer losses in a rotary will always be higher than in a reciprocating engine). Problems have been experienced with the rotary engine relative to seals and seal wear between rotor and housing. Improvements have been made over the years which have enabled current bsfc's to be attained. Operation of the rotary at speeds up to 10,000 rpm will depend upon further improvements in seals.

Scaling of data from a 60-in.³ or 90-in.³ single-rotor or two-rotor engine to a larger multirotor and larger-horsepower rotary engine is difficult. Indicated power is proportional to chamber size, number of rotors, and revolutions per minute. However, friction being a lower proportion of overall output power, slightly greater efficiencies can be achieved with large chamber sizes, whereas smaller sizes (having lower specific weight) are achievable with multirotor engines.

Currently available carbureted rotary engines can achieve a specific weight of approximately 1.2 lb/hp operating at speeds of approximately 5000 rpm; such engines possess a power per unit volume of approximately 40 hp/ft³. If seal problems and problems of thermal distortions of rotor and housing can be overcome, it would seem possible to achieve specific weights down to 0.6 or 0.5 lb/hp for an aluminum engine operating up to 10,000 rpm. With suitable development effort, a stratified-charge rotary engine operating at these speeds should be able to achieve brake specific fuel consumptions down to 0.5 lb/hp-hr.

4. Adiabatic Engines

With perhaps the eventual prospect of using high-temperature materials such as ceramics in Otto engines, it is reasonable to

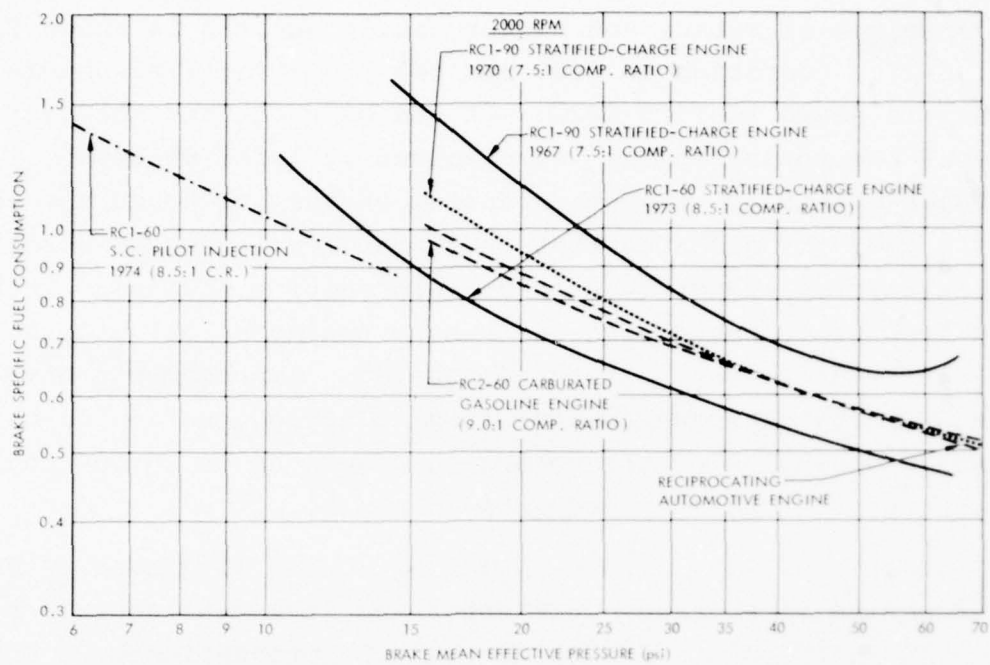


FIGURE C-27. Part-load fuel consumption of rotary and reciprocating engines (from Ref. C-8).

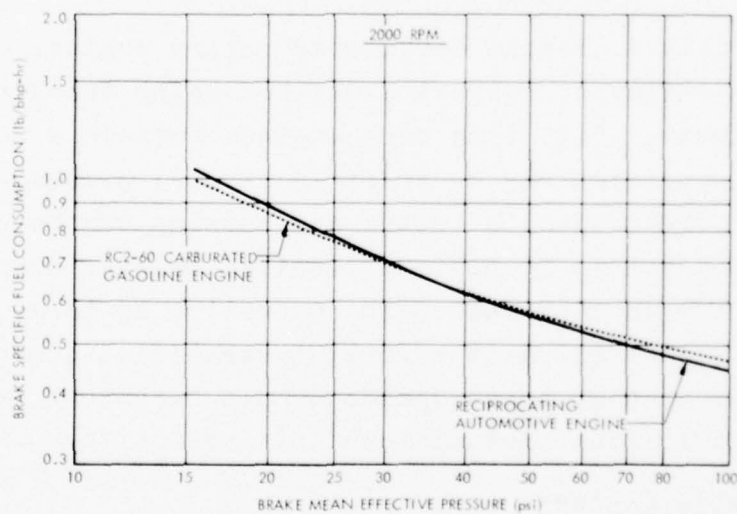


FIGURE C-28. Part-load fuel consumption, 2000 rpm (from Ref. C-8).

assess the potential of an adiabatic engine. From the previous analysis of losses, elimination of heat transfer effects would improve the sfc of an Otto engine by perhaps 10%. In addition, the need for a cooling system for an adiabatic engine could conceivably be eliminated, with an attendant decrease in specific weight of perhaps 20%.

5. Potential Limits for Otto Engines*

The analysis developed here can be used to estimate plausible limits in size and specific fuel consumption for Otto engines which cannot reasonably be expected to be exceeded in the foreseeable future, and which in fact may never be attainable. It has been observed that major impediments to further improvement in the Otto engine include the following:

1. Limited maximum compression ratio, due to knocking.
2. Real gas losses, which can be alleviated somewhat by lean operation in a stratified-charge engine.
3. Throttling and friction losses at representative part-power conditions, which can be alleviated by stratified-charge operation and, to some extent, by turbocharging.
4. Heat transfer losses, which can be reduced by adiabatic operation if suitable materials can be developed.
5. The weight and size associated with the limited volume-flow capabilities of reciprocating machinery, which can be alleviated by lightweight materials, turbocharging, and/or the rotary engine process.

To implement the cited potential improvements, at the same time circumventing the other penalties associated with the improvement mechanism, a "limit" engine can be postulated which, in reciprocating form, consists of:

1. Stratified-charge operation at part power and carbureted operation in the vicinity of maximum power.

*This section has been synthesized by one of the principal authors (DMD) on the basis of the contents of this appendix; any misinterpretations or errors are accordingly attributable to him.

2. Turbocharged operation at higher power levels, with variable compression ratio to permit maximum values at part power.
3. Adiabatic operation.
4. Use of lightweight materials.

Based on this type of an engine, it seems reasonable that

1. Compression ratios up to 12 might be possible.*
2. Operation at equivalence ratios down to the vicinity of 0.3 and with rapid combustion might be possible.
3. The losses presently associated with heat transfer, combustion time, and exhaust blowdown could possibly be reduced from their present level of 20% of the fuel-air cycle efficiency to 15% of the fuel-air cycle efficiency.
4. Suitable lightweight materials might be used.

Use of the previously developed loss relationships and scaling laws then permits an estimate of the specific fuel consumption-specific weight characteristics to be made, with the results shown in Fig. C-29. Consistent with the compression ratio limitation of 12, the lower part of the curve is not expected to be possible at all. Such a limit as shown in Fig. C-29 is of course always subject to both revision and misinterpretation. The interpretation here is that it is totally unreasonable to expect the performance of a reciprocating Otto engine to exceed that shown. Whether an Otto engine can indeed approach the limit shown depends upon whether the problems associated with lean operation, rapid combustion, no heat transfer losses, and lightweight materials can be simultaneously solved successfully. It is to be emphasized that currently no such simultaneous solutions are evident.

No corresponding estimate has been made here for the rotary engine, since the losses are somewhat difficult to quantify. It seems reasonable to expect the specific weight limit to be slightly less than 50% of that of the reciprocating Otto, but with a somewhat higher specific fuel consumption.

*There is some recent evidence that operation at low equivalence ratios might permit higher compression ratios, although probably not simultaneously with the other improvements indicated here.

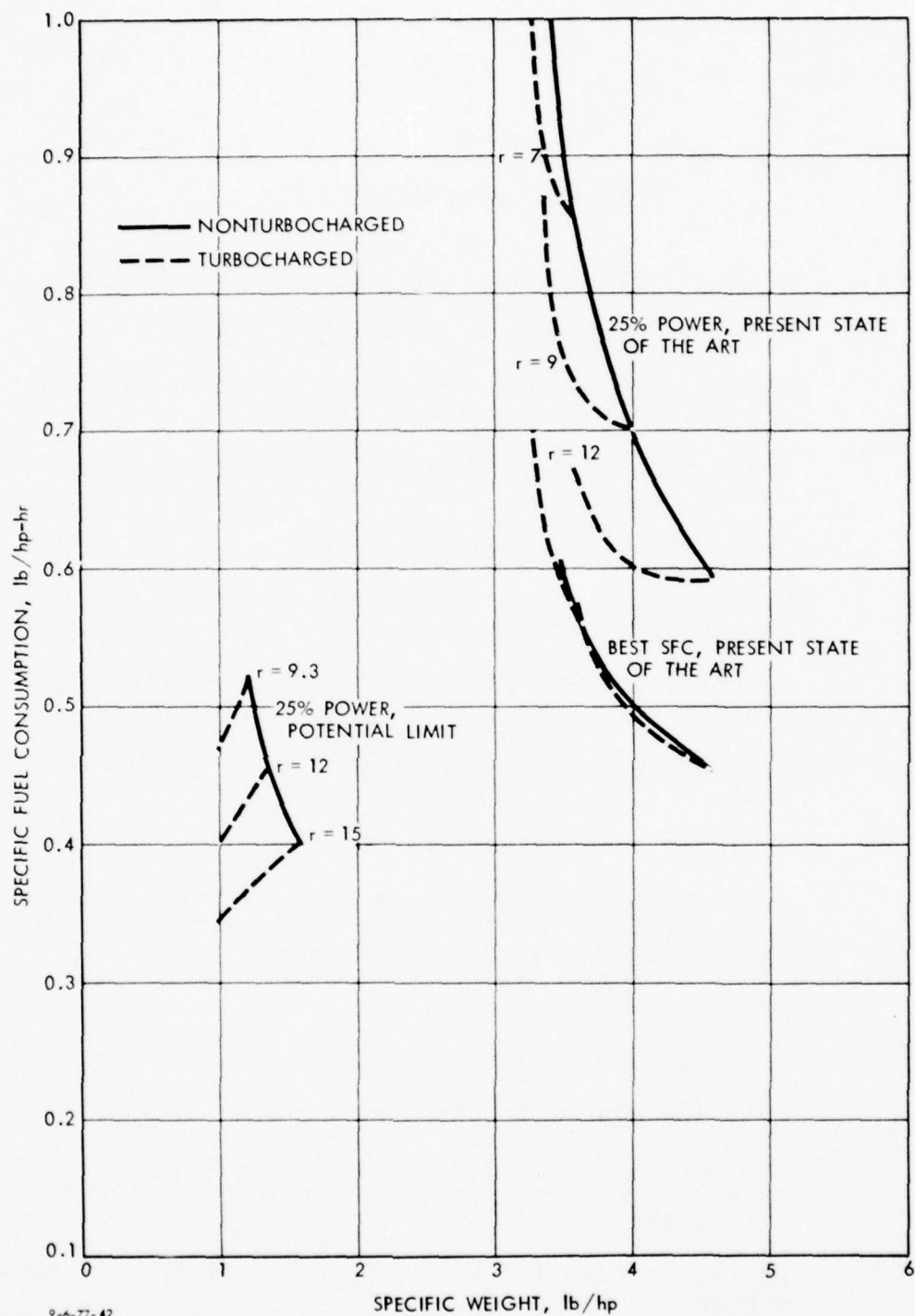


FIGURE C-29. Specific fuel consumption--specific weight limits for four-stroke Otto engines.

GLOSSARY, APPENDIX C

\bar{A}	Average cylinder surface area during a stroke
a_r	Cylinder form factor, $\pi D^2/4(V_D/N_{cyl})^{2/3}$
BDC	Bottom dead center; the piston position or crank angle at maximum cylinder volume.
bhp	Brake horsepower; the net horsepower delivered by an engine.
bmep	Brake mean-effective pressure
BSFC	Brake specific fuel consumption, fuel flow/brake horsepower, lb/hp-hr
c_p	Specific heat at constant pressure of the working fluid
c_v	Specific heat at constant volume of the working fluid
D	Cylinder bore (diameter)
e_v	Volumetric efficiency, the ratio of mass inducted into cylinder to that which would occupy the glide at working fluid inlet conditions.
f/a	Fuel-air ratio
fhp	Friction horsepower
fmep	Friction mean-effective pressure
F_s	Stoichiometric fuel-air ratio, the fuel-air ratio at which complete combustion can occur with no excess air.
\bar{h}	Average convective heat transfer coefficient during stroke
HV	Lower heating value of fuel

ihp	Indicated horsepower; the power which would be produced by the engine in the absence of frictional losses.
k	Thermal conductivity of working fluid
m	Mass of working fluid in cylinder
\dot{m}	Mass flow rate
m_c	Polytropic exponent for compression, $pv^{\dot{m}_c} = \text{constant}$
m_e	Polytropic exponent for expansion, $pv^{\dot{m}_e} = \text{constant}$
mep	Mean-effective pressure, defined on p. C-6.
N	Crankshaft rotational speed
N_{cyl}	Number of cylinders
N_m, N_{max}	Crankshaft rotational speed at maximum power
p	Pressure of working fluid
P_{add}	Rate of heat addition to working fluid, $\dot{m}(f/a)(HV)$
P_{cx}	Energy transfer rate to working fluid during ideal compression
P_i	Rate of energy transport associated with working fluid, $\dot{m}_c T_1$, where T_1 is the minimum temperature of the working fluid in the cycle.
P_{int}	Internal power transfer, the energy transfer rate to the working fluid before combustion from the working fluid after combustion.
$P_{\text{loss,cx}}$	Effective power loss associated with compression and associated expansion processes.
$P_{\text{loss,i}}$	Effective power loss associated with mechanism i
P_m, P_o	Maximum power output
$P_{o,\text{ideal}}$	Maximum power output of an ideal cycle
Pr	Prandtl number, $c_p u / k$
Q_c	Heat transfer to the working fluid during the compression stroke

Q_e	Heat transfer to the working fluid during the expansion stroke
Q_s	Combustion heat release per unit mass of working fluid
r	Compression ratio; ratio of cylinder volume or specific volume of the working fluid at beginning of compression to that at end of compression.
R	Gas constant of the working fluid
Re	Cylinder Reynolds number, $\rho v D / \mu$, where v is the piston speed.
RON	Research octane number
s	Entropy of the working fluid
S	Piston stroke, the maximum length of travel of the piston; or material yield stress.
sfc	Specific fuel consumption, lb/hp-hr
S_s	Yield stress of steel
T	Temperature of the working fluid
\bar{T}	Average temperature of the working fluid during a stroke
TDC	Top dead center, the piston or piston crank angle at minimum cylinder volume
u	Internal energy per unit mass of working fluid
v	Specific volume of the working fluid
V	Cylinder volume at a given piston position
V_D	Total piston displacement, the swept volume per stroke of the piston in a cylinder times the number of cylinders.
W	Weight
W_{cx}	Weight per unit displacement associated with compression and expansion processes
W_{cx}	Weight associated with compression and expansion processes

Z_d	Engine weight fraction that depends upon displacement
Z_r	Engine weight fraction that depends upon cylinder pressure
γ	Ratio of specific heats of the working fluid
$\Delta\eta_{bd}$	Efficiency loss due to blowdown losses (see pp. C-31--35)
$\Delta\eta_c$	Efficiency loss due to combustion process (see pp. C-21--27)
$\Delta\eta_f$	Efficiency loss due to frictional effects (see pp. C-35--38)
$\Delta\eta_{rg}$	Efficiency loss due to real-gas effects (see pp. C-18--20)
$\Delta\eta_{th}$	Efficiency loss due to throttling (see pp. C-40--44)
ϵ	Heat-exchange effectiveness
η	Thermodynamic efficiency, work output/heat input
η_{HX}	Efficiency loss due to heat transfer (see pp. C-27--31)
η_i, η_{id}	Thermodynamic efficiency of an ideal cycle
θ_b	Crank angle position at exhaust-valve opening, in degrees before bottom dead center.
μ	Viscosity of working fluid
ρ	Density of working fluid
ϕ	Equivalence ratio, the actual fuel-air ratio divided by the stoichiometric fuel-air ratio.
ψ	Ratio of part-load bmep to fuel-load bmep
V	Engine volume

REFERENCES, APPENDIX C

- C-1. Jet Propulsion Laboratory, "Should We Have a New Engine?" JPL SP 43-17, Vol. 11, p. 3-23.
- C-2. C.F. Taylor and E.S. Taylor, The Internal Combustion Engine in Theory and Practice, The Technology Press and John Wiley and Sons, Inc., New York, 1960.
- C-3. National Academy of Sciences, Report of the Committee on Motor Vehicle Emissions, November 1974, p. 28.
- C-4. J. John, Lean Burn Engine Concepts--Emissions and Economy, SAE 750930, October 1975.
- C-5. E.F. Obert, Internal Combustion Engines, Intext Publishers, New York, 1973.
- C-6. Mitchell, Alperstein, Cobb, and Faist, A Stratified Charge Multifuel Military Engine, SAE 720051, January 1972.
- C-7. Aerospace Corporation, Research Plan for Achieving Reduced Automotive Energy Consumption, NSF/RA-760008, October 1975, p. 3-105.
- C-8. C. Jones, A Progress Report on Curtiss-Wright's Rotary Stratified Charge Engine Development, SAE 741206, October 1974.

In addition, the following companies furnished engine data that was useful in the preparation of this appendix:

- American Motors Corporation, Detroit, Michigan
- AVCO-Lycoming, Williamsport, Pennsylvania
- Chrysler Corporation, Industrial Products Division, Marysville, Michigan
- Ford Motor Company, Industrial Engine Operations, Detroit, Michigan
- International Harvester Company, Woodfield, Illinois
- Teledyne-Continental Motors, Mobile, Alabama.

ANNEX C1

REPRESENTATIVE GASOLINE ENGINES

ANNEX C1. REPRESENTATIVE GASOLINE ENGINES

Make	Model	No. of Cyl. N _{Cyl}	Type	Piston Disp. V _D (in. ³)	Comp. Ratio r	Max. Power P (hp)	Weight W (lb)	Volume V (ft. ³)	N (rpm)	V _D /N _{Cyl} (in. ³)	W/V _D (lb/in. ³)	P/V _D (hp/in. ³)	W/P (lb/hp)	V/P (in. ³ /hp)	BSFC (Full) (lb/hp-hr)	BSFC (1/4 L) (lb/hp-hr)	Bmep (psi)	Piston Speed (fpm)	Equiv. Ratio φ	Comments
AVCO	0-235K	04	AC	235	8.5	118	222	12.26	2800	58.8	0.94	0.5021	1.881	179.6	0.500	0.976	142.0	1808	1.100	
	0-320H	04	AC	319.8	9.0	160	283	14.92	2700	80.0	0.88	0.5003	1.769	161.2	0.500		146.8	1744		
	0-360A	04	AC	360	8.5	180	256	14.16	2700	90.0	0.71	0.5000	1.422	135.9	0.500		146.7	1969		
	0-540E	06	AC	540	8.5	260	369	17.65	2700	90.0	0.68	0.4915	1.419	117.3	0.500		141.2	1969		
TCM	0-200A	04	AC	201	7.0	100	218	8.31	2750	50.2	1.08	0.4975	2.180	143.6	0.575	0.740	143.3	1788	1.205	
	0-300D	06	AC	301	7.0	145	270	12.16	2700	50.2	0.90	0.4817	1.892	144.9	0.520	0.707	141.3	1746	1.095	
	0-470B	06	AC	471	8.0	240	409	16.50	2600	78.5	0.87	0.5096	1.704	118.8	0.520		155.2	1733		
	0-470J	06	AC	471	7.0	225	381	19.28	2550	78.5	0.81	0.4777	1.693	148.1	0.500		148.4	1700		
AVCO	10-320B	04	AC	320	8.5	160	259	12.05	2700	80.0	0.81	0.5000	1.619	130.1	0.500		146.7	1744		Fuel Inj.
	10-360A	04	AC	361	8.7	200	324	11.43	90.2	90.2	0.90	0.5540	1.620	98.78	0.500	0.784	162.5	1969	1.152	Fuel Inj.
	10-540K	06	AC	541.5	8.7	300	470	15.12	90.2	90.2	0.87	0.5540	1.567	87.11	0.500	0.872	162.5	1969	1.152	Fuel Inj.
	10-720A	08	AC	720	8.7	400	566	20.72	90.0	90.0	0.79	0.5556	1.415	89.53	0.500	0.854	166.0	1932		Fuel Inj.
TCM	10-346	04	AC	346	7.5	165	296	13.03		86.5	0.86	0.4769	1.794	136.4	0.480	0.580	139.9	1800		Fuel Inj.
	10-360	06	AC	360	8.5	210	298	15.25		60.0	0.83	0.5833	1.419	125.5	0.480	0.752	165.0	1808		Fuel Inj.
	10-470F	06	AC	471	8.6	260	465	17.20		78.5	0.99	0.5520	1.788	114.3	0.480	0.790	166.6	1750	1.171	Fuel Inj.
	10-520C	06	AC	520	8.5	285	450	16.45		86.7	0.87	0.5481	1.579	99.71	0.500	0.854	160.8	1800	1.181	Fuel Inj.
AVCO	T10-360	04	AC	360	7.3	200	355	17.81		90.0	0.99	0.5556	1.775	153.9	0.700	0.847	173.3	1878		Turbocharged
	T10-540J	06	AC	541.5	7.3	350	549	23.03		90.2	1.01	0.6464	1.569	113.7	0.700		198.8	1878		Turbocharged
	T510-360	06	AC	360	7.5	210	334	16.27		60.0	0.93	0.5833	1.590	133.9			165.0	1806		Turbocharged
	T510-470	06	AC	471	7.5	260	511	16.27		78.5	1.08	0.5520	1.965	108.1			168.2	1733		Turbocharged
TCM	T510-520N	06	AC	520	7.5	310	510	15.56		86.7	0.98	0.5962	1.645	86.72	0.570	0.862	174.9	1800	1.106	Turbocharged
	GTS10-520	06	AC	520	7.5	375	547	22.82		86.7	1.05	0.7212	1.459	105.2	0.680	0.948	168.0	2267		Gear Box
	6-285	06	AC	406	9.0	285	433			67.7	1.07	0.7020	1.519		0.545		139.0	2417	1.123	Geared
	6-320	06	AC	406	9.1	320	440			67.7	1.08	0.7882	1.375		0.580	0.938	141.9	2658	1.209	Geared
Chry	H225	16	Auto	225	8.4	112	520	12.03	3600	37.5	2.31	0.4978	4.685	185.6			109.5	2475		
	LH318	V8	Auto	318	8.8	173	646	11.89	4000	39.8	2.03	0.5440	3.734	118.8			107.7	2207		
	LH360	V8	Auto	360	9.0	197	672	11.74	4000	45.0	1.87	0.5472	3.411	103.0			108.4	2387		
	H400	V8	Ind	400	8.2	204	785	13.62	4000	50.0	1.96	0.5100	3.948	115.4			101.0	2253		
Ford	2000F	16	Ind	200	8.3	104	377	11.79	4000	33.3	1.89	0.5200	3.625	195.9			103.0	2083		
	2500F	16	Ind	250	8.0	108	472	14.42	3500	41.7	1.78	0.4320	4.370	230.7			97.76	2169		
	3000F	16	Ind	300	7.9	132	533	15.54	3600	50.0	1.78	0.4400	4.038	203.4			96.80	2231		
	3510P	V8	Auto	351	8.0	179	671	13.34	4500	43.9	1.91	0.5100	3.749	128.8	0.530		89.75	2625		
Ford	3600P	V8	Auto	360	8.0	180	722	18.42	3600	45.0	2.01	0.5000	4.011	176.9			110.00	2100		
	3900P	V8	Auto	390	8.2	193	728	18.42	3600	48.8	1.87	0.4949	3.792	165.0	0.510		108.9	2269		
	4600P	V8	Auto	460	8.0	257	868	14.28	4400	57.5	1.89	0.5587	3.377	96.02	0.585		100.6	2823		
	534F	V8	Ind	534	7.3	222	1138	28.39	3000	66.8	2.13	0.4157	5.126	221.0	0.540		109.8	2100		
AMC	232-6	16	Auto	232		103	520	11.14	3750	38.7	2.24	0.4440	5.049	187.0	0.610	1.146	93.77	2188		
	258-6	16	Auto	258		129	531	11.14	3800	43.0	2.06	0.5000	4.116	149.3	0.570	1.048	104.2	2467		
	304-8	V8	Auto	304	8.25	165	660	11.84	4400	38.0	2.17	0.5428	4.000	124.0	0.560	1.019	97.70	2523		
	360-8	V8	Auto	360	8.25	218	699	11.84	3880	45.0	1.94	0.6056	3.206	93.85	0.670	1.153	123.5	2637		
AMC	401-8	V8	Auto	401	8.49	253		11.84	4600	50.1	--	0.6309		80.86	0.590	1.019	108.6	2821		

Footnotes are at end of table.

(Continued)

ANNEX C1. REPRESENTATIVE GASOLINE ENGINES (Cont'd)

Make	Model	No. of Cyl.	Type	Piston Disp. V _D (in. ³)	Comp. Ratio r	Max. Power P (hp)	Weight W (lb)	Volume V (ft. ³)	N (rpm)	V _D /N _{cyl} (in. ³ /rpm)	W/V _D (lb/in. ³)	P/V _D (hp/in. ³)	W/P (lb/hp)	V/P (in. ³ /hp)	BSFC (Full) (lb/hp-hr)	BSFC (1/4 L) (lb/hp-hr)	Bmep (psi)	Piston Speed (rpm)	Equiv. Ratio ϕ	Comments
IHC	C-345	V8	Ind	344.9	8.05	160	809	14.22	3000	43.1	2.35	0.4639	5.056	153.6	0.505		122.5	1828		
	C-392	V8	Ind	390.9	8.02	180	818	14.22	3000	48.9	2.09	0.4605	4.544	136.5	0.500		121.6	1828		
	C-446	V8	Ind	446.8	8.0	255	849	21.71	3800	55.8	1.90	0.5707	3.325	147.1	0.450		141.3	2229		
	C-537	V8	Ind	537.6	7.5	258	1141	27.98	3200	67.2	2.12	0.4799	4.422	187.4	0.533		118.8	2133		
MCC	4318A	04	AC	100	7.8	92	77	6.563		25.0	0.77	0.9200	0.837	123.3	0.900		89.82	2135		2-stroke
	6318K	06	AC	150	7.8	145	114	5.403		25.0	0.76	0.9667	0.786	64.4	0.850		93.37	2135		2-stroke
Ne1	H-63P	04	AC	63	8.0	48	68	4.077		15.8	1.08	0.7619	1.417	146.8	1.020		68.57	1742		2-stroke
CW	RC2-60-US	Rot	AC	120 ^b		185	285	4.93		60.0 ^c	0.79 ^d	1.542	1.541	46.02	0.600		122.1			Rotary-Lig.
	RC1-60	Rot	AC	60	8.5	155	284	8.00		60.0	1.58	2.583	1.832		0.570		146.1			Rotary-Lig.
	RC2-75	Rot	AC	150		330	352	9.26		75.0	0.78	2.200	1.067	48.48	0.530		145.2			Rotary-Lig.
	RC2-90-Y2	Rot	AC	180		310	407	14.08		90.0	0.75	1.722	1.313	78.50			113.7			Rotary-Lig.
Mazda	R100	Rot	Auto	60	9.4	110	297			60.0	1.65				0.600		103.7			Rotary-Lig.
	RK-2	Rot	Auto	70	9.4	116				70.0					0.635		109.4			Rotary-Lig.
Texasco	L-141	I4	Auto	141.5	10.0	56	403	9.08		35.4	2.85	0.3958	7.196	280.2	0.540		104	1500		TCCS-LB
	L-141 Std	I4	Auto	141.5	7.5	62	356	7.66		35.4	2.52	0.4382	5.742	213.6	0.620		115.1	1500		Std.

^aWeights do not include radiator, coolant, or oil.

^bBy convention, the piston displacement per rotor of a rotary engine is defined as the displacement of one element of a three-element rotor.

^cThe equivalent of displacement per cylinder for a rotary engine is defined here as the displacement of one element of a three-element rotor.

^dFor purposes of a reasonable comparison with reciprocating engines, the displacement used as a base for weight per unit displacement is the total displacement of all elements of all rotors.

APPENDIX D

SIZE AND SPECIFIC FUEL RELATIONSHIPS FOR DIESEL ENGINES

P.C.T. de Boer

CONTENTS

A.	Ideal Engine Performance	D-3
1.	The Ideal Cycles	D-3
a.	The Ideal Diesel Cycle	D-3
b.	Other Ideal Cycles	D-4
2.	Ideal Cycle Performance	D-9
a.	Ideal Gas, Standard Diesel Cycle	D-10
b.	Supercharged Diesel Cycle	D-11
c.	Turbocharged Diesel Cycle	D-15
d.	Compound Diesel Cycle	D-18
3.	Implications of Ideal-Cycle Results	D-19
B.	Relationship of Actual Performance to Ideal Performance	D-22
1.	Loss Mechanisms	D-22
a.	Real Gas Effects	D-22
b.	Friction and Flow Losses	D-23
c.	Internal Losses	D-26
2.	Impact of Losses on Performance	D-27
C.	Overall Engine Considerations	D-29
	References	D-35
	Annex D1--Increase of Specific Power Output by Supercharging	D-37
	Glossary	D-55

APPENDIX D
SIZE AND SPECIFIC FUEL RELATIONSHIPS FOR DIESEL ENGINES
P.C.T. de Boer

The performance of power plants can be characterized in many ways. Much attention has been given to such characterizations in the literature, including various well-known textbooks (e.g., Refs. D-1, D-2, D-3). However, the results available do not lend themselves conveniently to a technology assessment of advanced military propulsion concepts. It is the purpose of this appendix to outline methods by which such a technology assessment can be made with respect to Diesel engines.

A. IDEAL ENGINE PERFORMANCE

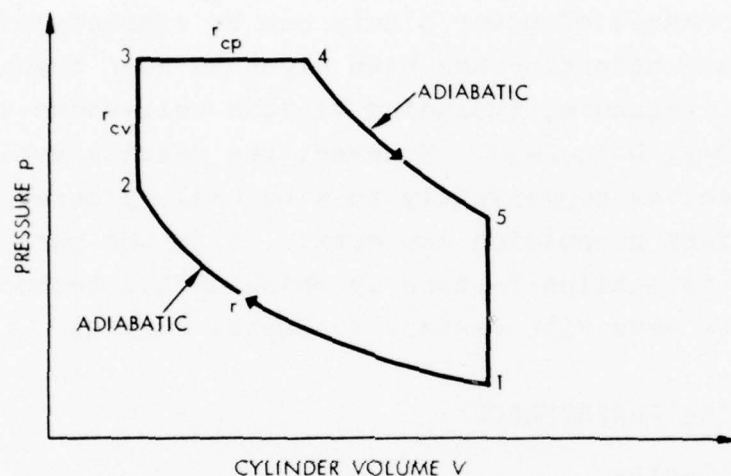
1. The Ideal Cycles

a. The Ideal Diesel Cycle. The well-known ideal-gas, standard Diesel cycle with limited-pressure combustion is shown in pressure-volume coordinates in Fig. D-1. It consists of four basic energy transfer processes:

1. Adiabatic compression (1-2)
2. Constant-volume combustion (2-3)
3. Constant-pressure combustion and power extraction (3-4)
4. Adiabatic expansion and power extraction (4-5).

Step 5-1 represents the exhaust process, which is taken to be cooling at constant volume in the ideal cycle. As indicated in Fig. D-1, the following conventional notation is introduced: compression ratio $r = V_1/V_2$, pressure ratio for constant-volume combustion $r_{cv} = p_3/p_2$, and volume ratio for constant-pressure

combustion $r_{cp} = V_4/V_3$. This cycle is usually referred to as the Diesel lp (limited-pressure) cycle, in contrast to the Diesel cp (constant-pressure) cycle. The latter is a special case of the former and obtains when $r_{cv} = 1$. The constant-pressure Diesel cycle is representative for the engine process in large, slowly running diesel engines.



9-30-77-8

FIGURE D-1. Ideal-gas, standard Diesel cycle (limited pressure). Compression ratio $r = V_1/V_2$, pressure ratio for constant-volume combustion $r_{cv} = p_3/p_2$, and volume ratio for constant-pressure combustion $r_{cp} = V_4/V_3$.

For a given fuel, the basic cycle parameters are the compression ratio, the fuel-air ratio, and either r_{cv} or r_{cp} . In terms of power transfers, in the context used in this report, the power required for compression is the internal power transfer, the rate of heat addition during combustion is the power added, and the difference between the power developed during combustion and expansion processes and that required for compression is the power output.

b. Other Ideal Cycles. As with the Otto cycle, major disadvantages of the Diesel cycle are associated with the size and

weight of the reciprocating machinery necessary to implement the cycle, and the relatively high energy content of the exhaust cycle. Variations of the basic cycle have accordingly been devised to alleviate these disadvantages, and three such cycles are considered here: the supercharged Diesel cycle, the turbocharged Diesel cycle, and the compound Diesel cycle.

The ideal supercharged Diesel cycle is shown in pressure-volume coordinates in Fig. D-2. The cycle 1-2-3-4-5 is identical to the standard Diesel cycle, and is augmented by adiabatic compression ($a' - 1$) in a separate compressor, transfer of gas from the compressor to the engine ($1 - c$ and $c - 1$), expansion of the remaining gas in the compressor ($c - b'$) and engine ($1 - a$), and inducting gas into the compressor ($b' - a'$) and expelling the gas in the engine ($a - b$). The principal intent of supercharging is that it increases the mass flow rate a given engine can handle--via the increase in density $\rho_1 - \rho_a$,--and hence tends to reduce the size of an engine required for a given power output. The basic cycle parameters are the overall compression ratio (V_a/V_2), the supercharging compression ratio (V_a/V_1), and the fuel-air ratio. The internal power transfer is that required for the entire compression process ($a' - 2$), and the power output is the total expansion power (3-4-5) plus the power developed by the engine intake and exhaust processes ($a-b-c-1$), less the power input to the supercharger ($a'-1-c-b'$) and the internal power transfer.

The ideal turbocharged Diesel cycle is shown in Fig. D-3. Again, the cycle 1-2-3-4-5 is identical to the standard Diesel cycle and is augmented by further expanding the exhaust gases (6-7) and using the power so generated to compress the intake air (0-1). The intent of turbocharging is again to increase the mass flow rate capabilities of a given engine and simultaneously to use the energy of the exhaust gases to effect the precompression. The basic cycle parameters are the overall compression ratio (v_0/v_2), the turbocharging compression ratio

(v_0/v_1) or pressure ratio (p_1/p_0), and the fuel-air ratio. The internal power transfer is that of the total compression process (0-2), and the power output is the power of the total expansion process (4-7) plus that developed by the engine intake and exhaust processes (6'-1), less the internal power transfer.

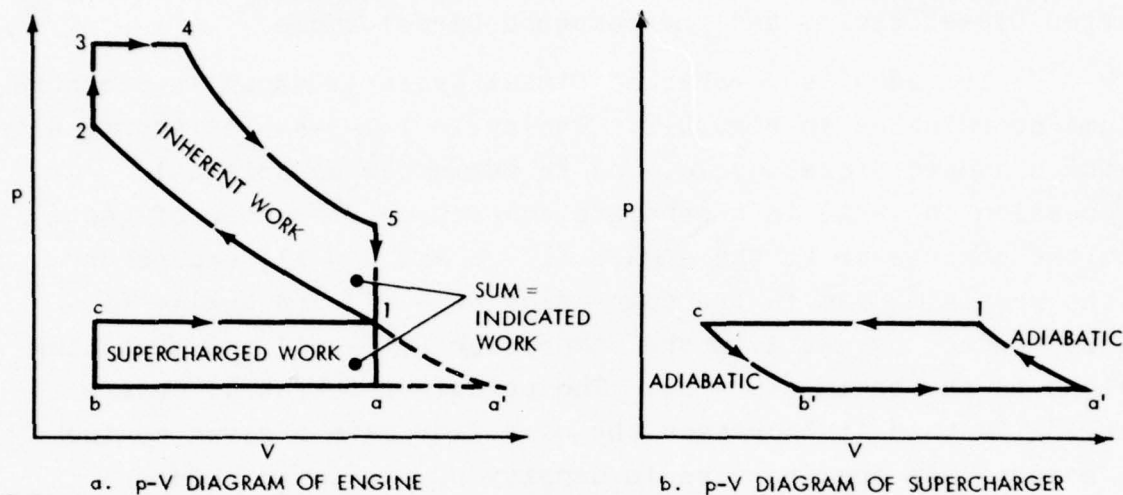
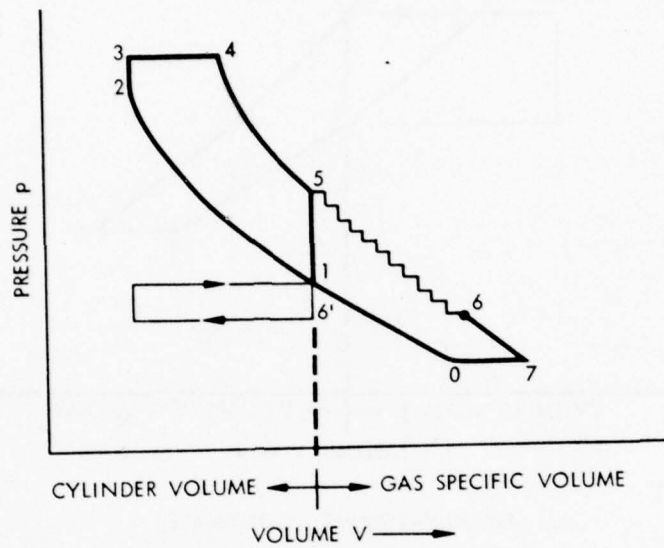


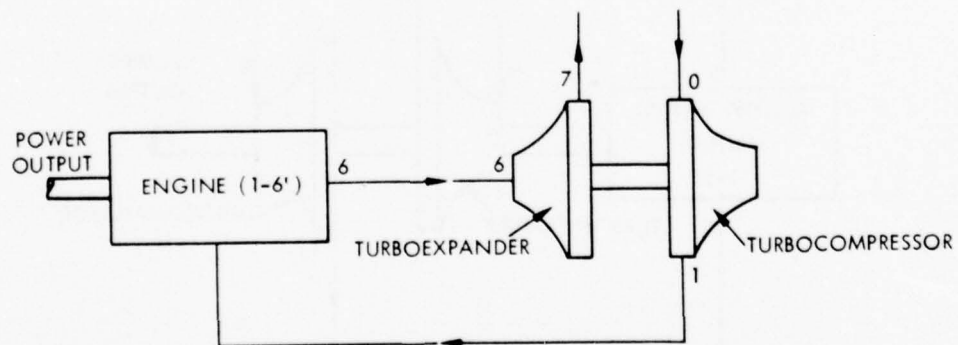
FIGURE D-2. Ideal-gas, standard supercharged Diesel cycle.

The ideal compound Diesel cycle is shown in Fig. D-4. The processes 1-2-3-4-5 are identical to those of the standard Diesel cycle; at point 5, however, the cylinder gases are transferred to a continuous-flow expander that expands the gases to their initial pressure (5-6),* and some of the power so derived is used to compress the intake air (0-1). Shaft power output may be obtained totally or partially from the turboexpander. The intent of the compound cycle is to utilize the maximum possible amount of the exhaust-gas energy of the diesel-cycle portion and simultaneously to achieve the reduced-size benefits of turbocharging. The basic cycle parameters are the overall

*For all of the cylinder gases to be (ideally) transferred without loss to a continuous-flow expander, it would be necessary for the cylinder exhaust stroke (the horizontal line originating at point 5 in Fig. D-4) to continue to zero volume.



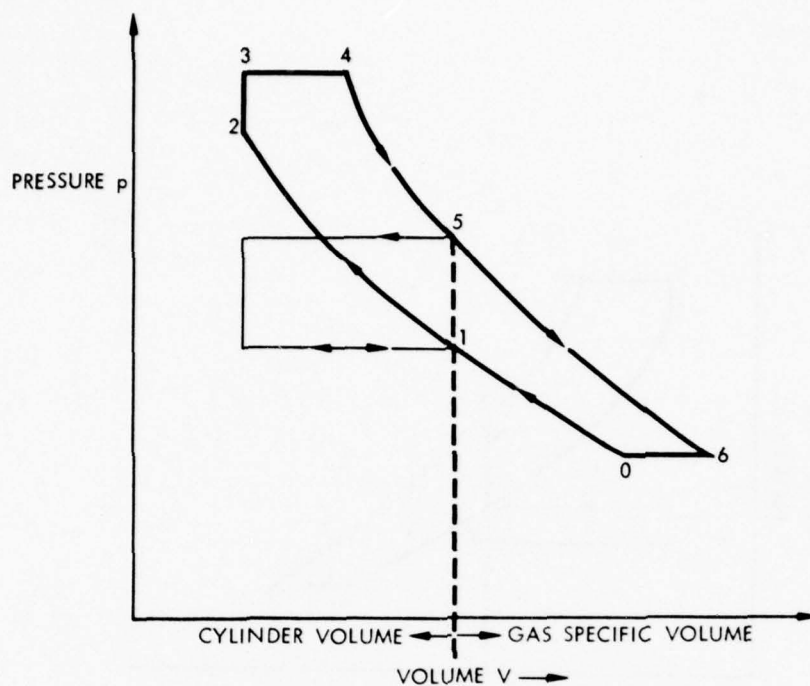
a. PRESSURE-VOLUME COORDINATES



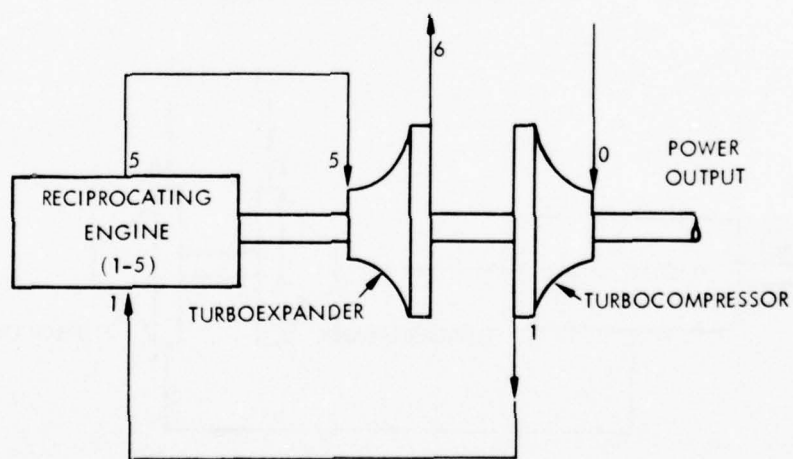
b. SCHEMATIC ARRANGEMENT

9-30-77-10

FIGURE D-3. Ideal turbocharged Diesel cycle.



a. PRESSURE-VOLUME COORDINATES



b. SCHEMATIC ARRANGEMENT

9-30-77-11

FIGURE D-4. Ideal compound Diesel cycle.

compression ratio (v_o/v_2), the intake air compression ratio (v_o/v_1) or pressure ratio (p_1/p_o), and the fuel-air ratio. The internal power transfer is that required for the compression process (0-2), and the power output is that developed during expansion (4-6) less both the power consumed by the intake and exhaust processes (5-1) and the internal power transfer.

2. Ideal Cycle Performance

Conventionally, as with Otto engines, the performance of Diesel cycles is expressed in terms of thermodynamic efficiency and mean effective pressure. For purposes of comparison with other engine cycles, it is convenient to express performance in terms of specific fuel consumption and a normalized power output per unit mass flow; for a fuel with a lower heating value of 18,400 Btu/lbm and a working fluid with constant specific heats, the interrelationships are identical to those for the Otto cycle:

$$sfc = \frac{0.138}{\eta} \quad (D-1)$$

and

$$\text{Specific Power} \equiv \frac{P_o}{P_i} \equiv \frac{P_o}{\dot{m} c_p T_1} = \frac{(mep)}{\left(\frac{\rho_c}{\rho_1}\right) p_1} \left(\frac{r_c^{-1}}{r_c}\right) \left(\frac{\gamma-1}{\gamma}\right) \quad , \quad (D-2)$$

where sfc = specific fuel consumption, lbm/hp-hr

η = thermodynamic efficiency

P_o = output power

P_i = rate of energy transport associated with the working fluid at inlet conditions ($= \dot{m} c_p T_1$)

\dot{m} = mass flow rate

c_p = specific heat at constant pressure

T_1 = working fluid temperature at machine inlet

mep = mean effective pressure

ρ_c = density of working fluid at beginning of compression
in displacement volume

ρ_1 = density of working fluid at machine inlet

r = compression ratio of displacement volume

p_1 = pressure of working fluid at machine inlet

γ = ratio of specific heats.

a. Ideal Gas, Standard Diesel Cycle. For the ideal Diesel cycle (Fig. D-1), with a working gas with constant specific heats, the performance characteristics are given by

$$\eta = \frac{0.138}{\text{sfc}} = 1 - \frac{r_{cp}^{\gamma} r_{cv} - 1}{r^{\gamma-1} [r_{cv} - 1 + \gamma r_{cv} (r_{cp} - 1)]} \quad (\text{D-3})$$

and

$$\frac{P_o}{P_i} = \frac{r^{\gamma-1}}{\gamma} [r_{cv} - 1 + \gamma r_{cv} (r_{cp} - 1)] - \frac{1}{\gamma} (r_{cp}^{\gamma} r_{cv} - 1) \quad (\text{D-4})$$

The power transfer parameters can also be expressed in terms of the three ratios r , r_{cv} , r_{cp} :

$$\frac{P_{int}}{P_i} = \frac{1}{\gamma} (r^{\gamma-1} - 1) \quad (\text{D-5})$$

$$\frac{P_{add}}{P_i} = \frac{r^{\gamma-1}}{\gamma} [r_{cv} - 1 + \gamma r_{cv} (r_{cp} - 1)] \quad , \quad (\text{D-6})$$

where P_{int} = internal power transfer = $\dot{m}c_v(T_2 - T_1)$

P_{add} = rate of heat addition = $\dot{m}\phi f_s(HV)$

ϕ = equivalence ratio

f_s = stoichiometric fuel/air ratio

HV = fuel lower heating value.

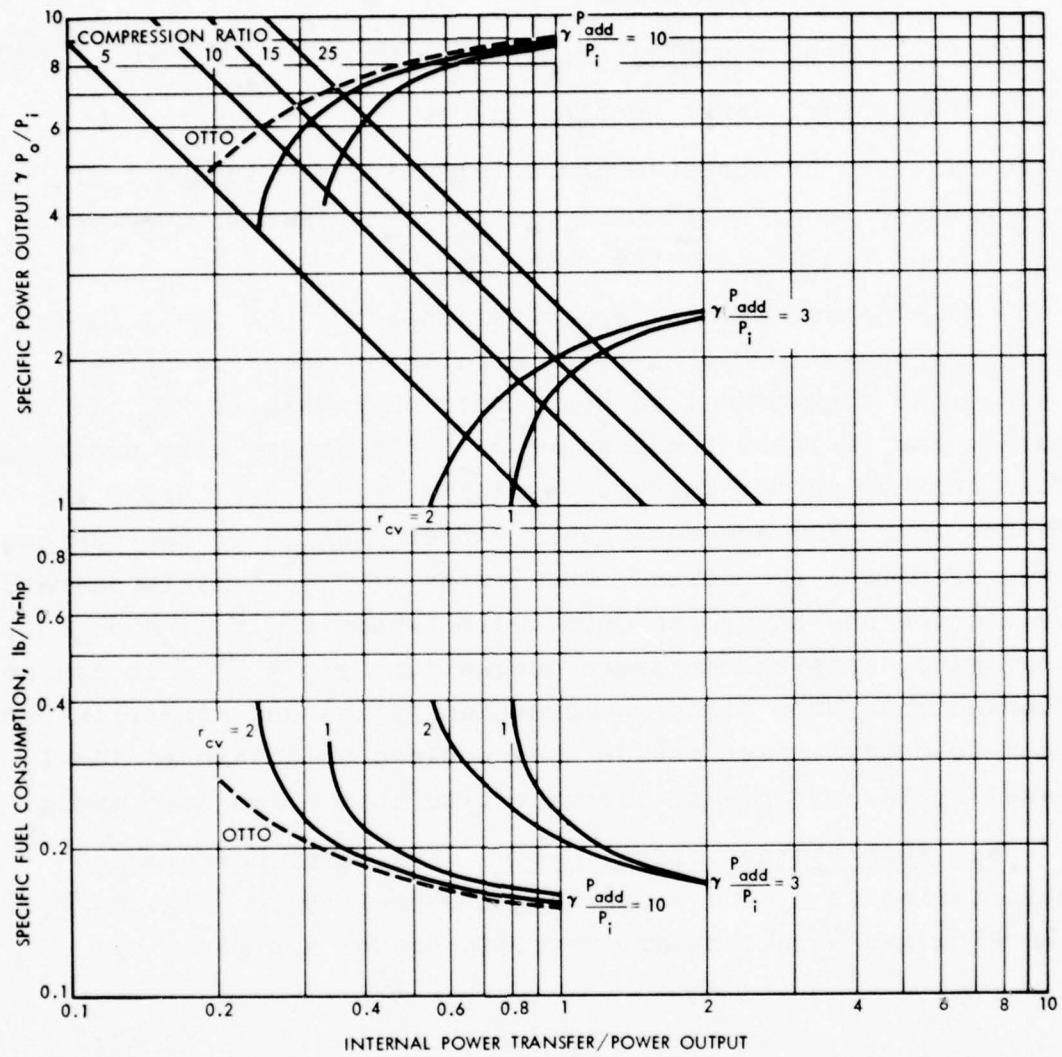
Obviously, the performance characteristics of sfc and P_o/P_i can be expressed as a function of the energy transfer parameters P_{int}/P_o and P_{add}/P_i and the ratio r_{cv} .

The performance characteristics of the ideal Diesel cycle are shown in Fig. D-5 for a ratio of specific heats $\gamma = 1.4$ and for normalized heat addition rates, $\gamma P_o/P_i$, of 10 and 3. For an inlet temperature of 520°R, these heat addition rates correspond to equivalence ratios, ϕ , of 0.73 and 0.22, respectively, and are reasonably representative of the current range of Diesel operation. The limits of Diesel cycle operation are, on the one hand, the Otto cycle (where $r_{cp} = 1$) and, on the other hand, constant-pressure combustion ($r_{cv} = 1$). It can be observed that both higher compression ratios and higher internal-power-to-output-power ratios are required to obtain an ideal Diesel cycle performance equivalent to that of an Otto cycle.

b. Supercharged Diesel Cycle. The ideal performance characteristics of the supercharged Diesel cycle (Fig. D-2), for a working gas with constant specific heats, are given by

$$\eta = 1 - \frac{1}{\gamma^{\gamma-1}} \left\{ \frac{r_{cp}^{\gamma} r_{cv}^{\gamma} - 1 - (1-1/r) \left[(\gamma-1)(1-1/r_s) - \gamma \left(1 - r_s^{-\frac{\gamma-1}{\gamma}} \right) \right]}{r_{cv} - 1 + \gamma r_{cv} (r_{cp} - 1)} \right\} \quad (D-7)$$

and



9-30-77-12

FIGURE D-5. Performance characteristics of the ideal-gas, standard Diesel cycle.

$$\frac{P_o}{P_i} = \frac{r_s^{-\frac{\gamma-1}{\gamma}}}{\gamma} \left\{ 1 - r_{cp}^{\gamma} r_{cv} + r^{\gamma-1} [r_{cv}^{-1} + \gamma r_{cv} (r_{cp} - 1)] \right. \\ \left. + \left(1 - \frac{1}{r}\right) \left[(\gamma-1) \left(1 - \frac{1}{r_s}\right) - \gamma \left(1 - r_s^{-\frac{\gamma-1}{\gamma}}\right) \right] \right\}, \quad (D-8)$$

where r = engine compression ratio (V_1/V_2 in Fig. D-2)

r_s = supercharging pressure ratio (p_1/p_a)

r_o = overall compression ratio (v_a/v_2) = $rr_s^{1/\gamma}$.

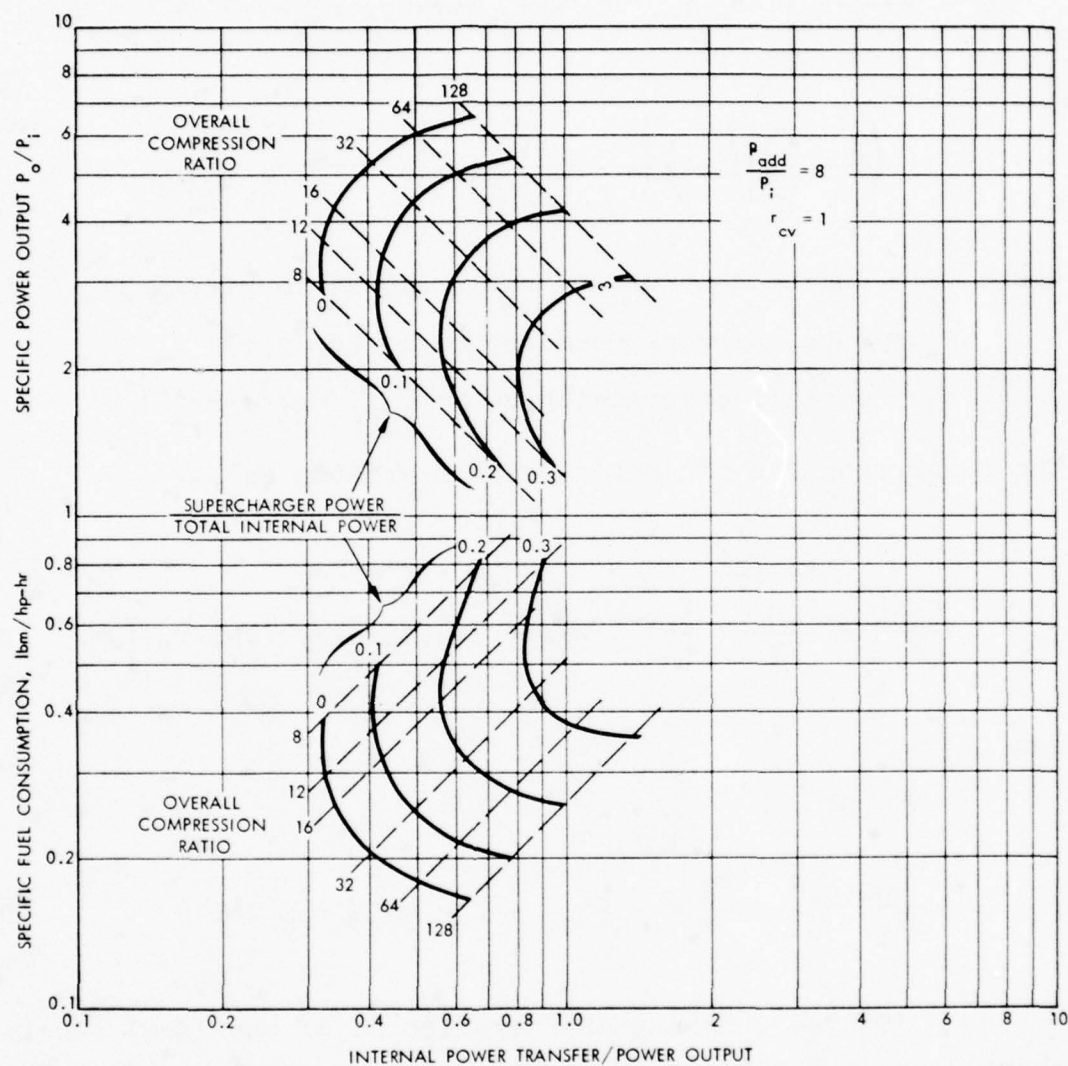
The power transfer parameters can be written as

$$\frac{P_{int}}{P_i} = \frac{r_s^{-\frac{\gamma-1}{\gamma}}}{\gamma} \left[r^{\gamma-1} - 1 + (\gamma-1)(1-1/r)(1-1/r_s) \right] \quad (D-9)$$

and

$$\frac{P_{add}}{P_i} = \frac{r^{\gamma-1} r_s^{-\frac{\gamma-1}{\gamma}}}{\gamma} [r_{cv} - 1 + \gamma r_{cv} (r_{cp} - 1)] \quad (D-10)$$

The performance characteristics of the ideal supercharged cycle are shown in Fig. D-6 for constant-pressure combustion ($r_{cv} = 1$) and $\gamma = 1.4$. The amount of supercharging is expressed in terms of the fraction of the total internal power transfer [$\dot{m}c_v(T_2 - T_a)$ in Fig. D-2] used to supercharge [$\dot{m}c_v(T_1 - T_a)$]. This fraction, F , is related to the overall compression ratio r_o and supercharging pressure ratio r_s by



9-30-77-13

FIGURE D-6. Performance characteristics of the ideal supercharged Diesel cycle.

$$F = \frac{r_s^{\frac{\gamma-1}{\gamma}} - 1}{r_o^{\gamma-1} - 1}$$

It is apparent from Fig. D-6 that substantial sacrifices in both specific fuel consumption and specific power output are associated with supercharging. These sacrifices are of course evident from the cycle diagram in Fig. D-2: for fixed initial conditions (a'), overall compression ratio, and heat addition, supercharging results in an increase in the temperature of the exhaust gases (5), and hence higher specific fuel consumption and lower specific output (see also Ref. D-1, Section 6.4). The impact of supercharging on the mass flow rate capability of the engine portion can be determined from the power output per unit volume flow at engine inlet, for a fixed maximum cycle pressure:

$$Y_p \equiv \frac{P_o}{\left(\frac{\dot{m}}{\rho_1}\right)P_3} = \frac{\gamma r_s^{\frac{1}{\gamma}} (P_o/P_i)}{(\gamma-1)r_o^{\gamma} r_{cv}} \quad (D-11)$$

The dependence of this parameter on the various cycle parameters is considered in detail in Annex D1; it can be observed, however, that as the amount of supercharging (r_s) is increased for a fixed overall compression ratio, the parameter Y_p will increase until the decrease of P_o/P_i (in Fig. D-6) with r_s exceeds the increase in $r_s^{1/\gamma}$.*

c. Turbocharged Diesel Cycle. The ideal performance characteristics of the turbocharged Diesel cycle (Fig. D-3), for constant-pressure combustion ($r_{cv} = 1$) and for a working gas with constant specific heats, are given by

$$\eta = \frac{P_o/P_i}{P_{add}/P_i} \quad (D-12)$$

*The location of the detailed treatment in Annex D1 is not intended to minimize the practical importance of supercharging (or turbocharging); the basic tradeoff, however, is as stated here.

$$\frac{P_o}{P_i} = r_o^{\gamma-1} (r_{cp} - 1) - \frac{r_s^{\frac{\gamma-1}{\gamma}}}{\gamma} (r_{cp}^{\gamma} - 1) \quad (D-13)$$

$$+ \frac{\gamma-1}{\gamma} \left\{ r_s^{\frac{\gamma-1}{\gamma}} - \left[\left(T_5/T_6 \right) \left(r_s^{\frac{\gamma-1}{\gamma}} - 1 \right) \left(r_{cp}^{\gamma} \right) \right]^{\frac{\gamma-1}{\gamma}} \right\} ,$$

where

$$\frac{P_{add}}{P_i} = r_o^{\gamma-1} (r_{cp} - 1) \quad (D-14)$$

r_o = overall compression ratio (v_o/v_2 in Fig. D-3)

r_s = supercharging pressure ratio,

and it has been assumed that the intake and exhaust strokes extend to zero clearance volume (which has little impact on the results). The temperature ratio T_5/T_6 varies between unity and γ , depending upon cycle parameters, and for simplicity it will be assumed to be unity here--an assumption which also has little impact on the results. The internal power transfer is given by

$$\frac{P_{int}}{P_i} = \frac{1}{\gamma} \left(r_o^{\gamma-1} - r_s^{\frac{\gamma-1}{\gamma}} \right) + \left(r_s^{\frac{\gamma-1}{\gamma}} - 1 \right) . \quad (D-15)$$

The performance characteristics of the ideal turbocharged cycle are shown in Fig. D-7. The amount of turbocharging is again expressed in terms of the fraction of total internal power transfer $[\dot{m}c_p(T_1 - T_0) + \dot{m}c_v(T_2 - T_1)]$ in Fig. D-3] transmitted by the turbocharger $[\dot{m}c_p(T_1 - T_0)]$. This fraction, F , is given by

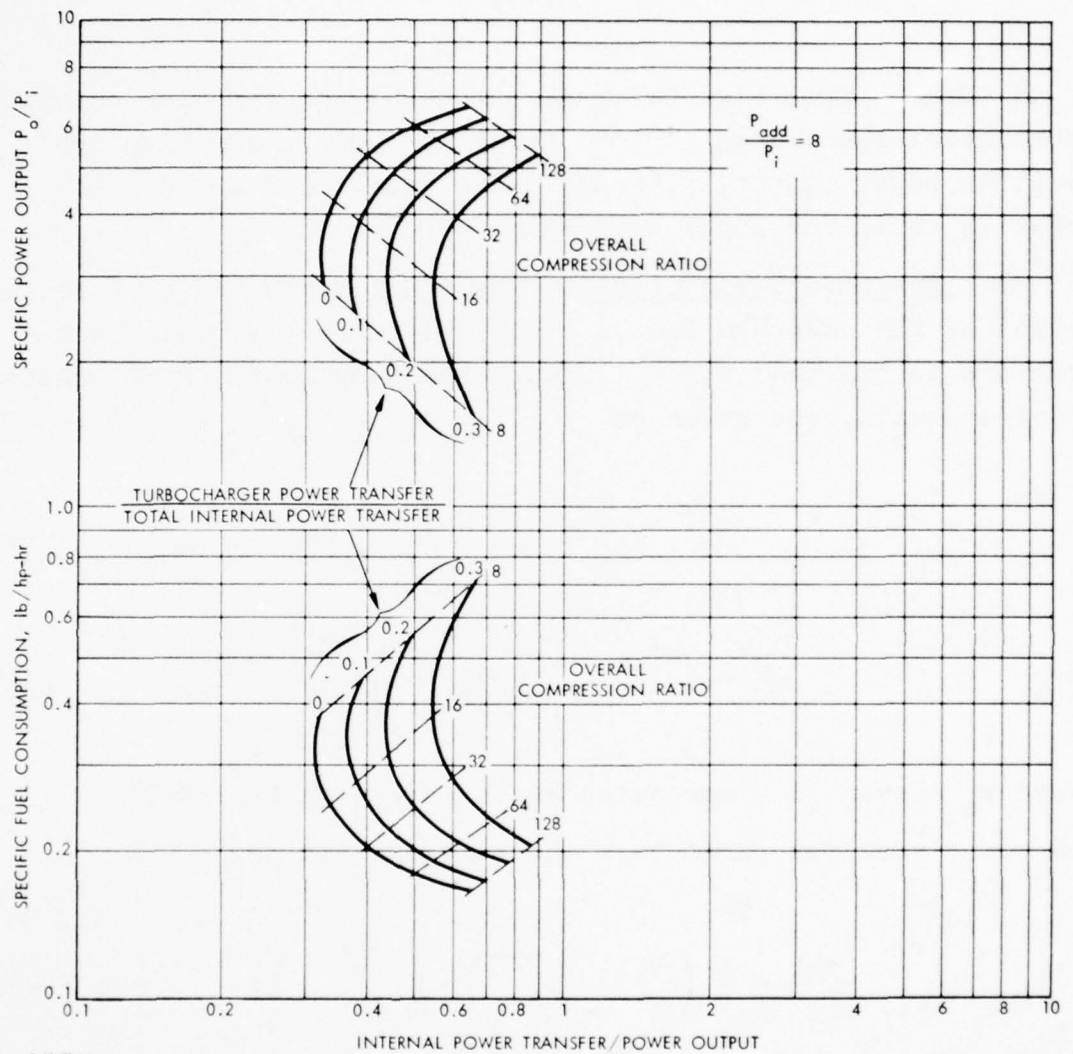


FIGURE D-7. Performance of ideal turbocharged constant-pressure Diesel cycle.

$$F = \frac{\gamma \left(r_s^{\frac{\gamma-1}{\gamma}} - 1 \right)}{r_o^{\gamma-1} - r_s^{\frac{\gamma-1}{\gamma}} + \gamma \left(r_s^{\frac{\gamma-1}{\gamma}} - 1 \right)} .$$

It is evident from Fig. D-7 that turbocharging can also entail substantial sacrifices in both specific fuel consumption and specific power output, although these sacrifices are not as great as those for supercharging.

d. Compound Diesel Cycle. The ideal performance characteristics of the compound Diesel cycle (Fig. D-4), for constant-pressure combustion ($r_{cv} = 1$) and for a working gas with constant specific heats, are given by

$$\eta = 1 - \frac{1}{r_o^{\gamma-1}} \quad (D-16)$$

$$\frac{P_o}{P_i} = \left(r_o^{\gamma-1} - 1 \right) \left(r_{cp} - 1 \right) , \quad (D-17)$$

where r_o = overall compression ratio (v_2/v_o in Fig. D-4).

The power transfer parameters can be expressed as

$$\frac{P_{int}}{P_i} = \frac{1}{\gamma} \left(r_o^{\gamma-1} - r_s^{\frac{\gamma-1}{\gamma}} \right) + \left(r_s^{\frac{\gamma-1}{\gamma}} - 1 \right) \quad (D-18)$$

and

$$\frac{P_{add}}{P_i} = r_o^{\gamma-1} (r_{cp} - 1) , \quad (D-19)$$

where r_s is the pressure ratio pertaining to the precompression process (0-1 in Fig. D-4).

The performance characteristics of the compound Diesel cycle are shown in Fig. D-8. The amount of precompression is again expressed in terms of the fraction of total internal power transfer $[\dot{m}c_p(T_1 - T_0) + \dot{m}c_v(T_2 - T_1)]$ in Fig. D-4 consumed by the precompression $[\dot{m}c_p(T_1 - T_0)]$. This fraction is related to the overall compression ratio and the precompression pressure ratio in identically the same way as for the ideal turbocharged cycle. It can be observed from Fig. D-8 that the ideal performance of the cycle (1) is superior to the standard Diesel cycle (compare with the zero-turbocharging case in Fig. D-7), (2) has a specific fuel consumption that depends only upon overall compression ratio (from Eq. D-16), and (3) has a performance which is relatively insensitive to the amount of precompression--only the internal power transfer increases slightly as the amount of precompression is increased.

The influence of the pressure rise during combustion (r_{cv}) is shown in Fig. D-9 for the special case of zero precompression. As might be anticipated, the results for $r_{cv} = 1$ are identical to the results for the conventional Otto cycle.

3. Implications of Ideal-Cycle Results

In this section, the results obtained for the various ideal cycles are summarized. Also, their implications for possible improvements in power output and specific fuel consumption are briefly discussed.

First of all, it can be seen from Fig. D-5 that the standard Diesel cycle gives best results for both specific power output, P_o/P_i , and specific fuel consumption, sfc, when the internal power transfer P_{int}/P_o is large (≥ 1 , say). The largest power outputs are obtained when the specific heat addition P_{add}/P_i is large. It is interesting that these correspond to the lowest sfc. For

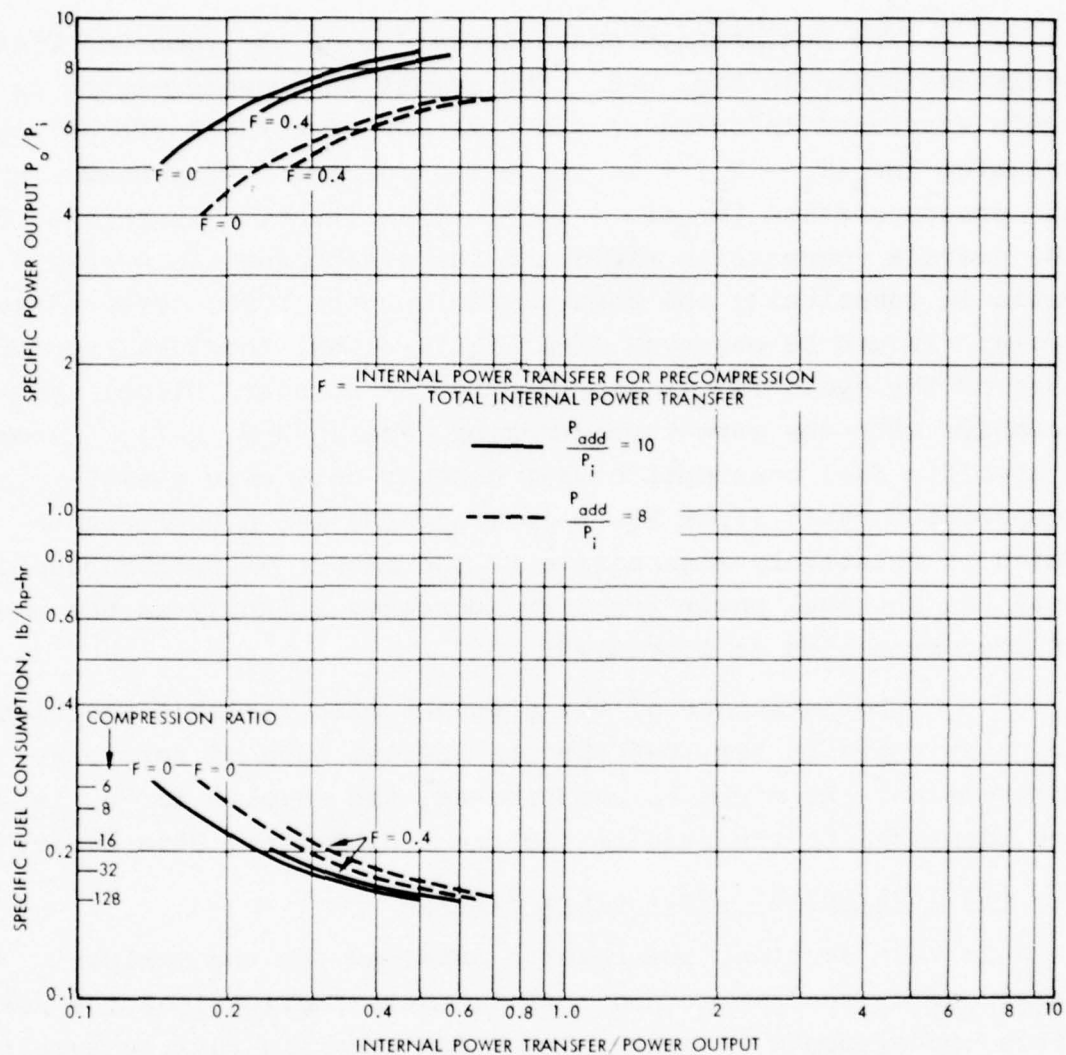


FIGURE D-8. Performance of ideal, compound, constant-pressure Diesel cycle.

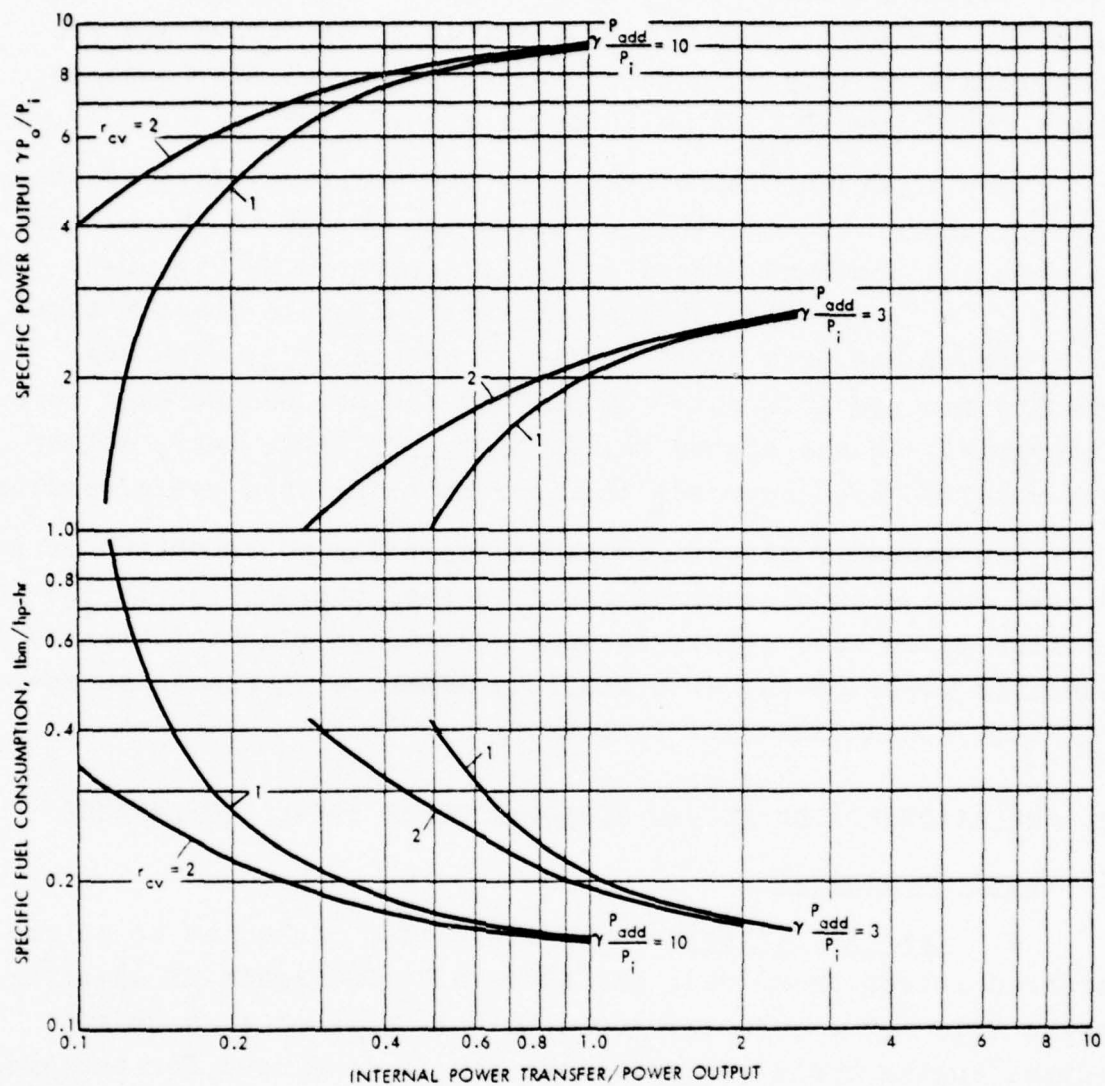


FIGURE D-9. Influence of pressure rise during combustion on compound Diesel cycle with no precompression.

$\gamma P_{\text{add}}/P_1 = 10$ and $P_{\text{int}}/P_o \geq 0.5$, the results for P_o/P_1 and sfc are very close to those for the Otto cycle, even though the specific power output parameter, Y_p , is much larger for the Diesel cycle than for the Otto cycle. Both specific power output and sfc deteriorate rapidly when the internal power transfer becomes small (≤ 0.5 for $\gamma P_{\text{add}}/P_1 = 10$ or ≤ 1 for $\gamma P_{\text{add}}/P_1 = 3$).

Very important improvements at the smaller values of internal power transfer are obtained by using the energy in the exhaust gas via the compound Diesel cycle, illustrated by Fig. D-8. For $r_{\text{cv}} = r_s = 1$, the results for the compound cycle are identical to those of the Otto cycle. With increasing r_{cv} , both the results for specific power output and for sfc become even more favorable. At the higher values of P_{int}/P_1 (≥ 1 , say), all of the results shown approach the corresponding Otto cycle results.

The tradeoff between increased specific power output of a Diesel engine and increased specific fuel consumption is investigated in some detail in Annex D1. Significant increases in specific power output with small to moderate increases in specific fuel consumption are indicated.

B. RELATIONSHIP OF ACTUAL PERFORMANCE TO IDEAL PERFORMANCE

1. Loss Mechanisms

a. Real Gas Effects. The first loss mechanism to be considered arises from "real gas effects." The ratio of specific heats γ is not a constant equal to 1.4 for each step of an actual engine cycle. Expressions can be developed for the cycle characteristics of interest, assuming that γ is different for each of the steps of the cycle, but constant during any step. A better assessment of the influence of "real gas effects" can be obtained by using combustion charts. For the standard Diesel cycle, this was done for $\gamma P_{\text{add}}/P_1 = 3$ by using Chart A of Ref. D-1, which is a combustion diagram for low fuel-air ratios of n-dodecane and air. For $\gamma P_{\text{add}}/P_1 = 10$, use was made of Chart C

of Ref. D-1, which is a chart of equilibrium properties of products of combustion of an iso-octane-air mixture with $\phi = 0.8$. The products of n-dodecane and air are not much different from those of iso-octane and air, for the same ϕ . The results were corrected to $\phi = 0.73$ ($\gamma P_{\text{add}}/P_1 = 10$) by noting that P_{int} and P_1 are independent of ϕ , while P_o is approximately proportional to ϕ . Hence the result obtained for P_o/P_1 was decreased by a factor $0.8/0.73$, while the value of P_{int}/P_o was increased by the same factor. These changes leave the result for sfc unaffected.

The results obtained from the ideal fuel-air cycle using combustion charts as described are included in Fig. D-10. It is seen that real gas effects cause an appreciable deviation from the ideal cycle results with $\gamma = 1.4$, even at mixtures as lean as $\phi = 0.22$ ($\gamma P_{\text{add}}/P_1 = 3$). This is caused mostly by a decrease of γ during the constant-pressure combustion process and during the expansion process. At low values of ϕ , the decrease in γ is not as pronounced as at high values of ϕ . On the other hand, the difference between expansion work and compression work is less at low values of ϕ , and a given decrease in expansion work has a relatively larger effect.

b. Friction and Flow Losses. The main mechanisms responsible for further power losses in Diesel engines are: (1) frictional losses in the engine, (2) flow losses, (3) losses arising from a finite combustion time, and (4) heat transfer to the walls of the cylinder and to the piston head during the combustion and expansion processes. Items (1) and (2) constitute the difference between IMEP (indicated mean effective pressure) and BMEP (brake mean effective pressure). This difference is denoted by FMEP (friction mean effective pressure). A detailed procedure to estimate the FMEP of both Diesel and Otto engines has been described by Bishop (Ref. D-4). This procedure involves the solution of 25 equations, with the final result representing the sum of friction losses in pumps, cam gear, and bearings and miscellaneous friction losses; valve pumping losses; throttle

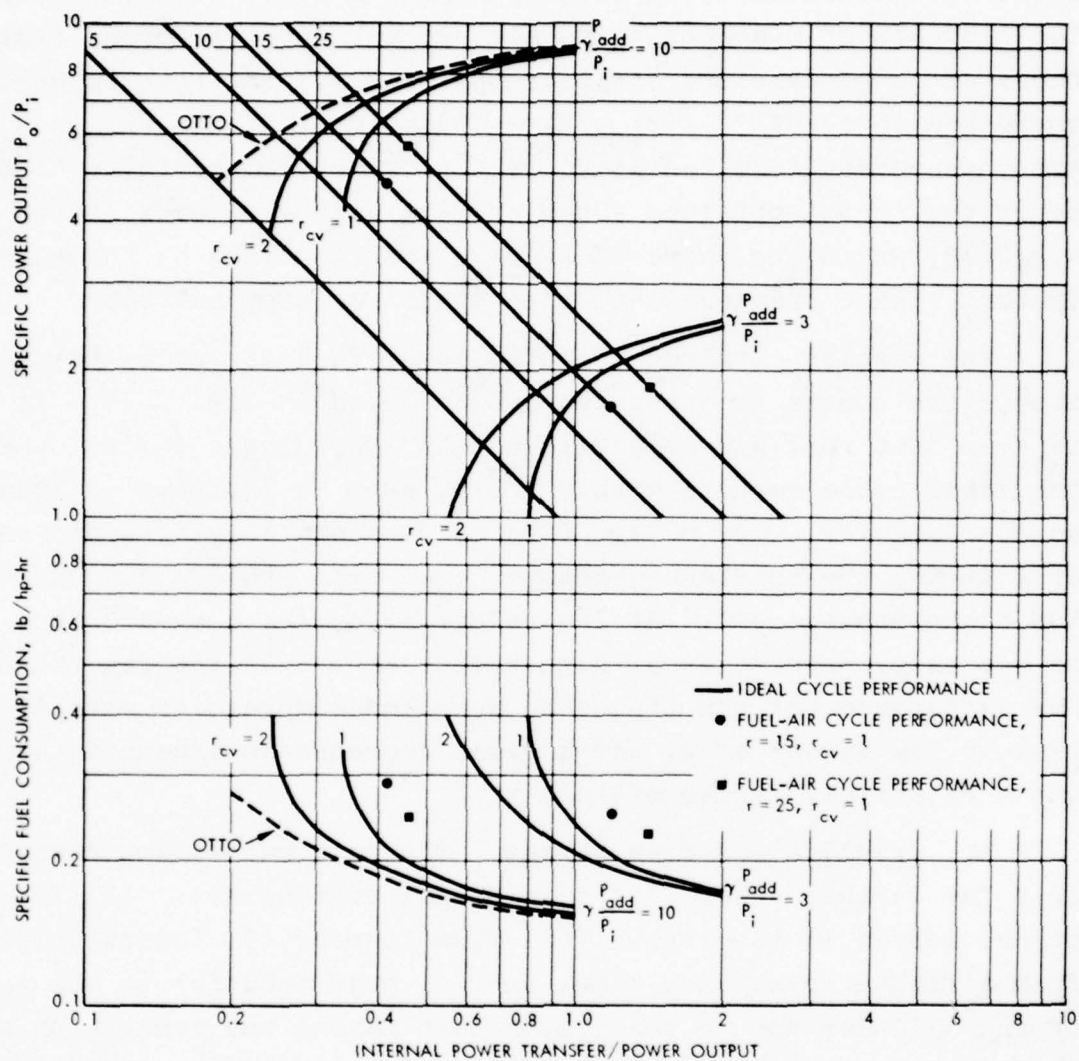


FIGURE D-10. Impact of real gas effects on performance of standard Diesel cycle.

losses; blowby losses; viscous piston losses; static ring tension losses; ring gas pressure losses; and prechamber losses. Bishop's procedure is quite suitable for present purposes. It was used to find FMEP and hence friction and flow losses for the four specific conditions of Fig. D-10, and representative values were employed for the many parameters involved (Table D-1).

The scaling laws for friction and flow losses follow directly from the equations presented in Ref. D-4. As can be seen from the numbers given in Table D-1, about half of the total FMEP losses consist of valve pumping losses; these scale as $N^{1.7}$, where N is the number of revolutions per minute. The dependence on N of the remaining losses contributing to FMEP is much weaker. It is possible to use these facts for constructing a simplified scaling law for dependence on engine speed.

TABLE D-1. ESTIMATION OF FMEP USING BISHOP'S PROCEDURE^a

Loss Source	FMEP (psi) ^b		Remarks
	$r = 15$	$r = 25$	
Crankcase	5.0	5.0	$\propto N$
Valve pumping	4.0	4.0	$\propto N^{1.7}$
Throttle	0.9	0.9	
Blowby	3.5	4.3	Decreases with N
Viscous piston	7.3	7.3	$\propto N$
Static ring tension	1.6	1.6	
Ring gas pressure	<u>3.4</u>	<u>6.1</u>	Decreases with N
Total FMEP	25.7	29.2	

^aSource: Ref. D-4.

^bIn making the estimation, the following values were substituted in Eqs. 1-25 on page 343 of Ref. D-4: $N = 2000$ rpm; intake valves per cylinder $G = 1$; intake valve head diameter $H = 2$ in.; cylinder bore diameter $B =$ piston stroke $S = 4$ in.; number of cylinders $C = 8$; displacement $D = (\pi/4)B^2 S = 402$ in³; firing exhaust back pressure at full load $p_e = 10$ psig; equivalent length of piston skirt $M = 2$ in.; total number of piston rings per cylinder $n = 3$; absence of prechamber, so that $R = 0$.

c. Internal Losses. The effect of finite combustion time and heat losses on thermal efficiency of Diesel engines is discussed in Ref. D-3, pp. 227-230. It is concluded that finite combustion time is responsible for a large part of the difference between the limited-pressure fuel-air cycle and the actual Diesel cycle as recorded on an indicator diagram. The difference between actual and ideal IMEP is of the order of 15%. In the best cases, it can be reduced to about 10%, while in engines without a well-developed injection system it can be considerably larger than 15%. Heat losses, on the other hand, generally do not appear to cause any important reduction of IMEP in Diesel engines, mostly because Diesel engines generally are large. There may be some effect of heat losses on IMEP in engines with combustion pre-chambers. Such chambers lead to a reduction in losses due to finite combustion time. For present purposes, it probably suffices to combine the finite combustion time losses and the cooling losses. It is assumed that these losses are 10% of the fuel-air cycle IMEP for a compression ratio of 15 and a specific heat addition $\gamma P_{\text{add}}/P_1 = 3$ ($\phi \approx 0.73$), corresponding to the best state of the art.

Scaling laws for heat losses are given in Chapter 8 of Ref. D-3. The relative reduction in power output arising from heat losses is given by Eq. 8-12 of Ref. D-3. For present purposes, it is useful to rewrite this equation as

$$\frac{\dot{BQ}}{P_1} = 10.4 \frac{\gamma B}{Pr R_g^{0.25}} \frac{T_g - T_c}{T_1} .$$

Here, \dot{Q} represents the total heat loss, B the fraction of the heat loss leading to a reduction in IMEP, Pr the Prandtl number ($= \mu c_p/k$), R_g the Reynolds number based on mass flow rate and piston area, T_g the gas temperature in the cylinder, and T_c the temperature of the coolant. To a good approximation,

$$T_g - T_c \approx 600 \phi^\circ R \approx 44 (\gamma P_{add}/P_1)^\circ R ,$$

(see Fig. 8-6 of Ref. D-3). It follows that for Diesel engines the heat losses scale approximately with specific heat addition (or equivalence ratio). The effect of compression ratio on heat losses is one of the factors determining B. In order to make this effect explicit, it seems reasonable to assume an approximate proportionality to T_2 , so that

$$B = B_0 (r/15)^{0.4} ,$$

where r is the compression ratio and B_0 the value of B for $r = 15$. Assuming that these scaling factors represent both the cooling losses and the finite combustion time losses with sufficient accuracy, and using $r = 15$, $\gamma P_{add}/P_1 = 10$ as the reference, these losses are estimated to be 3% of the ideal IMEP for $r = 15$, $\gamma P_{add}/P_1 = 3$, and 12% and 4% for $r = 25$ and $\gamma P_{add}/P_1 = 10$ and 3, respectively.

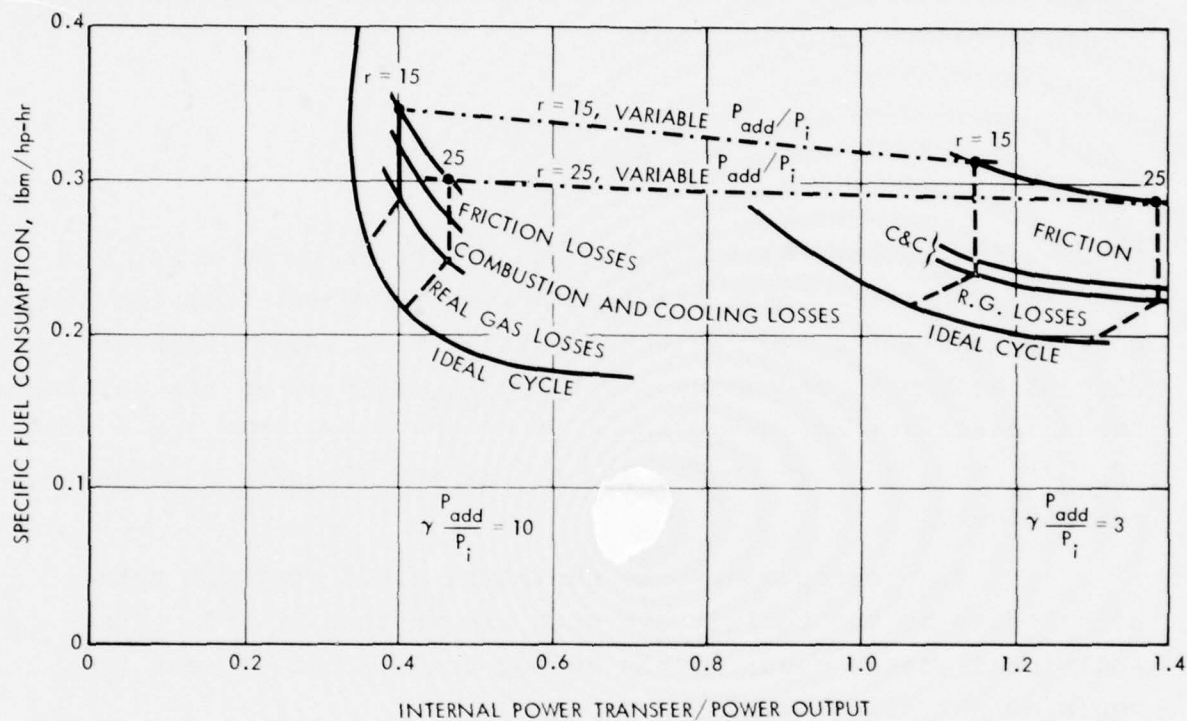
For completeness, it should be noted that the total heat losses to the coolant are much larger than 10-15%. The additional losses occur mostly during the exhaust process and hence do not affect IMEP.*

2. Impact of Losses on Performance

The impact of the various loss mechanisms on the specific fuel consumption of the standard, constant-pressure Diesel cycle are shown in Fig. D-11. It can be observed that the total impact of the losses is substantial; for example, for a compression ratio of 15 and $\phi = 0.72$ ($\gamma P_{add}/P_1 = 10$), the losses result in an increase in sfc from the ideal value of approximately 0.25 to a value of 0.35--a 40% increase.

It is interesting to note that the final results for actual sfc shown in Fig. D-11 are almost independent of $\gamma P_{add}/P_1$ (or ϕ),

*These losses, however, do affect the installed performance of a diesel engine, in that the cooling system requires both additional power and weight.



9-30-77-18

FIGURE D-11. Impact of losses on specific fuel consumption of standard, constant-pressure ($r_{cv} = 1$) Diesel cycle.

which, in the case of Diesel engines, means load. Furthermore, the results are on the order of 0.33 lbm/hp-hr. These results agree with data obtained from actual engines.

C. OVERALL ENGINE CONSIDERATIONS

In making a technology assessment of Diesel engines, it is useful to consider first the current state of the art with respect to specific weight and specific fuel consumption. Figure D-12 shows sfc as a function of specific weight, based on the manufacturers' specifications given in Ref. D-5. The points shown represent engines that are normally aspirated (circles), turbocharged (triangles), or turbocharged and aftercooled (squares). One of the most striking features of Fig. D-12 is that the specific weight varies over a wide range, but that specific fuel consumption is quite constant. The best specific fuel consumption obtained is on the order of 0.35 lbm/bhp-hr; typical values are 0.38 lbm/bhp-hr. This is true for normally aspirated as well as for turbocharged engines. Turbocharging and intake air cooling decrease specific weight, but not by drastic amounts.

An important parameter in determining the specific weight is the value of horsepower/cylinder (Ref. D-6). It was shown in Ref. D-6 that the minimum specific weight of currently available engines (about 5 lbm/bhp) occurs at about 20 horsepower/cylinder. At smaller values, the power output declines because of heat losses, while at larger values the engine walls have to be made relatively thicker, according to the principles of similitude (cf. Ref. D-3, Chapter 17).

Notable improvements in specific weight have resulted from increases in piston speed, combined with increases in BMEP (cf. Ref. D-7). The most striking results were obtained in a series of aircraft Diesels using aluminum engine blocks (Ref. D-8). These engines were developed just before World War II. They were abandoned after the war in favor of aircraft turbine

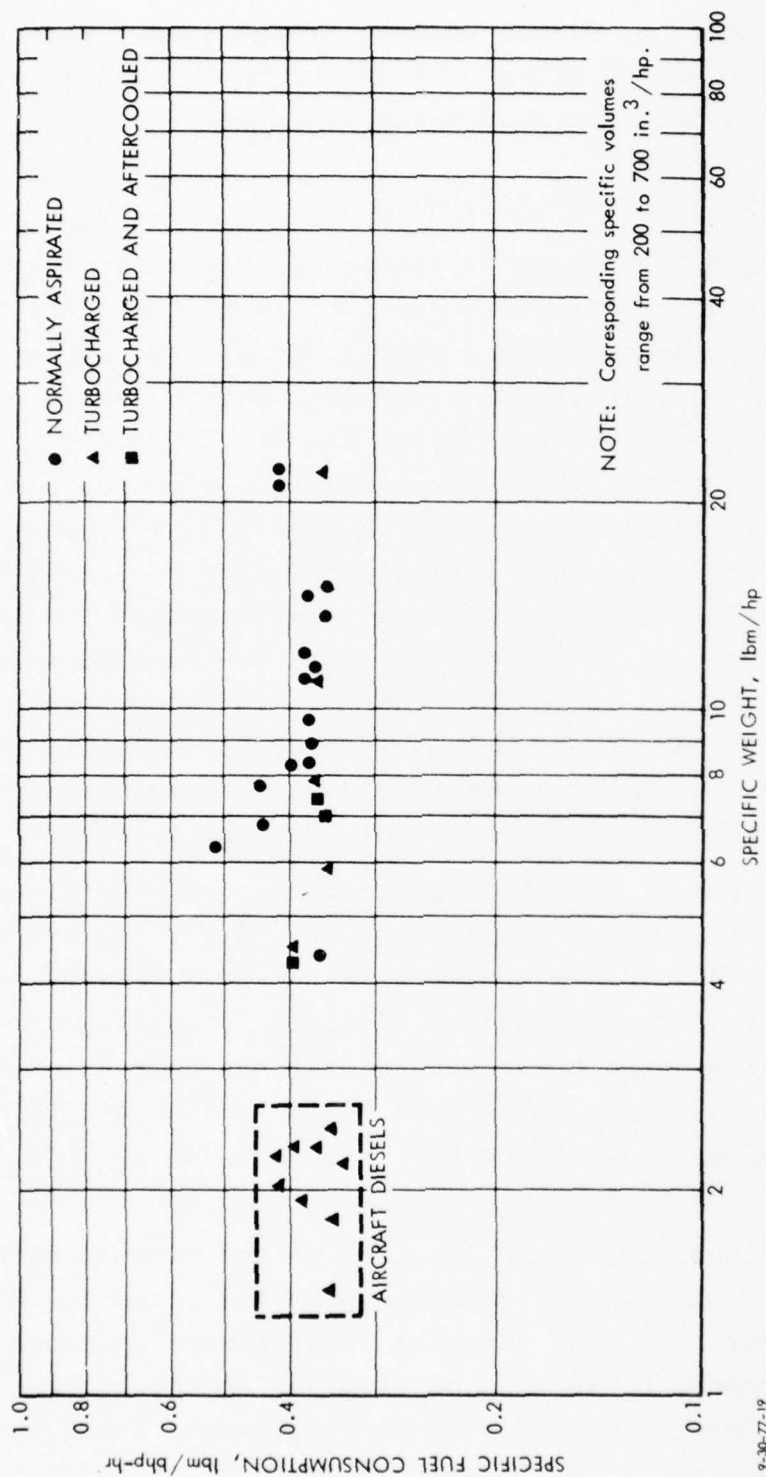


FIGURE D-12. Specific fuel consumption versus specific weight for Diesel engines based upon manufacturers' specifications (Source: Ref. D-5).

engines. Nevertheless, they still set a benchmark for potential improvements in Diesel engines.

In order to discuss potential improvements in more detail, we again refer to Fig. D-11. The ideal results show sfc's as low as 0.17-0.20 lbm/hp-hr. However, the various loss mechanisms combine in such a way that the actual sfc is 0.30-0.35 lbm/hp-hr. At high equivalence ratios (or P_{add}/P_i), about half of the losses are due to real gas losses, while the rest are due to the combined effects of finite combustion time, cooling, and friction. At low equivalence ratios, friction becomes relatively more important than real gas losses. In either case, it seems unlikely that these losses can be much reduced. It seems reasonable to conclude that significant improvements in sfc of Diesel engines beyond the current state of the art are not likely to occur. On the other hand, important improvements in specific weight can conceivably be realized by the use of lighter materials for the engine block and the main engine parts, and by higher piston speeds. While this may present a number of unresolved problems, it seems safe to state that specific weights on the order of 1.5 lbm/bhp should ultimately be attainable.

The present results can be used in still another way to study potential improvements in Diesel engines. This way is based on the specific power output parameter Y_p , or on its inverse $1/Y_p$. It will be recalled that the inverse can be written as

$$\frac{1}{Y_p} = \frac{(\dot{m}/\rho_1)p_3}{P_o} ,$$

where \dot{m}/ρ_1 is the volume flow rate into the cylinder (as distinguished from the volume flow rate into a precompression device), p_3 is the maximum cylinder pressure, and P_o is the power output. As noted in Chapter 17 of Ref. D-3, a group of similar

engines whose typical dimension is L will undergo deflections under the same pressure that are proportional to L . It can be concluded that the weight of such engines is approximately proportional to p_m . This conclusion is reinforced by the results of Ref. D-6. It follows that the specific weight of such engines is roughly proportional to C/Y_p , where the proportionality factor C depends on engine materials, piston speed, etc. This factor is not known a priori, and can best be determined from a comparison with actual engines. To this purpose, the results for Y_p corresponding to the standard, constant-pressure combustion Diesel (Fig. D-11) are shown in Fig. D-13, together with results for specific weight of actual engines (Ref. D-5). Similar results for ideal supercharged cycles are shown in Fig. D-14 (see Annex D1). Figures D-13 and D-14 indicate that the proportionality factor C for current state-of-the-art engines is of order 1. The figures also indicate that improvements in specific weight of state-of-the-art engines by further turbocharging would require sacrifices in sfc; their potential is severely limited by the large slope of the ideal curves of Fig. D-14. As mentioned previously, large improvements in specific weight without any sacrifices in sfc can in principle be obtained by using lighter engine materials combined with higher piston speeds.

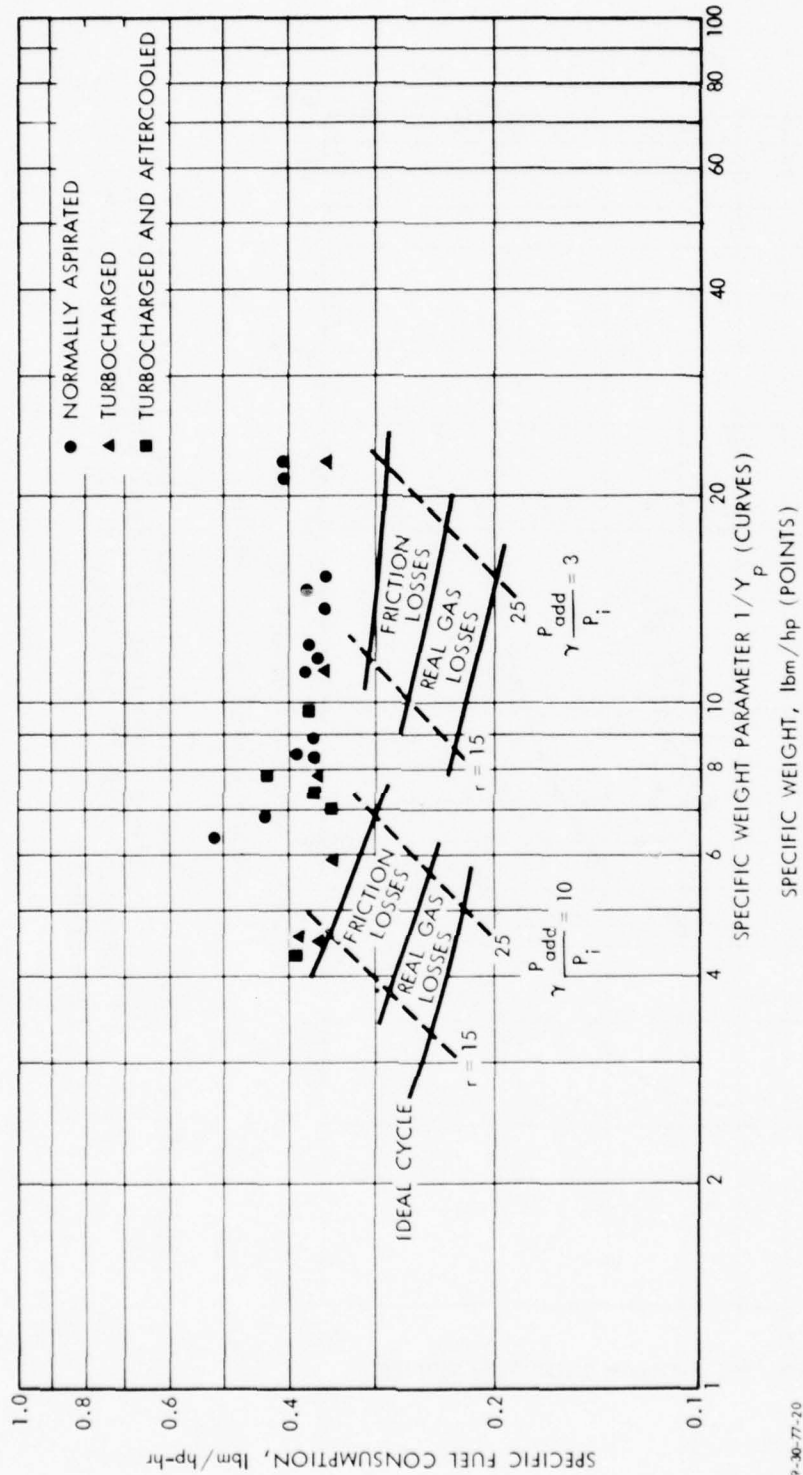


FIGURE D-13. Specific fuel consumption and specific weight of Diesel engines compared to estimated characteristics of standard Diesel cycle ($r_{cv} = 1$).

REFERENCES, APPENDIX D

- D-1. L.C. Lichty, Combustion Engine Processes, McGraw-Hill Book Company, New York, 1967.
- D-2. E.F. Obert, Internal Combustion Engines and Air Pollution, Intext Educational Publishers, New York, 1973.
- D-3. C.F. Taylor and E.S. Taylor, The Internal Combustion Engine, International Textbook Company, New York, 1970.
- D-4. I.N. Bishop, "Effect of Design Variables on Friction and Economy," SAE Paper 812A, January 1964, Transactions of the SAE, pp. 334-358, 1965.
- D-5. Diesel and Gas Turbine Worldwide Catalog, Vol. 42, Diesel and Gas Turbine Progress, Milwaukee, Wisconsin, 1977.
- D-6. P.C.T. de Boer, "Specific Power of Internal Combustion Engines," Appendix F of Institute for Defense Analyses, Survey of Advanced Propulsion Systems for Surface Vehicles, IDA Paper P-1073, F.R. Riddell, January 1975.
- D-7. W.P. Mansfield, "Transport Engines of Exceptionally High Specific Output," Proc. Institution of Mechanical Engineers 1968-69, Vol. 183, Part 3B, pp. 1-12, 1969.
- D-8. P.H. Wilkinson, Aircraft Diesels, Pitman Publishing Corporation, New York, 1940.

ANNEX D1

INCREASE OF SPECIFIC POWER OUTPUT BY SUPERCHARGING

CONTENTS

A. Otto Cycle with Adiabatic Supercharger	D-41
B. Diesel LP Cycle with Adiabatic Supercharger	D-46
C. Otto Cycle with Isothermal Supercharger	D-50
D. Diesel CP Cycle with Isothermal Supercharger	D-50
E. The Influence of Intake Air Temperature	D-51

PRECEDING PAGE BLANK-NOT FILMED

ANNEX D1

INCREASE OF SPECIFIC POWER OUTPUT BY SUPERCHARGING

The indicated power output (Eq. D-4) of the ideal-gas, standard Diesel cycle (Fig. D-1) can be written as

$$P_o = N_c p_1 V_1 (\gamma - 1)^{-1} \left\{ 1 - r_{cv} r_{cp}^\gamma + r^{\gamma-1} [r_{cv}^{-1} + \gamma r_{cv} (r_{cp} - 1)] \right\}, \quad (D1-1)$$

where N_c again is the number of cycles per second, and $V_1 = \nu R_o T_1 / p_1$ is the cylinder volume at point 1, ν being the number of moles inducted per cycle, and R_o the universal gas constant per mole. It follows from this expression that there are several ways to increase power output. These include raising the values of N_c , V_1 , or r_{cp} . All three of these parameters are subject to various practical limitations not to be discussed here. Other possible ways are raising the value of the compression ratio r or the pressure ratio r_{cv} . Both of these ways lead to an increase of the maximum pressure p_3 during the cycle. As a first approximation, the cylinder walls must have a thickness that increases proportionally with p_3 ; hence their weight will be proportional to p_3 for a given value of V_1 . Similarly, the weight of the moving parts must increase with p_3 . Consequently, little or no gain in specific power will result.

For present purposes, we focus attention on the possibility of increasing specific power output by *decreasing* the compression ratio r while keeping p_3 and hence the weights of the cylinder walls and the primary moving parts constant. This implies that the pressure p_1 must be raised ("supercharging," already considered in Section A-2-b of Appendix D). In contrast to the approach followed in Section A-2-b, this annex considers the effect of supercharging on the main engine only. It is assumed that the power required for the supercharging compressor is partly taken

from the energy in the exhaust gases, in such a way that no net power is required for the supercharging process.* In other words, only area 1-2-3-4-5 in Fig. D-2 is considered. The difference between areas 1-a-b-c and 1-a'-b'-c in Fig. D-2 is neglected. The weight of the supercharging equipment is also neglected; usually, this weight is considerably less than that of the main engine.

As was pointed out in Section A-2-b, the effect of supercharging on the power output of a given engine can be characterized by the parameter Y_p , which we call the *specific power output parameter*. Given the value of p_3 , there exists a value of p_1 for which Y_p is maximum. This follows from noting that Y_p is zero for $p_1 = 0$ and also for $p_1 = p_2$, in which case $r = 1$, $r_{cp} = 1$. The maximum value, Y_{pm} , of Y_p and the corresponding value, p_{1m} , of p_1 can be determined in a straightforward way. In the following subsections, the maximization is carried out for the Otto cycle ($r_{cp} = 1$), as well as for the general case of the Diesel lp cycle. The Otto cycle is more or less representative for small, high-speed Diesel engines. On the other hand, the engine process in large, slow-running Diesel engines may resemble the Diesel cp cycle ($r_{cv} = 1$). Many Diesel engines are best modeled by the Diesel lp cycle ($r_{cv} > 1$, $r_{cp} > 1$), the results for which are intermediate between those of the limiting cycles mentioned.

In considering the maximization procedure, it is useful to relate the effect of supercharging to the values of the parameters r_{cv} and r_{cp} . Taking the Diesel fuel to be n-dodecane, having a heating value of 3.12×10^6 Btu per poundmole and requiring 18.5 moles of oxygen to burn 1 mole of fuel, it can be shown that for $\gamma \approx 1.4$ and $r_{cp} = 1$ (Otto cycle)

$$r_{cv} = 1 + 7110 \phi(^{\circ}\text{R})/T_2 \quad . \quad (\text{D1-2})$$

*This assumption makes the following analysis more applicable to turbocharging, as conventionally defined, wherein the power required for compression is obtained by a turbine in the exhaust gases. Supercharging, as conventionally defined, involves using some power from the engine crankshaft to supply compressor power.

The corresponding expression for $r_{cv} = 1$ (Diesel cp cycle) is

$$r_{cp} = 1 + 5080 \phi(^{\circ}\text{R})/T_2 \quad . \quad (\text{D1-3})$$

It follows that the parameters r_{cv} and r_{cp} remain constant provided the ratio ϕ/T_2 remains constant. This situation corresponds to keeping ϕ fixed while using an *adiabatic supercharger* that takes in air at a given initial temperature. Another useful limit to consider is keeping ϕ fixed while using an *isothermal supercharger* compressing air at the given intake temperature T_1 . In the latter case, the parameters r_{cv} and r_{cp} depend on the compression ratio r , and the optimization procedure is slightly more involved.

A. OTTO CYCLE WITH ADIABATIC SUPERCHARGER

With $r_{cp} = 1$, it follows that

$$Y_p = (\gamma - 1)^{-1} (1 - r_{cv}^{-1}) f(r) \quad , \quad (\text{D1-4})$$

where $f(r) = r^{-1} - r^{-\gamma}$. The maximum value of $f(r)$ is

$$f_m = (\gamma - 1) \gamma^{-\frac{\gamma}{\gamma-1}} \quad , \quad (\text{D1-5})$$

which is achieved for $r = r_m = \gamma^{1/\gamma-1}$. We set

$$f = f_m g(r) \quad , \quad (\text{D1-6})$$

so that $0 \leq g(r) \leq 1$. The function $g(r)$ represents the fraction of the maximum specific power output that can be obtained. It is plotted in Fig. D1-1 for $\gamma = 1.4$, for which case $f_m = 0.123$, $r_m = 2.32$. The parameter r' used in Fig. D1-1 is identical to r for the Otto cycle.

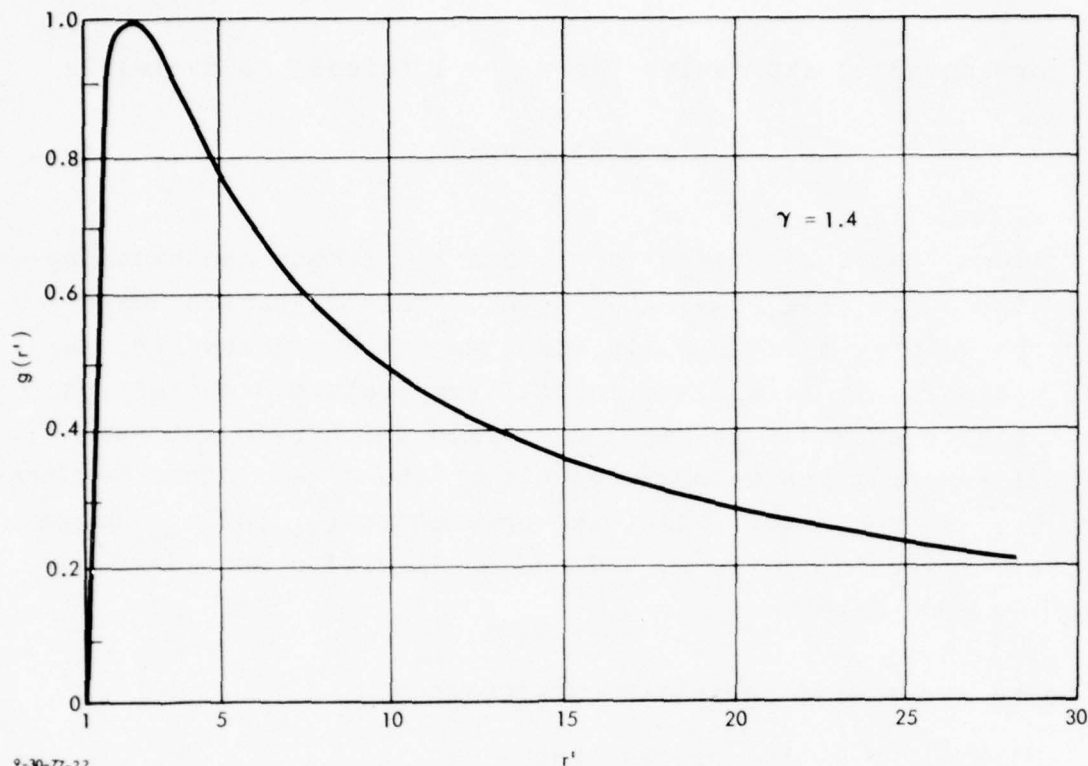


FIGURE D1-1. Specific power output function $g(r')$ for Otto cycle.

In order to obtain a deeper insight into the maximization process considered, the p - V diagrams of three cycles with constant p_3 and constant r_{cv} have been sketched in Fig. D1-2. In cycle (a), p_1 is very small, while in cycle (c) p_1 is close to p_2 . It is clear that the closed curves representing the engine process in both of these cases are very narrow, so that the area enclosed is very small. Cycle (b) is an intermediate case, with a much larger enclosed area.

It is illustrative to plot "partial power curves" in the graphs for P_o/P_i and sfc as function of P_{int}/P_o (Fig. D1-3). These curves are obtained by specifying the value of $g(r)$. This provides the value of r , and hence the value of the product $(P_{int}/P_o)(P_o/P_i) = r^{\gamma-1} - 1$, as well as the value of the specific fuel consumption $sfc = 0.138 (1 - r^{1-\gamma})^{-1}$. At $g = 1$ (maximum specific power output), $(P_{int}/P_o)_m (P_o/P_i)_m = r_m^{\gamma-1} - 1 = \gamma - 1$, $sfc = 0.138 (\gamma - 1)^{-1}$. The value of P_{add}/P_i varies along each

of the lines of constant g ; this value can be found from the intersections with the lines of constant P_{add}/P_1 .

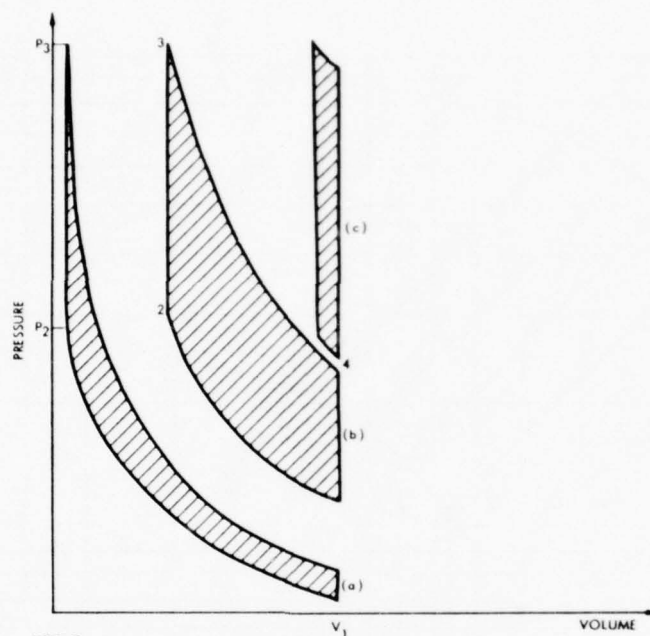


FIGURE D1-2. p - V diagrams for different degrees of supercharging in an Otto cycle with $p_3 = \text{constant}$, $r_{cv} = 2$.

Another illustrative way of displaying these results is to plot the fraction of maximum specific power output g as a function of the specific fuel consumption (see Fig. D1-4). Both of these quantities are functions of the compression ratio r , which becomes a parameter along the curve. It can be seen that appreciable gains in power output can be achieved at a relatively small increase in sfc, provided that the compression ratio r is not lowered too much (not below about 5, say).

By way of numerical illustration, we consider the case of an engine with compression ratio $r = 20$, corresponding to $g(r) = 0.283$ for $\gamma = 1.4$. The specific power output parameter Y_p can be increased by a factor $1/g = 3.53$ by supercharging to a pressure $(r/r_m)\gamma = (20/2.32)^{1.4} = 20.4$ times the original value of p_1 , while decreasing the compression ratio to $r_m = 2.32$. If

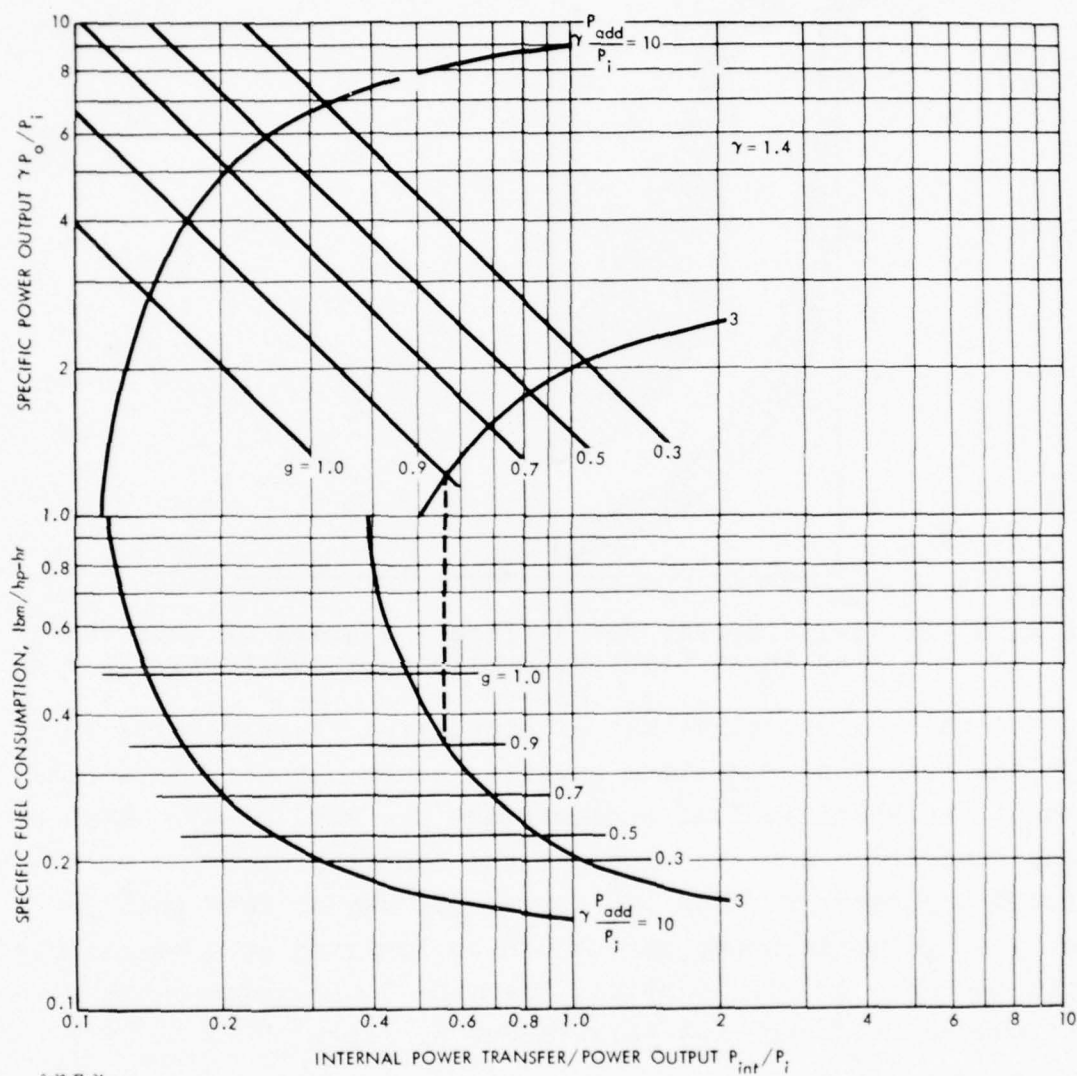


FIGURE D1-3. Performance characteristics of ideal Otto cycle at constant fractions, g , of specific power output parameter.

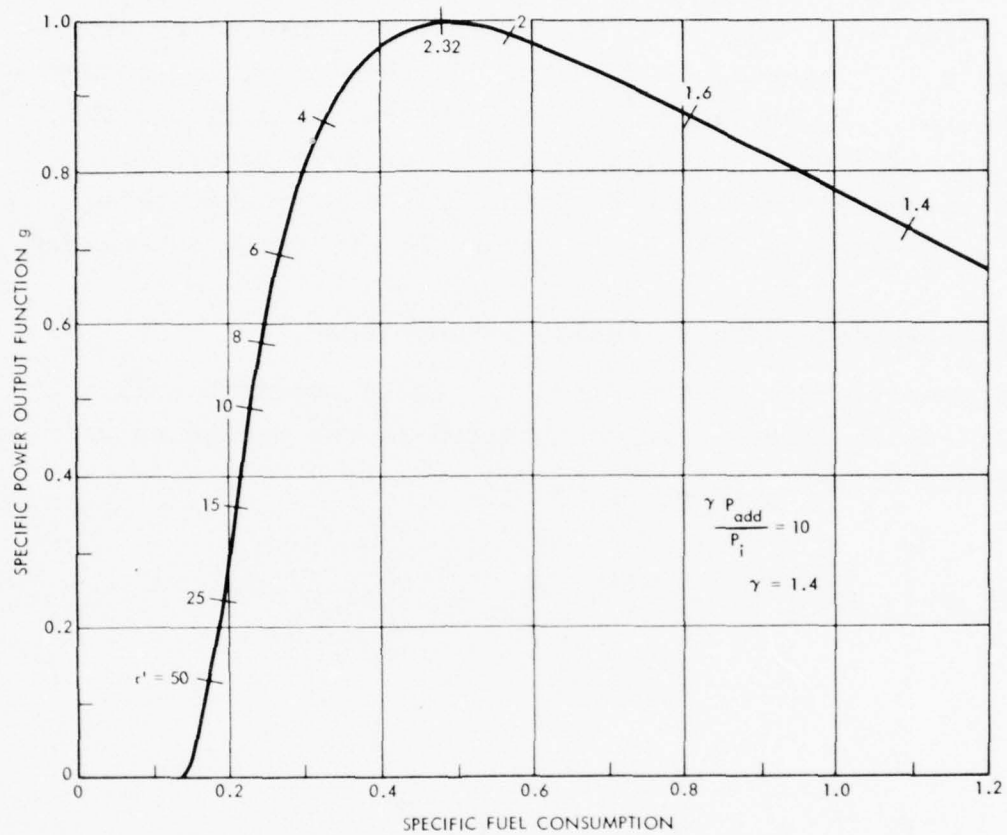


FIGURE D1-4. Specific power output function as a function of specific fuel consumption.

the original value of p_1 was 1 atm, this means supercharging to 20.4 atm, while $p_2 = 66.3$ atm. The specific fuel consumption increases from 0.198 to 0.483 lbm/hp-hr (a factor of 2.4). For $\gamma P_{add}/P_i = 10$ ($\phi = 0.73$) and $T_1 = 520^\circ R$, the value of the parameter r_{cv} is 4.0; the original value of Y_p is 0.065, while for the maximally supercharged case $Y_{pm} = 0.231$. Eighty percent of the maximum value of Y_p ($0.8 \times 0.231 = 0.185$) is achieved by supercharging to 7.7 instead of 20.4 atm. In this case, the compression ratio is 4.7, the power output increases by a factor 2.8, and the specific fuel consumption increases by a factor 1.5. The case discussed is illustrated in Fig. D1-5 by the curve marked "Otto adiabatic."* Other cases are discussed subsequently.

B. DIESEL LP CYCLE WITH ADIABATIC SUPERCHARGER

The general case of the Diesel lp cycle requires only a simple extension of the results obtained in the preceding section. The expression for $Y_p \equiv P_o/(N_c p_3 V_1)$ becomes

$$Y_p = (\gamma - 1)^{-1} \left[1 - r_{cv}^{-1} + \gamma(r_{cp} - 1) \right] b f_m g(r') \quad , \quad (D1-7)$$

where

$$b = \left[\frac{r_{cv} r_{cp} \gamma - 1}{r_{cv} - 1 + \gamma r_{cv} (r_{cp} - 1)} \right]^{-\frac{\gamma}{\gamma-1}} \quad , \quad r' = br \quad (D1-8)$$

while $sfc = 0.138 [1 - (r')^{1-\gamma}]^{-1}$. For $r_{cp} = 1$ the result for Y_p reduces to that of the preceding section, and $b = 1$, $r' = r$. It should be kept in mind that the Diesel lp cycle requires $r_{cp} \leq r$. For cases yielding a value of r_m below that of r_{cp} , the maximization procedure is invalid. However, such cases do not appear to be of practical importance and are left out of consideration here.

*It should be noted that the treatment of the Otto cycle here is only as one limit of the Diesel engine. In an Otto engine, of course, detonation limits could prohibit the high overall compression ratios considered here.

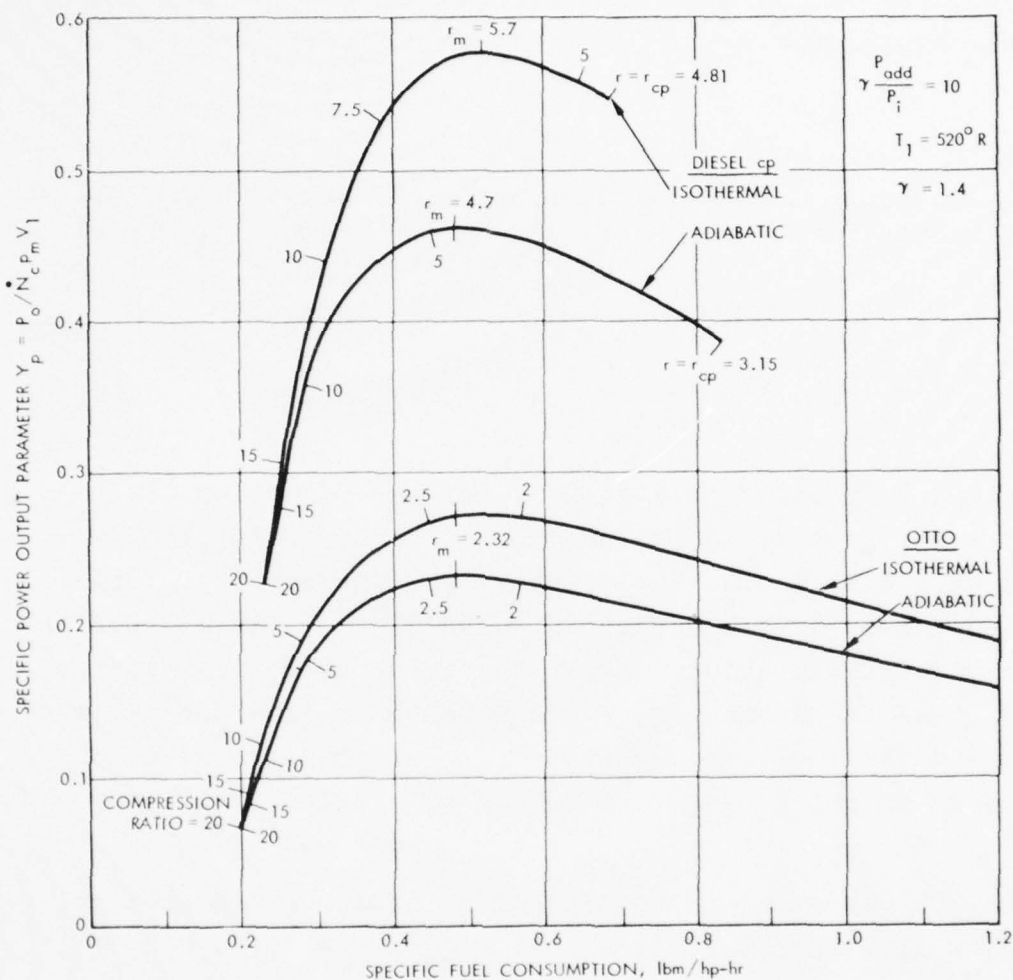


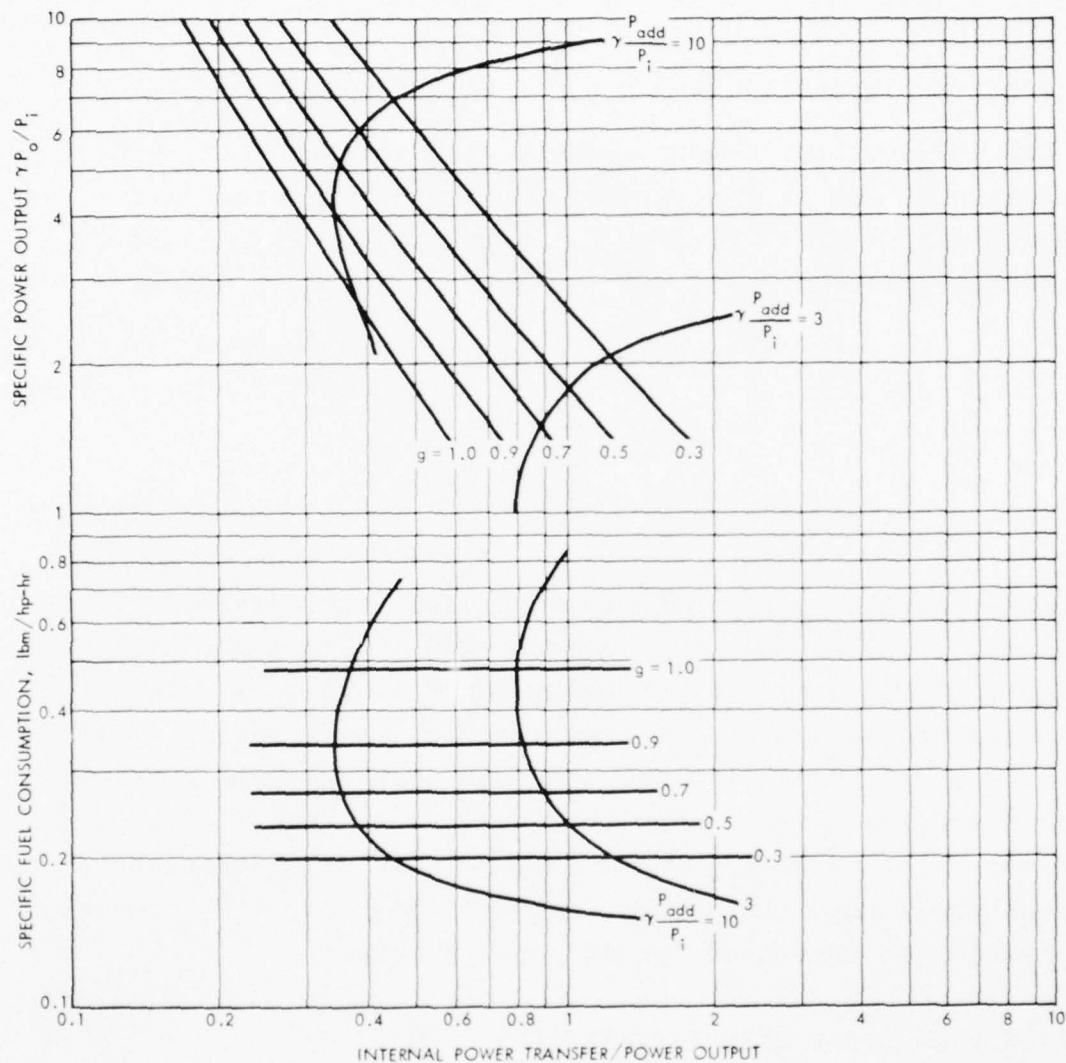
FIGURE D1-5. Specific power output parameter--specific fuel consumption relationship for ideal supercharged cycles.

It is again illustrative to plot the present results in the form of partial power curves in the graph for P_o/P_1 as a function of P_{int}/P_o . This is achieved by finding the value of r' corresponding to the specified partial power $g(r')$ and combining the results for P_{int}/P_o , P_o/P_1 , and P_{add}/P_1 into the relation

$$\frac{P_{int}}{P_o} = \frac{1}{1-(r')^{1-\gamma}} \frac{1}{(r_{cv}-1) + \gamma r_{cv} \left\{ \left[\frac{1}{r_{cv}} \left(1 + \frac{\gamma P_o/P_1}{(r')^{\gamma-1}-1} \right) \right]^{1/\gamma} - 1 \right\}} - \frac{1}{\gamma(P_o/P_1)} \quad (D1-9)$$

This relation is plotted in Fig. D1-6 for the Diesel cp cycle ($r_{cv} = 1$) with $\gamma = 1.4$, for values of r' corresponding to $g = 1.0, 0.9, 0.7, 0.5$, and 0.3 , respectively. The specific fuel consumption, given by $sfc = 0.138 [1 - (r')^{-0.4}]^{-1}$ is plotted in the lower part of Fig. D1-6. Again the value of P_{add}/P_1 varies along the lines of constant g , and can be found from the intersections with the lines of constant P_{add}/P_1 . The fraction of maximum power output g as a function of sfc again is given by Fig. D1-4.

By way of numerical illustration, we consider a Diesel cp cycle ($r_{cv} = 1$) with $r = 20$, $\gamma = 1.4$, $\gamma P_{add}/P_1 = 10$ ($\phi = 0.73$), $T_1 = 520^\circ R$, and $p_1 = 1$ atm. It follows that $r_{cp} = 3.15$, $b = 0.496$, $r' = 9.92$, $g(r') = 0.491$, $Y_p = 0.226$, $sfc = 0.230$ lbm/hp-hr. The power output can be increased by a factor $1/g = 2.03$ if the engine is supercharged to a pressure $(r'/r'_m)^\gamma = (9.92/2.32)^{1.4} = 7.65$ atm, which decreases the compression ratio to $r'_m/b = 4.7$. The specific fuel consumption is increased to 0.483 lbm/hp-hr. This case also is illustrated by Fig. D1-5 (curve marked "Diesel adiabatic"). The curve ends at the point where the value of r has decreased to that of r_{cp} ; this point is well beyond the maximum (point m).



9-30-77-27

FIGURE D1-6. Performance characteristics of the ideal Diesel constant-pressure cycle at constant fractions, g , of specific output parameter.

It is clear from Fig. D1-5 that for any value of specific fuel consumption the Diesel cp cycle provides considerably higher values of the specific power output parameter Y_p than does the Otto cycle.

C. OTTO CYCLE WITH ISOTHERMAL SUPERCHARGER

For an isothermal supercharger, the temperature T_2 after compression in the engine varies with the compression ratio r ; it is given by $T_2 = r^{\gamma-1} T_1$, where T_1 is constant. It follows that for an Otto cycle with $\gamma P_{add}/P_1 = 10$, $T_1 = 520^\circ R$, $\gamma = 1.4$,

$$r_{cv} = 1 + 9.98 r^{-0.4} \quad (D1-10)$$

$$Y_p = 0.308(1 + 0.100 r^{0.4})^{-1} g(r) \quad (D1-11)$$

The latter result is included in Fig. D1-5 (curve marked "Otto isothermal"). This type of supercharging yields higher values for the specific power output parameter Y_p than does adiabatic supercharging, because r_{cv} increases as r is decreased. This effect is unrelated to the circumstance that the work required for an isothermal compression process is less than for an adiabatic one. Consequently, there are two distinct advantages of the isothermal supercharger process over the adiabatic process, both leading to increased specific power output.

D. DIESEL CP CYCLE WITH ISOTHERMAL SUPERCHARGER

For a Diesel cp cycle ($r_{cv} = 1$) with $\gamma P_{add}/P_1 = 10$, $\gamma = 1.4$, $T_1 = 520^\circ R$, $p_1 = 1$ atm, we have

$$r_{cp} = 1 + 7.13 r^{-0.4} \quad (D1-12)$$

$$Y_p = 25.0 [r^{-1.4} - r^{-1.8} a(r)] \quad (D1-13)$$

$$a(r) = \left(r_{cp}^{1.4} - 1 \right) [1.4(r_{cp} - 1)]^{-1} \quad (D1-14)$$

The result for Y_p again is illustrated in Fig. D1-5 (curve marked "Diesel isothermal"). The curve ends at the point where the values of r and r_{cp} are equal. The figure shows that an isothermal supercharger can provide considerably higher specific power output than an adiabatic one, at the same specific fuel consumption.

E. THE INFLUENCE OF INTAKE AIR TEMPERATURE

The circumstance that an isothermal supercharger process provides a higher specific power output than does the corresponding adiabatic process is related to the influence of the intake air temperature on specific power output and fuel consumption. In investigating this influence explicitly, two important cases can be distinguished. First, if T_1 is varied but p_1 , V_1 , r , r_{cv} and r_{cp} are kept constant, there is *no change* in either the power output P_o , the specific power output parameter Y_p , or the specific fuel consumption. Because the temperature T_2 is proportional to T_1 , the fuel-air equivalence ratio ϕ must vary in proportion to T_1 in this case.

In the second case, T_1 is varied while keeping p_1 , r , and P_{add}/P_1 constant. This case applies to an engine running at given values of ϕ and p_1 , but with variable intake charge cooling or heating. The variation of T_1 here causes a variation of r_{cv} or r_{cp} . For the Otto cycle, it follows that the maximum pressure p_3 during the cycle varies, while the power output P_o is inversely proportional to T_1 :

$$P_o = \frac{N_c p_1 V_1}{\gamma - 1} 7110 \phi \left(1 - \frac{1}{r^{\gamma-1}} \right) \frac{1}{T_1}, \text{ or } \frac{P_o}{P_{or}} = \frac{T_{1r}}{T_1}.$$

Here, P_{or} and T_{1r} are the reference values. The latter result is plotted in Fig. D1-7, together with the corresponding result for the Diesel cp cycle (see below). The specific fuel consumption is constant, because the compression ratio r is constant. Furthermore, the specific power output parameter Y_p is nearly constant. For the case illustrated by Fig. D1-7, Y_p varies from 0.070 at $T_1/T_{1r} = 0.75$ to 0.062 at $T_1/T_{1r} = 1.25$; this represents a short vertical line segment in Fig. D1-5 (not shown).

For the Diesel cp cycle, p_2 remains constant if p_1 and r remain constant, so that the maximum pressure during the cycle remains constant. It is found that

$$\frac{Y_p}{Y_{pr}} = \frac{P_o}{P_{or}} = \frac{1 - \left(1 + \frac{5080 \phi}{T_{1r}^{\gamma-1}} \right)^{\gamma} + \gamma \frac{5080 \phi}{T_{1r}}}{1 - \left(1 + \frac{5080 \phi}{T_{1r}^{\gamma-1}} \right)^{\gamma} + \gamma \frac{5080 \phi}{T_{1r}}}.$$

This result is plotted in Fig. D1-7 for the case $r = 20$, $\gamma = 1.4$, $\gamma P_{add}/P_1 = 10$ and $T_1 = 520^\circ R$. Also indicated is the sfc at three points along the curve. It is seen that this quantity is nearly constant. The variation considered represents a nearly vertical line segment in Fig. D1-5, extending from the point $Y_p = 0.186$, sfc = 0.224 to the point $Y_p = 0.290$, sfc = 0.239.

It can be concluded that cooling the intake air while keeping the parameters r , P_{add}/P_1 , and p_1 constant is an effective way to increase the power output P_o . For the Otto cycle, the specific fuel consumption remains constant, and the parameter Y_p increases only slightly. For the Diesel cp cycle, there is a slight increase in sfc, while the parameter Y_p increases in proportion with p_o .

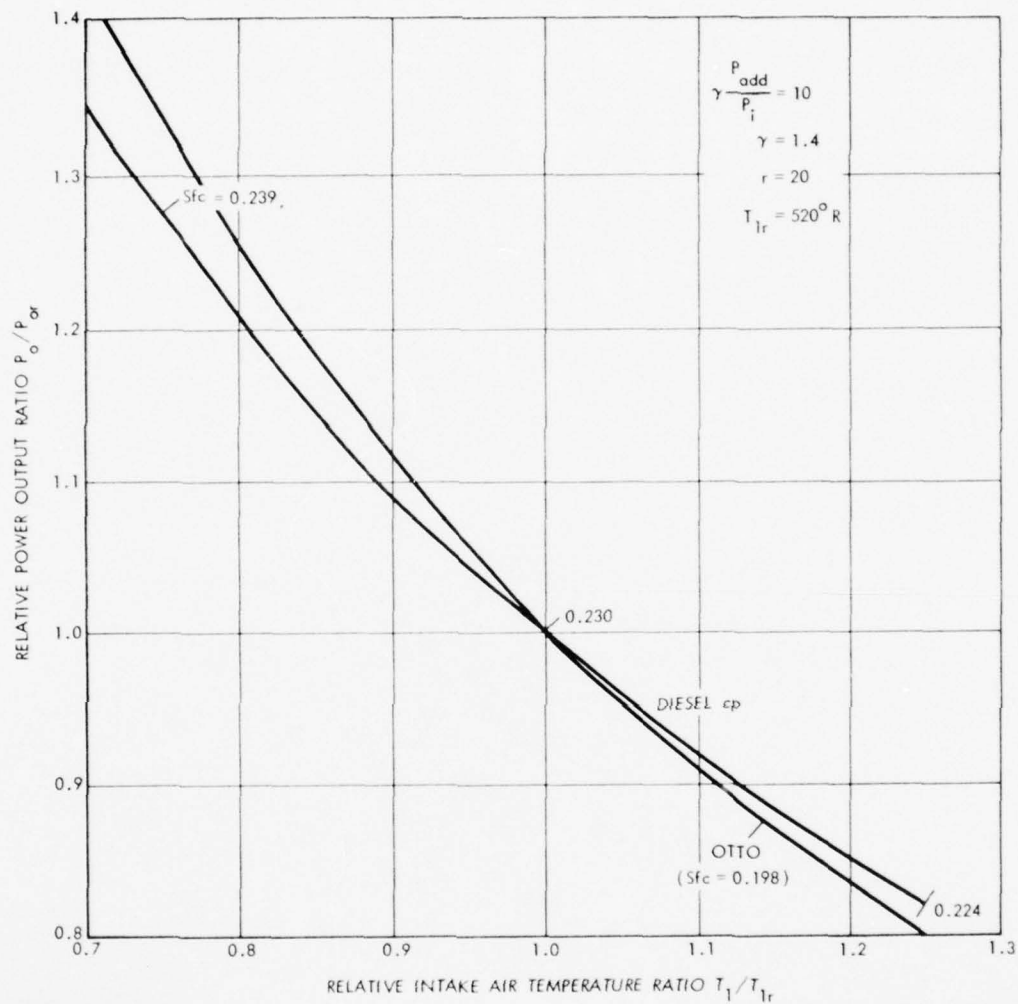


FIGURE D1-7. Influence of intake air temperature on power output and specific fuel consumption of Otto and Diesel constant-pressure cycles.

GLOSSARY, APPENDIX D

b	Defined by Eq. D1-8, p. D-46
B	Cylinder bore (diameter); or, the fraction of the total heat loss of the engine which leads to a loss in efficiency.
BMEP	Brake mean-effective pressure
C	Number of cylinders; or, a proportionality factor.
cp, CP	Refers to the constant-pressure Diesel cycle, see p. D-4.
c_p	Specific heat at constant pressure of the working fluid
c_v	Specific heat at constant volume of the working fluid
D	Piston displacement, the swept volume of the piston during one stroke.
F	Fraction of total internal power transfer used in precompression
FMEP	Friction mean-effective pressure
f_s	Stoichiometric fuel-air ratio, the fuel-air ratio at which complete combustion can be obtained with no excess air.
g	The ratio of the power output per unit inlet volume flow to the maximum obtainable by supercharging or turbocharging at a constant peak pressure.
HV	Lower heating value of the fuel
IMEP	Indicated mean-effective pressure
lp, LP	Refers to the limited-pressure Diesel cycle, see p. D-4.

\dot{m}	Mass flow rate
mep	Mean-effective pressure
N, N_c	Rotational speed of crankshaft
p	Pressure of the working fluid
P_{add}	Rate of heat addition to the working fluid, $\dot{m}f_s\phi(HV)$
P_i	Rate of energy transport associated with working fluid, $\dot{m}c_p T_1$, where T is the minimum temperature of the working fluid in the cycle.
P_{int}	Internal power transfer, the energy transfer rate to the working fluid before combustion from the working fluid after combustion.
P_o	Maximum power output
Pr	Prandtl number, $c_p \mu / k$, where μ and k are the viscosity and thermal conductivity, respectively, of the working fluid.
\dot{Q}	Total rate of heat loss from the engine
r	Compression ratio; ratio of cylinder volume or specific volume of the working fluid at beginning of compression to that at end of compression.
R	Gas constant of the working fluid
r^1	The compression ratio (cylinder-volume ratio) of an Otto cycle; or, as defined by Eq. D1-8 for Diesel cycles.
r_{cp}	Ratio of cylinder volume at end of constant-pressure combustion to that at the beginning, in the limited-pressure Diesel cycle (see Fig. D-1, p. D-4).
r_{cv}	Pressure ratio achieved in constant-volume combustion in the limited-pressure Diesel cycle (see Fig. D-1, p. D-4).
R_g	Reynolds number of the working fluid, based on mass flow rate and piston area.
r_o	Overall compression ratio in a supercharged or turbocharged engine; the ratio of working fluid specific volume at beginning of compression to that at end of compression.

r_s	Supercharging or turbocharging pressure ratio
S	Piston stroke; the maximum length of travel of the piston.
sfc	Specific fuel consumption; the fuel flow rate per unit power output, lb/hr-hp.
T	Temperature of the working fluid
V	Cylinder volume at a given piston position
v	Specific volume of the working fluid
Y_p	Ratio of the power output to the product of volume flow at cylinder inlet and maximum cycle pressure (see Eq. D-11).
γ	Ratio of specific heats of the working fluid
η	Thermodynamic efficiency, work output/heat input
ρ	Density of the working fluid
ϕ	Equivalence ratio, the actual fuel-air ratio divided by the stoichiometric fuel-air ratio.

APPENDIX E

SIZE AND FUEL CONSUMPTION RELATIONSHIPS FOR OPEN BRAYTON-CYCLE ENGINES

David Gordon Wilson

CONTENTS

A.	Ideal Engine Performance	E-3
1.	The Ideal Cycles	E-3
2.	Ideal-Cycle Performance	E-7
3.	Implications of Ideal-Cycle Performance	E-13
B.	Relationship of Actual Performance to Ideal Performance	E-14
1.	Components and Losses	E-14
a.	Compressor Losses	E-18
b.	Expander Losses	E-20
c.	Pressure Losses	E-21
d.	Heat Exchange Losses	E-22
2.	Impact of Losses on Engine Performance	E-24
3.	Part-Power Considerations	E-31
C.	Weight and Performance of Radial Turbomachinery	E-37
1.	Radial Turbomachinery Weight, Size, and Power	E-38
2.	Radial Turbomachinery Performance	E-43
D.	Weight, Size, and Performance of Combustors	E-45
1.	Specific Heat Release	E-45
2.	Combustor Weight	E-46
3.	Implications for Future Designs	E-48
E.	Size and Performance of Heat Exchangers	E-52
1.	Characterization of Heat Exchanger Losses	E-54
2.	Minimum Pressure Loss for Heat Transfer	E-60
3.	Heat-Transfer Fluid-Flow Relationship	E-62

F. Overall Engine Considerations	E-69
1. Effect of Component Losses on Specific Weight	E-69
a. Base-Case Engines	E-69
b. Compressors and Turbines	E-74
c. Combustors	E-76
d. Heat Exchangers	E-76
e. Discussion of Findings	E-77
f. Part-Load Component Losses	E-78
2. Improvements to the State of the Art	E-79
a. Turbomachinery	E-79
b. Combustors	E-80
c. Heat Exchangers	E-81
d. Intercoolers	E-81
3. Present and Future Brayton-Engine Specific Mass versus Specific Fuel Consumption	E-82
Glossary	E-84
References	E-89

APPENDIX E
SIZE AND FUEL CONSUMPTION RELATIONSHIPS
FOR OPEN BRAYTON-CYCLE ENGINES

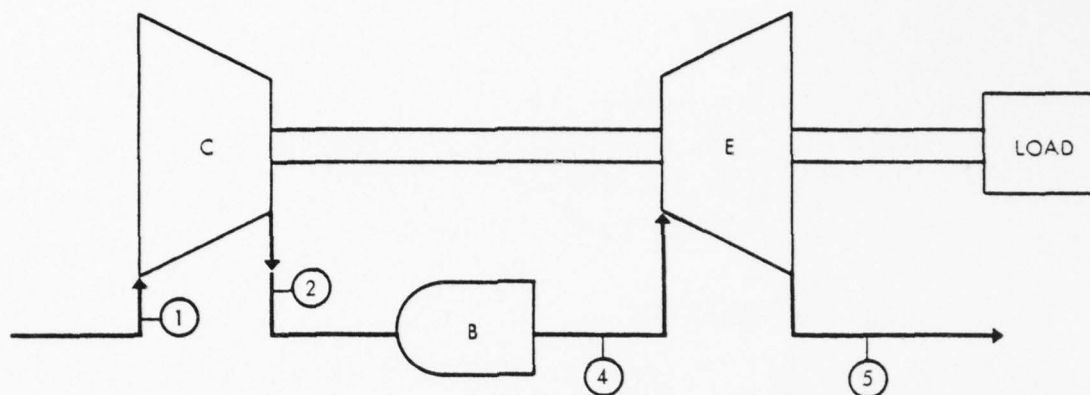
David Gordon Wilson

A. IDEAL ENGINE PERFORMANCE

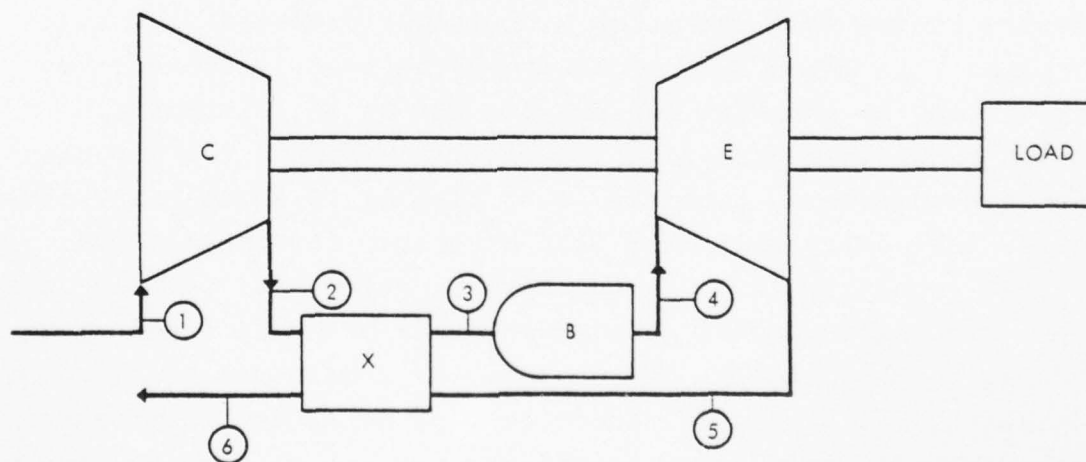
1. The Ideal Cycles

The open Brayton-cycle engine commonly takes one of two forms: a simple cycle or a regenerated cycle, with arrangements as shown in Fig. E-1. In either form, the ideal open Brayton-cycle engine takes air from the atmosphere (hence "open"); compresses it in a perfect heat-insulated ("adiabatic") compressor C (the combination of having no losses and no heat transfer makes it an "isentropic" compressor); heats the air without pressure losses in a combustor B, possibly preceded by a heat exchanger X in which some of the required heat is transferred from the engine exhaust; expands the air in an isentropic turbine or other expander E; and finally exhausts the air back into the atmosphere, possibly first passing it through the other side of the no-pressure-loss heat exchanger mentioned above. If the heat exchanger is used, the heat transfer must be accomplished with a temperature gradient of zero, this being an ideal cycle. For this to be possible, the air must be considered to have ideal properties. At the least, there must be no effect of pressure on the specific heat. For simplicity, we normally assume the air to have constant specific heat.

The ideal cycle can be conventionally defined in terms of the pressure ratio of the compressor, which is the same as (the inverse of) the expansion ratio of the expander, and of the temperature ratio (expander-inlet temperature/compressor-inlet



a. SIMPLE CYCLE (CBE)



b. REGENERATED CYCLE (CBEX)

9-23-77-1

FIGURE E-1. Open Brayton-cycle engine arrangements.

AD-A070 528

INSTITUTE FOR DEFENSE ANALYSES ARLINGTON VA SCIENCE A--ETC F/G 21/7
TECHNOLOGY ASSESSMENT OF ADVANCED PROPULSION SYSTEMS FOR SOME C--ETC(U)
SEP 78 F R RIDDELL, D M DIX DAHC15-73-C-0200

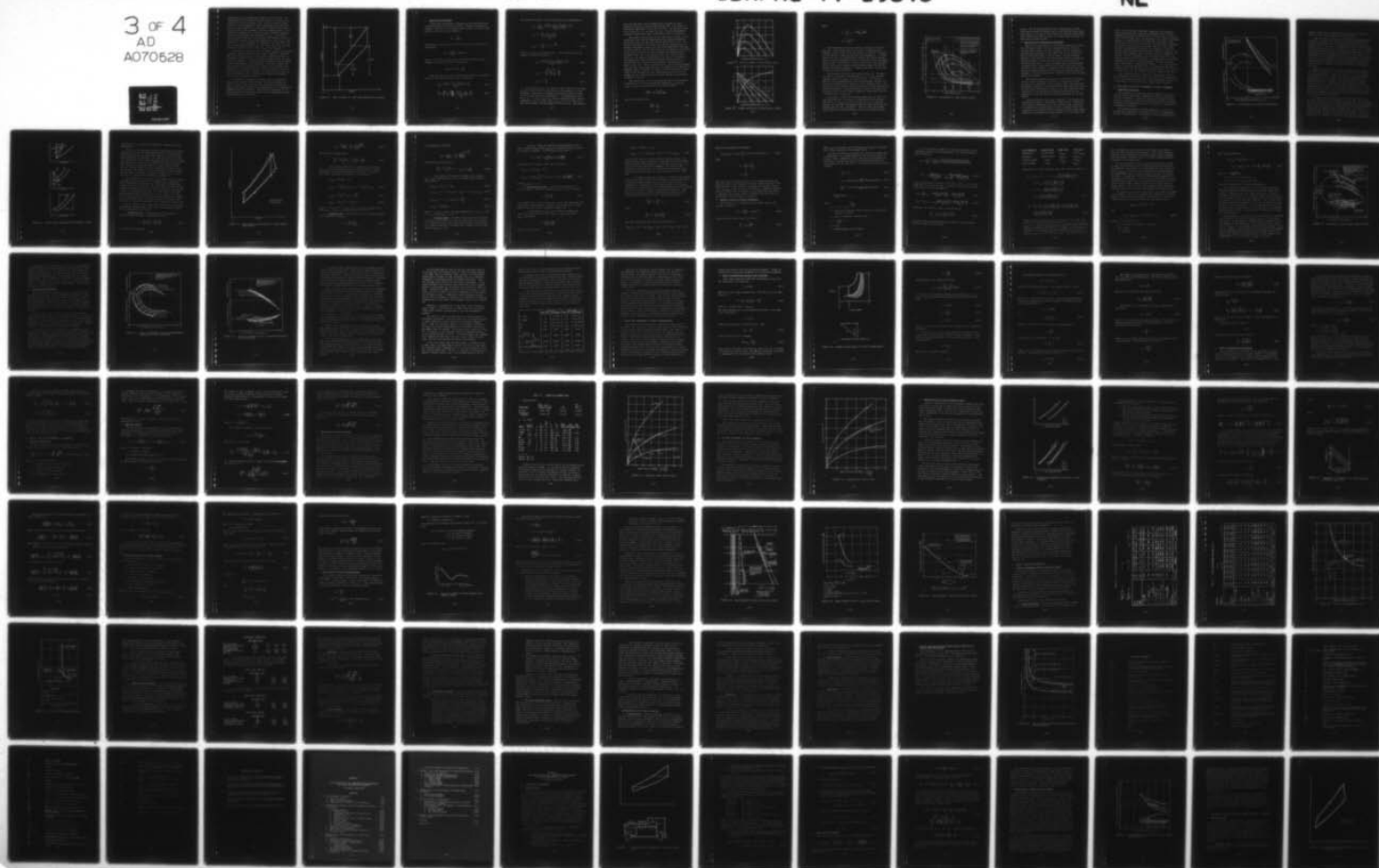
UNCLASSIFIED

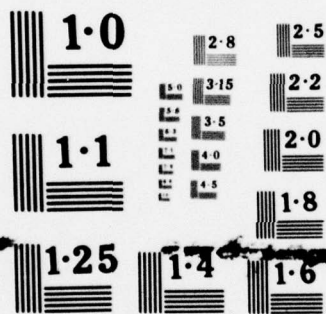
IDA-P-1278-VOL-2

IDA/HQ-77-19843

NL

3 of 4
AD
A070528



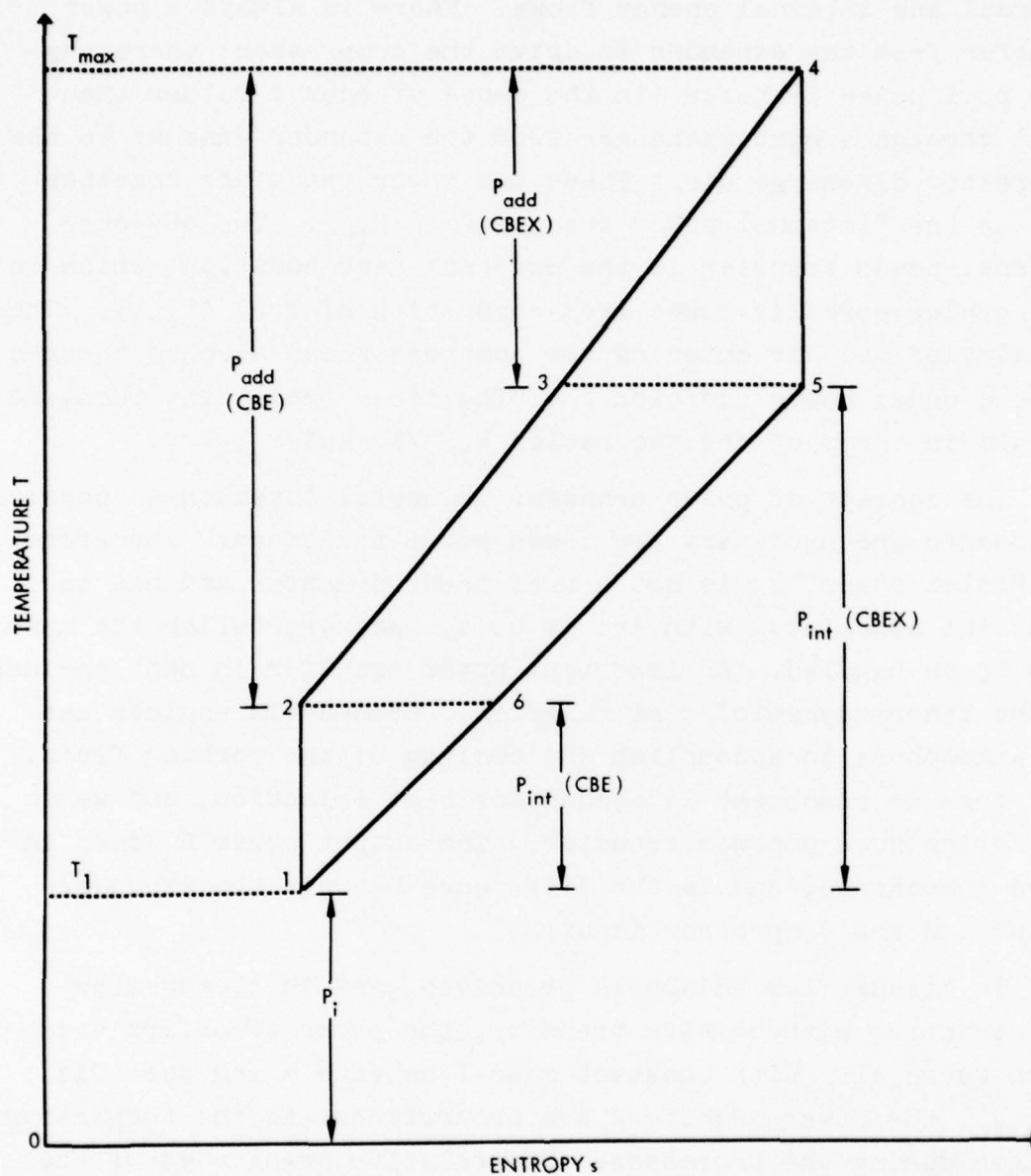


NATIONAL BUREAU OF STANDARDS
MICROCOPY RESOLUTION TEST CHART

temperature), both temperatures being in absolute units. An alternative way of defining the ideal cycle is in terms of the external and internal energy flows. There is always a power transfer from the expander to drive the compressor; there may also be a power transfer (in the sense of energy rather than work) through a heat exchanger from the expander exhaust to the compressor discharge air. These two power transfers together make up the "internal power transfer" or P_{int} . The obvious external power transfer is the external heat addition, which in real cycles normally comes from combustion of fuel (P_{add}). The enthalpy of the air entering the compressor can also be thought of as a quasi power addition P_i . The ideal cycle can, then, be defined in terms of the two ratios P_{int}/P_i and P_{add}/P_i .

The concept of power transfer is useful insomuch as physical components are necessary for these power transfers. Therefore the "inlet power" P_i is not a real power transfer and has no component associated with it; it does, however, define the mass flow to be handled. An important power transfer in heat engines is the (thermodynamic) heat rejected. Open-cycle engines use the atmosphere to accomplish the cooling of the working fluid. Therefore no component is needed for heat rejection, and we do not define such a power transfer. The output power P_o does involve components, and is the difference between the expander output and the compressor input.

In steady-flow adiabatic processes, and in steady-flow heat transfer without work transfer, the power transfers are given by $\dot{m} c_p \Delta T$. With constant mass-flow rate \dot{m} and specific heat c_p , the power transfers are proportional to the temperature changes during the processes. The relative magnitudes of the power transfers can thereby be shown on the temperature-entropy cycle diagram, as in Fig. E-2.



9-23-77-2

FIGURE E-2. Power transfers in ideal open Brayton-cycle engines.

2. Ideal-Cycle Performance

Ideal-cycle performance is measured by two characteristics: thermal efficiency and specific output. Thermal efficiency is defined as the ratio of the engine power output (as work or shaft power) to the rate of heat addition:

$$\eta_{th} \equiv \frac{P_o}{P_{add}} .$$

The thermal efficiency can also be related to the specific fuel consumption:

$$sfc = \frac{0.138}{\eta_{th}} \text{ lbm/hp-hr} ,$$

where a fuel with a heating value of 18,400 Btu/lbm has been assumed. The specific power is defined as

$$\text{Specific Power} = \frac{P_o}{P_i} .$$

When expressed in terms of temperature ratios, the specific power for both CBE and CBEX cycles is given by:

$$\frac{P_o}{P_i} = \frac{\dot{m}c_p(T_4 - T_5) - \dot{m}c_p(T_2 - T_1)}{\dot{m}c_p T_1} \quad (E-1)$$

$$\frac{P_o}{P_i} = \left[\frac{T_2 - T_1}{T_1} \right] \left[\left(\frac{T_4/T_1}{1 + \frac{T_2 - T_1}{T_1}} \right) - 1 \right] . \quad (E-2)$$

The thermal efficiency for the CBE cycle can be expressed as

$$\eta_{th} = \frac{P_o}{P_{add}} = \frac{\dot{m}c_p(T_4 - T_5) - \dot{m}c_p(T_2 - T_1)}{\dot{m}c_p(T_4 - T_2)}$$

$$\eta_{th} = 1 - \left[\frac{1}{1 + \frac{T_2 - T_1}{T_2}} \right] \quad (E-3)$$

$$\eta_{th} = 1 - \frac{T_1}{T_2} = 1 - r^{-\frac{\gamma-1}{\gamma}}, \quad (E-4)$$

where $r \equiv p_2/p_1$, the pressure ratio. For the CBEX cycle, the thermal efficiency is given by

$$\eta_{th} = \frac{\dot{m}c_p(T_4 - T_5) - \dot{m}c_p(T_2 - T_1)}{\dot{m}c_p(T_4 - T_3)} \quad (E-5)$$

$$\eta_{th} = 1 - \left(\frac{\frac{T_2 - T_1}{T_1} + 1}{\frac{T_4}{T_1}} \right) \quad (E-6)$$

$$\eta_{th} = 1 - \frac{T_1}{T_3} \quad (E-7)$$

For the ideal cycle, the specific power (power per unit mass flow of working fluid) is unaffected by the presence of a heat exchanger. Equation E-2 expresses the specific power in terms of the two important cycle parameters: the temperature ratio, T_4/T_1 , or $1 + (P_{add} + P_{int})/P_1$; and the temperature rise during compression, $(T_2 - T_1)/T_1$, which is P_{int}/P_1 for the CBE cycle. This relationship is shown graphically in Fig. E-3. The specific

power for the ideal cycle increases with increase of cycle temperature ratio, as can be seen from Eq. E-2. The effect of compressor temperature rise is less obvious. The specific power is zero when $T_2 = T_1$ and when $T_2 = T_4$. At some intermediate compressor temperature rise, the specific power is a maximum.

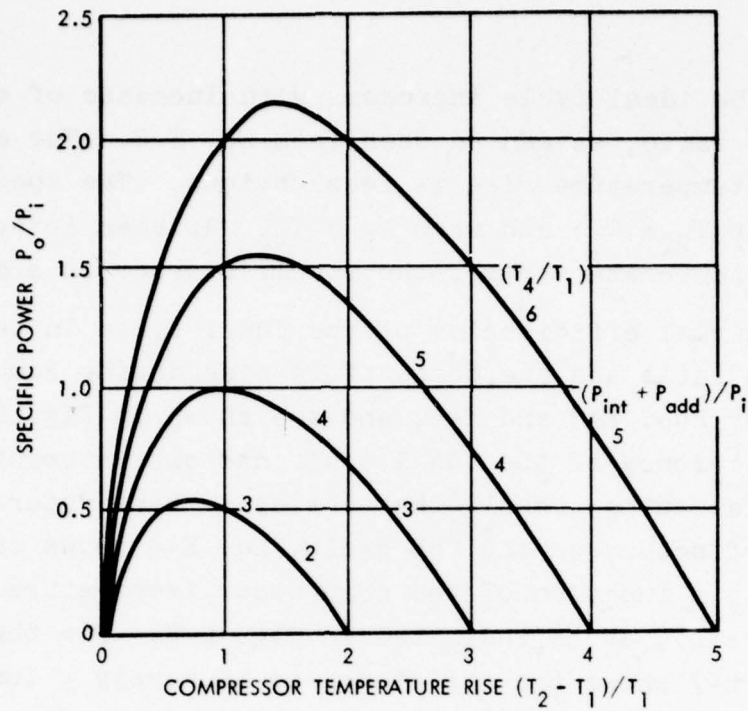
The thermal efficiencies of the ideal cycle in terms of the temperature ratio and the temperature rise during compression are given by Eqs. E-3 and E-6, and are shown in Fig. E-4. The thermal efficiency of the ideal cycle has the interesting, but somewhat misleading, result that the cycle temperature ratio has no direct effect. For the CBE cycle, Eq. E-4 shows the efficiency to be merely a function of the compressor temperature rise (or pressure ratio), as is indicated in Fig. E-4. For the CBEX cycle, Eq. E-7 shows the efficiency to be merely a function of the temperature before combustion begins, which accounts for the decrease in efficiency with compressor temperature rise shown in Fig. E-4. Thus, in either cycle, the efficiency depends only upon the inlet temperature and the temperature at which heat addition begins. However, in order to achieve a specific power close to the optimum, the cycle temperature ratio must be increased as the temperature prior to heat addition is increased, as shown in Fig. E-3.

The performance of the two cycles can also be portrayed as a function of the two power-transfer parameters P_{int}/P_o and $(P_{int} + P_{add})/P_i$ by noting that, for the CBE cycle,

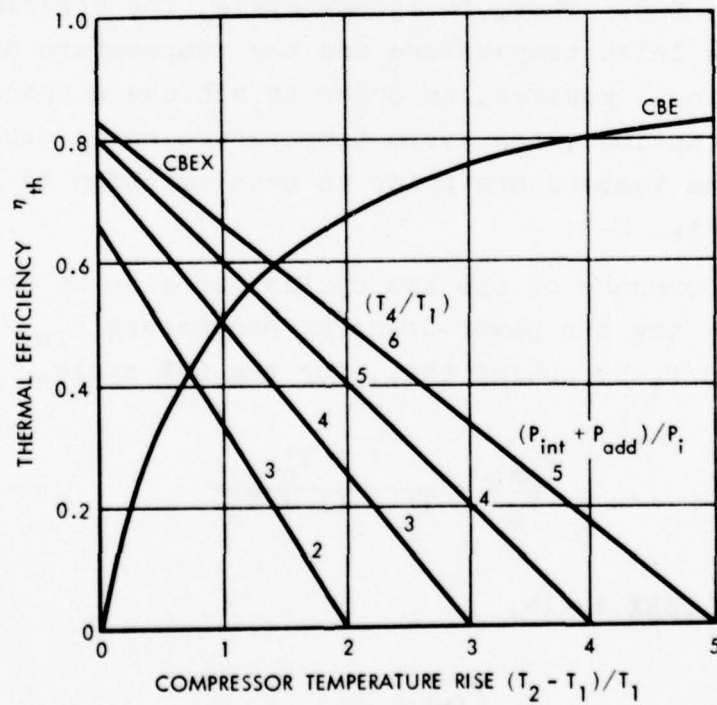
$$\frac{P_{int}}{P_o} = \frac{1 + T'_c}{T' - (1 + T'_c)} \quad (E-8)$$

and, for the CBEX cycle,

$$\frac{P_{int}}{P_o} = \frac{1}{T'_c} \quad , \quad (E-9)$$



9-23-77-4
FIGURE E-3. Specific power of ideal Brayton cycles.



9-23-77-3
FIGURE E-4. Thermal efficiency of ideal Brayton cycles.

where

$$T' \equiv \frac{T_4}{T_1} = 1 + \frac{P_{int} + P_{add}}{P_1}$$

$$T'_c \equiv \frac{T_2 - T_1}{T_1} .$$

The performance of the two cycles is shown in this way in Fig. E-5. When plotted against the ratio of internal power transfer to power output, the two cycles are identical in respect of both specific output and specific fuel consumption. In other words, the cycle is uninfluenced by whether the energy transfer from the post-energy-addition part of the cycle to the pre-energy-addition part is carried out by shaft power or by heat exchanger. In both cases, more internal energy transfer means that the external heat addition begins at a higher temperature, which leads to smaller irreversibilities.

The pressure ratios are also shown in Fig. E-5. The pressure ratio is plotted for generality as $(T_2 - T_1)/T_1$ with the pressure ratios for $(R/c_p) \approx 3.50$ also given. For the CBE specific fuel consumption the lines are horizontal, because for this cycle efficiency is a function only of pressure ratio. The lines correlating pressure ratio with specific output slope are at forty-five degrees. For the CBEX cycle, lines of constant pressure ratio are vertical, because compressor temperature rise is a function only of (P_{int}/P_o) .

The curves of Fig. E-5 illustrate again that the choice of even an ideal cycle, in respect of temperature ratio and pressure ratio, or $(P_{add} + P_{int})/P_1$ and P_{int}/P_o , is a compromise between the conditions for maximum specific output and those for minimum specific fuel consumption. Both the CBE and the CBEX ideal cycles have optimum pressure ratios for maximum specific

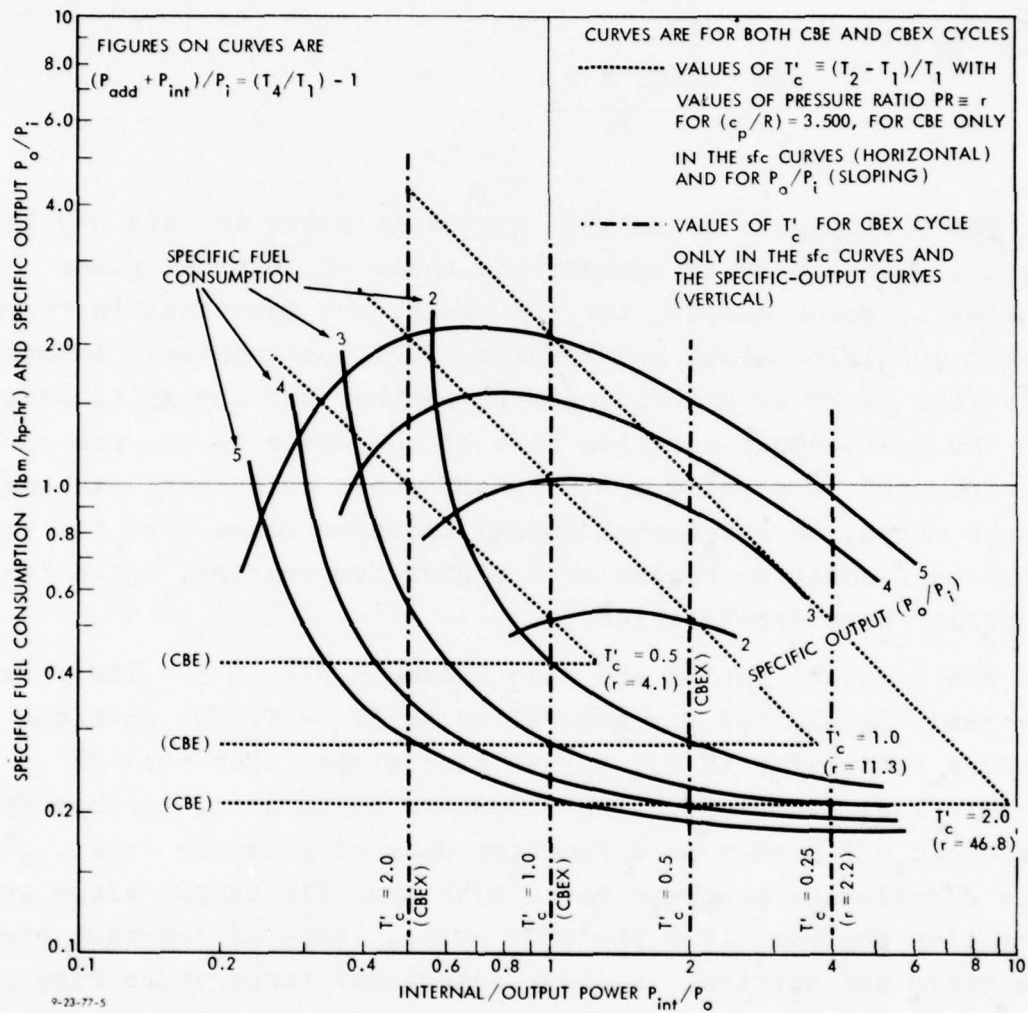


FIGURE E-5. Performance of ideal Brayton cycles.

output. But for minimum specific fuel consumption, the CBE cycle has an infinite pressure ratio, while the CBEX has a pressure ratio of 1.0, with, in the limit, the specific output being zero in both cases and the ratio of internal power transfer to power output being infinite.

3. Implications of Ideal-Cycle Performance

Many of the implications of the curves derived so far have been discussed above. One way of summarizing the effect of internal power transfer is the following. We are assuming an infinite heat exchanger for the CBEX cycle in all conditions, which nevertheless gives a finite amount of power transfer, whereas for the CBE cycle the finite power transfer through the compressor shaft is always given, except in the limit, by a finite pressure ratio. A heat exchanger with an effectiveness, or thermal ratio, approaching unity theoretically tends to be infinite in size, whereas a compressor with a pressure ratio increasing toward infinity does not necessarily become large (for instance, a positive-displacement compressor would add very small additional volumes).

The part-load implications are not seen in the ideal case, but may be very important in practice. An open-cycle high-pressure-ratio CBE engine will in general have a poor part-load performance, whereas a low-pressure-ratio CBEX engine will have a good part-load performance, because of the very different characteristics of the alternative power-transfer devices--the compressor in the CBE case, and the heat exchanger in the CBEX engine.

The ideal Brayton cycle can be improved. Any changes will semantically change it from being a Brayton cycle. Therefore, in considering improvements, we are opening up the possibility of reviewing all possible engine cycles. We shall limit this discussion to the possibility of introducing intercooling during compression and reheating during expansion. In the limit, the

ideal cycle would have isothermal compression and expansion. Such a cycle would have very poor performance unless a heat exchanger were used, in which case it would become the Ericsson cycle. For the same P_{add} , the expansion power would be increased because the expander work is proportional to expander inlet temperature, and this is held at the top temperature. Likewise, the compressor work would be reduced. The net output would thereby be increased by more than the increment by which the internal (shaft) power transfer would be reduced. However, the internal heat-exchanger power transfer would be somewhat increased. And the atmosphere could no longer be used to accomplish the heat rejection directly: the engine must carry a heat exchanger (or series of heat exchangers) for heat rejection during compression. This heat is termed P_x . For the characteristics of the ideal Ericsson cycle to be plotted to the same scales as those for the ideal Brayton cycle in Fig. E-5, P_x must be added to P_{int} on the abscissa; these are shown in Fig. E-6.

The large improvement in specific power and in specific fuel consumption over the Brayton cycle for similar temperature ratios can be seen from Fig. E-6. This improvement, however, is at the expense of increased total internal power transfer.

B. RELATIONSHIP OF ACTUAL PERFORMANCE TO IDEAL PERFORMANCE

1. Components and Losses

The components of open-Brayton-cycle engines are, as the symbols CBE and CBEX imply, compressors, burners, expanders, and heat exchangers. Connecting ducts can contribute significantly to losses, but they are incorporated into the four basic components by assigning each duct, or a portion of each duct, to a neighboring component.

The broadest and most precise definition of a loss is a process which results in a net reduction in the thermodynamic function "availability." In practice, for the components of an

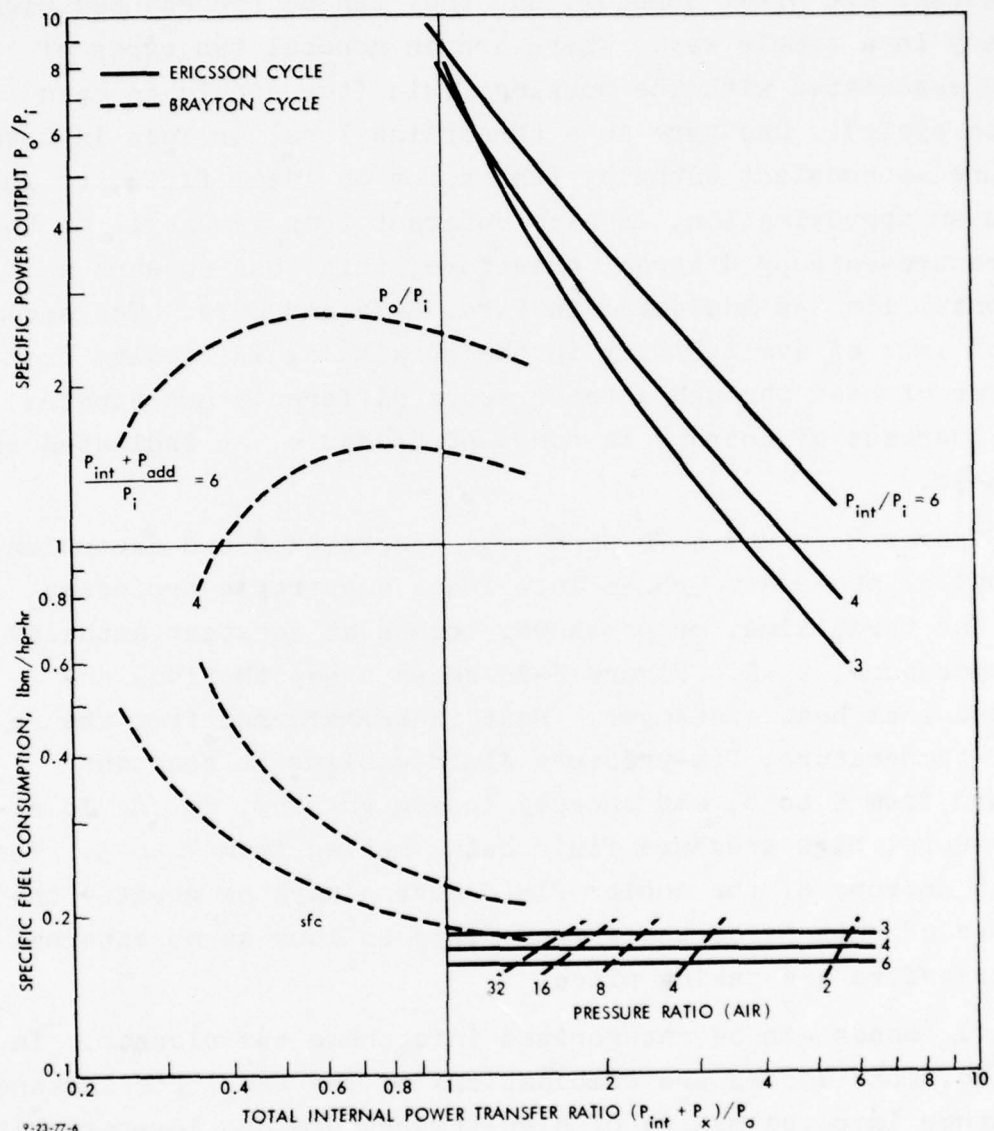


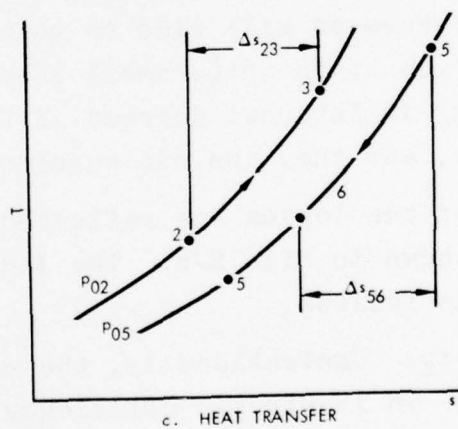
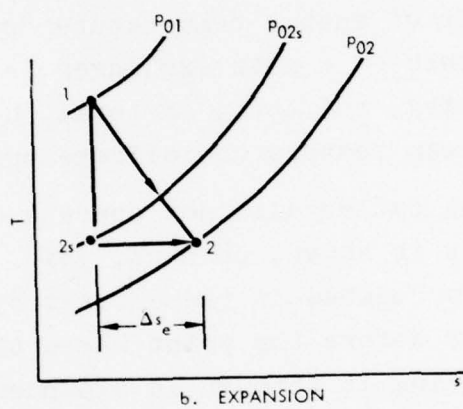
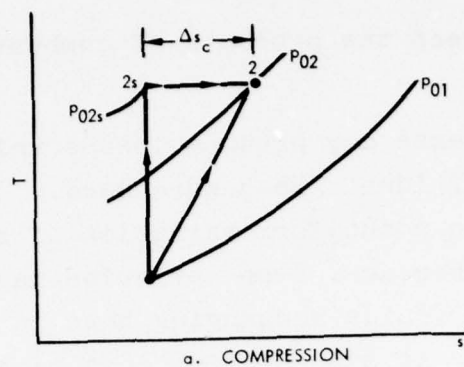
FIGURE E-6. Performance of the ideal Ericsson cycle.

engine, losses can be represented by increases in entropy in excess of those associated with the ideal cycles.

Losses are often complex, but they can be represented with accuracy in a simple way. There are in general two types of losses associated with the working fluid (the air in an open Brayton cycle). One type is a throttling loss, or loss in total pressure at constant enthalpy (which for an ideal fluid, to which air is an approximation, is also constant temperature). On the temperature-entropy diagram, therefore, this loss appears as a horizontal line as indicated in Figs. E-7a and E-7b. The second type of loss of availability in the working fluid results from transfer of heat through a temperature difference and appears as an increase of entropy at constant pressure, as indicated in Fig. E-7c.

Figures E-7a and E-7b show real compression and expansion (adiabatic) processes broken into ideal isentropic processes $1-2_s$, and throttling, or pressure, losses at constant enthalpy or temperature, 2_s-2 . Figure E-7c shows a hypothetical no-pressure-loss heat exchanger. Heat is transferred from the higher-temperature, low-pressure fluid cooling at constant pressure from 5 to 6, and thereby losing entropy, to the lower-temperature, high-pressure fluid being heated from 2 to 3. The gain in entropy of the cooler fluid must always be greater than the loss of entropy of the warmer fluid so long as no external heat transfers are taking place.

All losses can be categorized into these two classes. In practice, most losses are combinations of the two. For instance, the burner involves mixing of high-temperature and low-temperature streams and the dissipation of high-velocity jets within streams, forms of heat transfer and of pressure loss. (We are here idealizing the working fluid as a simple substance. If we consider the real case where many species may co-exist and mix, we should have to include also losses of availability between other



9-23-77-7

FIGURE E-7. Entropy gains associated with component losses.

potentials, e.g., between the products of combustion and the atmosphere.)

The use of real gases may produce losses which would hypothetically not occur if ideal gases were used. The principal causative factor is the nonuniform variation of specific heat with temperature and pressure. The variation may be such that the temperature of two fluids exchanging heat in a heat exchanger may approach each other at one location in a heat exchanger, while being more separated than for an ideal fluid in other places. The net result of such a temperature "pinch" is that the maximum effectiveness of a heat exchanger is limited even if the size went to infinity, and that, in total, heat is transferred over a larger mean temperature difference.

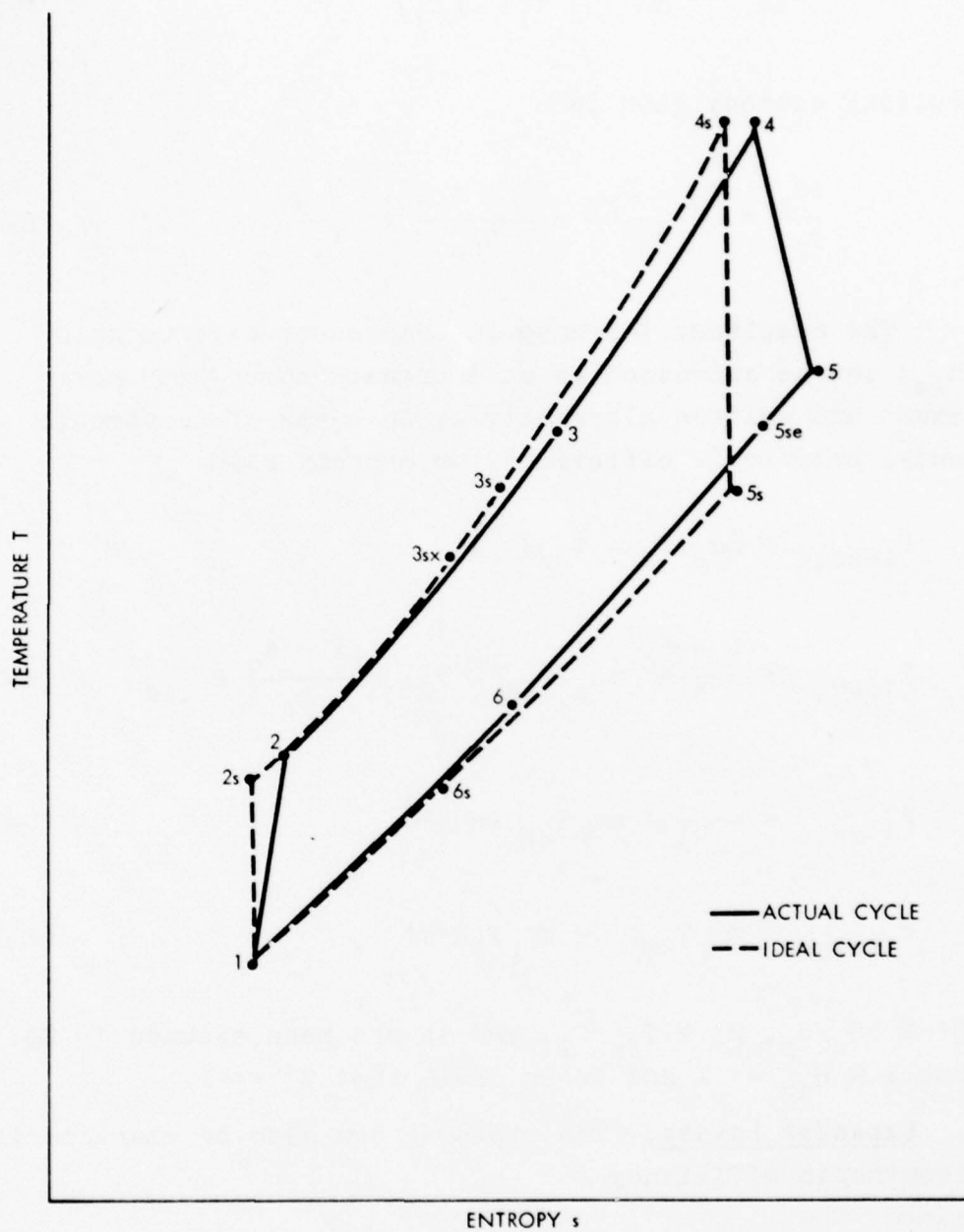
Some cryogenic gas cycles will not operate unless the heat-exchanger effectiveness is above, perhaps, 98%. Reversible, ideal conditions are approached in these cases by withdrawing high-pressure gas at or before the point where the specific heat reaches a maximum, passing it through an expander, and combining it with the low-pressure stream. It seems unlikely that OBE heat-exchanger effectivenesses will rise to this level. Real-gas effects presently result in quite small losses, due primarily to the increased energy in internal degrees of freedom in the products of combustion, and they are not considered further here.

The net results of the losses are reflected in the temperature-entropy diagram shown in Fig. E-8. The individual losses can be characterized as follows.

a. Compressor Loss. Conventionally, the compressor is characterized by either an isentropic efficiency

$$\eta_c \equiv \frac{h_{2s} - h_1}{h_2 - h_1} = \frac{T_{2s} - T_1}{T_2 - T_1} \quad (E-10)$$

or a polytropic efficiency



9-23-77-8

FIGURE E-8. Temperature-entropy diagram of actual Brayton-cycle engine.

$$\eta_{cp} \equiv \frac{dh_{isen}}{dh} ; \frac{T_2}{T_1} = \left(\frac{P_2}{P_1} \right)^{\frac{R}{c_p \eta_{cp}}} . \quad (E-11)$$

The resulting entropy gain is

$$\frac{\Delta S_c}{c_p} = \frac{S_2 - S_{2s}}{c_p} = \frac{1 - \eta_{cp}}{\eta_{cp}} \ln \frac{T_{2s}}{T_1} . \quad (E-12)$$

The resultant increase in compressor exit enthalpy ($h_2 - h_{2s}$) can be expressed as an increased compressor power requirement and written alternatively in terms of isentropic efficiency, polytropic efficiency, or entropy gain:

$$P_{loss,c} \equiv \dot{m} c_p (T_2 - T_{2s})$$

$$P_{loss,c} = \frac{1 - \eta_c}{\eta_c} \dot{m} c_p (T_{2s} - T_1) = \frac{1 - \eta_c}{\eta_c} P_{c,id} \quad (E-13)$$

$$P_{loss,c} = \frac{1 - \eta_c}{\eta_c} \dot{m} c_p T_{2s} \ln \frac{T_{2s}}{T_1} \quad (E-14)$$

$$P_{loss,c} = \dot{m} c_p T_{2s} C' = \dot{m} c_p T_1 R' C' , \quad (E-15)$$

where $C' \equiv \Delta S_c / c_p$, $R' \equiv T_{2s} / T_1$, and it has been assumed in Eq. E-14 that $1 - \eta_{cp} \ll 1$ and in Eq. E-15 that $C' \ll 1$.

b. Expander Losses. The expander can also be characterized by an isentropic efficiency

$$\eta_e \equiv \frac{h_4 - h_5}{h_4 - h_{5sE}} \quad (E-16)$$

or a polytropic efficiency

$$\eta_{ep} = \frac{dh}{dh_{isen}} ; \frac{T_5}{T_4} = \left(\frac{P_5}{P_4} \right)^{\eta_{ep} \frac{R}{c_p}} \quad (E-17)$$

The resulting entropy gain is

$$\frac{\Delta S_e}{c_p} = \frac{S_s - S_{5sE}}{c_p} = (1 - \eta_{ep}) \ln \frac{T_4}{T_{5sE}} \quad (E-18)$$

The resultant increase in expander exit enthalpy ($h_5 - h_{5sE}$), expressed as a loss in expander power output is, alternatively:

$$P_{loss,e} \equiv \dot{m} c_p (T_5 - T_{5sE}) \quad (E-19)$$

$$P_{loss,e} = (1 - \eta_e) \dot{m} c_p (T_4 - T_{5sE}) = (1 - \eta_e) P_{e,id} \quad (E-20)$$

$$P_{loss,e} = (1 - \eta_{ep}) \dot{m} c_p T_{5sE} \ln \frac{T_4}{T_{5sE}} \quad (E-21)$$

$$P_{loss,e} = \dot{m} c_p T_{5sE} E' \quad (E-22)$$

where $E' \equiv \Delta S_e / c_p$, and it has been assumed that $1 - \eta_p \ll 1$ and $E' \ll 1$, and $T_5 / T_{5sE} \cong 1 + E'$.

c. Pressure Losses. Pressure losses occur in the burner (3-4) and, in the CBEX cycle, in the regenerator (2-3 and 5-6). It is apparent from Fig. E-8 that these pressure losses result in a further reduction of expander power (relative to the ideal cycle), $\dot{m} c_p (h_{5sE} - h_{5s})$.

Pressure losses are generally characterized by fractional losses $\Delta p/p_{\max}$ where p_{\max} is the maximum pressure entering the relevant component. The resulting entropy gain is

$$\Delta S_L = R \sum \ln \frac{p_{\max}}{p_{\max} - \Delta p} \cong R \sum \left(\frac{\Delta p}{p} \right) \quad (E-23)$$

The reduction in expander power can be written as

$$P_{\text{loss},L} = \dot{m} c_p (T_{5sE} - T_{5s})$$

$$P_{\text{loss},L} \cong \dot{m} c_p T_{5s} \frac{\Delta S_L}{c_p} \equiv \dot{m} c_p T_{5s} L' = \dot{m} c_p T_{5s} \frac{R}{c_p} \sum \left(\frac{\Delta p}{p} \right) \quad (E-24)$$

where $T_{5sE}/T_{5s} \cong 1 + L'$.

d. Heat Exchange Losses. The thermal performance of a heat exchanger is generally characterized by its effectiveness,

$$\epsilon \equiv \frac{T_3 - T_2}{T_5 - T_2} \quad (E-25)$$

In the CBEX cycle, losses arising due to less than 100% effectiveness require additional heat addition and, in the sense of heat rather than work, can be considered a power loss.

In the absence of any other losses, the additional heat input required (Fig. E-8) is $\dot{m}(h_{3s} - h_{3sx})$, and since T_{3sx} is defined by

$$\epsilon = \frac{T_{3sx} - T_{2s}}{T_{3s} - T_{2s}} \quad ,$$

this can be written as

$$P_{\text{loss},x} \equiv \dot{m}c_p(T_{3s} - T_{3sx})$$

$$P_{\text{loss},x} = (1 - \epsilon)\dot{m}c_p(T_{3s} - T_{2s}) = (1 - \epsilon)P_{x,\text{ideal}} \quad (\text{E-26})$$

In the actual CBEX cycle, with the other losses present, the additional heat input (relative to the ideal cycle) associated with a non-unity effectiveness is, from Fig. E-8, $\dot{m}c_p(T_{5s} - T_3)$. For high-effectiveness heat exchangers, this quantity will normally be negative--that is, the effect of the other losses will decrease the required heat input from that for the ideal case.

In terms of entropy, we choose to represent the thermal losses associated with the heat exchanger as the entropy gain in a constant pressure change from T_3 to T_5 (Fig. E-8), the "temperature of approach." This entropy change is of course a surrogate, much larger than the entropy gain in the heat exchanger due to heat transfer through a temperature difference. (The actual loss would be given by deducting the entropy loss at constant pressure from T_6 to T_2 .) This entropy gain is

$$\frac{\Delta S_{3s}}{c_p} = \ln \frac{T_5}{T_3} \equiv x' \quad , \quad (\text{E-27})$$

where

$$\frac{T_5}{T_3} = \frac{1}{\epsilon} - \left(\frac{1 - \epsilon}{\epsilon} \right) \frac{T_2}{T_3} \quad . \quad (\text{E-28})$$

The total additional heat input can be written as

$$\dot{m}c_p(T_{5s} - T_3) = -\dot{m}c_p[(T_{5sE} - T_{5s}) + (T_5 - T_{5sE}) - (T_5 - T_3)]$$

and with some manipulation becomes

$$\dot{m}c_p(T_{5s}-T_3) = \dot{m}c_p T_1 \frac{T'}{R'} [x' - (1-x')(L'+E'+E'L')] , \quad (E-29)$$

where

$$R' \equiv \frac{T_{2s}}{T_1} = \frac{T_4}{T_{5s}}$$

$$T' = \frac{T_4}{T_1} .$$

The first term in brackets in Eq. E-29 is associated with the additional heat input required due to the ineffectiveness of the heat exchanger in the absence of expander and pressure losses (i.e., $P_{loss,x}$ in Eq. E-26 plus the effect of compressor losses), while the other term in brackets is associated with the effect of expander and pressure losses on reducing the heat input required when a heat exchanger is present.

2. Impact of Losses on Engine Performance

The specific fuel consumption of an actual engine, with losses, is given by

$$sfc = \frac{0.138}{\eta_{th}} \quad \text{lbm/hp-hr} \quad (E-30)$$

and the specific power output is given by

$$\frac{P_o}{P_i} = \eta_{th} \frac{P_{add}}{P_i} , \quad (E-31)$$

where η_{th} is the actual cycle efficiency and P_{add} is the actual rate of heat addition to the working fluid.

The cycle efficiency, including the effects of losses, can be determined in a straightforward way for specified values of pressure ratio, temperature ratio, compressor and expander efficiencies, fractional pressure loss, and heat-exchanger effectiveness (for the CBEX cycle). The results can be written as follows:

$$\frac{P_o}{P_1} = ET' - C \quad (E-32)$$

$$\eta_{th} = \frac{ET' - C}{T'[1 - \epsilon(1 - E)] - (1 - \epsilon)(1 + C)} \quad (E-33)$$

$$\frac{P_{int}}{P_o} = \frac{(1 - \epsilon)(1 + C) + \epsilon T'(1 - E) - 1}{ET' - C} \quad (E-34)$$

$$\frac{P_{add} + P_{int}}{P_1} = T' - 1, \quad (E-35)$$

where

$$E \equiv 1 - [(1 - f)r] - \frac{R\eta_{ep}}{c_p}$$

$f \equiv$ total cycle pressure losses relative to local total pressure $\equiv \Sigma(\Delta p/p)$

$r \equiv p_2/p_1 =$ compressor pressure ratio

$$C \equiv \gamma \frac{R}{c_p \eta_{cp}} - 1$$

$$T' \equiv T_4/T_1$$

$\epsilon \equiv$ heat-exchanger effectiveness.

It is also useful, however, to isolate the effects of the individual losses in the following way. The cycle efficiency can be written as

$$\eta_{th} = \frac{P_o}{P_{add}} = \frac{P_{o,id} - \text{losses reducing power output}}{P_{add,id} + \text{losses increasing heat input}}$$

or

$$\eta_{th} = \frac{\eta_{th,id}}{1 + \frac{\text{heat losses}}{P_{add,id}}} - \frac{\text{power losses}}{P_{add,id} \left(1 + \frac{\text{heat losses}}{P_{add,id}} \right)} \quad , \quad (E-36)$$

where the subscript id refers to the ideal cycle. If it is assumed that the losses are small compared to the ideal heat addition, Eq. E-36 can be expanded to

$$\eta_{th} = \left[\eta_{th,id} - \frac{\text{power losses}}{P_{add,id}} \right] \left[1 - \frac{\text{heat losses}}{P_{add,id}} \right] \quad (E-37)$$

$$\eta_{th} = \eta_{th,id} - \eta_{th,id} \left(\frac{\text{heat losses}}{P_{add,id}} \right) - \left(\frac{\text{power losses}}{P_{add,id}} \right) \quad . \quad (E-38)$$

Similarly, the specific output can be written as

$$\frac{P_o}{P_i} = \frac{P_{o,id} - \text{power losses}}{P_i} \quad . \quad (E-39)$$

From the previous characterization of losses, the power losses and heat losses are as follows:

<u>Loss Component</u>	<u>Equation Nos.</u>	<u>Power Loss</u>	<u>Heat Loss</u>
Compression	(E-13)-(E-15)	$P_{\text{loss},c}$	$-(1-\epsilon)P_{\text{loss},c}$
Expansion	(E-20)-(E-22)	$P_{\text{loss},e}$	$-\epsilon P_{\text{loss},e}$
Pressure Losses	(E-24)	$P_{\text{loss},L}$	$-\epsilon P_{\text{loss},L}$
Heat Exchange	(E-26)	0	$P_{\text{loss},x}$

Substitution of these losses into Eqs. E-37 and E-39 results in

$$\begin{aligned}
 \eta_{th} = \eta_{th,id} - [1 - (1-\epsilon)\eta_{th,id}] & \left(\frac{P_{\text{loss},c}}{P_{c,id}} \right) \left(\frac{P_{c,id}}{P_{\text{add},id}} \right) \\
 & - [1 - \epsilon\eta_{th,id}] \left(\frac{P_{\text{loss},e}}{P_{\text{loss},id}} \right) \left(\frac{P_{e,id}}{P_{\text{add},id}} \right) \\
 & - [1 - \epsilon\eta_{th,id}] \left(\frac{P_{\text{loss},L}}{\dot{m}c_p T_{5s}} \right) \left(\frac{\dot{m}c_p T_{5s}}{P_{\text{add},id}} \right) \\
 & - \eta_{th,id} \left(\frac{P_{\text{loss},x}}{P_{x,id}} \right) \left(\frac{P_{x,id}}{P_{\text{add},id}} \right) \quad (E-40)
 \end{aligned}$$

$$\begin{aligned}
 \frac{P_o}{P_i} = \frac{P_{o,id}}{P_i} \left[1 - \left(\frac{P_{\text{loss},c}}{P_{c,id}} \right) \left(\frac{P_{c,id}}{P_{o,id}} \right) - \left(\frac{P_{\text{loss},e}}{P_{e,id}} \right) \left(\frac{P_{e,id}}{P_{o,id}} \right) \right. \\
 \left. - \left(\frac{P_{\text{loss},L}}{\dot{m}c_p T_{5s}} \right) \left(\frac{\dot{m}c_p T_{5s}}{P_{o,id}} \right) \right] \quad (E-41)
 \end{aligned}$$

These relationships apply to both the CBE ($\epsilon=0$) and CBEX ($\epsilon \neq 0$) cycles. In these expressions, the terms $P_{\text{loss},c}/P_{c,id}$, $P_{\text{loss},e}/P_{e,id}$, etc., are all of the form of a ratio of a power "loss" to a power transferred, and hence are a measure of inefficiency, as reference to the relevant preceding equations will show (e.g., $P_{\text{loss},c}/P_{c,id} = (1-\eta_c)/\eta_c$ from Eq. E-13). The other factors in

Eqs. E-40 and E-41 are a function of the ideal cycle and, at most, the heat exchanger effectiveness. Thus, these equations associate cycle efficiency and specific power output decrements with the various component losses, in terms of energy transfer parameters of the ideal cycle.

It can be observed from Eq. E-40 that the impact of losses on ideal cycle efficiency can be reduced either by increasing the component efficiencies or by increasing the rate of heat addition $P_{add,id}$. The latter is synonymous with increased maximum temperature, and it is only through this effect of reducing the impact of component losses that the maximum temperature influences cycle efficiency. It is also to be noted from Eq. E-40 that the heat exchange losses (in the CBEX cycle) have no effect on the specific power output (relative to the ideal cycle)--a direct result of the fact that heat exchange losses require increases in heat addition rather than detract from power output.

For purposes of numerical evaluation of the impact of changes in the various losses, it is perhaps more convenient to express them in terms of the entropy gains. Substitution of the appropriate loss forms into Eq. E-37 yields, for the CBE cycle,

$$P_{add,id} = \dot{m} c_p T_1 (T' - R')$$

and

$$\eta_{th} = [\eta_{th,id} - C'' - E''] [1 + C''] \quad , \quad (E-42)$$

where $C'' \equiv C' / [(T'/R') - 1]$

$$E'' \equiv (L' + E' + E'L') / R' [1 - (R'/T')]$$

$$R' \equiv T_{2s} / T_1$$

$$T' \equiv T_4 / T_1,$$

and, for the CBEX cycle,

$$P_{add,id} = \dot{m} c_p T_1 \frac{T'}{R'} (R' - 1)$$

$$\eta_{th} = [\eta_{th,id} - C'' - E''] \left[1 - \frac{X''}{R' - 1} \right], \quad (E-43)$$

$$\text{where } C'' = \frac{(R')^2 C'}{T'(R' - 1)}$$

$$E'' = (L' + E' + E'L')/(R' - 1)$$

$$X'' = X' - (1 - X')(L' + E' + E'L').$$

These relationships will be useful subsequently.

The performance characteristics for both nonregenerated (CBE) and regenerated (CBEX) Brayton-cycle engines with representative component losses are shown in Fig. E-9. Here, the polytropic efficiencies of the compressor and turbine are 0.90 and 0.85, respectively, and the pressure losses for the CBE cycle are assumed to be 5% of the total pressure. For the CBEX cycle, the heat exchanger effectiveness is 0.9 and the pressure losses are 15% of the total pressure. All of these values are to some extent matters of design choice to be determined from tradeoffs between weight, volume, and specific fuel consumption, but they are representative.

The comparison of realistic and ideal performance characteristics shown in Fig. E-9 [for $(P_{add} + P_{int})/P_i = 5$] indicates that the sfc is substantially increased by the component losses. For example, for the CBE cycle, losses increase the sfc from a level of about 0.2 to a minimum of about 0.3--an increase of 50%. For the component values selected, the CBEX cycles yield somewhat better performance than the CBE cycles at higher values of internal power transfer, and particularly at lower turbine inlet temperatures [i.e., low values of $(P_{add} + P_{int})/P_i$].

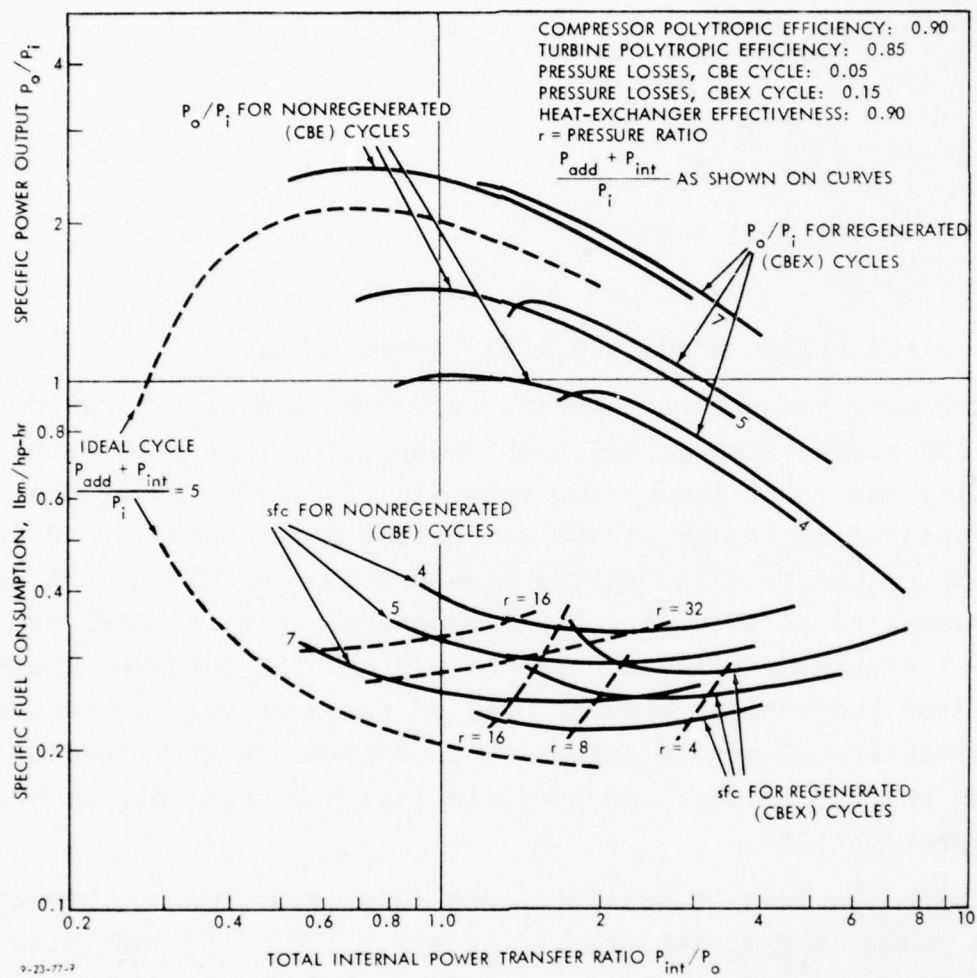


FIGURE E-9. Performance of some nonideal Brayton cycles.

The influence of the individual losses on the performance characteristics of CBE and CBEX cycles is shown in Figs. E-10 and E-11, respectively. The turbine loss is the largest contributor in the CBE cycle, as shown in Fig. E-10, closely followed by the compressor loss. The pressure loss is of minor significance. For the CBEX cycle (Fig. E-11) the heat exchanger loss is the dominant loss in the vicinity of the minimum sfc--even for the rather high effectiveness assumed. The remaining losses are relatively minor.

3. Part-Power Considerations

Because full-power considerations fix the specific power or size of the engine, the only performance parameter of significance for part power is the thermal efficiency or specific fuel consumption. Equation E-33 can be used to estimate the part-power thermal efficiency, just as at full power. However, all the parameters in that equation will, in general, change, and they will change in a way that is difficult to predict accurately.

The 25% power level has been chosen to represent part-power performance, because it is reasonably close to the cruising condition for many vehicular applications. The flow conditions in an open Brayton cycle can be markedly different from those at full power. This is particularly so for the compressor. There can be a strong effect on the compressor efficiency.

The reason for the sensitivity of the compressor at part power is as follows. The flow channels--impeller, diffuser, and so forth--are usually designed for a condition near the full-power level. The compressor will develop nearly its maximum pressure ratio and density ratio. If a channel at the compressor inlet were designed to produce the same flow velocity as one at the machine outlet, the ratio of the cross-sectional areas would be inversely the ratio of the design-point densities.

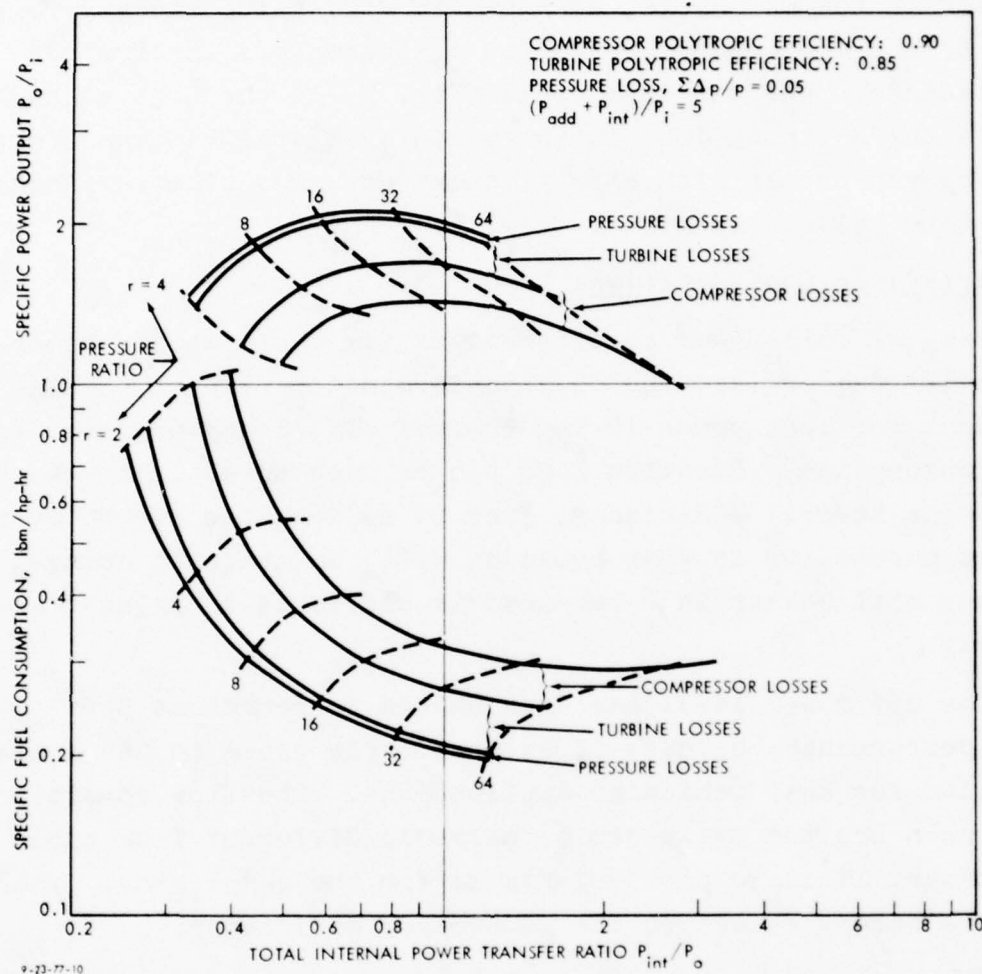


FIGURE E-10. Impact of component losses on nonregenerated Brayton-cycle (CBE) performance.

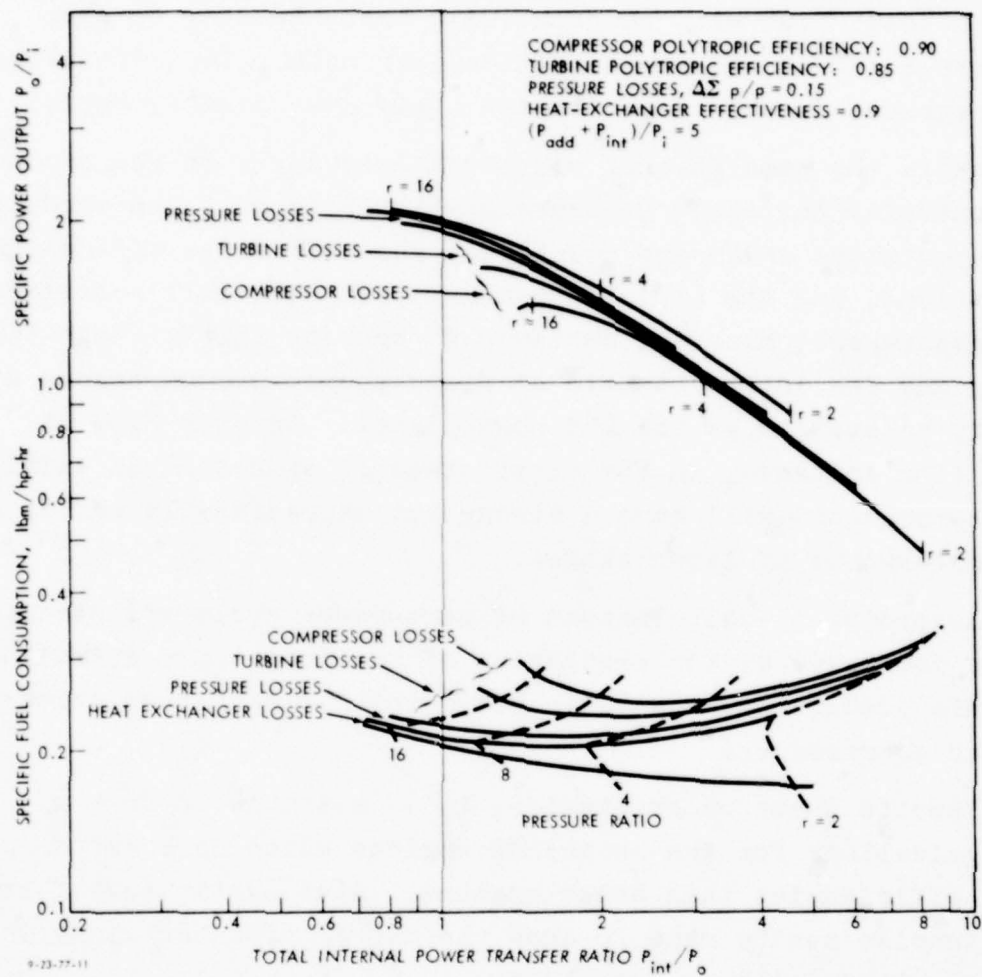


FIGURE E-11. Impact of component losses on regenerated Brayton-cycle performance.

At a quarter power, there may be only a very small density ratio across the compressor. Therefore the flow velocities, instead of being similar, will now be in the ratio of nearly the full-power densities. Therefore, either the inlet flow will be relatively slow, tending to produce positive stalling conditions, or the outlet flow will be relatively fast, tending to give negative stall or choking conditions, or both. The efficiency will degrade, further lowering the part-power density ratio.

While the same general considerations apply to the expander, the generally favorable pressure gradients found there produce flow conditions which are relatively insensitive to off-design distortions, and the efficiency usually changes only moderately. Compressors are, however, designed to operate fairly close to stall, and the inlet channels of fixed-geometry compressors will usually be stalled at the 25% power level. Stalled flow at inlet (for instance, in the first stage or stages of an axial-flow compressor) will have a strong but unpredictable effect on the performance of later stages.

Accordingly, calculations of part-power cycle efficiencies can be dominated by the prediction of the compressor efficiency, and this prediction is usually based on test characteristics of similar compressors.

Despite these uncertainties, it is possible to draw up some guidelines for the choice of engines which have better part-power efficiencies than other engines. Also, estimates of these efficiencies can be made to show the degree of uncertainty involved. These will be made below.

There are two principal forms of open Brayton cycle--the CBE and the CBEX--and two principal methods of part-power control--constant speed and reducing speed. (The shaft referred to is the compressor shaft, so we need not be concerned about the choice of a single shaft or a two-shaft machine with a separate power turbine, other than the choice implied by the control scheme.)

We have seen earlier that the CBE cycle produces high efficiencies when the pressure ratio is relatively high, whereas in the CBEX cycle the internal power transfer is accomplished predominantly through the heat exchanger, with the compressor temperature rise becoming small at maximum efficiency. This has important implications for part-power performance. A compressor designed for a density ratio near unity cannot degrade greatly in performance as the density ratio goes even closer to unity. Therefore the CBEX cycle will be more efficient at part power than will the CBE cycle from consideration of the compressor efficiency alone. In addition, heat exchangers actually improve their performance in Brayton-cycle part-power conditions, compensating to some extent the increased losses in the compressor.

Therefore, considerations of part-power cycle efficiency lead strongly to the choice of the CBEX cycle with as much internal power transfer accomplished in the heat exchanger as possible.

The choice of control system also has a strong effect on part-power performance. The cycle mass flow is a major function of shaft speed and a lesser function of compressor pressure ratio. When the compressor speed is held constant, therefore, the mass flow remains approximately at full-power level while the engine power is reduced. The pressure ratio reduces as less fuel is burned, so the compressor efficiency degrades because of the reduced density at outlet. More importantly, the expander-inlet temperature reduces as the fuel flow is reduced at part power, and the cycle thermal efficiency drops sharply.

On the other hand, when the shaft speed is allowed to fall at part power, the engine mass flow will also fall, so the maximum (expander-inlet) temperature will not drop as sharply as in the constant-speed case. The fall in compressor efficiency will depend on design pressure ratio, as discussed earlier, but in

general this form of control results in the compressor working line passing along or near the high-efficiency ridge.

In summary, the types of open-Brayton-cycle engine giving most favorable part-load efficiencies will have low design pressure ratios, high-effectiveness heat exchangers, and variable-speed compressor shafts. The most unfavorable type of engine will be one working on the CBE cycle with a high pressure ratio and maintaining constant compressor-shaft speed at part load.

It was pointed out earlier that the prediction by calculation of the part-load performance of a new Brayton-cycle engine is difficult and uncertain, even with very complex computer programs. All that will be attempted here will be calculations based on estimates of part-power conditions for a typical CBE cycle with constant compressor-shaft speed and for a typical CBEX cycle.

	CBE Cycle		CBEX Cycle	
	Des. Pt.	25% Power	Des. Pt.	25% Power
$T' \equiv T_4/T_1$	7	7×0.9	5.0	5.0×0.7
$T \equiv p_4/p_1$	32	32×0.7	4.0	4.0×0.75
η_{pc}	0.9	0.9×0.7	0.9	0.9×0.87
η_{pe}	0.9	0.9×0.9	0.85	0.85×1.0
f	0.05	0.04	0.06	0.04
$C \equiv \left[\frac{R}{\gamma} \frac{1}{c_p \eta_{pc}} - 1 \right]$	1.9371	2.9780	0.5387	0.4808
$E \equiv 1 - \left[(1-f)\gamma \right]^{-\frac{R}{c_p} \eta_e}$	0.5767	0.5011	0.2702	0.2224
$\eta_{th} = \frac{ET' - C}{ET' + (1-E)(T' - C - 1 - ET')}$	0.517	0.077	0.520	0.354
ϵ	0	0	0.90	0.94

This type of calculation serves perhaps more to emphasize the importance of compressor-efficiency drop in a CBE cycle rather than to give useful numbers. The drop in efficiency of the CBEX cycle to 25% load, which is approximately 60% of the full-load efficiency, is similar to actual low-pressure-ratio cycles. No figures for the part-load efficiency of actual high-pressure-ratio, constant-speed CBE cycles were available to the author.

Thus far, consideration of engine performance has been limited to specific fuel consumption and specific power output, the latter in the form of $P_o / \dot{m}_c T_1$. The specific power measures of ultimate interest are of course power per unit weight or volume. To develop these measures, it is necessary to examine the size-weight-loss characteristics of the various components. Accordingly, the next three sections deal with these relationships for three of the major types of components in open Brayton-cycle engines: radial turbomachinery, combustors, and heat exchangers. The other type of component commonly found in these engines, axial turbomachinery, is treated in Appendix F.

C. WEIGHT AND PERFORMANCE OF RADIAL TURBOMACHINERY

The derivation of correlating relations for radial turbomachinery used for Brayton cycles is made easier by the similarity of the design conditions which generally apply. The shape, or specific speed, can be chosen to be near the optimum, and the number of blades also can be selected to give maximum efficiency without significantly compromising weight, frontal area, or volume. Some form of vaned diffuser is always used for compressors, and vaned nozzles for turbines. Backward-sloped blades are used to the maximum degree allowed by blade-root stresses. Variable-geometry inlet or outlet vanes are generally not used. The hub-to-tip ratio of the blades at compressor inlet and turbine outlet can generally be chosen to give optimum performance even where there is a power takeoff, because the shaft diameter is

usually much smaller than the optimum hub diameter. These considerations are employed throughout the following developments.

1. Radial Turbomachinery Weight, Size, and Power

Some useful geometric quantities are defined in Fig. E-12. The stage power P_s is given by

$$P_s = \dot{m} \Delta h_o \quad , \quad (E-44)$$

where Δh_o is the stage enthalpy rise. From Fig. E-12, the mass flow \dot{m} is

$$\dot{m} = C_{x1} \rho_1 \frac{\pi}{4} d_{s1}^2 (1 - \lambda_1^2) \quad , \quad (E-45)$$

where $\lambda_1 \equiv \text{hub/tip ratio} = d_{h1}/d_{s1}$.

The stage enthalpy rise can be expressed in terms of the stage work coefficient ψ

$$\psi \equiv \Delta h_o / u_2^2 \quad ,$$

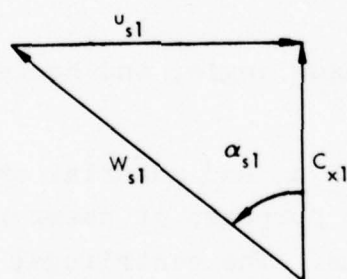
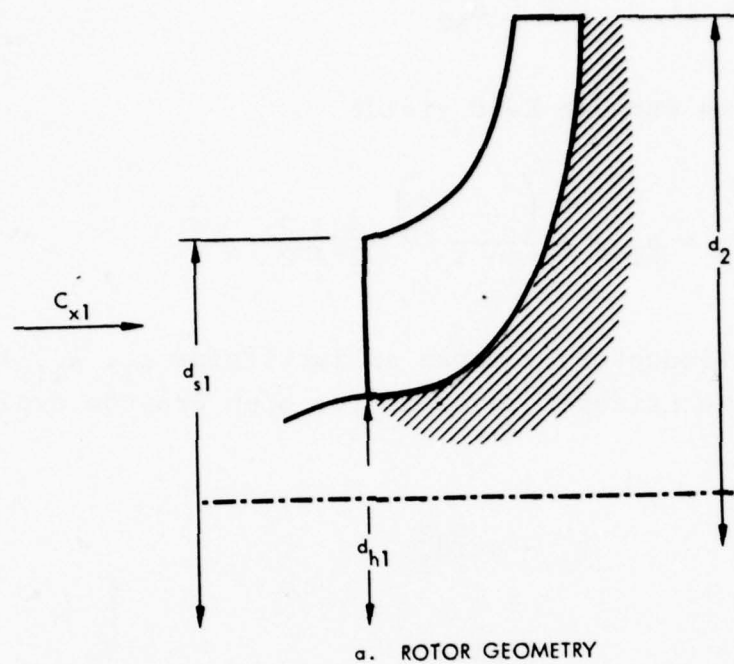
where u_2 is the rotor tip speed (at d_2). Thus

$$\Delta h_o = \psi u_2^2 \quad . \quad (E-46)$$

From the inlet velocity triangle,

$$\tan \alpha_{s1} = \frac{u_{s1}}{C_{x1}} \quad . \quad (E-47)$$

This angle is selected to minimize W_{s1} , and turns out to be near 60 deg for most applications. The specific speed can be defined (or represented) by the shroud-to-tip diameter ratio:



9-23-77-12

FIGURE E-12. Geometric definitions in radial turbomachinery.

$$\lambda_2 \equiv \frac{d_{s1}}{d_{s2}} \quad . \quad (E-48)$$

Combining Eqs. E-44 through E-48 yields .

$$P_s = \rho_1 \frac{\pi}{4} \psi \frac{(1 - \lambda_1^2)}{\tan \alpha_{s1}} \lambda_2^3 u_2^3 d_2^2 \quad . \quad (E-49)$$

If we take the introductory remarks as justifying ρ_1 , λ_1 , λ_2 , and $\tan \alpha_{s1}$ being considered constant for open Brayton cycles, then

$$P_s \sim \psi u_2^3 d_2^2 \quad (E-50)$$

$$d_2 \sim \frac{\dot{m}^{1/2}}{u^{1/2}} \quad (E-51)$$

or

$$P_s \sim \dot{m} \psi u_2^2 \quad , \quad (E-52)$$

where ψ is a function of blade angle, and hence of u_2 and material properties.

The variation of ψ with u_2 and material properties is not simple, but for the present purposes it seems reasonable to make the following approximations. The centrifugal stresses σ_c vary approximately as

$$\sigma_c \sim \rho_r u_2^2 \quad ,$$

where ρ_r is the material density.

The bending stresses vary approximately as

$$\sigma_b \sim \rho_r u_2^2 \sin \beta ,$$

where β is the backslope angle. The maximum stress σ is then

$$\sigma \sim \rho_r u_2^2 (1 + A \sin \beta) , \quad (E-53)$$

where A is a constant of order unity. The relationship between ψ and β is determined from angular momentum considerations, and can be approximated by

$$\psi \sim 1 - \frac{\psi \tan \beta}{2}$$

or

$$\psi \sim \frac{1}{1 + \frac{1}{2} \tan \beta} . \quad (E-54)$$

Equations E-53 and E-54 can be combined approximately as

$$\sigma \sim \frac{\rho_r u_2^2}{\psi}$$

or expressed as a determinant of tip speed

$$u_2^2 \sim \frac{\sigma \psi}{\rho_r} , \quad (E-55)$$

where σ can be interpreted as the allowable working stress of the material. Equations E-52 and E-55 then yield

$$P_s \sim \dot{m} \psi^2 \frac{\sigma}{\rho_r} . \quad (E-56)$$

The weight of the stage can be considered in two parts-- the rotor and the stationary parts. The rotor weight W_R scales approximately as

$$W_R \sim \rho_r d_2^3 .$$

With Eqs. E-51 and E-55, this can be written as

$$W_R \sim \frac{\dot{m}^{3/2}}{\psi^{3/4}} \frac{\rho_r^{7/4}}{\sigma^{3/4}} . \quad (E-57)$$

The weight of the stationary parts, W_S , scales approximately as

$$W_S \sim \rho_s d_2^2 t , \quad (E-58)$$

where t is a characteristic (small) thickness. The thickness is governed largely by pressure stresses similar to those in a thin-walled cylinder; thus

$$t \sim \frac{p d_2}{\sigma_s} ,$$

where p is the maximum pressure and σ_s is the allowable stress in the material. Then the weight will vary as

$$W_S \sim \frac{\rho_s p d_2^3}{\sigma_s} .$$

With Eqs. E-52 and E-55, this yields

$$W_S \sim \frac{\dot{m}^{3/2}}{\psi^{3/4}} \frac{\rho_s \rho_r^{3/4}}{\sigma_s^{3/4}} \quad (E-59)$$

Equations E-56, E-57, and E-59 can be combined to produce the specific weight

$$\frac{W}{P_s} = \frac{W_R + W_S}{P_s}$$

or

$$\frac{W}{P_s} \sim \frac{\dot{m}^{1/2}}{\psi^{11/4}} \frac{\rho_r^{11/4}}{\sigma^{7/4}} \left[A + (1 - A) \frac{\rho_s}{\rho_r} \frac{p}{\sigma} \right] \quad (E-60)$$

where A is the ratio of rotor weight to total stage weight in a base stage.

The stage volume V scales as

$$V \sim d_2^3 \quad ,$$

and hence the specific volume scales as

$$\frac{V}{P_s} \sim \frac{\dot{m}^{1/2} \rho_r^{7/4}}{\psi^{11/4} \sigma^{7/4}} \quad (E-61)$$

2. Radial Turbomachinery Performance

The best measure of efficiency is the polytropic total-to-static efficiency from inlet to outlet "flange." This assumes that the outlet head is of no utility, which is generally true except for jet engines. The losses can be measured as $(1 - \eta_{cp})$.

For a single-stage compressor, the efficiency degrades as the backward sweep of the rotor blades at outlet decreases, and hence as ψ increases, due to the increasing amount of flow deceleration required in the rotor. Further, as ψ and hence blade speed increase, Mach number effects eventually further degrade the efficiency. For simplicity, it is assumed here that the efficiency variation is linear with ψ and independent of the magnitude of blade speed. Available data (e.g., Ref. E-1) suggest that a reasonable approximation is

$$1 - \eta_{pc} = 0.2 \left(\frac{\psi}{0.9} \right) \quad (E-62)$$

for single-stage compressors. For multistage compressors, the outlet dynamic head could conceivably be useful, and different limiting values of η_{pc} are suggested:

$$1 - \eta_{pc} = L \left(\frac{\psi}{0.9} \right) , \quad (E-63)$$

where $L = 0.2$ for 1 stage

$L = 0.15$ for 2 stages

$L = 0.13$ for 3 stages

$L = 0.12$ for 4 or more stages.

This relationship is at best approximate and tentative, and envelope values need to be established for existing "well-designed" engines. Given the problems associated with the inaccuracy with which the efficiency is known, reported, and even defined by the engine manufacturers, such an effort was beyond the scope of the present investigation.

Multistage radial turbines (of the type used in Brayton-cycle engines) are not used, because multistage axial turbines are smaller, lighter, and more efficient.

Equation E-63 can be combined with Eqs. E-60 and E-61 to provide relationships between efficiency and specific weight and specific volume:

$$\frac{W}{P_s} \sim \frac{\dot{m}^{1/2} \rho_r^{11/4}}{(1 - \eta_{pc})^{11/4} \sigma^{7/4}} \left[A + (1 - A) \frac{\rho_s}{\rho_r} \frac{p}{\sigma} \right] \quad (E-64)$$

$$\frac{V}{P_s} \sim \frac{\dot{m}^{1/2} \rho_r^{11/4}}{(1 - \eta_{pc})^{11/4} \sigma^{7/4}} \quad (E-65)$$

It is worth emphasizing that these relationships are based upon the assumption, among others, that the maximum permissible tip speed is always employed, which therefore implies a value of loading ψ for a given stage pressure ratio. If the maximum tip speed is not employed, the variation of specific weight with loss level will be considerably less.

D. WEIGHT, SIZE, AND PERFORMANCE OF COMBUSTORS

1. Specific Heat Release

A widely accepted relation governing heat release in hydrocarbon-burning combustors is due to Clarke (Ref. E-2):

$$\frac{P_{add}}{A_x p_3} = 786.10^6 \epsilon \eta_t \eta_v \sqrt{T_3} \sqrt{\frac{\Delta p_o}{p_o}} / T_h \text{ CHU/ft}^2\text{-hr-atm}, \quad (E-66)$$

where $A_x \equiv$ cross-sectional area

$\epsilon \equiv$ excess combustion factor for vortex

$\eta_t \equiv$ vortex refreshment efficiency

$\eta_v \equiv$ vortex velocity efficiency

$T_h \equiv$ temperature of vortex gas, °K.

It is assumed here that the factors ϵ , η_t , η_v and T_h all tend to certain terminal values in "good" design, for all combustors. The reason for this assumption is the independence of the primary vortex, which burns approximately stoichiometrically, from the other combustion-chamber characteristics or specifications. Then

$$\frac{P_{add}}{\ell A_x} = \frac{P_{add}}{\text{volume}} \sim \frac{\sqrt{T_3} \sqrt{\frac{\Delta p_o}{p_o}} p_3}{\left(\frac{\ell}{d_c}\right) d_c} \quad (E-67)$$

This applies to circular or annular combustors, d_c being appropriately defined.

2. Combustor Weight

The combustor is here simplified to be a cylindrical pressure casing (subscript c) and an inner cylindrical flame tube (subscript ft), neglecting any ends, flanges, injectors, etc. The weight of the combustor can then be written as

$$W_{cc} = N\pi d_c \left(\frac{\ell}{d_c}\right) d_c t_c \rho_c + N\pi d_c K_1 \left(\frac{\ell}{d_c}\right) d_c t_{ft} \rho_{ft} \quad , \quad (E-68)$$

where N = number of combustors

t = material thickness

K_1 = flame tube/casing diameter ratio.

The casing thickness t_c will be governed by pressure stresses, at least at higher pressure ratios; hence

$$t_c \sim \frac{p_3 d_c}{2\sigma_c} \quad .$$

The flame-tube wall thickness t_{ft} will be some minimum to allow for a small oxidation loss and to give sufficient strength against collapse under the pressure-drop forces and resistance to fluttering vibration.

$$W_{cc} = N\pi d_c^2 \left(\frac{\ell}{d_c} \right) \left[\frac{p_3 d_c \rho_c}{2\sigma_c} + K_1 t_{ft} \rho_{ft} \right]$$

$$W_{cc} \sim N d_c^3 \left(\frac{\rho_c}{\sigma_c} \right) \left[p_3 + K' \right] \left(\frac{\ell}{d_c} \right) , \quad (E-69)$$

where $K' \equiv K_1 \frac{t_{ft}}{d_c} \frac{\rho_{ft}}{\rho_c} \sigma_c$.

The combustor volume V_{cc} can be written as

$$V_{cc} = N\pi \frac{d_c^2}{4} \left(\frac{\ell}{d_c} \right) d_c$$

and hence, from Eq. E-69,

$$\frac{W_{cc}}{V_{cc}} = \frac{\frac{N\pi d_c^3}{2} \left(\frac{\rho_c}{\sigma_c} \right) \left[p_3 + K' \right] \left(\frac{\ell}{d_c} \right)}{\frac{N\pi d_c^3}{4} \left(\frac{\ell}{d_c} \right)} = 2 \left(\frac{\rho_c}{\sigma_c} \right) (p_3 + K') . \quad (E-70)$$

The combustion-chamber specific weight is obtained by dividing Eq. E-68 by E-70:

$$\frac{P_{add}}{W_{cc}} \sim \frac{p_3 \sqrt{T_3} \sqrt{\frac{\Delta p_o}{p_o}}}{d_c \left(\frac{\ell}{d_c} \right) (p_3 + K')} \left(\frac{\sigma_c}{\rho_c} \right) . \quad (E-71)$$

If the contribution of the flame tube to the total mass is regarded as small, which is usually the case, and if (l/d_c) is taken as constant for good design (a function of outlet temperature profile), then

$$\frac{P_{add}}{W_{cc}} \sim \left(\frac{\sigma_c}{\rho_c}\right) \frac{\sqrt{T_3}}{d_c} \sqrt{\frac{\Delta p_o}{p_o}} \quad (E-72)$$

For an annular combustor a similar relation is obtained, the outer diameter D substituting for the individual casing diameter d_c :

$$\frac{P_{add}}{W_{cc}} \sim \left(\frac{\sigma_c}{\rho_c}\right) \frac{\sqrt{T_3}}{D} \sqrt{\frac{\Delta p_o}{p_o}} \quad (E-73)$$

3. Implications for Future Designs

Equations E-67, E-72, and E-73 can be used to guide selection of new combustion systems or to evaluate proposals for improved materials or techniques. Both specific heat releases as functions of volume and of mass are proportional to the square root of the relative pressure drop and to the square root of absolute inlet temperature. Claimed improvements in combustion-chamber volume or weight can therefore be judged from existing specifications for good systems.

Both volume and mass can be reduced by using many small-diameter combustors or an annular combustor with as small an outside diameter as is practicable. The principal reason is that the mixture of secondary air after the primary near-stoichiometric zone is normally accomplished by large-diameter jets that have to penetrate the center of the flow to produce an acceptable outlet temperature profile. The smaller the thickness of the flow, the less distance must be penetrated by these jets and the larger the number of smaller jets which can be used. Thus the mixing

length can be reduced approximately by keeping the length-to-diameter ratio constant.

With regard to material properties, the ratio of allowable working stress to density in the conditions of operation is the significant variable, other things being equal. Because most of the mass is in the casing, which is normally at a relatively low temperature, improved cooling of the liner or the use of a ceramic liner (flame tube) should not greatly affect the weight. Improved flame-tube materials or design would, however, enable the mixing air to be ducted into the hot stream, greatly reducing mixing pressure losses and overall volume.

Catalytic combustion would in the limit be accomplished over the whole stream, the temperature of which would gradually rise to the turbine-inlet temperature. Mixing would presumably not be involved. Scaling laws and rate limits are not yet known to this contributor. For the present, obviously, proposed catalytic combustion systems can be compared with the best present systems.

Some representative present data are shown in Table E-1. The usable data from Table E-1 are plotted in Fig. E-12. The large variability in quality is noteworthy. Some of this variability is undoubtedly due to poor definition of the data. For instance, some of the industrial gas turbines have combustors that are connected to the turbine expanders by relatively long ducts. It is possible to have a short combustor, ending with a "peaky" temperature profile, because the temperature distribution will become more uniform as the gas travels along the connecting duct. There may also be actual errors in the data.

Nevertheless, even if all inconsistencies were removed, there would remain considerable variation in performance, showing that most combustors are imperfectly developed and that combustor design is an art rather than a science.

TABLE E-1. COMBUSTION-CHAMBER DATA

1. Russian Data^a

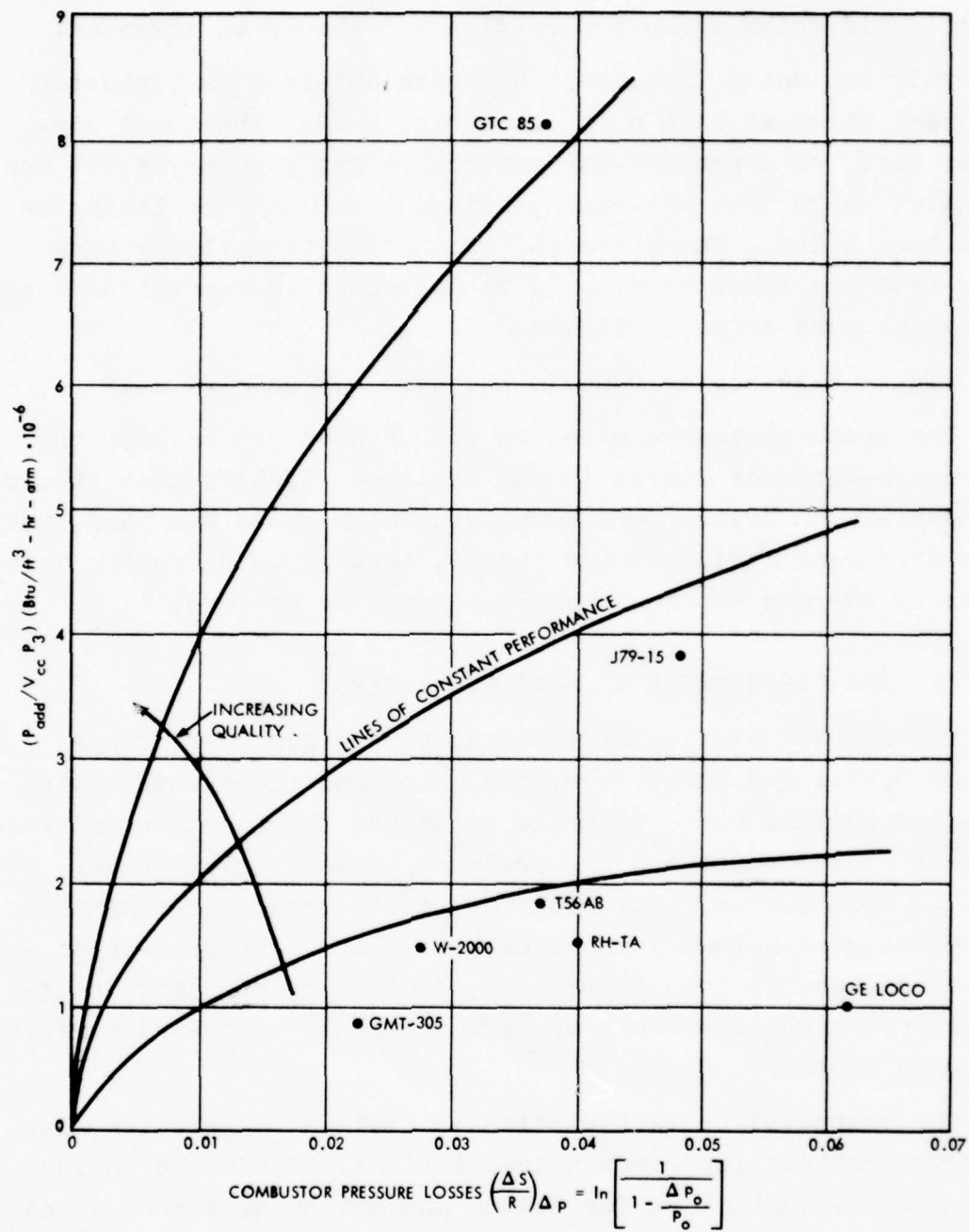
Engine Type	$\frac{P_{add}}{V_{cc} P_3} \frac{kJ}{m^3-hr-atm}$	$\frac{l}{d}$	$\frac{\Delta p_o}{p_o}, \%$
Aircraft	$30-70 \times 10^6$	2.0-3.0	3.5-4.5
Stationary & Transport	$8-30 \times 10^6$	2.5-3.5	4.5-5.5

2. U.S. Data^b

Engine	Pressure Ratio	N	P_3 , psia	$\frac{\Delta p_o}{p_o}, \%$	T_3 , °F	d_{ft} , in.	$\frac{P_{add}}{V_{cc} P_3} \frac{Btu}{ft^3-hr-atm}$	$\left(\frac{l}{d}\right)_{ft}$
J 79-15	11.5	10	169	4.7	761	?	3.86×10^6	?
T 56A8	9.2	6	136	3.6	605	5.53	1.88×10^6	4.36
T 58	8.66	Ann.	128	5.5	580	(D=16)	8.5×10^6	?
BBC	7.2	1	102	5.1	528	66	0.87×10^6	2.39
GTC-85	3.67	1	54	3.7	370	5.0	8.1×10^6	2.62
GMT-305	3.46	2	51	2.2	1100	6.0	0.9×10^6	2.08
RH-TA	4.0	1?	59	4?	700	14	1.54×10^6	2.21
GE Loco	?	6	37	6.0	500	9.6	1.0×10^6	3.54
W-2000	?	12	74	2.7	475	4.63	1.5×10^6	5.83

^aSource: Ref. E-3.^bSource: Ref. E-4.

Figure E-13 should be a useful device for evaluating new or proposed combustor systems. It can also be used to establish the optimum combustor specifications for a given "quality" of combustor (line of constant performance) for any one mission. The mission will provide the tradeoffs for combustor pressure losses and for volume that will result in an optimum specification at a point along each line. There will therefore be a



9-23-77-13

FIGURE E-13. Combustor volume versus losses.

locus of optima for any one mission, showing more precisely the direction in which combustor development should be advanced.

Only one datum (Ref. E-5) has been obtained on combustor mass, and this has been plotted in Fig. E-14. The total combustor mass for a present-day automobile gas turbine of 150 bhp was given as 39 lbm, the casing being 30 lbm and the lining or flame tube 1 lbm. Therefore the assumption tentatively made above that the liner mass could be neglected in comparison with the casing mass seems justified.

Figure E-14 may be used in the same way as Fig. E-13.

The pressure losses given in the data do not include the compressor-diffuser losses in CBE engines. Ideally they should. If a combustion system were developed which could burn the fuel in an airstream moving at 600 ft/sec, very large diffusion losses presently charged to the compressor could be avoided.

E. SIZE AND PERFORMANCE OF HEAT EXCHANGERS

The characteristics of interest to the designer of open Brayton cycles are the volume, the mass, and the steady-state full-load performance. It could be argued that the thermal performance at 25% power and the pressure losses at full power would be more appropriate. However, the thermal performance of heat exchangers normally improves, at least in Brayton-cycle applications, as the load is reduced, so that by studying the full-power performance the designer is being conservative with regard to cruise economy.

The transient characteristics of heat exchangers can also be very important for certain applications. A vehicle engine which has been optimized for volume and weight will tend to have minimum thermal lag in the heat exchanger (which will be the principal transient performance characteristic of interest). Thus primary concern can be safely directed at steady-state full-load performance.

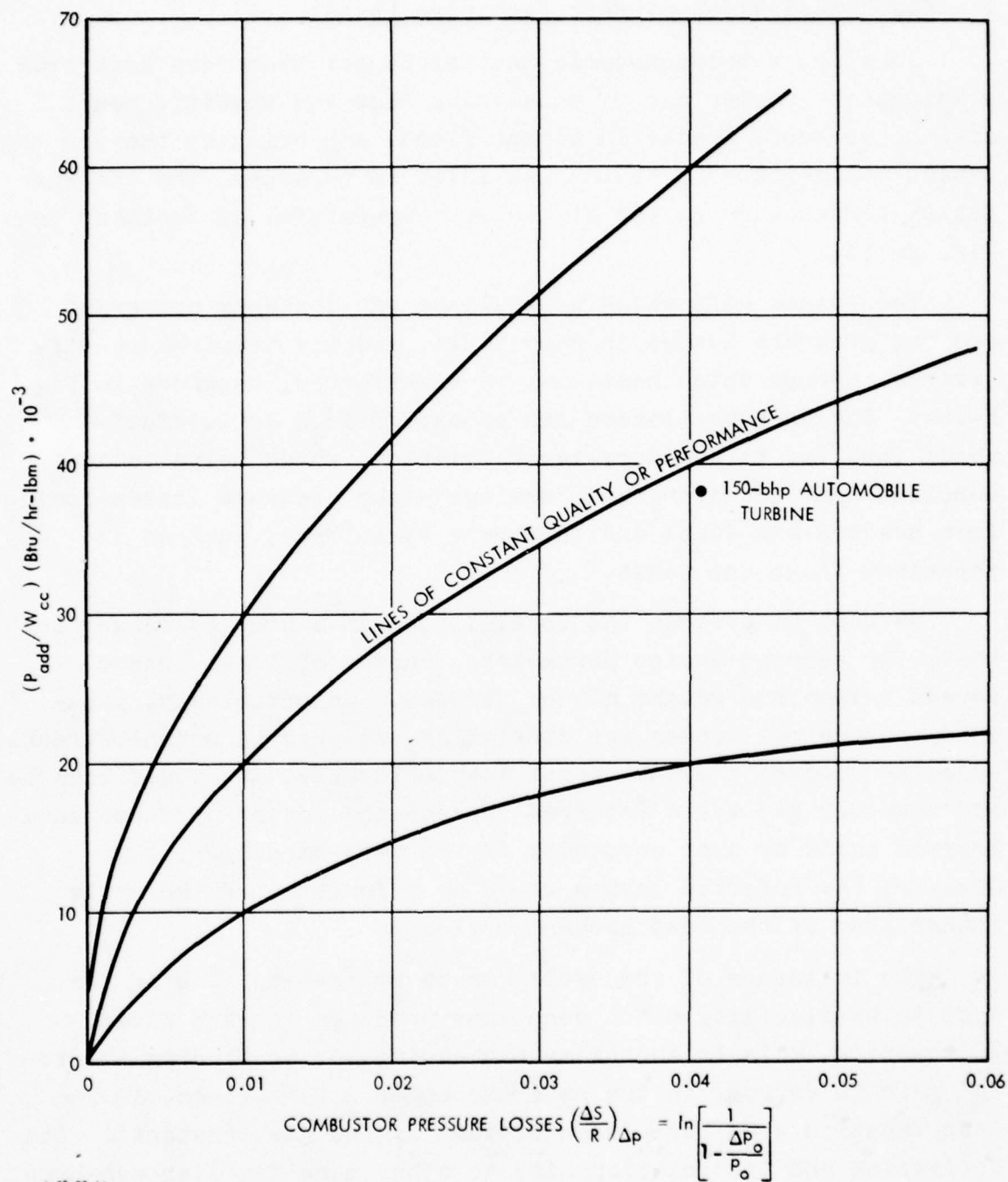


FIGURE E-14. Combustor mass versus losses.

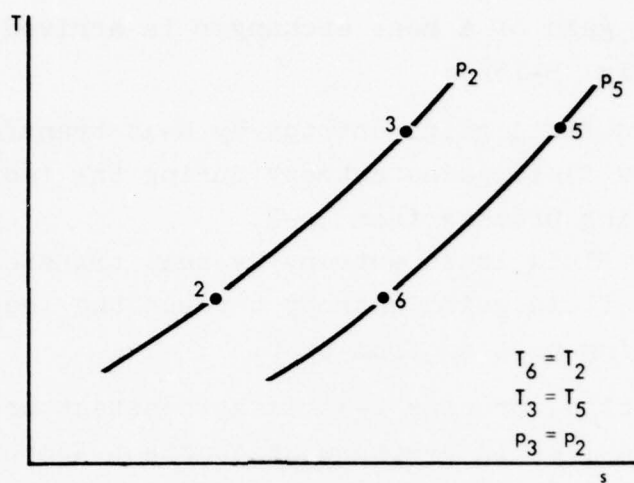
1. Characterization of Heat Exchanger Losses

Ideally, a Brayton-cycle heat exchanger transfers heat from a hot gas to cooler air of equal mass flow and specific heat, with no pressure losses in either fluid, and bringing the air outlet temperature up to the gas inlet temperature, and the gas outlet temperature to the air inlet temperature, as depicted in Fig. E-15a.

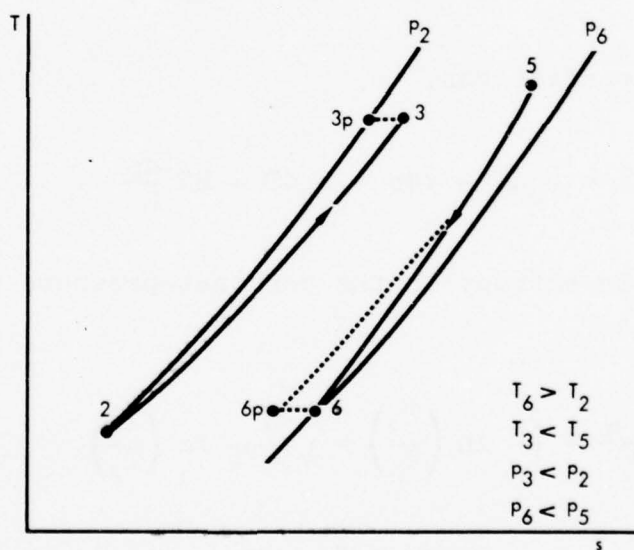
The losses with which we shall be particularly concerned are the pressure losses in each fluid, and the temperature difference through which heat must be transferred, as shown in Fig. E-15b. The pressure losses can be categorized as "useful"--those involved in boundary-layer friction, which helps to accomplish heat transfer, and "useless"--the pressure losses coming from headers and ducts and in stream turbulence, such as in separated flows and wakes.

We want to present the total losses in a heat exchanger so that, for varying design parameters, curves of total losses versus volume and weight may be derived. Unfortunately, pressure and thermal losses are dissimilar, so they cannot be directly added to produce a useful total loss. Ideally, one would like to add together the cycle referred losses--the losses produced in a Brayton cycle by each component of the heat-exchanger loss. However, the referred losses would be a function of the cycle rather than of the heat exchanger alone.

The influence of the cycle can be avoided by finding the loss in availability which each loss produces in each fluid. In practice, this is approximately equivalent to finding the total gain in entropy in the heat exchanger. This, then, is the loss function used here (when divided by the gas constant). Its derivation and its relationships to other more familiar measures of heat-exchanger performance and loss are given below.



a. IDEAL HEAT EXCHANGER



b. ACTUAL HEAT EXCHANGER

9-23-77-15

FIGURE E-15. Pressure and temperature difference in heat exchangers.

The entropy gain of a heat exchanger is arrived at in the following way (Fig. E-15b):

1. The cold fluid gains entropy by heat transfer from 2-3p.
2. The cold fluid gains entropy during the (equivalent) throttling process from 3p-3.
3. The hot fluid loses entropy by heat transfer from 5-6p.
4. The hot fluid gains entropy through the (equivalent) throttling process from 6p-6.

In this idealization, process 2-3p is at constant pressure, and process 3p-3 is a loss in pressure at constant temperature. Likewise, process 5-6p is cooling at constant pressure, and 6p-6 is a loss in pressure at constant temperature. An ideal fluid is assumed so that a constant-temperature change is also one at constant enthalpy. From Gibbs' equation,

$$Tds = du + pdv = dh - vdp ,$$

and, assuming a perfect gas,

$$Tds = c_p dT - vdp = c_p dT - RT \frac{dp}{p} .$$

Then the change in entropy in the constant-pressure process 2-3p can be written as

$$\frac{\Delta S_{23p}}{R} = \frac{c_p}{R} \ln \left(\frac{T_3}{T_2} \right) = \frac{\gamma}{\gamma - 1} \ln \left(\frac{T_3}{T_2} \right) \quad (E-74)$$

and similarly for the process 5-6p. The entropy change in the constant-temperature change 3p-3 can be written as

$$\frac{\Delta S_{3p3}}{R} = \ln \left(\frac{p_2}{p_3} \right) \quad (E-75)$$

and similarly for the process 6p-6. For a two-fluid heat exchanger with unequal heat-capacity flows defined by

$$C_{\text{rat}} = \frac{\dot{m}_5 \bar{c}_{p56}}{\dot{m}_2 \bar{c}_{p23}},$$

the net increase in entropy can accordingly be written as

$$\sum \frac{\Delta S}{R} = \frac{\gamma}{\gamma - 1} \ln \left[\left(\frac{T_3}{T_2} \right) \left(\frac{T_6}{T_5} \right)^{C_{\text{rat}}} \right] + \ln \left[\left(\frac{p_2}{p_3} \right) \left(\frac{p_5}{p_6} \right)^{C_{\text{rat}}} \right]. \quad (\text{E-76})$$

As a simplification, C_{rat} will be set equal to 1.0, and only counterflow heat exchangers will be considered in the succeeding development. This leads to a constant heat-transfer-driving temperature difference, θ , as shown in Fig. E-16. This difference, and the temperature rise of the cold fluid ΔT_c , can be used to determine the relationship between the temperature ratios in Eq. E-76 and the heat-exchanger effectiveness, as follows:

$$\frac{T_3}{T_2} \cdot \frac{T_6}{T_5} = \frac{T_3}{T_3 - \Delta T_c} \cdot \frac{T_3 + \theta - \Delta T_c}{T_3 + \theta} = \left[1 - \frac{1}{\frac{T_3}{\Delta T_c} + \frac{\theta}{\Delta T_c}} \right] \bigg/ \left[1 - \frac{\Delta T_c}{T_3} \right]. \quad (\text{E-77})$$

Defining a specific temperature rise

$$Q' \equiv \frac{\Delta T_c}{T_3} \quad (\text{E-78})$$

and the heat-exchanger effectiveness

$$\epsilon \equiv \left[\frac{T_5 - T_2}{T_3 - T_2} \right]^{-1} = \left[\frac{\theta + \Delta T_c}{\Delta T_c} \right]^{-1} = \left[\frac{\theta}{\Delta T_c} + 1 \right]^{-1}, \quad (\text{E-79})$$

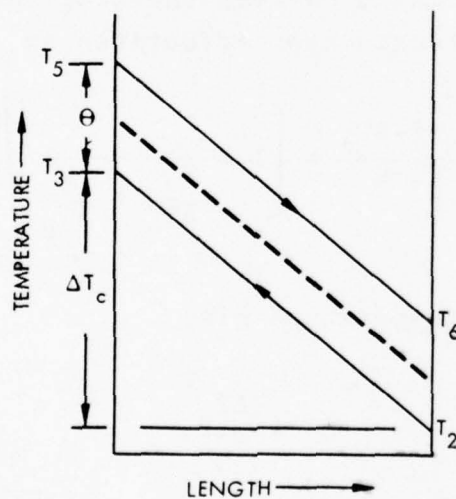
then

$$\frac{\theta}{\Delta T_c} = \frac{1}{\epsilon} - 1 = \frac{1 - \epsilon}{\epsilon}, \quad (\text{E-80})$$

and so

$$\frac{T_3}{T_2} \frac{T_6}{T_5} = \frac{1 - \frac{1}{\frac{1}{Q'} + \left(\frac{1 - \epsilon}{\epsilon}\right)}}{1 - Q'}. \quad (\text{E-81})$$

Equation E-81 confirms that $(1 - \epsilon)/\epsilon$ alone is an insufficient measure of heat-exchanger thermal losses (as represented by entropy increases).



9-23-77-16

FIGURE E-16. Temperature distribution in a counterflow heat exchanger, $C_{rat} > 1.0$.

The pressure ratios in Eq. E-76 can also be converted to a more familiar form,

$$\left(\frac{p_2}{p_3}\right)\left(\frac{p_5}{p_6}\right) = \frac{p_2}{p_2 - \Delta p_{23}} \cdot \frac{p_5}{p_5 - \Delta p_{56}} , \quad (\text{E-82})$$

which, since $\Delta p/p$ should be much less than unity, becomes

$$\left(\frac{p_2}{p_3}\right)\left(\frac{p_5}{p_6}\right) = 1 + \frac{\Delta p_{23}}{p_2} + \frac{\Delta p_{56}}{p_6} = 1 + \sum \left(\frac{\Delta p}{p}\right) , \quad (\text{E-83})$$

where $\sum(\Delta p/p)$ is the sum of all of the relative pressure losses.

Equation E-76 can then be written as

$$\sum \left(\frac{\Delta S_x}{R}\right) = \frac{\gamma}{\gamma-1} \ln \left[\frac{1 - \frac{1}{\frac{Q'}{1-\epsilon} + \frac{1-\epsilon}{\epsilon}}}{1-Q'} \right] + \ln \left[1 + \sum \left(\frac{\Delta p}{p}\right) \right] \quad (\text{E-84})$$

or, expressing the losses as $\Delta S/c_p$,

$$\sum \left(\frac{\Delta S_x}{c_p}\right) = \ln \left[\frac{1 - \frac{1}{\frac{Q'}{1-\epsilon} + \frac{1-\epsilon}{\epsilon}}}{1-Q'} \right] + \frac{R}{c_p} \ln \left[1 + \sum \left(\frac{\Delta p}{p}\right) \right] . \quad (\text{E-85})$$

Assuming that both $\sum(\Delta p/p)$ and $Q'(1-\epsilon)/\epsilon$ are small compared to unity, Eq. E-85 simplifies to

$$\sum \left(\frac{\Delta S_x}{c_p}\right) = \left(\frac{Q'}{1-Q'}\right)\left(\frac{1-\epsilon}{\epsilon}\right) + \frac{R}{c_p} \sum \left(\frac{\Delta p}{p}\right) \quad (\text{E-86})$$

$$\equiv H' + L'_x . \quad (\text{E-87})$$

A simpler form for heat-exchanger thermal losses was used in assessing the impact of losses on the cycle (Eq. E-27):

$$X' \equiv \frac{\Delta S_{35}}{c_p} = \ln \frac{T_5}{T_3} .$$

This is related to H' above by

$$H' \equiv \left(\frac{Q'}{1 - Q'} \right) \left(\frac{1 - \epsilon}{\epsilon} \right) = \frac{X'}{1 - Q'} . \quad (E-88)$$

Up to this point we have merely defined the heat-exchanger thermal and pressure losses in forms which allow them to be added. We now introduce Reynolds analogy to relate heat transfer in convective flow in channels to the minimum pressure loss necessary.

2. Minimum Pressure Loss for Heat Transfer

Consider flow within a series of channels of arbitrary cross section, defined by

A_x = cross-sectional area of one channel

A_h = inside surface area of one channel

N = number of parallel channels

ℓ = length of each channel

P = perimeter of each channel

θ_w = fluid-to-wall temperature difference

h = heat-transfer coefficient

u = mean flow velocity.

Then the total heat-transfer rate to the channel walls is

$$\dot{Q} = h N A_h \theta_w = h N \ell P \theta_w . \quad (E-89)$$

The pumping power required to produce the heat transfer is

$$\dot{W} = \dot{V}\Delta p = N A_x u \Delta p \quad ,$$

Where \dot{V} = volume flow = $Nu A_x$

Δp = pressure drop.

The Δp is the "useful" pressure drop, resulting from boundary-layer drag:

$$\Delta p A_x = \tau_w P l = \tau_w A_h \quad , \quad (E-90)$$

where τ_w is the skin-friction shear stress. Reynolds analogy between skin friction and heat transfer is

$$St = \text{Stanton Number} \equiv \frac{h}{\rho u c_p} = \frac{c_f}{2} \equiv \frac{\tau_w}{\rho u^2} \quad . \quad (E-91)$$

Equations E-89 through E-91 can be combined to yield

$$\frac{\dot{W}}{\dot{Q}} = \left(\frac{\gamma R}{c_p} \right) \left(\frac{T_3}{\theta_w} \right) \left(\frac{u^2}{\gamma R T_3} \right) \quad . \quad (E-92)$$

Noting that

$$\frac{u^2}{\gamma R T_3} = M_3^2 = (\text{Mach number})^2$$

and

$$\frac{T_3}{\theta_w} = \frac{2T_3}{\theta} = \frac{2}{Q^*} \left(\frac{\epsilon}{1 - \epsilon} \right)$$

$$\frac{\dot{Q}}{\dot{Q}^*} = \dot{m} c_p T_3 \quad ,$$

then Eq. E-92 can be written as

$$\frac{\epsilon}{1 - \epsilon} = \frac{(\Delta p/p)}{2\gamma M_3^2} .$$

If we make the numerator the sum of the pressure drops on both sides of the channel (assumed equal for simplicity in calculation), we obtain

$$\left[\frac{\epsilon}{1 - \epsilon} \right] = \frac{\sum \left(\frac{\Delta p}{p} \right)}{4\gamma M_3^2} . \quad (E-93)$$

This equation gives the minimum pressure drop to give a desired effectiveness at a given mean channel Mach number in convective heat transfer in laminar or turbulent flow. (Low Mach numbers yield low pressure drops.) There are three variables; another relation is needed before the effect of, say, $\sum(\Delta p/p)$ on ϵ can be found. A unique relation will not be given by one additional equation, because a fourth variable, which appears in the loss equation (Eq. E-86) but not in Reynolds analogy (Eq. E-93), will appear as a parameter. This additional variable is $Q' \equiv \Delta T_c/T_3$.

3. Heat-Transfer Fluid-Flow Relationship

A continuous function between heat transfer and fluid flow from laminar to turbulent conditions is the Colburn modulus, $St Pr^{2/3}$ [$Pr \equiv$ Prandtl Number $\equiv c_p \mu/k$] as a function of Reynolds number, depicted schematically in Fig. E-17. The Colburn modulus can also be written in terms of the Nusselt number:

$$Nu \equiv \frac{hd_h}{k}$$

$$St Pr^{2/3} = \frac{Nu}{Re Pr^{1/3}} = f(Re, \text{ passage shape}) , \quad (E-94)$$

where d_h = hydraulic diameter of channel $\equiv 4A_x/P$

k = thermal conductivity,

and universal relationships with Reynolds number are, for laminar flow,

$$\begin{aligned} \text{Nu} &= \text{constant} = 3.0 \text{ for triangular passages} \\ &= 3.6 \text{ for square passages} \\ &= 4.4 \text{ for circular passages} \\ &= 8.2 \text{ for parallel plates} \end{aligned}$$

and, for turbulent flow,

$$\text{Nu} = 0.023(\text{Re})^{0.8}(\text{Pr})^{1/3}.$$

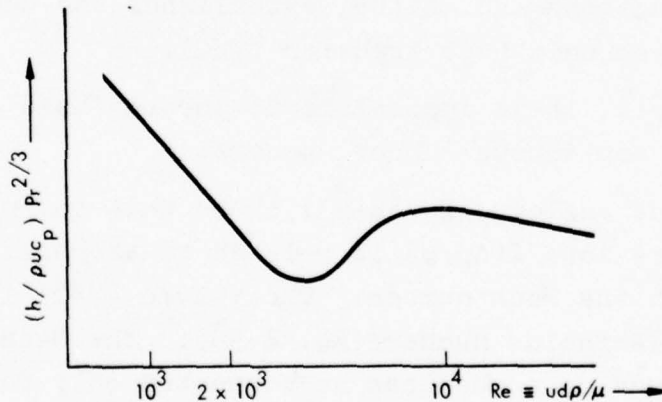


FIGURE E-17. Typical variation of Colburn modulus with Reynolds number.

The Nusselt number can be used to relate heat flow to channel volume by noting that

$$h = \frac{\dot{Q}}{(\theta/2)NA_h}$$

$$V = 2V_1 = 2A_x \ell N = \frac{1}{2} d_h A_h N ,$$

so

$$Nu = \left(\frac{\dot{Q}}{V}\right)\left(\frac{d_h^2}{k\theta}\right) = \left(\frac{\dot{Q}}{V}\right)\left(\frac{d_h}{k\dot{Q}T_3}\right)\left(\frac{\epsilon}{1-\epsilon}\right) d_h . \quad (E-95)$$

Equations E-94 and E-95 combine to give

$$\frac{\left(\frac{\dot{Q}}{V}\right)\left(\frac{d_h^2}{k\theta}\right)}{RePr^{1/3}} = f(Re, \text{ passage shape}) . \quad (E-96)$$

This relationship, in conjunction with Reynolds analogy (Eq. E-93) and the loss functions (Eq. E-86), establishes the dependence of loss on volume per unit heat transfer (V/\dot{Q}).

Unfortunately, it is impossible to portray this relationship in a universal, continuous manner, because:

1. Reynolds analogy (Eq. E-93) shows that the minimum pressure loss $\Sigma(\Delta p/p)$ is related to the heat transfer through the Mach number. The volume (V/\dot{Q}) is a function of the Reynolds number (Eq. E-96). The Mach number and the Reynolds number can be connected only for specific properties and for a specific hydraulic diameter d_h .
2. In the laminar region the Nusselt number is constant. Because $Nu \sim (\dot{Q}/V)(d_h^2/k\theta)$, the heat-exchanger volume becomes independent of Mach number, Reynolds number, and all fluid properties except the thermal conductivity.

Continuous curves of $\Sigma(\Delta p/p)$ versus (V/Q) can be made, therefore, only for specific fluid properties, hydraulic diameters, and values of Q' or θ .

The only possible universal relations (i.e., without a large number of parameters for different fluid properties, hydraulic diameters, and temperature ratios Q') are those shown in Fig. E-18, in which the laminar heat exchangers are shown as a series of vertical lines, specific to channel shape, with the volumes independent of Mach number and the losses decreasing with Mach number. The turbulent limit line is shown to a different scale incorporating many more fluid properties (which could of course be combined into one rather complex property) and with a limiting volume that is Mach-number dependent.

Despite all these limitations, it is instructive to plot heat-exchanger losses versus volumes, recognizing that boundaries of ideal heat exchangers cannot be specified because a heat exchanger designed to operate under unusual conditions might go past the boundary, even though it were far from ideal in its performance. The rather limited range of fluid properties, hydraulic diameters, and temperature ratios (Q') used in heat exchangers for open-Brayton-cycle engines makes such a plot more useful than were it to be applied to all types of heat exchangers. Two versions are given (Figs. E-19 and E-20) with some representative heat-exchanger designs.

Figure E-19 shows how the minimum-loss condition is approached for constant-Mach-number heat exchangers whose volumes are increased by increasing flow lengths. The effectiveness and the pressure drop both increase, so that the thermal losses at first decrease faster than the pressure-drop losses increase. The minimum-loss conditions are generally reached at relatively high values of the pressure loss, e.g., 10-15%, and high values of the effectiveness, e.g., 90-98%, both higher than values generally used for gas turbines. One would expect, of course,

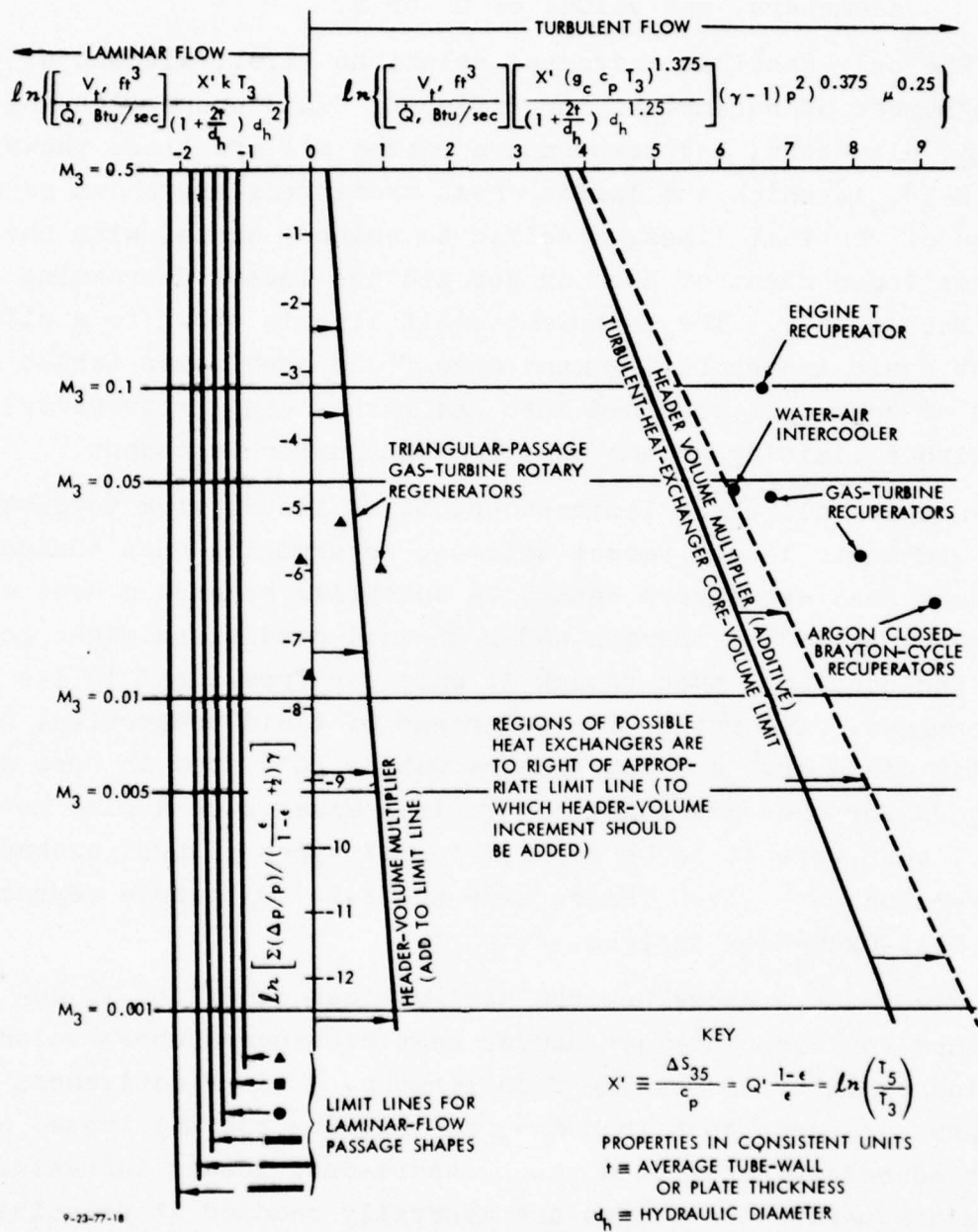
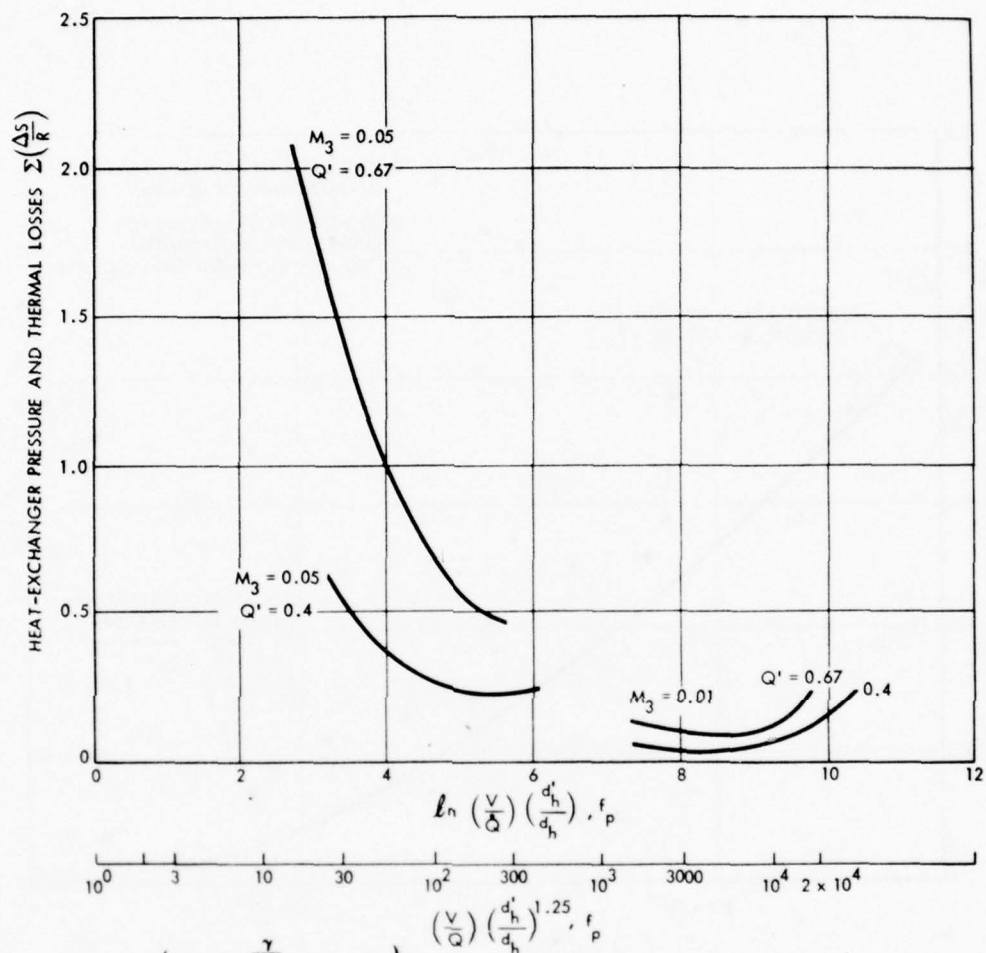


FIGURE E-18. Heat-exchanger minimum loss versus volume.



$$\Sigma\left(\frac{\Delta S}{R}\right) = \ln \left\{ \left[\frac{T_3}{T_2} \frac{T_6}{T_5} \right]^{\frac{\gamma}{\gamma-1}} \left[1 - \Sigma \frac{\Delta p}{p} \right] \right\}$$

V = CORE VOLUME, ft^3

$Q \equiv P_{HX}$, Btu/sec

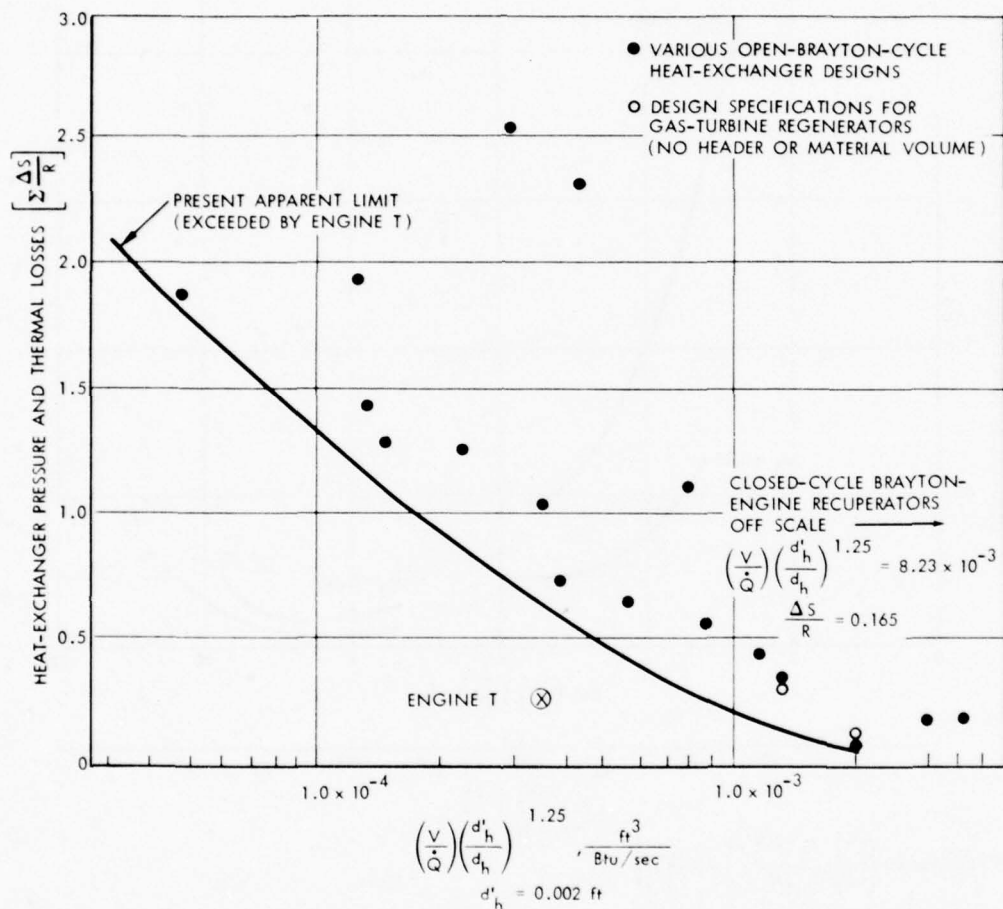
$d'_h \equiv 0.002$ ft

d_h = HYDRAULIC DIAMETER, ft

f_p = PROPERTY FUNCTION $\equiv \left[93.39 c_p \mu^{0.25} \rho^{0.75} (g_c \gamma R)^{0.375} (T(R))^{1.375} \right]$

UNITS OF ft, Btu, lbf, lbm, sec
9-23-77-19

FIGURE E-19. Heat-exchanger specific volume versus losses.



$$\Sigma \left[\frac{\Delta S}{R} \right] = \ln \left[\left(1 - \Sigma \left(\frac{\Delta p}{p} \right) \right) \left(1 - \left(Q' \left(\frac{1-\epsilon}{\epsilon} \right) \right) / \left(\frac{1}{Q'} - 1 + \frac{1-\epsilon}{\epsilon} \right) \right)^{\frac{\gamma}{\gamma-1}} \right]^{-1}$$

9-23-77-20

FIGURE E-20. Heat-exchanger losses versus specific volume.

that the economic optimum would be found at smaller values corresponding to smaller heat exchangers.

Figure E-20 plots losses against relative volume with no attempt to correlate fluid properties. However, the effects of hydraulic diameter are removed for turbulent flow by normalizing the hydraulic diameter with a value representative of current good practice, 0.002 ft. The points shown are various gas-turbine heat exchangers. An apparent limit line has been drawn in "by eye" as an envelope. However, this may be misleading. Because of the varied effects of fluid properties and heat-exchanger temperature ratio (Q'), designs which plot close to the apparent limit line may in fact be poor heat exchangers, while some that are far removed may in fact be nearly ideal. Only Fig. E-18 will show how close to the limits the designs actually are.

F. OVERALL ENGINE CONSIDERATIONS

1. Effect of Component Losses on Specific Weight

Alternative methods of finding the effects of component losses on cycle efficiency and specific power were discussed in Section B-2. One method explicitly introduces component loss functions as deductions from ideal cycle efficiency. In this section we incorporate into this method the relations connecting component specific mass with component losses to find the influence coefficients of each component loss on the specific mass and the specific fuel consumption of the complete engine.

Summaries of the calculations are given in Table E-2 for the CBE cycle and in Table E-3 for the CBEX cycle. The results are plotted in Figs. E-21 and E-22.

Explanations of the values chosen are made below.

a. Base-Case Engines. The Chrysler-derived "mature" engine, 150 hp, as described in Ref. E-5, was used as a reference case.

TABLE E-2. LOSS CALCULATIONS FOR CBE CYCLE

$$\frac{P_{add} + P_{int}}{P_i} = 4$$

$$(T' = 5)$$

$$\frac{P_{int,id}}{P_i} = 1.5$$

$$(R' = 2.5)$$

$$\eta_{id} = 1 - \frac{1}{R^T} = 0.6$$

$\eta_{is,c}$	0.78					0.87	0.90	0.78	→
$\eta_{is,e}$	0.88							0.83	0.78
$\Sigma(\frac{\Delta P}{P})$	0.09	0.05	0.07	0.12	0.09				→
$L' \equiv \frac{R}{c_p} \Sigma(\frac{\Delta P}{P})$.0257	.0143	.020	.0343	.0257				→
$C' \equiv (1 - \frac{1}{R'}) (\frac{1}{\eta_{is,c}} - 1)$.1692			→	.0897	.0667		.1692	→
$E' \equiv (1 - \eta_{is,e}) (\frac{R'}{1 + L'} - 1)$.1725	.1758	.1741	.1701	.1725	→	→	.2444	.3162
$C'' \equiv C' [(T'/R') - 1]$.1692			→	.0897	.0667		.1692	→
$L'' \equiv L' + E'L' + E'$.2026	.1926	.1976	.2102	.2026	→	→	.2763	.3500
$E'' \equiv L'' / [R'(1 - R'/T')]$.1621	.1541	.1581	.1682	.1621	→	→	.2211	.2800
$\eta_{th} = (\eta_{id} - C'' - E'')(1 + C'')$.3142	.3236	.3189	.3070	.3795	.3960		.2452	.1763
$sfc = 0.1383/\eta_{th} \frac{lbm}{bhp-hr}$.4402	.4248	.4338	.4505	.3645	.3493		.5640	.7846
$\Delta m \text{ lbm}$?	+25.5	+8.8	-7.2	+160	+280		-150	-250
$\Delta m/hp \text{ lbm/hp}$	0	+0.19	-0.06	-0.05	+1.07	1.87		-1.0	-1.67
Effect of losses in	Base Case	Combustor			Compressor			Expander	

TABLE E-3. LOSS CALCULATIONS FOR CBEX CYCLE

$\frac{P_{add} + P_{int}}{P_i} = 4$	$(T' = 5)$										$\eta_{id} = 1 - \frac{R'}{T'} = 0.7$									
$\frac{P_{compressor}}{P_i} = 0.5$	$(R' = 1.5)$																			
$\eta_{is,c}$	0.78	0.87	0.90	0.91	0.78	0.78	0.78	0.78	0.78	0.78	0.78	0.78	0.78	0.78	0.78	0.78	0.78	0.78	0.78	0.78
$\eta_{is,e}$	0.88	0.88	0.88	0.88	0.88	0.88	0.88	0.88	0.88	0.88	0.88	0.88	0.88	0.88	0.88	0.88	0.88	0.88	0.88	0.88
$\Sigma(\Delta p/p)$	0.15	0.15	0.15	0.15	0.21	0.33	0.15	0.15	0.15	0.15	0.15	0.15	0.15	0.15	0.15	0.15	0.15	0.15	0.15	0.15
$(\Delta p/p)_{combustor}$	0.04	0.04	0.04	0.04	0.04	0.04	0.04	0.04	0.04	0.04	0.04	0.04	0.04	0.04	0.04	0.04	0.04	0.04	0.04	0.04
$(\Delta p/p)_{HX}$	0.06	0.06	0.06	0.06	0.12	0.24	0.06	0.06	0.06	0.06	0.06	0.06	0.06	0.06	0.06	0.06	0.06	0.06	0.06	0.06
$H' = \frac{T_5 - T_3}{T_2} \approx (1 - \epsilon) \left(\frac{T_5}{T_2} - 1 \right)$.113	.113	.113	.113	.226	.452	.113	.113	.113	.113	.113	.113	.113	.113	.113	.113	.113	.113	.113	.113
ϵ	.89	.89	.89	.89	.79	.55	.89	.89	.89	.89	.89	.89	.89	.89	.89	.89	.89	.89	.89	.89
$LK' \equiv \frac{R}{C_p} \left(\frac{\Delta p}{p} \right)_{HX}$.0171	.0171	.0171	.0171	.034	.068	.0171	.0171	.0171	.0171	.0171	.0171	.0171	.0171	.0171	.0171	.0171	.0171	.0171	.0171
$X' = \left[\frac{T_5}{T_2} \frac{1}{H'} - 1 \right]^{-1}$.0561	.0561	.0561	.0561	.1188	.2697	.0561	.0561	.0561	.0561	.0561	.0561	.0561	.0561	.0561	.0561	.0561	.0561	.0561	.0561
$L' \equiv \frac{R}{C_p} \Sigma \left(\frac{\Delta p}{p} \right)$.0429	.0429	.0429	.0429	.060	.0941	.0429	.0429	.0429	.0429	.0429	.0429	.0429	.0429	.0429	.0429	.0429	.0429	.0429	.0429
$E' \equiv (1 - \eta_{is,e}) \left[\frac{R'}{T'} + L' - 1 \right]$.0526	.0526	.0526	.0526	.0498	.0446	.0526	.0526	.0526	.0526	.0526	.0526	.0526	.0526	.0526	.0526	.0526	.0526	.0526	.0526
$L'' \equiv L' + E'L' + E'$.0978	.0978	.0978	.0978	.1126	.1425	.0978	.0978	.0978	.0978	.0978	.0978	.0978	.0978	.0978	.0978	.0978	.0978	.0978	.0978
$E'' \equiv L''/(R' - 1)$.1955	.1955	.1955	.1955	.2252	.2850	.1955	.1955	.1955	.1955	.1955	.1955	.1955	.1955	.1955	.1955	.1955	.1955	.1955	.1955
$X''' \equiv \left[1 - \frac{X'}{(R' - 1)} \right]^{-1}$	1.0723	1.0723	1.0723	1.0723	.9609	.6688	1.0723	1.0723	1.0723	1.0723	1.0723	1.0723	1.0723	1.0723	1.0723	1.0723	1.0723	1.0723	1.0723	1.0723
$C'' = \frac{R'}{T'} \left[\frac{1}{\eta_{is,c}} - 1 \right]$.0846	.0448	.0323	.0297	.0946	.0846	.0846	.0846	.0846	.0846	.0846	.0846	.0846	.0846	.0846	.0846	.0846	.0846	.0846	.0846
$\eta_{th} = [\eta_{id} - C'' - E'']X'''$.4503	.4929	.5053	.5091	.3749	.2209	.4503	.4503	.4503	.4503	.4503	.4503	.4503	.4503	.4503	.4503	.4503	.4503	.4503	.4503
$sfc = 0.1383/\eta_{th} \frac{lbm}{bhp-hr}$.3072	.2806	.2737	.2716	.3689	.6260	.3072	.3072	.3072	.3072	.3072	.3072	.3072	.3072	.3072	.3072	.3072	.3072	.3072	.3072
$\Delta m/hp \text{ } lbm/hp$	0	+.31	+.54	+.73	-.244	-.327	0	0	0	0	0	0	0	0	0	0	0	0	0	0
$m/hp \text{ } lbm/hp$	3.59	3.90	4.13	4.32	3.34	3.26	3.59	3.59	3.59	3.59	3.59	3.59	3.59	3.59	3.59	3.59	3.59	3.59	3.59	3.59
Effect of Losses In	Base Case	Compressor				HX		Expander				Combustor								

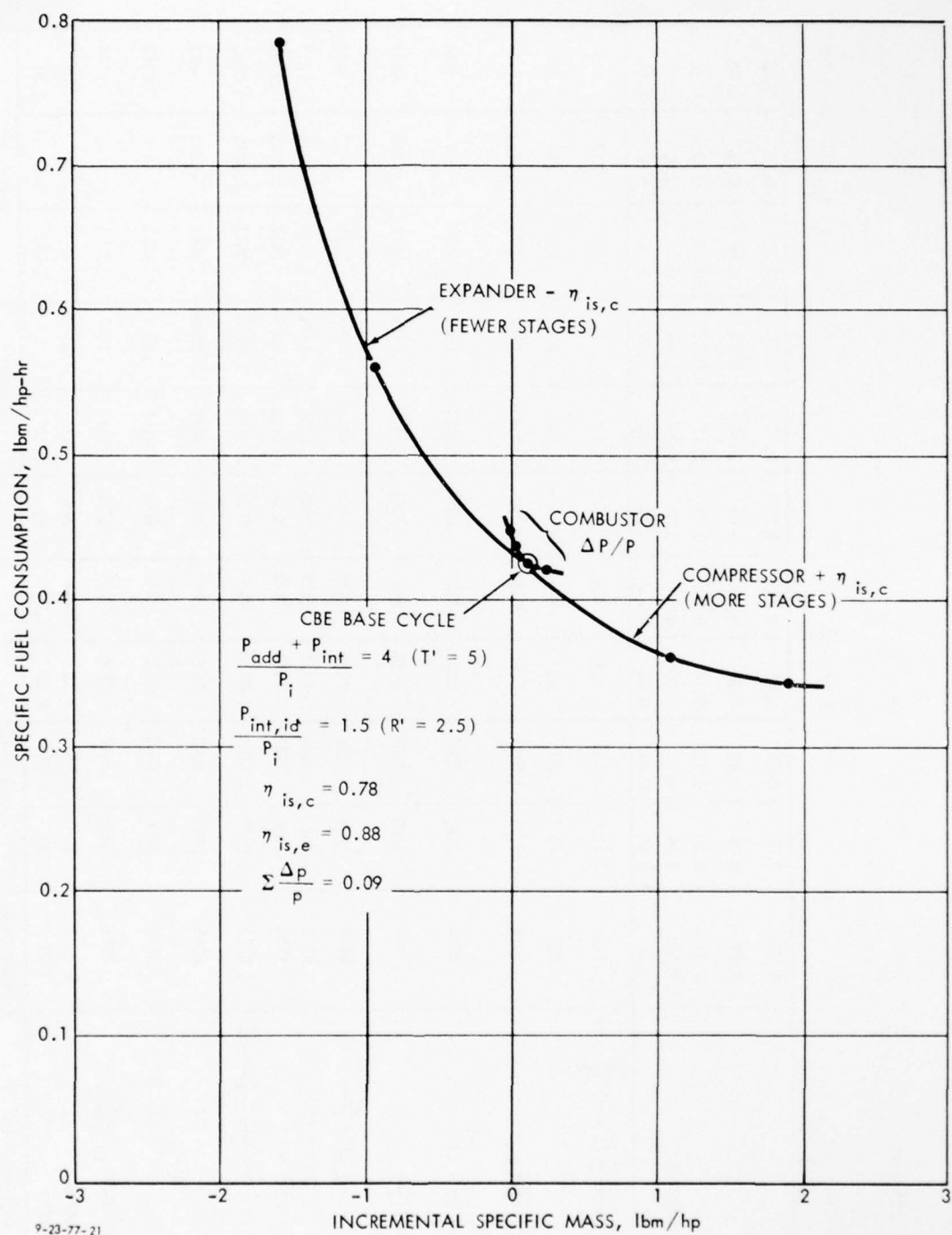


FIGURE E-21. Effect of CBE component losses.

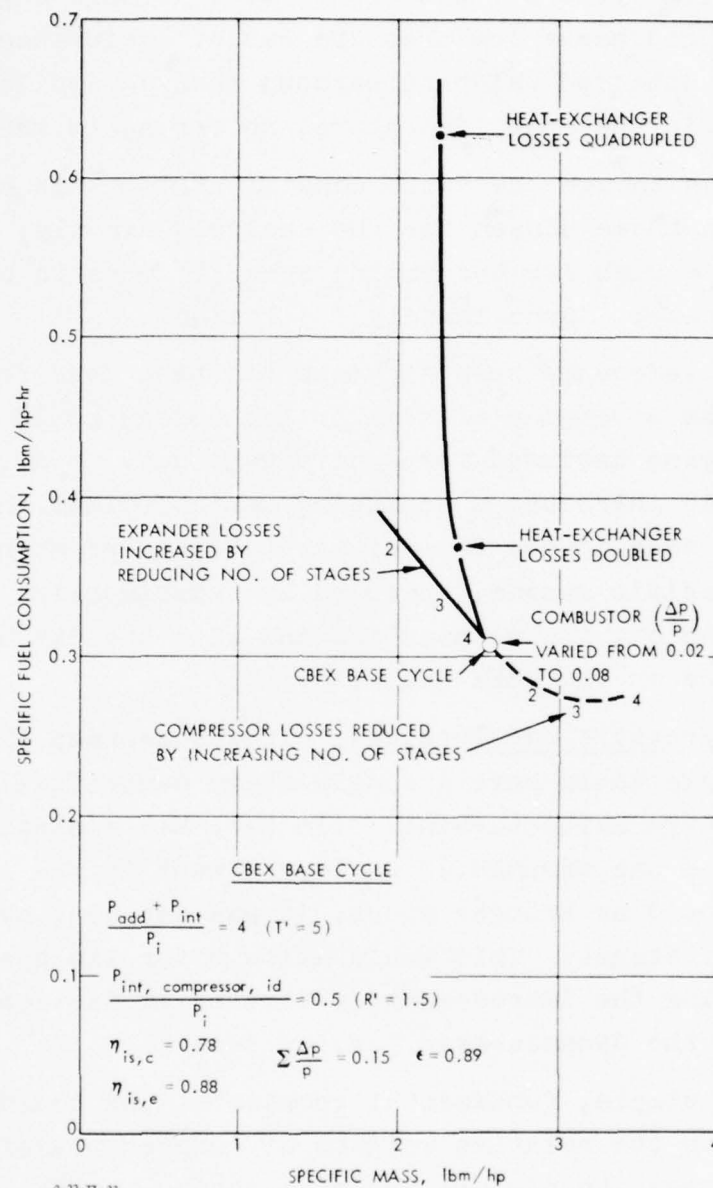


FIGURE E-22. Effect of CBEX component losses.

This is especially so for the CBEX cycle, as this engine is regenerative and has a low pressure ratio. Reference E-5 contains a more detailed weight breakdown than is available for any other engine in the open literature, so far as is known.

Even though the cycle conditions for this engine did not match those chosen for the analysis exactly, they seemed close enough for the engine specific mass to be used as the base case: approximately 2.5 lbm/hp.

No reference specific mass has been used for the CBE cycle, because no engine of similar technology could be located. To use an engine designed for a different duty, e.g., for helicopters, would introduce a confusing variable into the comparisons. It is easy to see the relative effects of using different base-case specific masses, however, by superimposing Fig. E-21 on Fig. E-22 with sfc scales matching and with the CBE base case at a chosen value on the CBEX scale.

b. Compressors and Turbines. It was assumed that the base-case CBEX cycle would have a single-stage centrifugal compressor and a four-stage axial turbine. (In Ref. E-5 a single-stage radial turbine was assumed.) An improvement in the compressor efficiency would be brought about, it was assumed, by increasing the number of stages. This would allow rotor tip speeds to be reduced, giving the improvements estimated in Section C-2, and would reduce the dynamic-head leaving loss.

No simple, fundamental considerations could be derived for estimating the relative weights of compressors of varying numbers of stages to perform the same duty. The following assumptions were made, based on pure judgment.

CENTRIFUGAL COMPRESSOR

	<u>CBEX Base Case</u>			
	↓			
No. of stages	1	2	3	4
Isentropic efficiency	0.78	0.87	0.90	0.91
Compressor mass	58 lbm			
Mass multiplier	1.0	1.8	2.4	2.9
Incremental mass/hp	0	0.31	0.54	0.73
Mass/hp	2.5	2.81	3.04	3.23

The single-stage radial turbine of the Ref. E-5 engine weighs 95 lbm (from Table 5-4 of the reference). The turbine mass and efficiency for various numbers of stages, based again on judgment rather than analysis, are given below.

AXIAL-FLOW TURBINES

	<u>CBEX Base Case</u>		
	↓		
No. of stages	4	3	2
Isentropic efficiency	0.88	0.83	0.78
Turbine mass	190	150	110
Incremental mass/hp	0	-0.27	-0.53
Mass/hp	2.5	2.23	2.97

On a similar basis, the CBE turbomachinery efficiencies and weights are listed below.

CENTRIFUGAL COMPRESSOR

	<u>CBE Base Case</u>		
	↓		
No. of stages	2	4	6
Isentropic efficiency	0.78	0.87	0.90
Compressor mass, lbm	200	360	480
Incremental mass/hp	0	1.07	1.87

AXIAL-FLOW TURBINE

	<u>CBE Base Case</u>		
	↓		
No. of stages	8	6	4
Isentropic efficiency	0.88	0.83	0.78
Turbine mass, lbm	400	250	150
Incremental mass/hp	0	-1.0	-1.67

E-75

The similarity of the base-case isentropic efficiencies should be taken as coincidental. For these cycles to be compared, the polytropic efficiencies should be the same. Here the polytropic efficiencies of compression are 0.819 for the CBEX cycle and 0.854 for the CBE cycle.*

c. Combustors. The base-case combustor mass was taken from Ref. E-5 (pp. 5-17) as 39 lbm. Of this, the housing mass is 30 lbm, and the liner 1 lbm, so justifying the previous supposition that the contribution of the liner or flame tube to the total mass is small.

The variation of combustor mass with design factors given in Eq. E-71 was used:

$$\frac{P_{add}}{W_{cc}} \sim \left(\frac{\sigma_c}{\rho_c} \right) \frac{\sqrt{T_3} \sqrt{\frac{\Delta p_o}{p_o}}}{d_c \left(\frac{\ell}{d_c} \right) (1 + K')}$$

The symbols have been previously defined, but for any one engine design, the only significant variable of interest here is the pressure drop. The designer can trade off combustor pressure drop against size and mass of the combustor.

The combustor pressure drop of the base-case combustor was not given, and has been assumed to be 4%. The same pressure drop and specific mass were used for the CBE and CBEX cycles because inlet pressure is not a factor in combustor mass, to a first order of accuracy.

d. Heat Exchangers. The problems of making universal relations for heat-exchanger size versus losses were discussed

*The conversion formula is

$$\eta_{p,c} = \ln R' / \ln \left[\frac{R' - 1}{\eta_{is,c}} + 1 \right]$$

earlier (Section E-3). For the purposes of getting some indications of the influence of heat-exchanger design choices on overall engine specific size and fuel consumption, however, the apparent limit line of Fig. E-20 was used. Heat exchangers were assumed to have the reference hydraulic diameter of 0.002 ft: the heat exchanger of Ref. E-5 had somewhat smaller passages.

The heat-exchanger pressure losses of the base-case heat exchanger were not given in Ref. E-5. For the base-case engine the pressure losses were assumed to be 6%, and the effectiveness approximately 90% (0.89). (The heat-exchanger effectiveness in Ref. E-5 was also 90%.) The regenerator assembly weighed 61 lbm (pp. 5-16 of Ref. E-5), of which the core was 20 lbm and the housing 30 lbm. The volume was assumed to be proportional to the mass for different sizes of heat exchanger. The thermal loss factor H' and the pressure-drop loss factor L_x were calculated for the base case, and both factors were doubled and then quadrupled for alternative heat-exchanger designs. The sizes and masses were then estimated from the trend or limit line of Fig. E-20. The results are listed in Table E-3 and Fig. E-22.

e. Discussion of Findings. The approximations used in the calculations are such that the conclusions drawn cannot be unduly dogmatic. However, the following findings seem to be reasonable.

1. The heat-exchanger thermal losses have the greatest impact on specific size and fuel consumption. Despite the uncertainties of the heat-exchanger analysis, the large increase in fuel consumption for a small decrease in mass (and volume) shown in Fig. E-22 must withstand questioning of the accuracy of the quantified results.
2. The influence of turbomachinery efficiency is at least as great as is shown on Fig. E-22. It is felt that the masses of compressors and turbines were, if anything, overestimated. Good design would lead to a

smaller increase in machine mass with increase in the number of stages than was estimated. The compressor and turbine lines in Figs. E-21 and E-22 could therefore be steeper, leading to an optimum engine for some missions having a larger number of turbomachinery stages.

3. The influence of combustor pressure drop is small. By varying the pressure drop over more than the range normally considered as reasonable, from two to eight percent, an almost insignificant change in the specific engine mass and in the specific fuel consumption is produced, at least in comparison with the effects of changes in the other components.

There are, of course, other influences which cannot be quantified here. A single-stage compressor in a vehicle engine may be dictated not so much by considerations of optimality, but by the necessity of fitting the engine in a compartment of fixed size. A short combustor may be required because a longer one would lead to the requirement of an additional shaft bearing to avoid critical-speed problems. There may be room for more heat-exchanger core surface, but fitting it in may present an insurmountable packaging problem or require additional large ducting volume.

f. Part-Load Component Losses. All the above calculations and discussion were for full-load conditions. It would have been preferable to have calculated the specific mass for full load, and the specific-fuel-consumption effects for quarter-power conditions. As discussed earlier (Section B-3) the calculation of part-power performance of components and of the full engine seems presently too complex to attempt to establish quantitative general trends. However, the following qualitative conclusions, repeating to some extent those in Section B-3, seem justified.

The findings of component influence coefficients have reinforced the previous suggestions that the CBEX cycle is preferable for engines which must operate for long periods at cruise, part-power conditions. The off-design losses of turbines and particularly compressors increase with design pressure ratio, whereas the off-design losses of heat exchangers decrease over the range of interest. The full-power influence coefficients indicate that heat exchangers with even higher effectivenesses than are presently used, say 95%, might be justified. The higher the heat-exchanger effectiveness, the lower the optimum cycle pressure ratio, and the lower, therefore, are the turbomachinery losses at off-design. The two effects reinforce each other to give a double incentive towards a low-pressure-ratio highly regenerated cycle.

These considerations are based on the assumed use of simple constant-geometry turbomachinery. Variable-geometry compressors or, better, multispool engines largely overcome the part-load problems of high-pressure-ratio CBE engines. Gas bearings could make the use of small multispool engines very attractive.

There is also the possibility of combining a cruise engine with a boost engine in one unit. The low-pressure-ratio regenerative engine for cruise could divert its flow from the heat exchanger to a turbosupercharger shaft for boost, giving a high-pressure-ratio engine operating at maximum specific power rather than maximum efficiency.

2. Improvements to the State of the Art

a. Turbomachinery. Maximum polytropic efficiencies which have been achieved in the past appear to be about 94% for axial turbines, 93% for axial compressors, 92% for radial turbines and 87% for radial compressors. These are total-to-total efficiencies, and can be approached as useful efficiencies only with multistage machines (e.g., ten stages) or by the use of diffusers

much more effective than are presently available. Small (e.g., 1%) improvements in these levels could be expected

There is need for research on series diffusers, or other means of lowering the dynamic head by more than 75%. Diffusers for radial turbines could be greatly improved.

This contributor believes that there is usually too much emphasis on the use of the minimum possible number of stages in Brayton-cycle engines. Some of the efficiency considerations have been given above. Another is stress. High-temperature ceramic turbines might be feasible now if they were contemplated for use in multistage turbines having a tip speed of 1,000 or 1100 ft/sec instead of 1550 ft/sec or more.

There is a very wide range in turbomachinery specific mass, accentuated because aircraft turbines are light and also have higher stage loadings, whereas many industrial machines are heavy and may also have low stage loadings. It seems desirable to have lightweight construction techniques spread to machines of lower stage loadings. There are few advantages and many disadvantages of heavy construction.

b. Combustors. It was shown earlier that combustor design and performance seems to be scattered over a range of "quality" values, so that there is considerable scope for most combustion systems to be brought up to the level of the best. However, the influence of the combustion system on the engine specific power and fuel consumption is not large.

The use of ceramics for combustor liners could lead to a further improvement in combustors through the use of ducts instead of the present jets for mixing. The pressure-drop requirements of combustors are largely dictated by the need to achieve jet penetration through the primary combustor flow. By ducting the mixing flows together in, for instance, corrugated interleaved channels, a good outlet temperature distribution could be achieved in a shorter length with a lower pressure drop. If

the ceramic duct walls were partly effusion cooled, this arrangement should soon be practicable.

Ceramic combustors would also make easier the introduction of reheated turbine expanders (Ericsson-cycle approaches).

c. Heat Exchangers. Rotary ceramic regenerators have already achieved high standards of compactness, and only small improvements in surface/volume ratio are seen as possible because considerations such as fouling will dominate those of manufacturing and cost. Further improvements are needed in material compatibility with the composition and temperature of future engine working fluids. Significant gains could probably be realized from improved headers and ducts.

Further major improvements to regenerative heat exchangers would require alternative forms of moving surface, such as particles or ribbons that could also reduce the intrinsic carryover losses and reduce ducting volume and pressure losses.

d. Intercoolers. As shown earlier, the introduction of the intercooled, reheated cycle (approaching the Ericsson cycle) could lead to large gains in engine specific power, thermal efficiency, and part-power efficiency. However, if the heat is to be rejected at a low temperature, a large volume of air must pass through the intercoolers in order that the air temperature rise be small. It is this large air volume that controls the size and power losses of intercoolers more than design details.

For vehicular applications of the intercooled cycle, it might be preferable to use an intermediate heat-transfer fluid, as in an internal-combustion spark-ignition engine, so that the atmospheric air side of the heat exchanger can be optimally placed without unduly compromising the working-fluid side.

3. Present and Future Brayton-Engine Specific Mass Versus Specific Fuel Consumption

The performance of some advanced present and projected engines were plotted on Fig. E-23. Two state-of-the-art lines for 1977 and 2000 were drawn by eye and judgment.

There is little continuity between the lightweight engines and those of medium weight (developed or under development for automobiles). The same is true for the relationship between the medium-weight and the heavyweight engines, which include most of the world's nonaircraft gas-turbine horsepower, and which would be off the chart. In the present state of the art, there does not seem to be a conscious tradeoff between mass and sfc. Many lightweight engines have better sfc's than the heavyweight engines. The reason is cost, in that lightweight engines tend to use an aircraft-engine approach, which includes high turbine-inlet temperature and which is costly to develop.

The effects of the high inlet temperature overshadow the component losses introduced to save weight, such as high-Mach-number compressors, turbines, diffusers, and ducts.

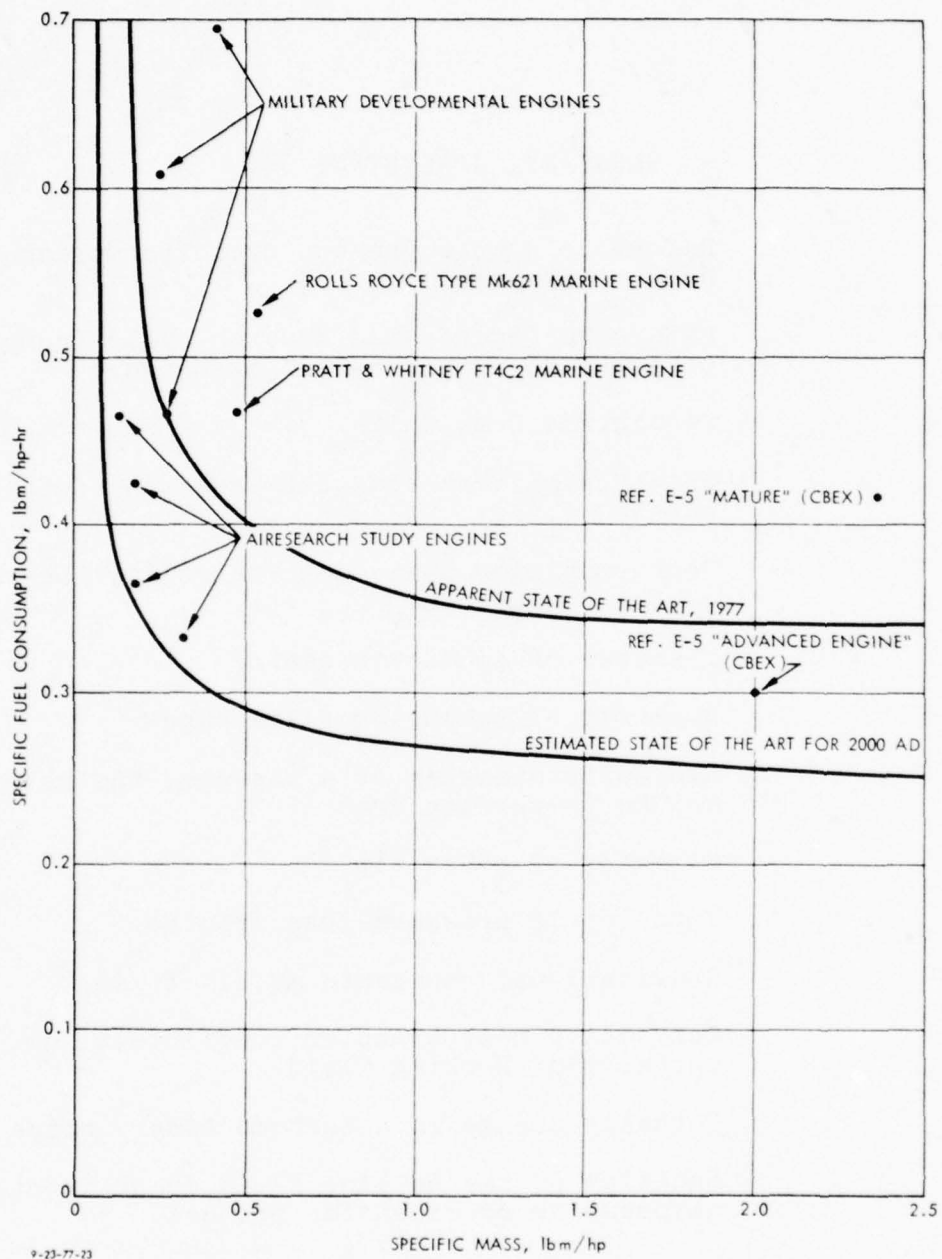


FIGURE E-23. Brayton engine specific mass versus specific fuel consumption.

GLOSSARY, APPENDIX E

CBE	Refers to simple Brayton cycle (compressor-burner-expander)
CBEX	Refers to regenerated Brayton cycle (compressor-turbine-expander-heat exchanger)
CHU	Centigrade heat unit
c_p	Specific heat at constant pressure of the working fluid
C_{rat}	Heat-exchanger heat-capacity ratio, the ratio of the products $\dot{m}c_p$
d_c	Diameter of combustor casing
d_{ft}	Diameter of combustor flame tube
d_h	Hydraulic diameter of a passage, the ratio of volume to surface area
d_2	Diameter of rotor tip
f	Total cycle pressure-loss fraction
g_c	Gravitational constant, 32.174 ft/sec ²
h	Convective heat-transfer coefficient; or, enthalpy of working fluid
Δh_o	Enthalpy change in a turbomachinery stage
h_{isen}	Enthalpy of the working fluid in an isentropic compression or expansion process
k	Thermal conductivity of working fluid
ℓ	Length
m	Mass
\dot{m}	Mass flow rate

M_3	Mach number at heat exchanger exit
Nu	Nusselt number, hd_h/k
p	Pressure of working fluid
P_{add}	Rate of heat addition to the working fluid in an actual cycle
$P_{add,id}$	Rate of heat addition to the working fluid in an ideal cycle
$P_{c,id}$	Power required for compression in an ideal cycle
$P_{e,id}$	Power produced by expansion in an ideal cycle
P_{HX}	Heat transfer rate in heat exchanger
P_i	Rate of energy transport associated with the working fluid, $\dot{m}c_p T_1$
P_{int}	Internal power transfer, the energy transfer rate to the working fluid before combustion and from the working fluid after combustion
$P_{int,id}$	Internal power transfer in an ideal cycle
$P_{loss,c}$	Equivalent power loss in the compressor; the difference between the actual power used and that required for isentropic compression.
$P_{loss,e}$	Equivalent power loss in the expander; the difference between the power produced by isentropic expansion and the actual power produced.
$P_{loss,L}$	Equivalent power loss associated with cycle pressure losses; the reduction in expander power output due to pressure losses.
$P_{loss,x}$	Additional rate of heat addition required, for a given maximum temperature, due to heat-exchanger ineffectiveness.
P_o	Power output
$P_{o,id}$	Power output of an ideal cycle
Pr	Prandtl number, $C_p \mu / k$

	Heat transfer rate in heat exchanger.
$\dot{q}_{x,id}, \dot{P}_{x,ideal}$	Heat transfer rate in heat exchanger in an ideal cycle
p	Pressure of the working fluid
p_1	Pressure of the working fluid at compressor inlet
Q'	Specific temperature rise in heat exchanger; ratio of the temperature rise on cold side to the maximum cold-side temperature
\dot{Q}	Heat transfer rate in heat exchanger (P_x)
r	Compressor pressure ratio
R	Gas constant of the working fluid
Re	Reynolds number, $\rho u d_h / \mu$
s, S	Entropy of the working fluid
sfc	Specific fuel consumption, fuel flow per unit power output, $lbm/hp-hr$
St	Stanton number, $h / \rho u c_p$
t	Material thickness
T	Temperature of the working fluid
T'	A temperature ratio
t_c	Thickness of combustor casing
T'_c	Specific temperature rise in compressor; the ratio of compressor temperature rise to inlet temperature.
t_{ft}	Thickness of combustor flame tube
T_{max}	Maximum cycle temperature
T_1	Temperature of working fluid at compressor inlet
u	Fluid velocity; or, tangential velocity of a rotating part

u_2	Rotor tip speed
v	Specific volume of working fluid
V	Volume
\dot{V}	Volume flow rate
V_{cc}	Volume of combustion chamber
V_t	Total core volume of heat exchanger
W	Weight
\dot{W}	Pumping power required for heat transfer
W_{cc}	Weight of combustion chamber
W_R	Weight of turbomachinery rotor
W_S	Weight of turbomachinery stationary parts
γ	Ratio of specific heats of the working fluid
ΔS_c	Entropy increase during compression
ΔS_e	Entropy increase during expansion
ΔS_L	Entropy increase due to pressure losses
ΔS_x	Entropy increase due to heat-exchanger ineffectiveness
ΔT_c	Temperature rise of cold-side fluid in heat exchanger
ϵ	Heat exchanger effectiveness
$\eta_c, \eta_{is,c}$	Isentropic efficiency of compressor
η_{cp}	Polytropic efficiency of compressor
$\eta_e, \eta_{is,e}$	Isentropic efficiency of expander
η_{ep}	Polytropic efficiency of expander
η_{id}	Thermodynamic efficiency of an ideal cycle
η_p	Polytropic efficiency
η_{th}	Thermodynamic efficiency, work output/heat input

$\eta_{th,id}$	Thermodynamic efficiency of an ideal cycle
θ	Effective temperature difference between hot-side and cold-side fluids in heat exchanger
θ_w	Fluid-to-wall temperature difference in heat exchanger
μ	Viscosity of the working fluid
ρ	Density of the working fluid; or, material density
ρ_{ft}	Density of combustor flame-tube material
ρ_r	Density of turbomachinery rotor material
ρ_s	Density of turbomachinery stationary-part material
σ	Mechanical stress; allowable working stress in a material
σ_b	Bending stress
σ_c	Centrifugal stress
σ_s	Allowable stress in turbomachinery stationary parts
ψ	Turbomachinery stage loading coefficient, $\Delta h_o / u_2^2$

REFERENCES, APPENDIX E

- E-1. Creare, Inc., Hanover, N.H., The Fluid-Dynamic Design of Centrifugal Compressors, Technical Note TN-153, Robert C. Dean, Jr., September 1972.
- E-2. J.S. Clarke, The Relation of Specific Heat Release to Pressure Drop in Aircraft-Gas-Turbine Combustion Chambers, Inst. Mech. Engrs.--ASME Joint Conference on Combustion, 1955.
- E-3. Foreign Technology Division, Air Force Systems Command, Combustion Chambers of Gas-Turbine Engines, FTD-MT-24-306-70, Yu. M. Pchelkin, May 1971. (AD 727 960)
- E-4. Herbert R. Hazard, "Combustors," in Gas-Turbine Engineering Handbook, GT Publications, Inc., Stamford, Connecticut, 1966.
- E-5. Jet Propulsion Laboratory, Should We Have a New Engine?, Report JPL SP 43-17, Vol. II, August 1975.

APPENDIX F

SIZE AND SPECIFIC FUEL CONSUMPTION RELATIONSHIPS FOR CLOSED BRAYTON-CYCLE ENGINES

A. Douglas Carmichael

CONTENTS

A. Ideal Engine Performance	F-3
1. The Ideal Cycle	F-3
2. Ideal Cycle Performance	F-6
3. Implications of Ideal Cycle Performance	F-8
B. Relationship between Actual Performance and Ideal Performance	F-10
1. Component Losses	F-10
a. Compressor Loss	F-10
b. Regenerator and Heater Pressure Loss	F-12
c. Regenerator Loss	F-12
d. Turbine Loss	F-13
e. Regenerator and Cooler Pressure Losses	F-14
f. Heater Losses	F-14
g. Cooler Losses	F-15
h. Mechanical Losses	F-15
i. Auxiliary Power Consumption	F-15
2. Impact of Losses on Performance	F-15
3. Part-Power Considerations	F-19
4. Implication of Thermodynamic Analysis of Practical Engine	F-21
C. Weight, Size, and Performance of Axial Flow Compressors	F-22
1. Outline of the Method	F-23
2. Aerodynamic Design Considerations	F-24
3. Mechanical Design Considerations	F-26
a. Blade Design	F-26
b. Compressor Disc	F-30
c. Compressor Casing	F-31
4. Compressor Stage Weight	F-32
5. Approximate Method of Compressor Weight Estimation	F-37

6. Volume/Horsepower for Axial-Flow Compressors	F-37
D. Weight, Size, and Performance of Axial-Flow Turbines	F-40
1. Outline of the Method	F-40
2. Aerodynamic Design Considerations	F-43
3. Mechanical Design Considerations	F-44
a. Blade Design	F-44
b. Turbine Disc	F-47
c. Turbine Casing	F-48
4. Total Stage Weight	F-49
5. Weight-Performance Characteristics of Multistage Turbines	F-49
E. Weight, Size, and Performance of Tubular Heat Exchangers	F-54
1. Basic Relationships	F-54
2. Illustrative Example	F-59
F. Overall Engine Considerations	F-60
1. Limitations to Performance and Size of Closed Brayton Cycle Engines	F-63
2. Performance, Size, and Weight of Closed Brayton Cycle Engines	F-64
a. The Core Engine	F-64
b. The Heat Source	F-66
c. The Complete Engine	F-66
G. Research and Development Areas--The Closed-Cycle Brayton Engine	F-66
Glossary	F-72
References	F-78

APPENDIX F
SIZE AND SPECIFIC FUEL CONSUMPTION RELATIONSHIPS
FOR CLOSED BRAYTON-CYCLE ENGINES

A. Douglas Carmichael

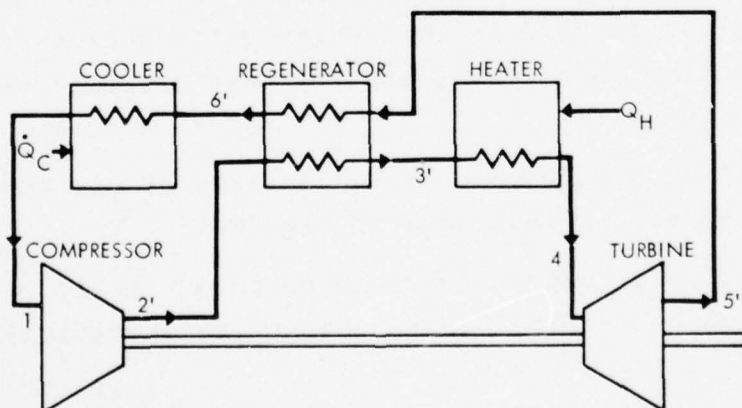
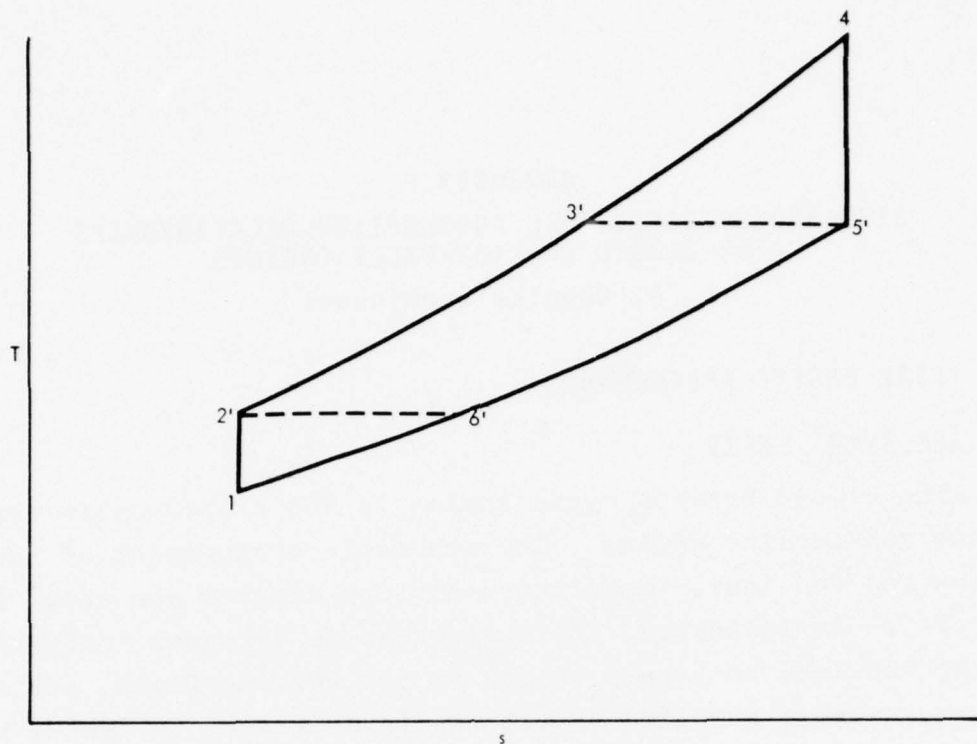
A. IDEAL ENGINE PERFORMANCE

1. The Ideal Cycle

The closed Brayton cycle engine is the closed-cycle version of the gas-turbine engine. The schematic arrangement of the engine and the ideal temperature-entropy diagram are shown in Fig. F-1. As indicated, the engine has an external combustion source (heater) to supply energy to the working fluid, and a cooler, usually supplied by either air or water, to remove waste heat from the working fluid. A regenerator is normally employed to enhance the cycle efficiency. The regenerator transfers heat from the turbine exit to the compressor exit to reduce the heat supplied from the heater. The working fluid in the cycle is a gas, often at high pressure in order to reduce the size of the unit. Helium is used in the larger units because of the good heat transfer properties, and the peak pressure may be in the range of 600 psi.

The ideal closed Brayton cycle consists of six energy transfer processes, as indicated in Fig. F-1:

1. Isentropic compression from p_1 to p_2 (1-2')
2. Constant-pressure heat-exchange (regeneration) utilizing turbine exhaust gas (2'-3')
3. Constant-pressure heat-addition (heating) from an external heat source (3'-4)
4. Isentropic expansion from p_2 to p_1 (4-5')



9-6-77-43

FIGURE F-1. T-s diagram and arrangement of the ideal Brayton cycle.

5. Constant-pressure heat exchange (regeneration) with gas leaving the compressor (5'-6')
6. Constant-pressure heat-extraction (cooling) to state 1 (6'-1).

In the ideal cycle there are of course no irreversibilities due to friction and due to heat transfer across a finite temperature difference. Hence the compressor and turbine efficiencies are 100%, there is no pressure drop across the system heat exchangers, and the effectiveness of the regenerator is 100%, i.e., $T_3' = T_5'$ and $T_2' = T_6'$ for a perfect-gas working fluid.

For a perfect gas with constant specific heats the energy transfer rates associated with the processes and their corresponding components are:

$$\begin{aligned}
 \text{Compressor:} \quad \dot{W}_c &= \dot{m} c_p (T_2' - T_1) \\
 \text{Regenerator:} \quad \dot{Q}_R &= \dot{m} c_p (T_3' - T_2') \\
 \text{Heater:} \quad \dot{Q}_H &= \dot{m} c_p (T_4 - T_3') = \dot{m} c_p (T_4 - T_5') \\
 \text{Turbine:} \quad \dot{W}_t &= \dot{m} c_p (T_4 - T_5') \\
 \text{Regenerator:} \quad \dot{Q}_R &= \dot{m} c_p (T_5' - T_6') = \dot{m} c_p (T_3' - T_2') \\
 \text{Cooler:} \quad \dot{Q}_C &= \dot{m} c_p (T_6' - T_1),
 \end{aligned}$$

where \dot{m} is the mass flow rate of the working fluid, and c_p is the specific heat at constant pressure. The energy transfer parameters, in the context of this report, are then appropriate combinations of the energy transfer rates:

1. The active internal power transfer, P_{int} , which is the energy transferred from post-heat-addition to pre-heat-addition is

$$\begin{aligned}
 P_{int} &= \dot{W}_c + \dot{Q}_R = \dot{m} c_p [(T_2' - T_1) + (T_3' - T_2')] \\
 &= \dot{m} c_p (T_3' - T_1) = \dot{m} c_p (T_5' - T_1) .
 \end{aligned} \tag{F-1}$$

2. The power addition, P_{add} , is the rate of heat addition:

$$P_{add} = \dot{Q}_H = \dot{m}c_p(T_4 - T_{5'}) \quad (F-2)$$

3. The power output, P_o :

$$P_o = \dot{W}_t - \dot{W}_c = \dot{m}c_p[(T_4 - T_{5'}) - (T_{2'} - T_1)] \quad (F-3)$$

4. The intermediate power transfer, P_x , is the energy transfer rate, excluding active internal power transfer, across other internal surfaces:

$$\begin{aligned} P_x &= \dot{Q}_H + \dot{Q}_C = \dot{m}c_p[(T_4 - T_{5'}) + (T_{6'} - T_1)] \\ &= \dot{m}c_p[(T_4 - T_{5'}) + (T_{2'} - T_1)] \end{aligned} \quad (F-4)$$

5. The total internal power transfer, P_{it} , is then

$$P_{it} = P_{int} + P_x \quad (F-5)$$

6. The reference, or inlet, power transfer, P_i , is

$$P_i = \dot{m}c_p T_1 \quad (F-6)$$

2. Ideal Cycle Performance

The ideal cycle efficiency of a closed Brayton cycle is

$$\eta_{id} = \frac{P_o}{P_{add}} = 1 - \frac{T_{2'} - T_1}{T_4 - T_{5'}} = 1 - \frac{T_1}{T_{5'}} = 1 - \left(\frac{T_1}{T_4}\right)\left(\frac{T_{2'}}{T_1}\right) \quad (F-7)$$

which can also be expressed in terms of the specific fuel consumption (sfc) as

$$\text{sfc} = \frac{0.138}{\eta_{id}} \text{ lbm/hp-hr} \quad (\text{F-8})$$

for a representative fuel having a lower heating value of 18,400 Btu/lbm. The specific power output is

$$\frac{P_o}{P_i} = \frac{(T_4 - T_{5'}) - (T_{2'} - T_1)}{T_1} = \left(\frac{T_4}{T_1} - \frac{T_{2'}}{T_1} \right) \left(1 - \frac{T_1}{T_{2'}} \right) . \quad (\text{F-9})$$

It is evident that the ideal performance, in the above terms, can be expressed in terms of only temperature ratios (T_4/T_1 and $T_{2'}/T_1$); the pressure ratio of the cycle and the specific heat ratio, γ , are not required to define the performance of the ideal cycle. Further, in defining two power transfer ratios--the total internal power transfer ratio

$$\begin{aligned} \frac{P_{it}}{P_o} &= \frac{P_x + P_{int}}{P_o} = \frac{(T_4 - T_1) + (T_{2'} - T_1)}{(T_4 - T_{5'}) - (T_{2'} - T_1)} \\ &= \frac{\left(\frac{T_4}{T_1} - 1 \right) + \left(\frac{T_{2'}}{T_1} - 1 \right)}{\left[\frac{T_4}{T_1} - \left(\frac{T_4}{T_1} \right) \left(\frac{T_1}{T_{2'}} \right) \right] - \left(\frac{T_{2'}}{T_1} - 1 \right)} \end{aligned} \quad (\text{F-10})$$

and the power-added ratio (a measure of maximum temperature)

$$\frac{P_{int} + P_{add}}{P_i} = \left(\frac{T_4}{T_1} - 1 \right) , \quad (\text{F-11})$$

it can be seen that the ideal performance can be presented in terms of the power transfer ratios rather than the two temperature ratios.

The performance of the ideal Brayton cycle is presented in Fig. F-2, in terms of sfc and specific power output (P_o/P_i), as a function of the total internal power transfer ratio (P_{it}/P_o) with the power-added ratio as a parameter. The values of the latter of 3, 4, and 6 correspond to temperature ratios (T_4/T_1) of 4, 5, and 7, or for $T_1 = 520^\circ\text{R}$, maximum temperatures of 2080°R , 2600°R , and 3640°R . Values of the pressure ratio (p_2/p_1) are also shown for any monatomic gas ($\gamma = 5/3$).

3. Implications of Ideal Cycle Performance

The performance characteristics of the ideal Brayton cycle presented in Fig. F-2 indicate that the best performance (low sfc and high power output ratio P_o/P_i) occurs at higher values of turbine inlet temperature [i.e., high $(P_{add} + P_{int})/P_i$]. However, at particular values of turbine inlet temperature, the lowest sfc occurs at high internal power transfer ratio P_{it}/P_o , while the highest power output occurs at close to the lowest internal power transfer ratio. If the size and weight of the energy transfer components can be represented in an approximate manner by the total internal power transfer ratio P_{it}/P_o , then there is an important tradeoff between size (and/or weight) and sfc for the ideal engine. In this context, the performance characteristics for the ideal engine also indicate that the pressure ratio of the engine is likely to be relatively low (<4.0) for most applications, the larger portion of the active internal power transfer being accomplished in the regenerator rather than in the compressor.

Most of the characteristics presented in Fig. F-2 are essentially independent of gas properties (within the constraints of a perfect gas), with the previously mentioned exception of pressure ratio. Since the cycle is closed, the performance of the cycle, in different terms, can be affected by the choice of working fluid. In particular, the power output per unit mass flow rate can be increased by selecting a working fluid with

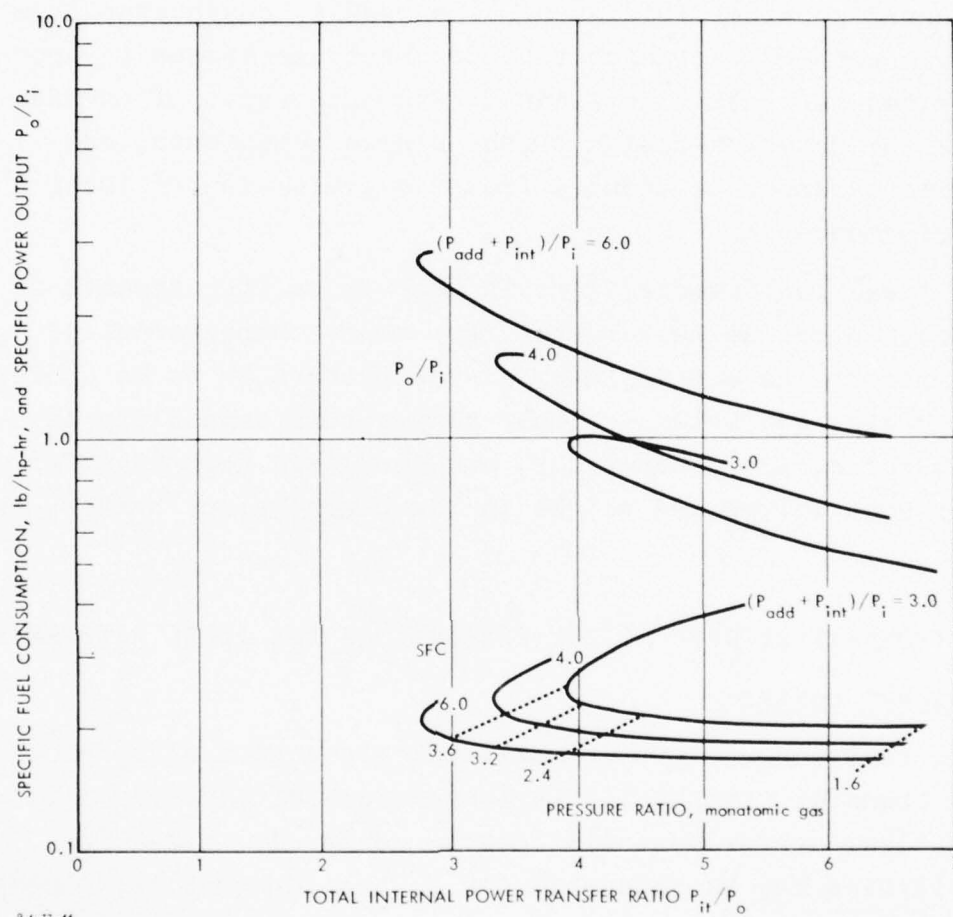


FIGURE F-2. Performance characteristics of ideal closed-Brayton cycles.

high specific heat (low molecular weight and/or many internal degrees of freedom); the pressure ratio required can be reduced by selecting a working fluid with a high ratio of specific heats (few internal degrees of freedom). Currently, helium is the preferred working fluid, and, as a result, deviations from perfect gas properties, which tend to introduce losses in open-cycle engines, are not significant. Gas properties of course influence the detailed design of the engine components, but these effects cannot be deduced from the evaluation of ideal cycle performance.

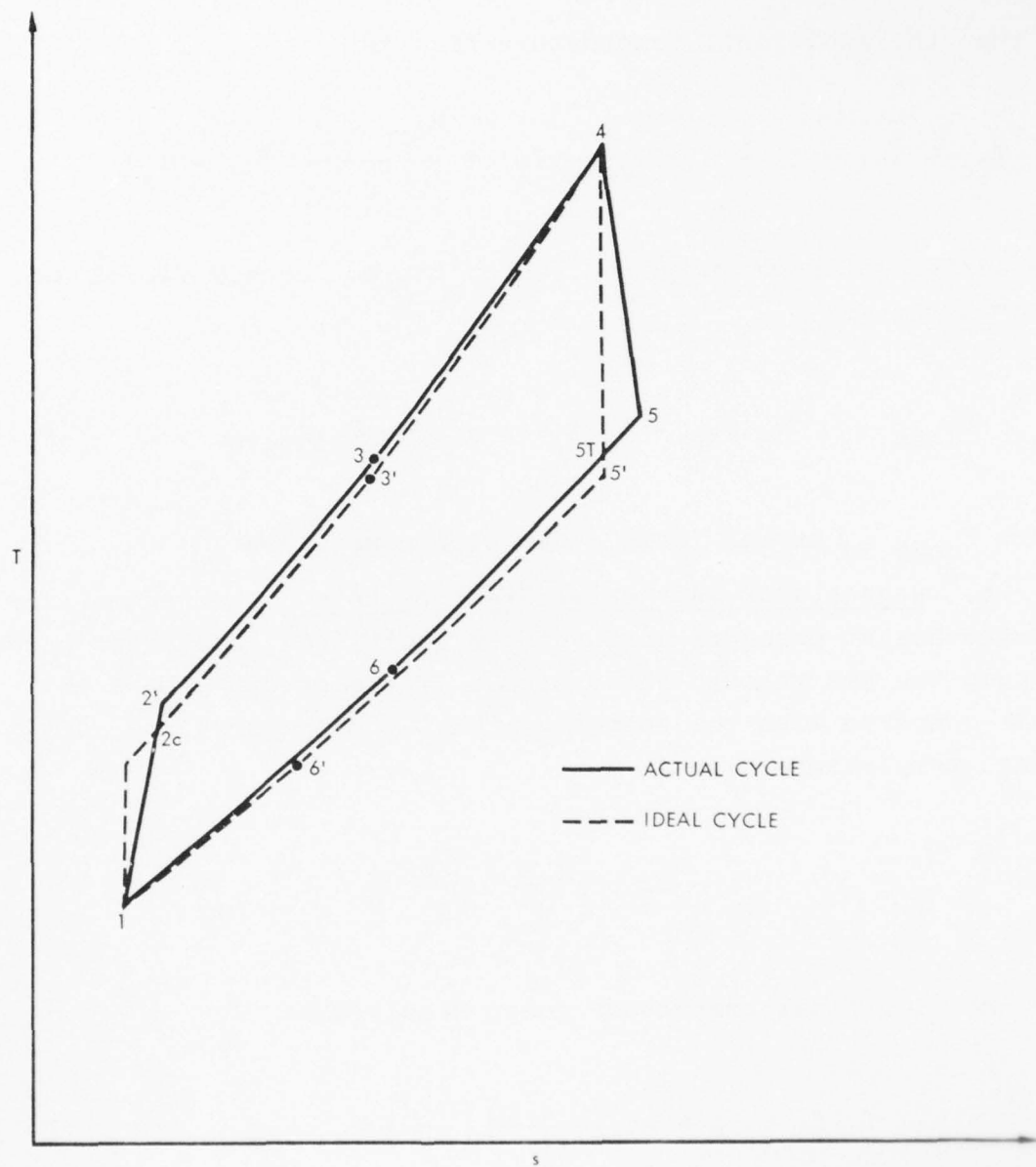
The ideal performance suggests that major improvements in closed Brayton cycles must result from those characteristics which permit the necessary internal power transfer to be achieved in minimum size and weight--higher temperature capability in heater, turbine, and regenerator, and increased heat transfer rates per unit volume and weight in the regenerator, heater, and cooler.

B. RELATIONSHIP BETWEEN ACTUAL PERFORMANCE AND IDEAL PERFORMANCE

1. Component Losses

In a real engine irreversibilities associated with friction and heat transfer through finite temperature differences imply that the ideal performance will not be achieved. These irreversibilities may be accounted for by the conventional concepts of isentropic efficiency for the compressor and turbine, effectiveness for the regenerator, and pressure loss in the heat exchangers and ducting. A T-s diagram for a practical cycle is presented in Fig. F-3. The various losses can be characterized as follows.

a. Compressor Loss. The compressor requires more than the ideal power input, and the loss is usually characterized by the isentropic efficiency



9-6-77-45

FIGURE F-3. T-s diagram of the actual Brayton-cycle engine and the ideal cycle.

AD-A070 528

INSTITUTE FOR DEFENSE ANALYSES ARLINGTON VA SCIENCE A--ETC F/G 21/7
TECHNOLOGY ASSESSMENT OF ADVANCED PROPULSION SYSTEMS FOR SOME C--ETC(U)
SEP 78 F R RIDDELL, D M DIX DAHC15-73-C-0200

UNCLASSIFIED

IDA-P-1278-VOL-2

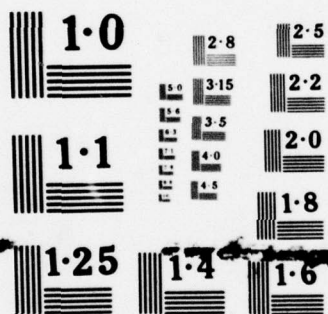
IDA/HQ-77-19843

NL

4 OF 4
AD
A070528



END
DATE
FILMED
8-79
DDC



NATIONAL BUREAU OF STANDARDS
MICROCOPY RESOLUTION TEST CHART

$$\eta_c \equiv \frac{T_{2'} - T_1}{T_{2c} - T_1}$$

so that the additional temperature rise is

$$T_{2c} - T_{2'} = (1 - \eta_c)(T_{2c} - T_1) = \frac{(1 - \eta_c)}{\eta_c} (T_{2'} - T_1) .$$

The additional power required, which can be loosely viewed as a power loss, is

$$P_{\text{loss},c} = \dot{m} c_p (T_{2c} - T_{2'}) = \frac{(1 - \eta_c)}{\eta_c} P_{\text{comp,id}} , \quad (\text{F-12})$$

where $P_{\text{comp,id}}$ is the ideal compressor power input.

b. Regenerator and Heater Pressure Loss. The regenerator and the heater pressure loss require additional compressor power to pump the gas through the system. If the pressure loss is small compared with the compressor exit temperature, the additional temperature rise is

$$T_2 - T_{2c} = \frac{\gamma - 1}{\eta_c \gamma} \frac{\Delta p_H}{p_2} T_{2c}$$

and the additional compressor power required is

$$P_{\text{loss},H} = \dot{m} c_p \left(\frac{\gamma - 1}{\eta_c \gamma} \right) \left(\frac{\Delta p_H}{p_2} \right) T_{2c} . \quad (\text{F-13})$$

c. Regenerator Loss. The necessity for heat transfer through a non-zero temperature difference is a source of loss

in the regenerator. This is usually characterized by the heat-transfer effectiveness:

$$\epsilon = \frac{T_3 - T_2}{T_5 - T_2} .$$

If the difference between the heat actually transferred and the theoretically maximum value is viewed as a loss, one obtains

$$P_{\text{loss},r} = \dot{m}c_p(T_5 - T_3) = (1 - \epsilon)P_{\text{reg},i} = \frac{1 - \epsilon}{\epsilon} P_{\text{reg}} , \quad (\text{F-14})$$

where P_{reg} is the actual heat transfer rate in the regenerator, and $P_{\text{reg},i}$ is the corresponding heat transfer rate in an ideal regenerator.

d. Turbine Loss. The turbine produces less than the ideal power, and the loss is usually characterized by the isentropic efficiency

$$\eta_T = \frac{T_4 - T_5}{T_4 - T_{5T}}$$

so that the additional temperature rise is

$$T_5 - T_{5T} = \frac{(1 - \eta_T)}{\eta_T} (T_4 - T_5) = (1 - \eta_T)(T_4 - T_{5T})$$

and the power loss from the turbine is

$$P_{\text{loss},t} = \dot{m}c_p(T_5 - T_{5T}) = \frac{1 - \eta_T}{\eta_T} P_{\text{turb}} = (1 - \eta_T)P_{\text{turb},i} , \quad (\text{F-15})$$

where P_{turb} is the actual power output of the turbine, and $P_{\text{turb},i}$ is the corresponding output of an ideal turbine.

e. Regenerator and Cooler Pressure Losses. These pressure losses detract from the turbine output power, and if they are small compared to the turbine exit pressure, the additional temperature rise is

$$T_{5c} - T_{5'} = \frac{\gamma - 1}{\gamma} \frac{\Delta p_E}{p_1} T_{5c}$$

and the corresponding power loss is

$$P_{\text{loss},E} = \dot{m} c_p \left(\frac{\gamma - 1}{\gamma} \right) \left(\frac{\Delta p_E}{p_1} \right) T_{5c} \quad . \quad (F-16)$$

f. Heater Losses. The combustor-heater system uses the oil fuel and atmospheric air to provide the heat energy to be transferred to the working fluid of the Brayton cycle. The main loss in the heater results from the energy carried away by the hot gases released to the atmosphere up the stack. This loss is minimized by cooling the exhaust gases by means of air preheaters and by pressure charging. Other smaller energy losses result from heat transfer to the environment at the external surfaces of the heater and by incomplete combustion.

The energy loss in the heater is not charged to the thermodynamic cycle but to the complete power plant. The heater efficiency η_h is defined as

$$\eta_h = \frac{\text{Heat Transfer to the Cycle Heater}}{\text{Energy in the Fuel}} = \frac{\dot{Q}_H}{\dot{m}_f (HV)} \quad ,$$

where HV is the fuel heating value, and \dot{m}_f is the flow rate of fuel.

g. Cooler Losses. As with the regenerator, there is an irreversibility in the cooler associated with heat transfer through a non-zero temperature difference. The effect of this loss is to raise the minimum temperature of the cycle (T_1) and, as such, it is not charged directly to the cycle here. The effect on cycle performance, in terms of energy transfer parameter, is to reduce the value of $(P_{add} + P_{int})/P_1$ for a given maximum temperature.

h. Mechanical Losses. There are friction losses in the bearings and seals of the unit that do not appear in the simple thermodynamic model of the cycle. These losses tend to be small and are accounted for by the mechanical efficiency, defined as

$$\eta_m = \frac{\text{Mechanical Power Output}}{\text{Thermodynamic Power Output}} .$$

i. Auxiliary Power Consumption. Power is required to circulate the combustion gases through the heater and to pass the coolant fluid through the cooler. These losses are neglected here.

2. Impact of Losses on Performance

The specific fuel consumption of a practical engine is given by

$$\text{sfc} = \frac{0.138}{\eta \eta_h \eta_m} \quad \text{lbm/hp-hr} , \quad (\text{F-17})$$

and the specific power output is given by

$$\frac{P_o}{P_1} = \eta \eta_m \frac{P_{add}}{P_1} , \quad (\text{F-18})$$

where η is the cycle efficiency, and P_{add} is the actual heat added to the working fluid.

Although the cycle efficiency, including the losses, can be determined in a straightforward way, it is useful to isolate the effects of the ideal efficiency and the various losses, as follows:

$$\eta = \frac{(T_4 - T_5) - (T_2 - T_1)}{T_4 - T_3}$$

$$= \frac{(T_4 - T_{5'}) - (T_2 - T_1) - (T_5 - T_{5c}) - (T_{2c} - T_2) - (T_{5c} - T_{5'}) - (T_2 - T_{2c})}{(T_4 - T_{3'}) - (T_3 - T_{3'})}$$

By using the substitution

$$\epsilon = \frac{T_3 - T_2}{T_5 - T_2}$$

this can be written as

$$\eta = \frac{(T_4 - T_{5'}) - (T_2 - T_1) - (T_5 - T_{5c}) - (T_{2c} - T_2) - (T_{5c} - T_{5'}) - (T_2 - T_{2c})}{(T_4 - T_{3'}) - (1 - \epsilon)[(T_2 - T_{2c}) + (T_{2c} - T_2) - (T_3 - T_{3'})] - \epsilon[(T_5 - T_{5c}) + (T_{5c} - T_{5'})]}$$

If it is assumed that the various temperature differences $(T_2 - T_{2c})$, $(T_{2c} - T_2)$, etc., appearing in the denominator are small compared with the heater ideal temperature rise $(T_4 - T_3)$, and if the previously defined losses are introduced, this equation may be written as

$$\eta = \eta_{1d} - [1 - \eta_{1d}(1 - \epsilon)] \left(\frac{P_{\text{loss},c}}{P_{\text{comp},1d}} \right) \left(\frac{P_{\text{comp},1d}}{P_{\text{add},1d}} \right) - [1 - \eta_{1d}\epsilon] \left(\frac{P_{\text{loss},t}}{P_{\text{turb},1}} \right) \left(\frac{P_{\text{turb},1}}{P_{\text{add},1d}} \right)$$

$$- \eta_{1d} \left(\frac{P_{\text{loss},r}}{P_{\text{reg},1}} \right) \left(\frac{P_{\text{reg},1d}}{P_{\text{add},1d}} \right) - [1 - \eta_{1d}(1 - \epsilon)] \left(\frac{P_{\text{loss},H}}{P_{\text{RH},1d}} \right) \left(\frac{P_{\text{RH},1d}}{P_{\text{add},1d}} \right) \quad (\text{F-19})$$

$$- [1 - \eta_{1d}(1 - \epsilon)] \left(\frac{P_{\text{loss},E}}{P_{\text{RC},1d}} \right) \left(\frac{P_{\text{RC},1d}}{P_{\text{add},1d}} \right)$$

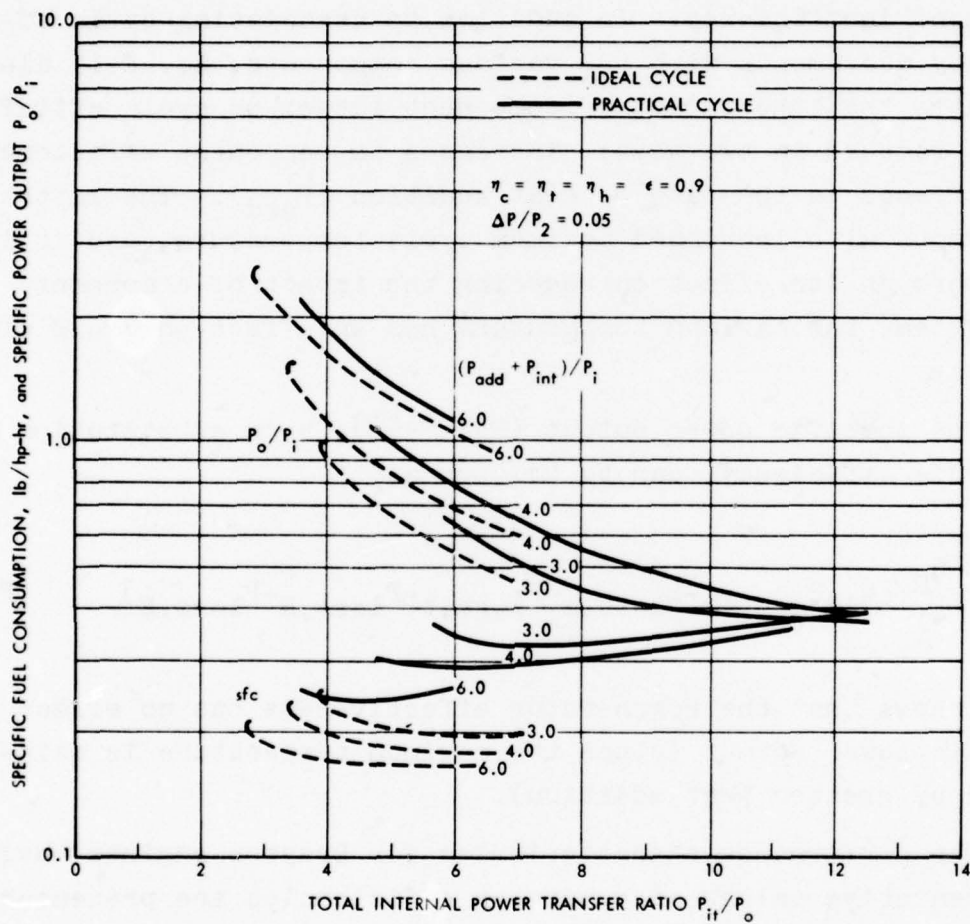
where P_{RH} and P_{RC} are the energy transfer rates in regenerator plus heater, and regenerator plus cooler, respectively. In this expression, the terms $(P_{loss,c}/P_{comp,id})$, $(P_{loss,t}/P_{turb,i})$, etc., are all of the nature of a ratio of power "lost" to power transferred in a particular component, and are thus a measure of component inefficiency. In addition to associating cycle efficiency decrements with the various components, Eq. F-19 also indicates that the impact of component losses on cycle efficiency can be reduced in two ways: increases in component efficiencies or increases in the rate of heat addition (P_{add}). The latter is synonymous with increased maximum cycle temperature, and it is only through its effect on reducing the impact of component losses that the maximum temperature has an effect on cycle efficiency.

The specific power output (Eq. F-18), upon substitution of the cycle efficiency, can be written as

$$\frac{P_o}{P_i} = \frac{\eta_m}{P_i} [\eta_{id} P_{add,id} - P_{loss,c} - P_{loss,t} - P_{loss,H} - P_{loss,E}] \quad , \quad (F-20)$$

which shows that the regenerator effectiveness has no effect on specific power output (since the maximum temperature is maintained by greater heat addition).

The performance characteristics for Brayton engines having representative values of component efficiencies are presented in Fig. F-4. It has been assumed that the polytropic efficiencies of the compressor and turbine are 0.90, the regenerator effectiveness is 0.90, the heater efficiency is 0.9, and the pressure loss in the system is 5% of the maximum cycle pressure. The mechanical efficiency would be expected to be close to unity, and is so assumed here. The assumed component efficiencies are extremely good, would require careful design, and are unlikely to be improved in the future. The selected regenerator



9-6-77-46

FIGURE F-4. Performance characteristics of Brayton cycles.

effectiveness and overall pressure loss are under the control of the designer and would be selected from tradeoff studies of weight and volume against fuel consumption, but are representative values for helium systems.

The comparison of the practical and ideal performance characteristics presented in Fig. F-4 shows that the predicted sfc for the practical engine is dramatically reduced by the irreversibilities in the various components. For example, at $(P_{\text{add}} + P_{\text{int}})/P_i = 3.0$, losses increase the sfc from a level of about 0.2 to a minimum of about 0.32, corresponding to a reduction in efficiency from 69% to 43%. The effect of increased heat addition in reducing the impact of component losses on sfc is clearly indicated by the higher values of the energy addition ratio. For a given pressure ratio, the irreversibilities also reduce the specific power output, as evidenced by the first point on the corresponding curves, which are at the same pressure ratio. For the same ratio of internal power transfer to power output, however, the actual engine achieves a slightly higher specific power output--at the expense of increased specific fuel consumption.

The influence of the losses on the performance characteristics is presented in Fig. F-5 for a value of $(P_{\text{int}} + P_i)/P_o$ of 3.0 (corresponding to a maximum cycle temperature of 2080°R if $T_1 = 520^\circ\text{R}$). This figure shows the regenerator effectiveness has the most significant influence on sfc. The other losses are approximately of equal importance. As indicated previously, power output is not influenced by regenerator effectiveness. It is to be noted here that the compressor pressure ratio applies to both ideal and actual cycles, but that the internal power transfer ratio applies only to the actual cycle.

3. Part-Power Considerations

The closed-cycle Brayton engine would normally operate at fixed temperatures and pressure ratios over the normal operating

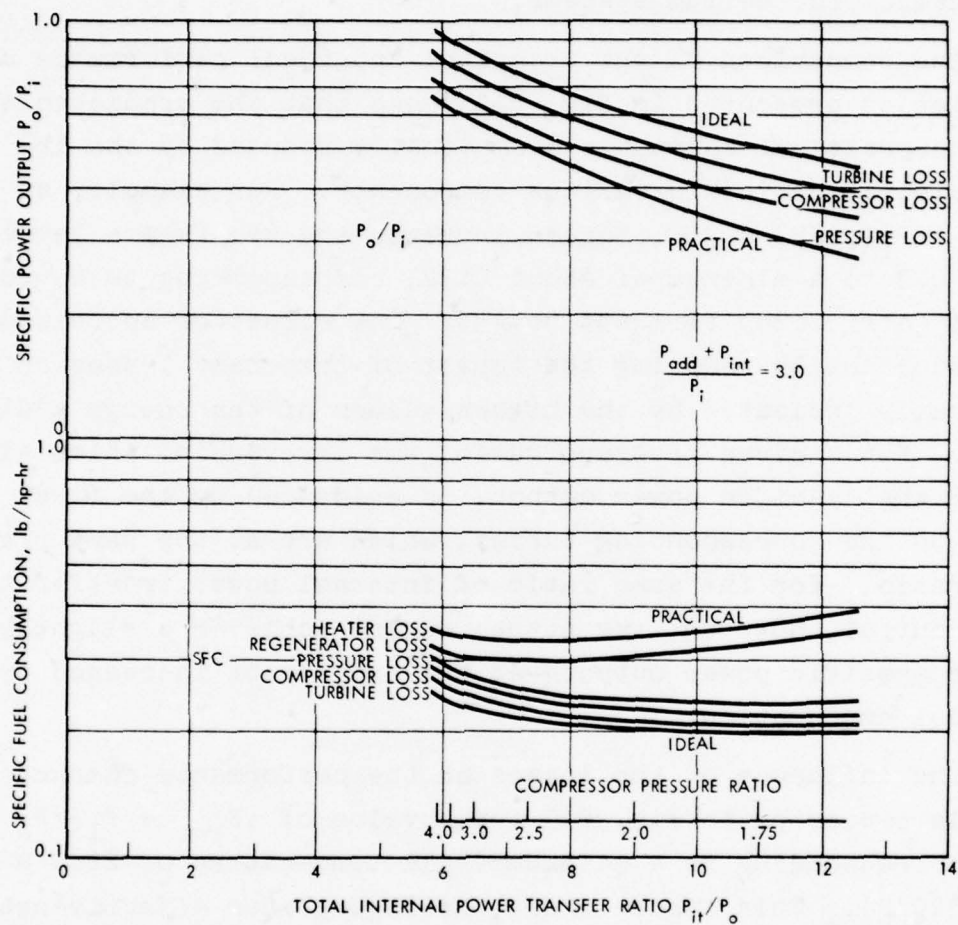


FIGURE F-5. Influence of component losses on Brayton-cycle engine performance.

power levels. Changes in required power would be controlled by varying the mass flow rate of gas in the components by raising or lowering the pressure (density) level in the system. The basic efficiency of the engine should remain at a value close to the design-power value. It would be expected that there would be only small increases in sfc at part power, depending on the output speed schedule as a function of power for the driven load. Perhaps an area of investigation would be the part-load performance of the combustor unit, but this is not expected to be significant.

4. Implication of Thermodynamic Analysis of Practical Engines

The closed-cycle Brayton engine, in common with other closed-cycle engines, has a high ratio of internal energy transfer to power output, compared with open-cycle engines. Since much of the energy transfer is by heat exchangers, the volume and weight of the engines may be expected to be high. Since the pressure level in the system is a design variable, the volume and weight of practical engines can be minimized to some extent by choosing high internal pressure levels. Nevertheless, any further major improvements must result from other ways to reduce the size, weight, and performance loss associated with the internal energy transfer.

The largest heat exchanger in the system is likely to be the regenerator because regenerator effectiveness has such an important influence on efficiency. A potential topic for research and development is the technology of compact, high-pressure regenerators.

The specific fuel consumption of the engine and the power output are improved by raising the turbine inlet temperature T_4 , since it reduces both the ratio of internal energy transfer to power output and the impact of the losses associated with it. The level that can be utilized in a power plant is essentially a materials and fabrication problem. The heater provides a very

serious challenge because of the combined effects of corrosion due to the products of combustion, high stress due to the helium pressure, and high operating temperature.

The part-load performance of the closed-cycle Brayton engine is likely to be better than almost any other engine because the power will be controlled by varying the pressure level in the system. The thermodynamic, aerodynamic, and heat-transfer parameters will remain unchanged as power is reduced.

The extent to which the benefits of a closed-cycle Brayton engine can be realized and further improvements can be made obviously depends on the factors which control the size-weight-loss relationships of the various components. Accordingly, the next three sections deal with these relationships for the three major types of components in closed-cycle Brayton engines: axial compressors, axial turbines, and heat exchangers.

C. WEIGHT, SIZE, AND PERFORMANCE OF AXIAL-FLOW COMPRESSORS

The axial-flow compressor achieves compression by imparting angular momentum to the fluid by means of a rotating blade-row, the rotor, and removing it in a stationary blade-row, the stator. The fundamental weight- and/or size-performance relationship is dictated by the fact that although the energy transfer rate in a stage (a rotor-stator pair) can be increased with little increase in stage weight or size, more turning, and hence acceleration and deceleration, of the fluid is required, thus leading to higher flow losses. Hence, for a given state of technology and a given application, possible designs range from a few "highly loaded" stages of lower efficiency to several "lightly loaded" stages of higher efficiency. The limits on this relationship are examined here, both to serve as a benchmark for axial-flow compression devices, and to identify those physical variables that most influence the relationship.

1. Outline of the Method

The weight-performance relationships for axial-flow compressors are governed by aerodynamic and mechanical design interactions. In order to determine appropriate relationships, an analytical procedure is developed here that is similar to the design process used for axial-flow compressors. The procedure centers around a single compressor stage, depicted schematically in Fig. F-6

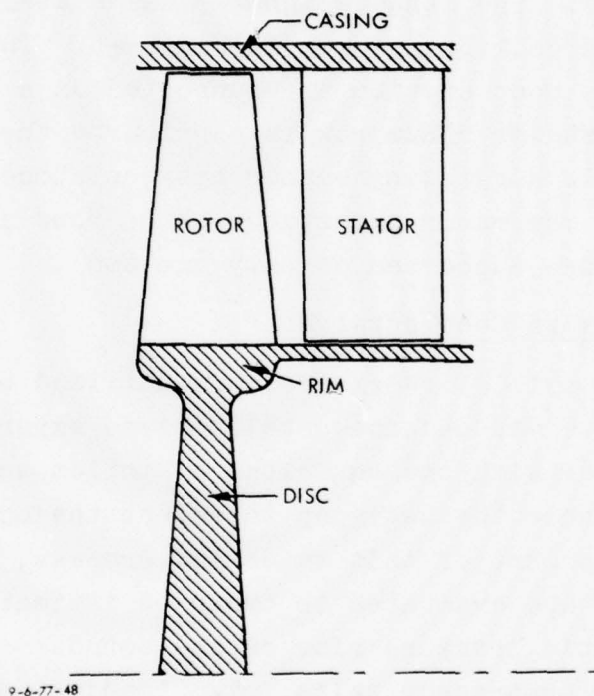


FIGURE F-6. Compressor-stage arrangement.

Briefly, it is assumed that the achievable performance of a compressor stage is largely determined by the value of the aerodynamic loading parameter ($\Delta h_o/u^2$) at the tip radius, where Δh_o is the stagnation enthalpy rise across the stage and u is the tip speed. In order to achieve this performance, it is necessary that the static pressure rise and fluid decelerations not exceed some empirically determined limits, and these limits

are used to establish the basic geometrical characteristics of the blades. Other factors which are known to influence performance but not stage weight, such as Mach number, Reynolds number, and tip clearance, can be introduced to further refine the performance estimate.

Given the basic geometrical characteristics of the stage, more detailed dimensions and weights are determined from an estimate of steady and vibratory stress levels as functions of material properties. The stage weight is calculated for a stage having a prescribed geometry, shown in Fig. F-6. The rotor blade row and blade root section are supported on a constant-stress disc. The stator blade row is carried by the outside casing, and there is a rotating spacer between successive discs. It is assumed that the rotor and stator blade rows are unshrouded (i.e., the blades are supported at only one end).

2. Aerodynamic Design Considerations

The design of axial-flow compressors utilized blade-element performance data (termed cascade data) derived experimentally. These data, together with the equations of motion and conservation of energy, enable the designer to select the optimum geometry for the design. As part of this selection process, empirical loading parameters are evaluated in order to estimate the influence of the static pressure rise on the boundary layers on the blades and the compressor walls. Two loading parameters are used in this study:

1. The parameter $\Delta p/q$ at the rotor tip
2. The blade diffusion factor to select the blade solidity.

The stage loading parameter $\Delta p/q$ is a measure of the blade row static pressure rise Δp compared with the inlet velocity head q . Experimental studies have indicated that losses increase as the value of $\Delta p/q$ is increased. It is very difficult to achieve high values of $\Delta p/q$ because of boundary layer separation.

The tip sections of the compressor stages are assumed to have representative vector diagrams corresponding to the rotor relative inlet angle β of 60 deg and V_x/u of 0.5. By using a range of values of $\Delta p/q$ and these design assumptions, the basic design features of the compressor stages are established.

The other loading parameter, the diffusion factor,* is used to determine the solidity of the blades. The diffusion factor is an empirically derived parameter that is intended to allow the designer to establish the conditions of the boundary layers on the blade surfaces. High values of diffusion factor correspond to large losses. A representative value of 0.45 is selected for this study. This value, together with vector diagram data determined by using the loading parameter $\Delta p/q$, enables the solidity of the blades to be established. Solidity is the ratio of the blade chord length c to the circumferential distance s between the blades and defines the way the blades are packed into the stage.

The design limitations at the rotor tip were used to define conditions at the mid- and hub-sections of the blades. However, at low values of hub/tip ratio in some cases, the blade designs can be unacceptable because of very high fluid deflections in the rotor blade row at the hub. To overcome this problem, an upper limit of the parameter $(g_o J \Delta h_o / u^2)$ of 1.0 is set at the hub. When this limit is exceeded, the blade geometry is modified to reduce the blade loadings to correspond to the limit at the hub. In this study, as in practice, limitations at the rotor hub reduce the pressure rise attainable in low hub/tip ratio designs.

The resulting performance data for the axial-flow compressor stages are summarized in Table F-1 (the polytropic efficiency is obtained from Ref. F-1). The polytropic efficiency ($\eta_p \equiv dh_{isen}/dh_{actual}$) is the basic measure of stage performance, and

*The diffusion factor is defined as

$$1 - (\cos \beta_1 / \cos \beta_2) + [\cos \beta_1 (\tan \beta_1 - \tan \beta_2) / 2\sigma],$$

where σ is the solidity, β_1 is the inlet fluid angle, and β_2 is the outlet fluid angle.

is related to overall isentropic efficiency as shown in Fig. F-7. Table F-1, then, defines the achievable efficiency of axial compressor stages as a function of the aerodynamic loading parameter ($g_o J \Delta h / u^2$) and the tip solidity required to attain this performance.

The blade height and tip radius for the compressor rotor are determined from the continuity equation, assuming that the average value of axial velocity is the same as the value at the tip radius.

TABLE F-1. COMPRESSOR PERFORMANCE AND DESIGN DATA

Rotor $\Delta p/q$	0.44	0.47	0.50	0.54	0.58
$(g_o J \Delta h_o / u^2)_{tip}$	0.307	0.334	0.362	0.405	0.451
Tip Solidity	0.77	0.83	0.93	1.14	1.56
Polytropic Efficiency η_p	0.925	0.92	0.88	0.84	0.80
Lower Limit of Hub/Tip	0.55	0.58	0.60	0.64	0.67

3. Mechanical Design Considerations

The construction of the compressor stage is idealized in Fig. F-6. The main purpose of the mechanical design study is to determine the stage weight and volume. To do this, the method of designing each component is first established, then the weights are calculated. The aerodynamic design data for the compressor blades, together with the dimensions and velocities, provide the input information for the mechanical design process.

a. Blade Design. Rotor blades are subject to steady gas-bending loads and steady centrifugal loads. Unsteady loads occur because of asymmetry and instability in the flow to and from the blading. The blade chord and the number of rotor blades are determined by evaluating the steady blade stresses, the oscillating stresses, and the properties of the blade material.

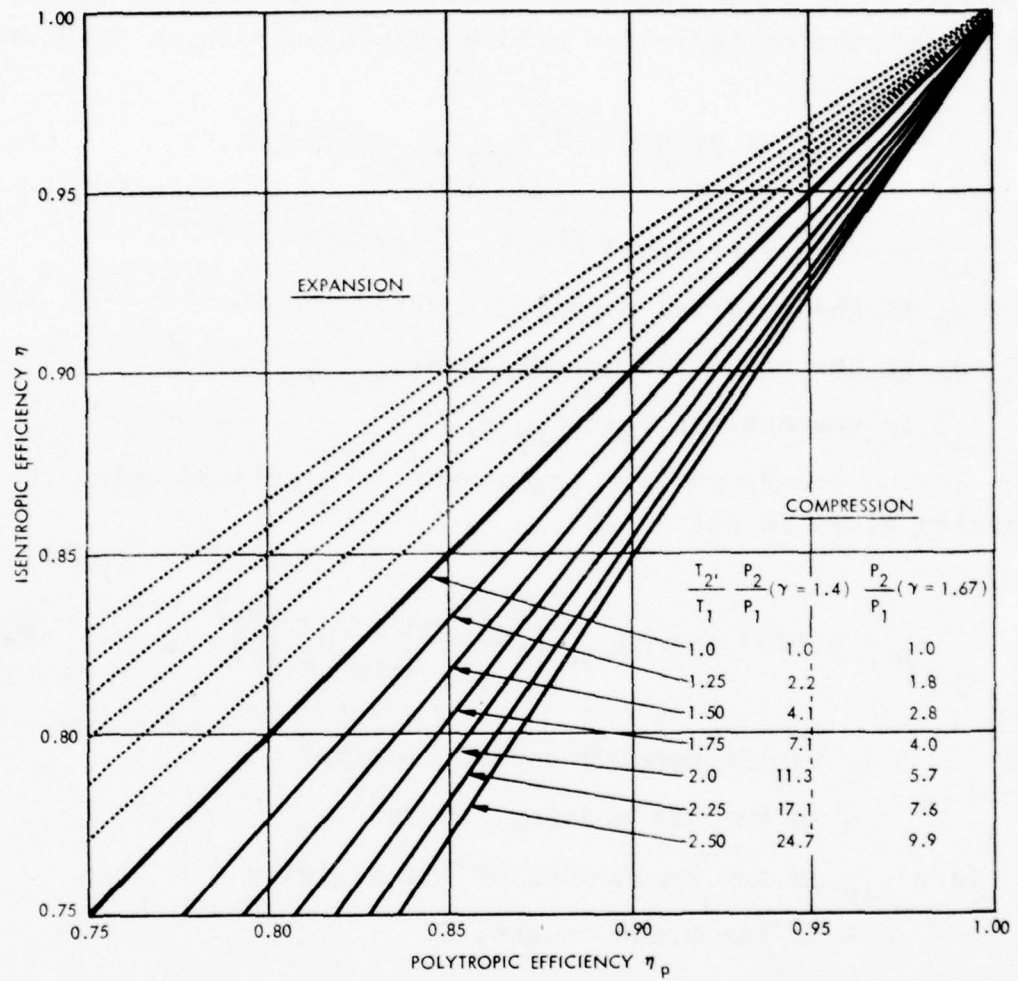


FIGURE F-7. Relationship between polytropic and isentropic efficiencies.

The rotor blades are assumed to have uniform chord length and thicknesses tapering from 4% of chord at the tip to 9% at the hub. The centrifugal stresses are predicted for the assumed geometries of the rotor blades by the expression (Ref. F-2)

$$\sigma_{CF} = 71.8 \times 10^{-6} \rho_m u_t^2 (1 - \lambda^2) , \quad (F-21)$$

where σ_{CF} is the centrifugal stress, lbf/in.²

ρ_m is the material density, lb/ft³

u_t is the rotor tip speed, ft/sec

λ is the hub/tip ratio r_h/r_t .

The steady gas bending stress is predicted using the expression given in Ref. F-2:

$$\sigma_B = 0.0824 \rho (s/c)_{tip} \left(\frac{g_o J \Delta h_o}{u^2} \right)_{tip} u_t^2 \left(\frac{l}{c} \right)^2 , \quad (F-22)$$

where σ_B is the bending stress, lbf/in.²

ρ is the gas density, lb/ft³

$(s/c)_{tip}$ is the reciprocal of tip solidity

l is the blade length, ft

u_t is the tip speed, ft/sec

c is the blade chord, ft.

From this expression, the product $(\sigma_B c^2)$ is established.

The allowable oscillating bending stress is assumed to be a factor "a" times the steady gas bending stress, where "a" is termed the amplification factor. The value of the amplification factor "a" used in turbomachinery designs reflects the fact that the asymmetry of flow in the region of the blade is likely to

excite higher resonant amplitudes in the blading when the blades have low natural frequencies. This effect is indicated in the form of the expression for the amplification factor (Ref. F-3)

$$a = 40 n/f , \quad (F-23)$$

where n is the rotational speed, rev/sec

f is the fundamental natural frequency, Hz.

The natural frequency of compressor blading of the geometry assumed here is given approximately by (Ref. F-4)

$$f = 1.08 \sqrt{\frac{E}{\rho_m}} \frac{c}{\ell^2} , \quad (F-24)$$

where f is the natural frequency, Hz

E is Young's modulus, lbf/in.²

ρ_m is the material density, lb/ft³

c is the blade chord, ft

ℓ is the blade length, ft.

The fatigue properties of materials are often presented in Goodman diagrams, where the fatigue strength (for 10^7 cycles) is plotted against the applied steady stress. For this study a representative Goodman diagram is utilized in which the allowable fatigue stress due to oscillating loads is assumed to vary linearly from a value of 0.75 of the yield stress σ_y at zero applied steady stress to zero fatigue stress when the steady stress reaches the yield stress σ_y . Thus, if the allowable fatigue stress is $a\sigma_B$, one obtains

$$\sigma_B = \frac{\sigma_y - \sigma_{CF}}{\left(\frac{a}{0.75} + 1\right)} . \quad (F-25)$$

Equations F-22 through F-25 may be combined to estimate the design value of blade chords:

$$c = \left[\frac{4.07 \rho \left(\frac{s}{c} \right)_{\text{tip}} \left(\frac{g_o J \Delta h_o}{u^2} \right)_{\text{tip}} u_t^2 \ell^4 n \sqrt{\frac{\rho_m}{E}}}{\sigma_y - \sigma_{CF}} \right]^{1/3} \quad (\text{F-26})$$

This relatively simple expression is obtained by assuming a $\gg 0.75$. The total weight of the compressor blades, assuming that the stator blades are similar to the rotor blades, is estimated from the expression

$$W_B = 0.54 \rho_m c \ell r_t / (s/c)_{\text{tip}} , \quad (\text{F-27})$$

where W_B is the total blade weight, lb.

b. Compressor Disc. The rim of the disc carrying the rotor blades is assumed to be equivalent to an unsupported annular ring having a depth $1/5$ of the blade height and the width equal to the blade chord c . The weight of the spacer is assumed to be included with the rim.

The weight of rim is given by

$$W_R = 1.257 \rho_m c \ell r_h , \quad (\text{F-28})$$

where W_R is the rim weight, lb

r_h is the hub radius, ft.

The load on the disc imposed by the blades and the unsupported rim is utilized to determine the minimum thickness of the uniformly stressed disc, t_D .

$$t_D = \frac{2.15 \times 10^{-5}}{\sigma_D} \left[\frac{1 - \lambda^2}{(s/c)_{tip}} + \lambda(1 - \lambda)(11\lambda - 1) \frac{\rho_m c u_t^2}{(6\lambda - 1)} \right], \quad (F-29)$$

where t_D is the disc minimum thickness, ft

σ_D is the disc stress, lbf/in²

This equation may be substituted into the equation for the weight of a uniformly stressed disc (see, for example, Ref. F-5)

$$W_D = \frac{2\pi(\sigma_D \times 144)r_t^2 t_D g_o}{u_t^2} \left[e^{\frac{\rho_m u_D^2}{2g_o(\sigma_D \times 144)}} - 1 \right], \quad (F-30)$$

where W_D is the disc weight, lb

σ_D is the disc stress, lbf/in²

u_D is the disc speed at the minimum thickness radius, ft/sec

g_o is the gravitational constant, 32.2 ft-lbm/lbf-sec².

c. Compressor Casing. The casing is designed as a thin-walled cylinder with the load provided by the pressure difference p across the casing wall. The casing thickness is expressed as

$$t_c = r_t p / \sigma_c, \quad (F-31)$$

where t_c is the casing thickness, ft

p is the maximum pressure difference, lbf/in²

σ_c is the casing stress, lbf/in²

The casing weight was estimated by assuming that the width of the stage is twice the blade chord:

$$W_C = 4\pi\rho_m \frac{p}{\sigma_c} r_t^2 c \quad . \quad (F-32)$$

4. Compressor Stage Weight

The weight of the compressor stage is the sum of the components:

$$W_{TOTAL} = W_B + W_R + W_D + W_C \quad . \quad (F-33)$$

The weights of the blades, rim, disc, and casing, given by Eqs. F-27, F-28, F-30, and F-32, respectively, may be combined to give the total stage weight. The blade chord c , given by Eq. F-26, and the disc thickness t_D , given by Eq. F-29, may be substituted into the expressions to provide the total stage weight. Two additional equations are required in order to be able to express the stage weight in terms of the fundamental aerodynamic and material property parameters: the continuity equation

$$\dot{m} = \rho V \pi (r_t^2 - r_h^2) = \rho u_t \frac{\pi}{2} r_t^2 (1 - \lambda^2) \quad , \quad (F-34)$$

where \dot{m} is the mass flow rate, lbm/sec, and the definition of the blade height

$$l = r_t - r_h = r_t (1 - \lambda) \quad . \quad (F-35)$$

The total stage weight can be expressed as

$$W_{TOTAL} = \left[A + B \left(e^{cu_t^2} - 1 \right) \right] \frac{D}{u_t^{1/2}} \left(\frac{E}{F - Gu_t^2} \right)^{1/3} \quad , \quad (F-36)$$

where

$$A = \frac{0.54}{(s/c)_{tip}} (1 - \lambda) + 1.257 \lambda (1 - \lambda) + 4\pi p/\sigma_c$$

$$B = \frac{0.627}{(6\lambda - 1)} \left[\frac{1 - \lambda^2}{(s/c)_{tip}} + \lambda(1 - \lambda)(11\lambda - 1) \right]$$

$$C = \frac{\rho_m (6\lambda - 1)^2}{231840 \sigma_D}$$

$$D = \rho_m (1 - \lambda)^{4/3} \left[\frac{2/\pi \dot{m}}{\rho(1 - \lambda^2)} \right]^{3/2}$$

$$E = 0.648 \rho \left(\frac{s}{c} \right)_{tip} \left(\frac{g_o J \Delta h_o}{u^2} \right)_{tip} \sqrt{\frac{\rho_m}{E}}$$

$$F = \sigma_y$$

$$G = 71.8 \times 10^{-6} \rho_m (1 - \lambda^2) .$$

The power absorbed by the compressor stage is

$$P_c = 1.414 \dot{m} \Delta h_o ,$$

where P_c is the power, hp

\dot{m} is the mass flow rate, lb/sec

Δh_o is the stagnation enthalpy rise, Btu/lb.

This expression may be rewritten as

$$P_c = 5.647 \times 10^{-5} \dot{m} \left(\frac{g_o J \Delta h_o}{u^2} \right)_{tip} u_t^2 . \quad (F-37)$$

The weight per unit power of the stage is therefore given by

$$\frac{W_{TOTAL}}{P_c} = \left[A + B \left(e^{cu_t^2} - 1 \right) \right] \frac{D^1}{u_t^{2.5}} \left(\frac{E}{F - Gu_t^2} \right)^{1/3}, \quad (F-38)$$

where

$$D^1 = 17710 \rho_m (1 - \lambda)^{4/3} \left[\frac{\frac{2}{\pi}}{\rho (1 - \lambda^2)} \right]^{3/2} \frac{\dot{m}^{1/2}}{\left(\frac{g_o J \Delta h_o}{u^2} \right)_{tip}}.$$

The other coefficients A, B, C, E, F, and G remain unchanged. Equation F-38 indicates that the weight/power for a compressor varies as

$$\frac{W_{TOTAL}}{P_c} \propto \left(\frac{g_o J \Delta h_o}{u^2} \right)^{-2/3} \dot{m}^{1/2} E^{1/6} \rho^{-7/6}. \quad (F-39)$$

In addition, there is an approximate relationship:

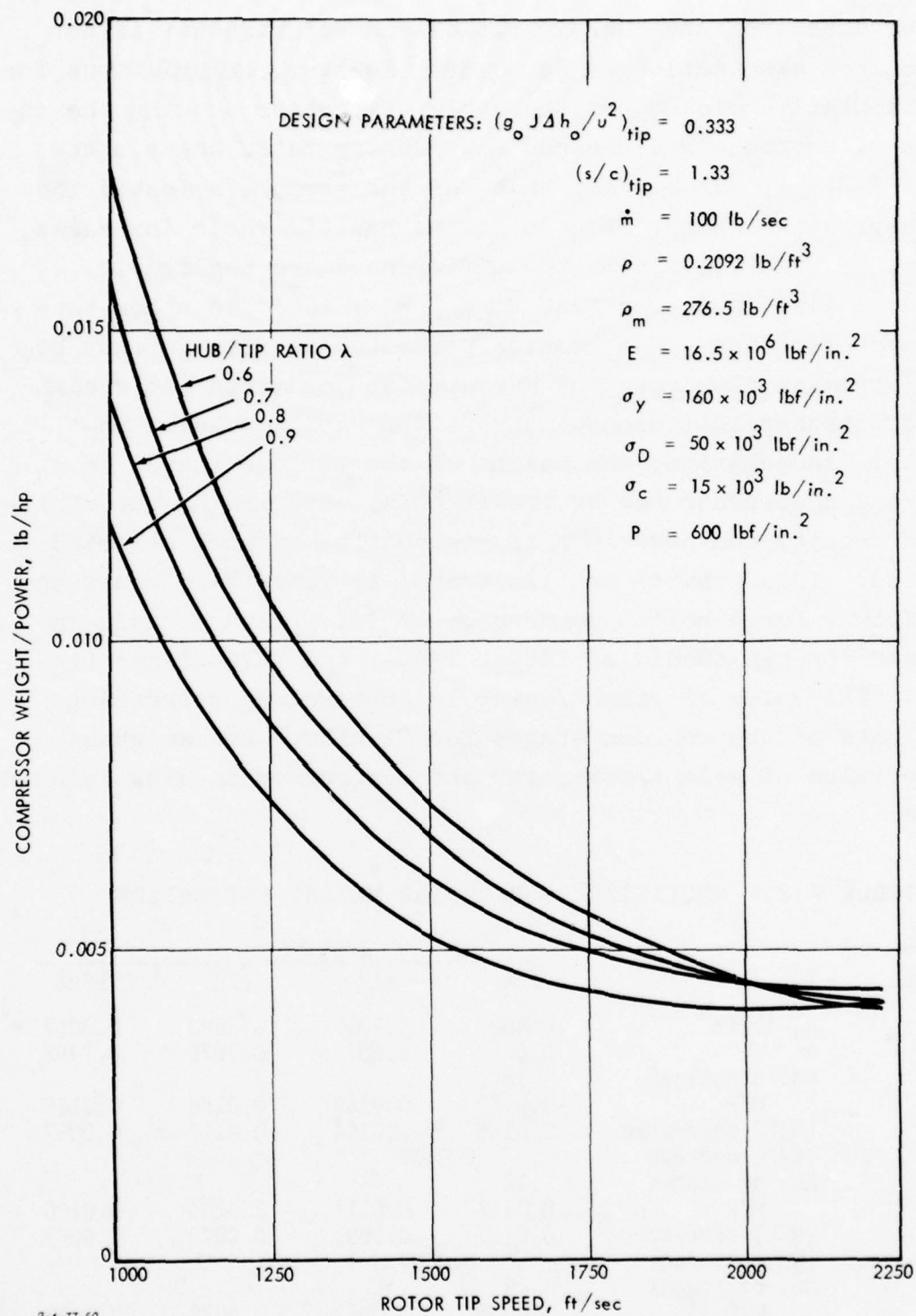
$$\frac{W_{TOTAL}}{P_c} \propto u_t^{-2.5} \rho_m^{7/6}. \quad (F-40)$$

It can be seen from Eq. F-38 that at high values of u_t the terms $e^{cu_t^2}$ and Gu_t^2 become important and would eventually cause the compressor weight/power to rise as u_t increases further. This situation would occur when the centrifugal stress in the rotor blades approaches the yield stress level and when the centrifugal loads in the disc are very high. It can be expected that there is a rotor tip speed yielding minimum compressor stage weight/power.

The effect of the hub/tip ratio λ on weight/power is not obvious from examination of Eq. F-38. However, calculations for a representative closed Brayton cycle compressor showing the influence of compressor tip speed and hub/tip ratio are plotted in Fig. F-8. It can be seen that for the example selected the compressor weight/power reduces as the hub-tip ratio increases, but that at high tip speeds the differences are negligible. This curve also indicates that $W_{\text{TOTAL}}/P_c \propto u_t^{-2.5}$ is a low-tip-speed approximation. The results presented in Fig. F-8 may be scaled for mass flow rate and gas density (provided the design level of pressure differences across the casing remains unchanged). In addition, the weight of the various stages in a multistage compressor may be predicted by determining the variation in density and hub/tip ratio by continuity at a selected tip speed. This process is illustrated in Table F-2, where the weight/power for a helium compressor of 2:1 pressure ratio is estimated for tip speeds of 1000-, 1200-, and 1400-ft/sec tip speeds. The value of weight/power is obtained by correcting the weights of the various stages for density. The weighted average value of weight/power for the compressor is also calculated.

TABLE F-2. MULTISTAGE COMPRESSOR WEIGHT ESTIMATION

Tip Speed, ft/sec		Stage			
		1st	1/3	2/3	Last
1000	ρ , lb/ft ³	0.2092	0.2357	0.2683	0.3017
	λ	0.6	0.657	0.7078	0.7458
	No. of stages	18			
	W/P	0.0176	0.0166	0.0156	0.0149
	(W/P) corrected	0.0176	0.0144	0.0117	0.0097
	(W/P) average	0.0133			
1200	No. of stages	12			
	W/P	0.0117	0.0111	0.0105	0.0100
	(W/P) corrected	0.0117	0.0097	0.0079	0.0065
	(W/P) average	0.0089			
	No. of stages	9			
1400	W/P	0.0085	0.0083	0.0078	0.0075
	(W/P) corrected	0.0085	0.0072	0.0058	0.0049
	(W/P) average	0.0066			



9-6-77-50
FIGURE F-8. Compressor weight/power for closed Brayton-cycle engine, helium working fluid.

5. Approximate Method of Compressor Weight Estimation

It is possible to provide an approximate method for estimating weight/power for representative compressors if the centrifugal stresses in the blades are a small proportion of the material yield stress and the centrifugal loads and stresses in the disc are not high. The procedure is to simplify Eq. F-38 using the above assumptions and then to derive a nondimensional expression from the resulting equation for average stages in representative compressors. The resulting expression is of the form

$$\left(\frac{W_{\text{TOTAL}}}{P_c} \right)_{\text{average}} = \frac{(\text{Function of stage loading})(0.46 + 144p/\sigma_y)}{\frac{u_t^{2.5} \rho^{7/6} E^{1/6} \sigma_y^{1/3}}{m^{1/2} \rho_m^{7/6}}} \quad (\text{F-41})$$

Since stage loading influences the efficiency of a compressor stage (as in Table F-1), it is possible to develop an approximate method for providing the relationship between the polytropic efficiency and weight/power for representative multistage compressors. This is shown in Fig. F-9. The method tends to underestimate the weights of compressors with high centrifugal stresses (i.e., at high rotor tip speeds). In addition, it is implied that the components are of reasonable size and can be manufactured. Furthermore, corrections to polytropic efficiency for low Reynolds number and high Mach number would have to be made.

6. Volume/Horsepower for Axial-Flow Compressors

The volume of an axial-flow compressor stage is easily established from the dimensions of the stage as

$$V = 2\pi r_t^2 c \quad , \quad (\text{F-42})$$

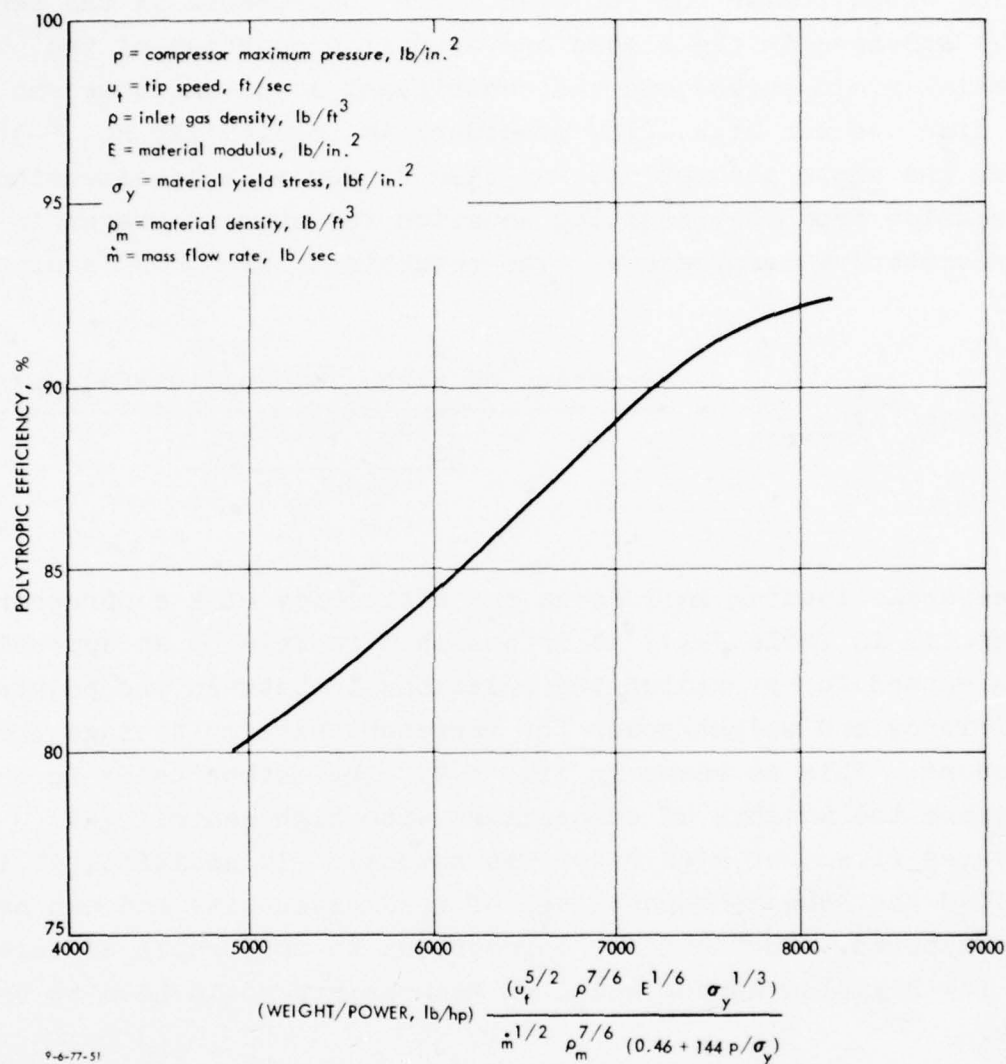


FIGURE F-9. Compressor weight and performance.

where V is the volume, ft^3

r_t is the tip radius, ft

c is the rotor chord, ft .

It is assumed that the stator blade chord is the same as the rotor blade chord. The spacing of the blade rows is accounted for because the blade chords are measured at the setting angle of blades (about 35° at the hub), hence the spacing between the blades is about $(1 - \cos 35^\circ)(\text{chord})$ or 0.18 chord.

The horsepower of the stage from Eq. F-37 is

$$P_c = \frac{1}{550 g_o} \left(\frac{g_o J \Delta h_o}{u^2} \right)_{\text{tip}} u_t^2, \quad (\text{F-43})$$

hence the V/P_c is given by

$$V/P_c = \frac{2\pi r_t^2 c g_o 550}{m \left(\frac{g_o J \Delta h_o}{u^2} \right)_{\text{tip}} u_t^2} \quad (\text{F-44})$$

The value of r_t^2 can be substituted from Eq. F-34, while c can be obtained from Eq. F-26 to give

$$V/P_c = \frac{48.8 \times 10^3 m^{1/2} \left[\frac{(s/c)_{\text{tip}} \sqrt{\frac{\rho_m}{E}}}{\sigma_y - 71.8 \times 10^{-6} \rho_m u_t^2 (1-\lambda^2)} \right]^{1/3}}{\rho^{7/6} u_t^{2.5} (1+\lambda)^{3/2} (1-\lambda)^{1/6} \left(\frac{g_o J \Delta h_o}{u^2} \right)_{\text{tip}}^{2/3}} \quad (\text{F-45})$$

When the centrifugal blade stress is a small proportion of the yield stress of the material, Eq. F-45 may be provided in an approximate form as

$$V/P_c = [\text{Function of Stage Loading}] \left(\sqrt{\frac{\rho_m}{E}} \frac{1}{\sigma_y} \right)^{1/3} \left(\frac{\dot{m}^{1/2}}{\rho^{7/6} u_t^{2.5}} \right) . \quad (F-46)$$

The relationship between stage loading and polytropic efficiency provides the method of predicting (approximately) the volume/horsepower and polytropic efficiency of multistage axial-flow compressors, presented in Fig. F-10. The prediction method underestimates the volume of compressors when, at tip speed, the rotor blade centrifugal stresses are a high proportion of the material yield stress.

D. WEIGHT, SIZE, AND PERFORMANCE OF AXIAL-FLOW TURBINES

The axial-flow turbine achieves expansion by imparting angular momentum to the fluid by means of a stationary blade row (the stator) and removing it by means of a rotating blade row (the rotor). As with the compressor, the fundamental weight-and/or size-performance relationship is dictated by the fact that although the energy transfer rate in a stage can be increased with little weight or size increase, more turning of the fluid is required and hence more losses are incurred. Again, the limits on the resulting relationship between a few stages of lower efficiency and several stages of higher efficiency are examined here.

1. Outline of the Method

Briefly, it is assumed that the achievable performance of a turbine stage is determined by the stage loading coefficient $\psi = \Delta h_o / u_m^2$, where Δh_o is the stagnation enthalpy decrease across the stage and u_m is the blade speed at the mean radius. To achieve this performance, it is necessary that both the flow coefficient $\phi = V_x / u_m$, where V_x is the axial through-flow velocity, and the chord-to-spacing ratio of the blades be optimally selected. Other factors that are known to affect

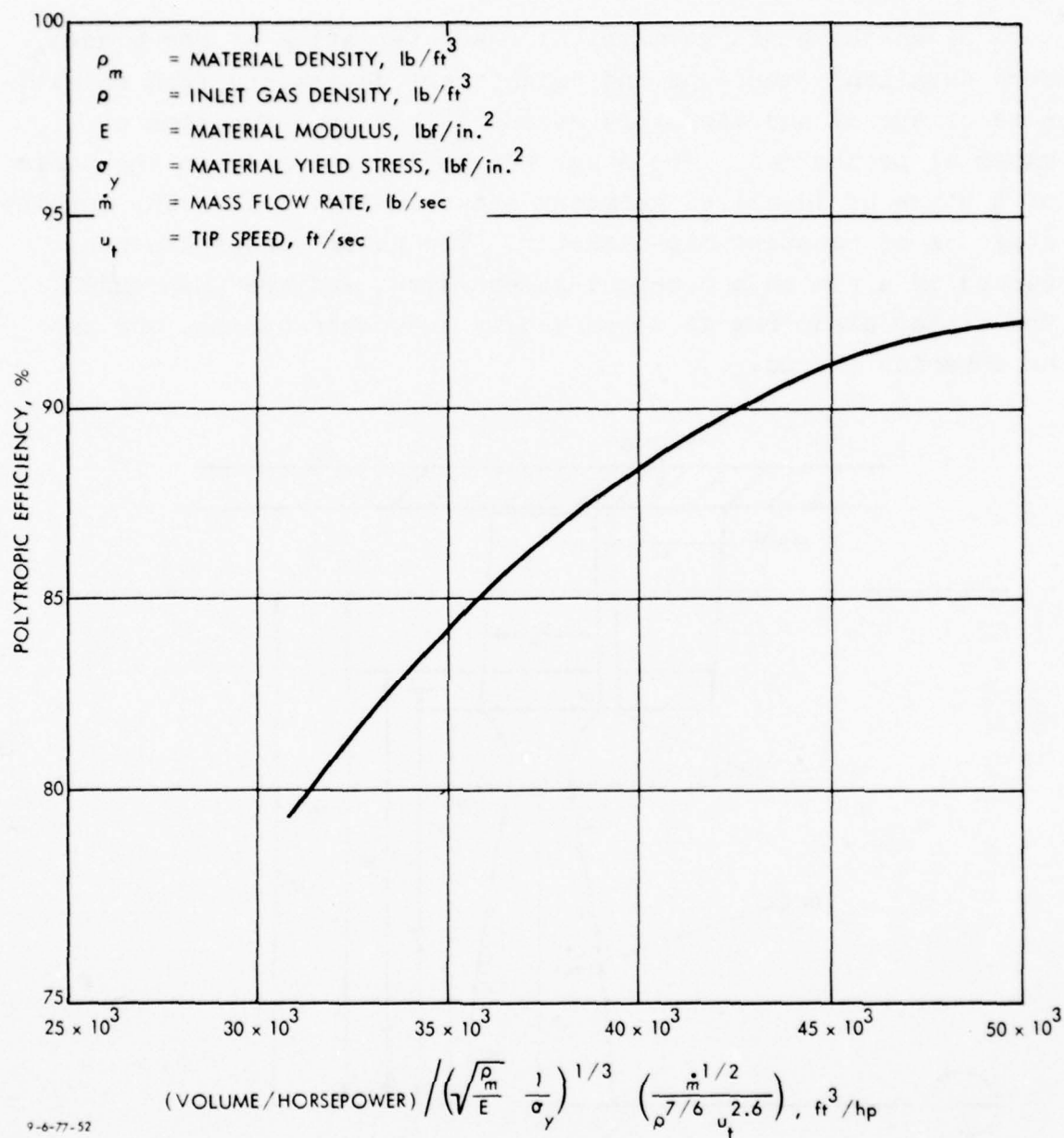
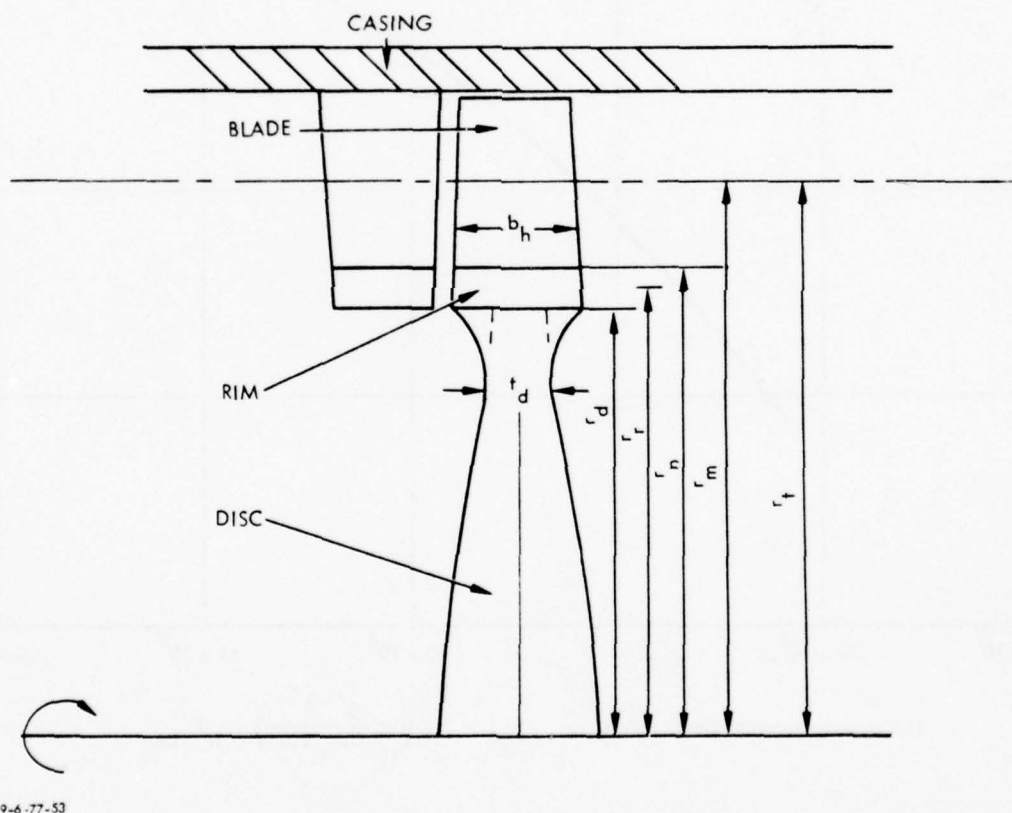


FIGURE F-10. Compressor volume and performance.

stage performance--Reynolds number, Mach number, aspect ratio, and tip clearance--are not considered here.

Given the basic geometrical characteristics of the blades, more detailed dimensions and weights are determined from an estimate of steady and vibratory stress levels as a function of material properties. The stage weight is estimated on the basis of a stage of idealized geometry shown in Fig. F-11. The turbine stage is of constant mid-diameter. The rotor blades are supported by a rim on a constant-stress disc, and are unshrouded. The stator blade row is supported by the outer casing, and has an interior shroud.



9-6-77-53

FIGURE F-11. Idealized turbine-stage geometry.

2. Aerodynamic Design Considerations

The range of the loading coefficient ψ considered is from 1.3 (rather lightly loaded) to 2.1 (rather heavily loaded). From the empirical correlation of Ref. F-6, the corresponding range of the flow coefficient ϕ is from 0.65 to 0.75, and the range of the achievable polytropic efficiency η_p is from 0.91 to 0.94. The optimum solidity (chord-to-spacing ratio) is established as a function of inlet and exit angles according to Ref. F-10. The resulting performance and solidity are summarized in Table F-3.

TABLE F-3. TURBINE AERODYNAMIC PERFORMANCE AND DESIGN DATA

Loading Coefficient $\psi = \Delta h_o / u_m^2$	1.3	1.68	1.8	2.1
Flow Coefficient $\phi = V_x / u_m$	0.65	0.71	0.73	0.75
Solidity $(c/s)_m$	1.29	1.35	1.37	1.41
Polytropic Efficiency η_p	0.94	0.93	0.92	0.91

The power delivered by a stage is

$$P_s = \dot{m} \Delta h_o = \dot{m} \left(\frac{\Delta h_o}{u_m^2} \right) u_m^2 \quad (F-47)$$

If every turbine stage has an equal enthalpy drop, then the power delivered by an entire turbine is

$$P = \sum_i P_s = \dot{m} N_s \left(\frac{\Delta h_o}{u_m^2} \right) u_m^2 \quad (F-48)$$

where N_s is the number of stages. Thus, as the loading coefficient $(\Delta h_o / u_m^2)$ is increased, the number of stages required for

a given output power decreases. Further, continuity requires that

$$\pi \rho \left(\frac{V_x}{u_m} \right) u_m \left(\frac{\ell}{D_m} \right) D_m^2 = \dot{m} , \quad (F-49)$$

where ρ is the gas density and ℓ is the blade height. Thus, for any selected value of loading coefficient, which also determines V_x/u_m , Eq. F-49 establishes the relationship between blade speed u_m and mean diameter D_m , provided that ℓ/D_m is known. Finally, by noting that

$$u_m = \pi D_m N , \quad (F-50)$$

where N is the rotative speed, Eq. F-49 can also be viewed as a relationship between blade speed and rotative speed.

3. Mechanical Design Considerations

a. Blade Design. The turbine blades are assumed to be geometrically similar to all cross sections. The tip cross-sectional area is assumed to be two-thirds of the hub cross-sectional area, and the thickness-to-chord ratio is assumed to be 20%.* All dimensions of the blade are then fixed by determining the chord length at the hub from the following stress and material properties considerations.

The centrifugal stresses σ_z are given, for the blade sections employed, by the relation:

$$\sigma_z = 3.02 \times 10^{-4} \rho_m u_m^2 (1/D_m) , \quad (F-51)$$

where σ_z = centrifugal stress at the hub, lbf/in.²

ρ_m = density of blade material, lbm/ft³

u_m = peripheral speed in middle section, ft/sec.

*Twenty percent is a representative value of thickness-to-chord ratio for highly loaded turbine blades.

The gas bending stresses σ_B are derived, by the method of momentum balance across the blade row, as:

$$\sigma_B = 0.0187 \rho^4 (s/c)_h u_m^2 (\ell/c_h)^2, \quad (F-52)$$

where σ_B = gas bending stress, lbf/in.²

ρ = gas density, lbm/ft³

$(s/c)_h$ = reciprocal of solidity at hub

u_m = peripheral speed at middle section, ft/sec

ℓ = blade length

c_h = blade chord at hub.

The maximum steady stress level σ_s is given by

$$\sigma_s = \sigma_z + \sigma_B. \quad (F-53)$$

If one assumes a direct relationship between the aerodynamic vibration excitation and the gas-bending forces, the vibratory stress σ_v can be expressed in the following form, where a , the amplification factor, is related to the blade resonance order:

$$\sigma_v = a\sigma_B. \quad (F-54)$$

In closed-cycle turbine applications, blades can be assumed to be relatively short and stiff, so that the asymptotic value of 2.5 for a at high harmonics can be assumed (Ref. F-3).

As in the case of compressors, a representative Goodman diagram is assumed for fatigue strength, wherein the allowable fatigue stress due to oscillating loads is assumed to vary linearly from a value of 0.75 of the 100,000-hour creep-rupture strength σ_c at zero applied steady stress to zero fatigue stress

when the steady stress reaches the creep strength. Thus the allowable vibratory stress is

$$\sigma_v = 0.75(\sigma_c - \sigma_s) ,$$

and hence the allowable bending stress is

$$\sigma_B = \frac{\frac{\sigma_c - \sigma_z}{a}}{0.75 + 1} . \quad (F-55)$$

Equations F-49, F-52, and F-55 can be combined to determine the blade chord:

$$c_h = 0.194 \left[\dot{m} \left(\frac{\ell}{D_m} \right) \frac{\psi(s/c)_h}{\sigma_c - \sigma_z} u_m \right]^{1/2} . \quad (F-56)$$

The weight of the rotor blades is simply

$$W_B = \left(\frac{\pi D_m}{s_m} \right) \left(\frac{5}{6} A_h \ell \rho_m \right) ,$$

where the first factor is the number of blades, and A_h is the blade cross-sectional area at the hub. If one introduces Eq. F-49 and some obvious geometrical relationships, this becomes

$$W_B = 0.415 \rho_m \left(\frac{\dot{m}}{\rho} \right) \left(1 - \frac{\ell}{D_m} \right) \frac{B}{(s/c)_h \phi} \frac{c_h}{u_m} , \quad (F-57)$$

where ρ_m = material density, lbm/ft³

\dot{m} = mass flow rate, lbm/sec

ρ = gas density, lbm/ft³

c_h = blade chord, ft

u_m = mean blade velocity, ft/sec.

It is assumed that the weight of the stator blades is equal to the weight of the rotor blades.

b. Turbine Disc. The disc rim is assumed to be an integrated ring having a width equal to the chord and a depth equal to two-thirds of the rim width. The weight of the rim is accordingly given by

$$W_R = 0.67 \pi \rho_m D_r c_h^2 ,$$

which, by introducing Eq. F-49 and some geometrical relationships, can be written as

$$W_R = 0.989 \rho_m \left(\frac{\dot{m}}{\rho} \right)^{1/2} \frac{(1 - \ell/D_m)}{(\ell/D_m)^{1/2}} \frac{1}{\phi^{1/2}} \frac{c_h^2}{u_m^{1/2}} . \quad (F-58)$$

It is assumed that the stator shroud is of equal weight.

The turbine disc is assumed to be uniformly stressed, supporting the blades and the rim. The weight of the disc is thus

$$W_D = \frac{2\pi\sigma_D r_D^2 t_D}{u_D^2} \left[\exp\left(\frac{\rho_m u_D^2}{2\sigma_D}\right) - 1 \right] ,$$

where r_D = disc radius

u_D = disc peripheral speed

t_D = disc thickness

σ_D = allowable material stress level

ρ_m = density of disc material.

The minimum thickness of the disc t_D is determined by the requirement that it support the blades and the rim:

$$(W_B + W_R) = \frac{2u_m^2}{D_m} = 2\pi r_D t_D \sigma_D$$

with the result that, after some manipulation, the weight of the disc can be expressed as

$$W_D = \frac{W_B + W_R}{1 - \frac{\ell}{D_m} - \frac{4}{3} \frac{c_h}{D_m}} \left\{ \exp \left[\frac{\rho_m u_m^2 \left(1 - \frac{\ell}{D_m} - \frac{4}{3} \frac{c_h}{D_m} \right)^2}{9266 \sigma_D} \right] - 1 \right\}, \quad (F-59)$$

where lbm/ft^3 , ft/sec , and lbf/in^2 are the units used for density, speed, and stress, respectively.

c. Turbine Casing. The casing is assumed to be a thin-walled cylinder with the load provided by the maximum pressure difference Δp across the casing wall. Thus, the thickness of the casing is

$$t = \Delta p r_t / \sigma_y,$$

where r_t is the tip radius and σ_y is the allowable stress level in the casing wall. The casing weight, assuming it is of length $2c_h$, is

$$W_c = 4\pi \rho_m \frac{\Delta p}{\sigma_y} r_t^2 c_h,$$

which can be written, with some effort, as

$$W_c = \rho_m \left(\frac{\dot{m}}{\rho} \right) \left(\frac{\Delta p}{\sigma_y} \right) \frac{(1 + \ell/D_m)^2}{(\ell/D_m)\phi} \frac{c_h}{u_m} . \quad (F-60)$$

4. Total Stage Weight

The total stage weight is simply

$$W_s = 2W_B + 2W_R + W_D + W_c . \quad (F-61)$$

Inspection of Eqs. F-56 through F-60 shows that for a selected level of stage loading (which also fixed the polytropic efficiency, the solidity, and the flow coefficient) and a selected tip speed, the only remaining parameter is the blade height-to-diameter ratio ℓ/D_m . Minimum weights are generally obtained at smaller values of ℓ/D_m , until the tip clearance losses become overwhelming. A minimum value of $\ell/D_m = 0.05$ is accordingly selected here. It is then a simple matter to estimate the weight of a multistage turbine, stage by stage, by determining subsequent values of gas density and ℓ/D_m for each stage. This process is illustrated in Table F-4, for a turbine using helium, at an inlet temperature and pressure of 1805°R and 25 atmospheres, respectively, with a mass flow of 83.6 lbm/sec. Nominal pressure ratio and horsepower are 1.43 and 33,500, respectively.

5. Weight-Performance Characteristics of Multistage Turbines

As in the case of compressors, the results of these rather detailed weight estimates can be satisfactorily approximated for complete multistage units. Inspection of Eqs. F-56 through F-60 shows that the basic dependence of stage weight on material and fluid properties is

$$\text{Stage Weight} \sim \frac{\rho_m}{\sigma_c^{1/2}} \frac{\dot{m}^{3/2}}{u_m^{1/2}} \left[\frac{K_1}{\rho} + \frac{K_2}{\rho} \frac{\Delta p}{\sigma_y} \right] f_1(SL) ,$$

TABLE F-4. ILLUSTRATION OF STAGE WEIGHT ESTIMATION

Working Fluid: Helium

Mass Flow Rate: 83.6 lbm/sec

Pressure Ratio: 1.43

Material Density ρ_m : 480 lbm/ft³

Material Creep Strength σ_c : $(250-0.95T)10^3$ psi

Casing Allowable Stress σ_y : 14,500 psi

Mean Blade Speed u_m : 1043 ft/sec

	<u>First Stage</u>	<u>Middle Stage</u>	<u>Last Stage</u>
p (atm)	25.0	21.0	17.4
T (°R)	1805	1691	1578
σ_z (psi)	20,700	23,100	26,000
ℓ (ft)	0.26	0.29	0.32
c_h (ft)	0.11	0.104	0.106
$2W_B$ (lbm)	25.3	26.3	29.4
$2W_R$ (lbm)	20.5	18.1	18.4
W_D (lbm)	88.2	49.6	43.8

where $f_1(SL)$ is some function of stage loading, and K_1 and K_2 are essentially constants. This dependence is precise if the tip speed is not too high (in the sense that there is an optimum tip speed just as for compressors), if the centrifugal stresses are small compared to the vibratory stresses, and if the rim depth is proportional to blade height rather than blade chord. The stage power is merely $\dot{m}(\Delta h/u_m^2)u_m^2$, and hence

$$\text{Stage Weight/Power} \sim \frac{\rho_m}{\sigma_c^{1/2}} \frac{\dot{m}^{1/2}}{u_m^{5/2}} \left[\frac{K_1}{\rho} + \frac{K_2}{\rho} \frac{\Delta p}{\sigma_y} \right] f_2(SL) .$$

The first term in brackets, which is associated with blades, rim, and disc, varies from stage to stage due to the change in inlet density; the second term, which is associated with the casing, depends on the inlet density to the first stage. Hence total weight to total power can be written as

$$\text{Total Weight/Power} \sim \frac{\rho_m \dot{m}^{1/2}}{\sigma_c^{1/2} u_m^{5/2} \rho} \left[K_1 \left(1 + \frac{\rho}{\rho_{out}} \right) + K_2 \frac{\Delta p}{\sigma_y} \right] f_2(SL) ,$$

where ρ refers to the inlet density and ρ_{out} refers to the exit density. Noting that

$$\frac{\rho}{\rho_{out}} \approx \left(\frac{p}{p_{out}} \right)^{\frac{1}{\gamma}} ,$$

it was found that the detailed results could be adequately represented by

$$\left[\frac{\text{Weight}}{\text{Power}} \right] \left[153,000 m^{1/2} \frac{\rho_m}{\sigma_c^{1/2}} \frac{1}{\rho u_m^{2.5}} \left(1 + \pi^{\frac{1}{\gamma}} + 25 \frac{\Delta p}{\sigma_y} \right) \right]^{-1} = r(\text{SL}) = r_1(\eta_p) \quad (\text{F-62})$$

where π is the pressure ratio and the dimensions are

$$[\text{Weight/Power}] = \text{lbm/hp}$$

$$[\dot{m}] = \text{lbm/sec}$$

$$[\rho] = \text{lbm/ft}^3$$

$$[\sigma] = \text{lbf/in}^2$$

$$[u_m] = \text{ft/sec}$$

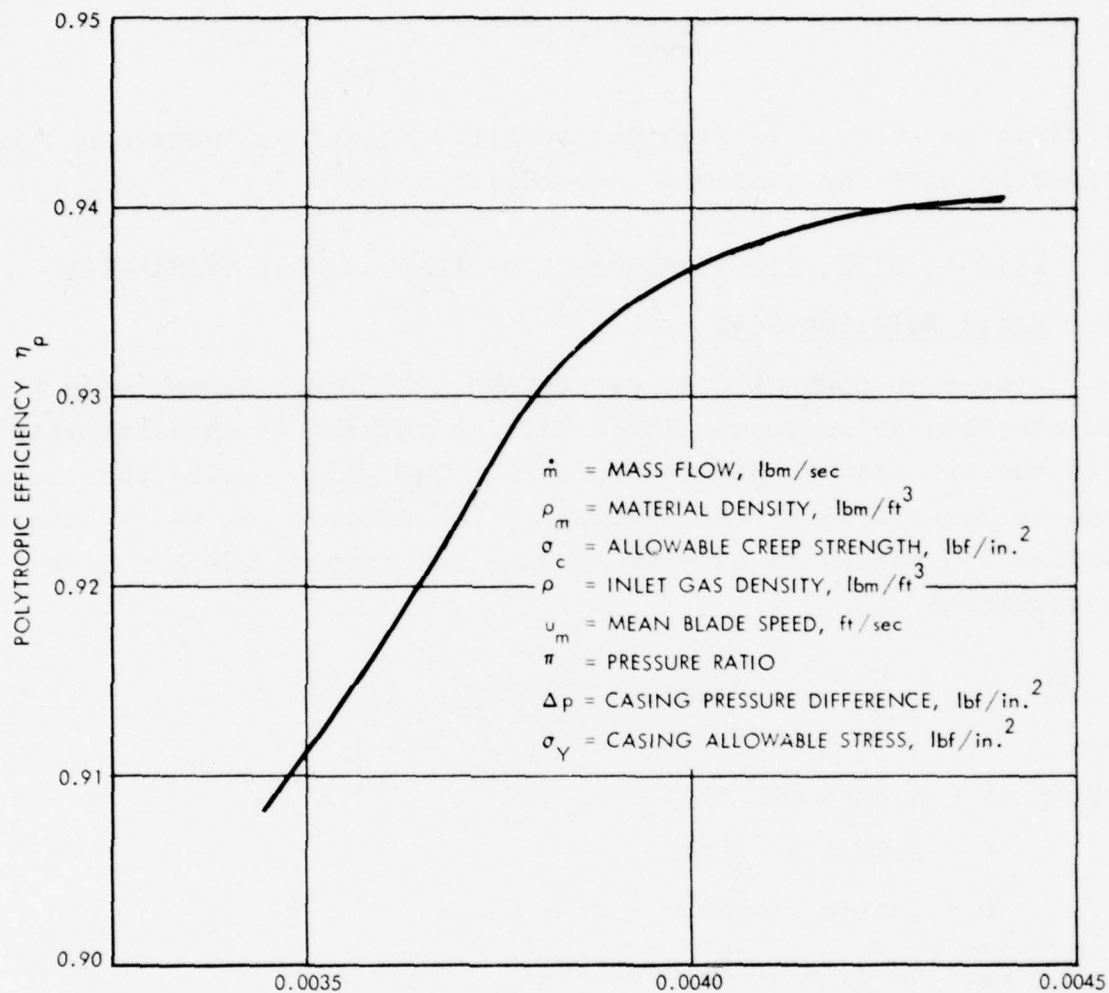
$$[\Delta p] = \text{lbf/in}^2$$

This relationship is displayed graphically in Fig. F-12. The weight tends to be underestimated at high tip speeds (high centrifugal stresses), and does not include the weight of shafts, bearings, seals, and necessary supporting structure. It is implied the components are of reasonable size and can be manufactured. Finally, the polytropic efficiencies do not include deleterious effects associated with tip clearance, low blade aspect ratios, and low Reynolds numbers. Thus, the relationship represents a lower bound on weight and an upper bound on efficiency.

As noted previously, there is an implied relationship between blade speed and rotative speed. Equations F-49 and F-50 yield

$$\frac{N_m^2}{\rho u_m^3} = \frac{3600}{\pi} \left(\frac{\ell}{D_m} \right) \left(\frac{V_x}{u_m} \right),$$

where N is in revolutions per minute. Since ℓ/D_m for the first stage is approximately 0.05 and V_x/u_m is a function of stage loading (and hence efficiency), this relationship can also be displayed as a function of polytropic efficiency. More



$$\left[\frac{\text{WEIGHT}}{\text{POWER}} \right] \left[163,000 \dot{m}^{1/2} \left(\frac{\rho_m}{\sigma_c^{1/2}} \right) \frac{1}{\rho u_m} 2.5 \left(1 + \pi^{1/\gamma} + 25 \frac{\Delta p}{\sigma_Y} \right) \right]$$

9-6-77-54

FIGURE F-12. Weight and performance of axial turbines.

importantly, for constant material and fluid properties, it implies the relationship

$$\frac{\text{Weight}}{\text{Power}} \sim N^{-5/3} ,$$

indicating that decreasing the specific weight by increasing tip speed requires an increase in rotative speed.

E. WEIGHT, SIZE, AND PERFORMANCE OF TUBULAR HEAT EXCHANGERS

1. Basic Relationships

The most compact heat exchangers have small passages in the counterflow arrangement. This will be assumed in this analysis for tubular heat exchanger surfaces. The flow outside the tubes can be controlled by the spacing of the tubes. The weight and volume can easily be determined when the product LND has been established.

$$\text{Weight} = (\text{LND})\pi\rho_m t , \quad (\text{F-63})$$

where L = length of tubes

N = number of tubes

D = inside diameter of the tubes

ρ_m = tube material density

t = tube thickness.

For a neat exchanger arrangement with the tubes placed at the corners of equilateral triangles, side S, the volume is

$$\text{Volume} = \sqrt{\frac{3}{2}} (\text{LND}) \left(\frac{S}{D}\right)^2 D , \quad (\text{F-64})$$

where S/D is the spacing-to-diameter ratio of the tubes. It is

assumed that the wall thickness of the tube is small, so the inside diameter may be used to characterize the tube size.

The product LND is established by heat transfer and pressure loss considerations, as follows. The heat transfer is given by

$$\dot{Q} = \dot{m}\Delta h = hA\overline{\Delta t} \quad , \quad (F-65)$$

where \dot{m} = mass flow rate

Δh = enthalpy change

\dot{Q} = heat transfer rate

h = heat transfer coefficient

A = area = πDLN

$\overline{\Delta t}$ = (log) mean temperature difference.

By definition, the heat transfer coefficient can be written as

$$h = Nu \, k/D \quad ,$$

where Nu is the Nusselt number and k is the thermal conductivity of the fluid. Thus, one has

$$\dot{Q} = \pi \, Nu \, k \, L \, N \, \overline{\Delta t} \quad . \quad (F-66)$$

For laminar flow in the tubes, the Nusselt number is, from Reynolds analogy,

$$Nu = 4.36 \quad , \quad (F-67)$$

while for turbulent flow, the Nusselt number is

$$Nu = 0.023 \, Re^{0.8} \, Pr^{0.4} \quad , \quad (F-68)$$

where Re = Reynolds number

Pr = Prandtl number.

The pressure loss in tubes is given by

$$\frac{\Delta p}{\rho} = 2 C_f V^2 L/D , \quad (F-69)$$

where C_f = friction coefficient

V = average fluid velocity.

For laminar flow, the friction coefficient is given by

$$C_f = 16Re^{-1} , \quad (F-70)$$

and for turbulent flow, the friction coefficient is

$$C_f = .079Re^{-1/4} . \quad (F-71)$$

From continuity, the fluid velocity is

$$V = \frac{4}{\pi} \frac{\dot{m}}{\rho D^2 N} , \quad (F-72)$$

and hence

$$Re = \frac{VD\rho}{\mu} = \frac{4}{\pi} \frac{\dot{m}}{DN\mu} \quad (F-73)$$

For laminar flow, the heat transfer is independent of Reynolds number, and hence it is independent of pressure loss. From Eqs. F-66 and F-67 one has

$$\dot{Q} = 4.36\pi k LN\Delta\bar{t} = 13.7 k LN\Delta\bar{t} \quad (F-74)$$

$$\frac{LND}{\dot{Q}} = \frac{D}{13.7 k \Delta t} \quad (F-75)$$

It is apparent that the weight/heat transfer rate and volume/heat transfer rate are minimized when the diameter is minimized. The pressure drop can be determined from Eqs. F-69, F-70, F-72, and F-73 as

$$\frac{\Delta p}{\rho} = \frac{128 \dot{m} \mu L}{\pi \rho^2 D^4 N} \quad (F-76)$$

For turbulent flow, both the heat transfer and the pressure loss are functions of Reynolds number and are thus interconnected. Using equations F-65, F-66, F-68, F-69, F-71, F-72, and F-73, it is possible to determine the value of the product LND independently of L and N, as follows:

$$\frac{LND}{\dot{Q}} = 17.27 \frac{\mu^{1.23} D^{.18}}{(k \Delta t)^{1.41} Pr^{.56} \rho^{.82}} \left(\frac{\Delta h}{\Delta p / \rho} \right)^{0.41} \quad (F-77)$$

This equation indicates that weight/heat transfer rate and volume/heat transfer rate increase with viscosity, diameter, and enthalpy change and decrease with conductivity, temperature difference, density, and pressure drop, as expected. The conditions on the outside of the tube must be compatible with those on the inside. For the regenerator, the conditions may be made to be compatible by considering the pressure-drop equation and equating the tube lengths. This yields

$$\left(\frac{\rho^2 D^{4.75}}{\mu^{1/4} \rho} \frac{\Delta p}{\rho} \right)_{\text{inside}} = \left(\frac{\rho^2 d_h^{4.75}}{\mu^{1/4} \rho} \frac{\Delta p}{\rho} \right)_{\text{outside}} \quad (F-78)$$

where d_h is the hydraulic diameter of the outside tube geometry.

One interesting feature of this development is that it enables all the heat exchangers in the working fluid circuit to be optimized at one time by selecting the pressure loss in each individual heat exchanger to minimize the total weight of the cores. That is, Eq. F-77 can be written for any heat exchanger as

$$W_1 = K_1 \left(\frac{\Delta p}{p} \right)_1^{-0.41}, \quad (F-79)$$

where K_1 is a function of properties and conditions. The total weight of all the heat exchangers is

$$W = \sum_{i=1}^n K_i \left(\frac{\Delta p}{p} \right)_i^{-0.41} \quad (F-80)$$

subject to the condition that

$$\sum_{i=1}^n \left(\frac{\Delta p}{p} \right)_i = \left(\frac{\Delta p}{p} \right)_{\text{total}}, \quad (F-81)$$

where $(\Delta p/p)_{\text{total}}$ is the total fractional pressure loss in the cycle. Using Lagrange multipliers, it can be demonstrated that minimum weight occurs when

$$\left(\frac{\Delta p}{p} \right)_i = \frac{\left(\frac{\Delta p}{p} \right)_{\text{total}}}{\sum_{i=1}^n \left(\frac{K_j}{K_i} \right)^{0.71}}. \quad (F-82)$$

The fact that one of the heat exchangers is a regenerator complicates this process. However, by specifying that the pressure drops on the two sides of the regenerator are the same the process

is simplified. If the subscripts r, h, and c refer to the re-generator (one side), heater, and cooler, respectively, the optimum pressure drops are as follows:

$$(\Delta p/p)_r = \frac{(\Delta p/p)_{\text{total}}}{\left[2 + \left(\frac{2K_h}{K_r} \right)^{0.71} + \left(\frac{2K_c}{K_r} \right)^{0.71} \right]} \quad (\text{F-83})$$

$$(\Delta p/p)_h = \frac{(\Delta p/p)_{\text{total}}}{\left[2 \left(\frac{K_r}{2K_h} \right)^{0.71} + \left(\frac{K_c}{K_h} \right)^{0.71} + 1 \right]} \quad (\text{F-84})$$

$$(\Delta p/p)_c = \frac{(\Delta p/p)_{\text{total}}}{\left[2 \left(\frac{K_r}{2K_c} \right)^{0.71} + \left(\frac{K_h}{K_c} \right)^{0.71} + 1 \right]} \quad (\text{F-85})$$

2. Illustrative Example

The procedure outlined above was used to determine the heat exchanger core weights for a closed-cycle Brayton engine having the following design conditions:

Working Fluid	Helium
T_1	560°R
T_3	2080°R
ΔT compressor	200°R
$\Delta p/p$	0.05
Polytropic efficiencies	0.9.

For a mass flow rate of 1 lb/sec, the following values are obtained from Eqs. F-63, F-77, F-83, F-84, and F-85:

	<u>Heater</u>	<u>Regenerator</u>	<u>Cooler</u>
$K = W(\Delta p/p)^{0.41}$	0.43	11.33	0.978
Optimum ($\Delta p/p$)	0.0033	0.0204	0.00595
Weight/mass flow rate	4.476	55.88	7.99

Using the property data for the selected design point but varying the overall pressure drops and the values of regenerator effectiveness, the weights of the heat exchanger cores are scaled from the base values for pressure drops, enthalpy changes, and temperature differences. The results are presented in Fig. F-13. Finally, the weights of the heat exchanger cores for the various designs are estimated and are presented with other performance parameters in Table F-5. The assumptions used to estimate the heat exchanger core weights are given with the table.

The air preheater is essentially a regenerator with air on one side and combustion products on the other. It is assumed that the combustion side of the heater is pressurized to four atmospheres. The air preheater weight is estimated by the methods presented here, assuming a pressure loss of 5% for the two sides. The estimated air preheater weight is 10.6 lb/lb per sec of helium. For the example considered here, this value corresponds to about 0.03 lb/output horsepower.

F. OVERALL ENGINE CONSIDERATIONS

The complete Brayton engine includes the components of the Brayton cycle, the fossil-fueled heat source, the pipes and shafts connecting the components, auxiliary systems, and structural support. The weight, volume, and performance of the main Brayton cycle components have been predicted. The prediction methods can also be applied to the turbomachinery and heat exchangers in the heat source. The weight and volume of the auxiliary systems and the structural supports are beyond the scope of this study.

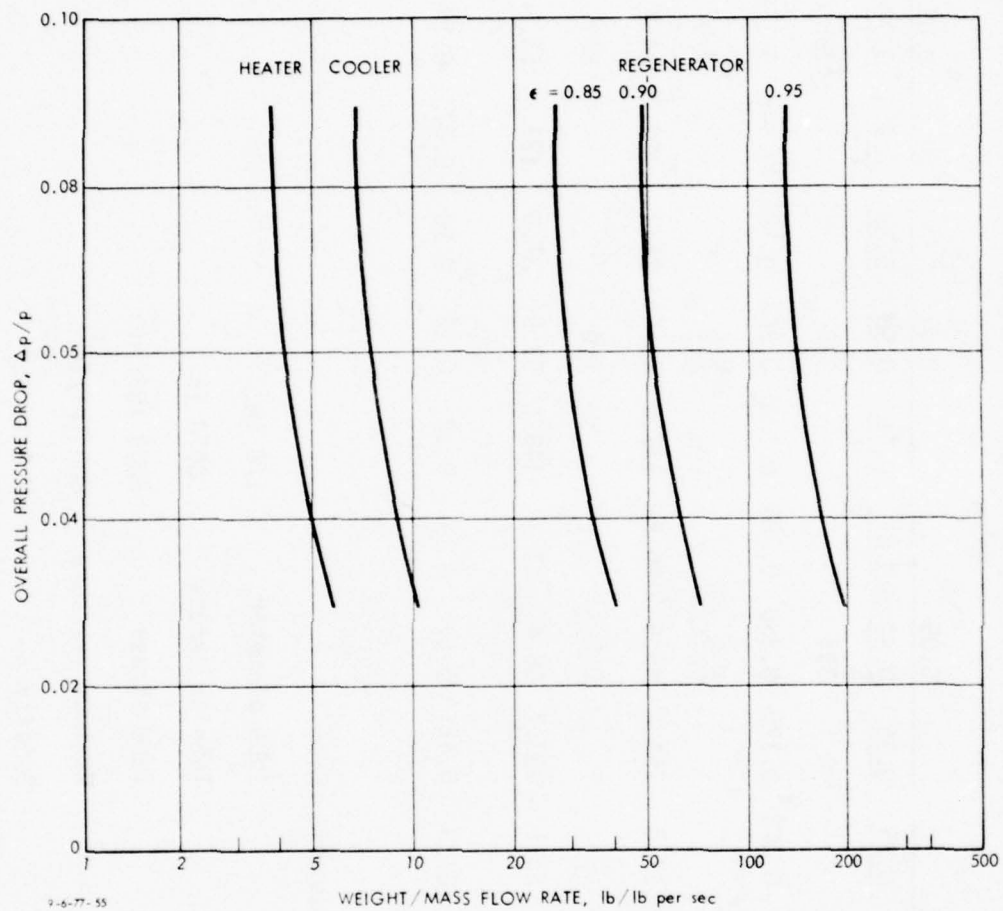


FIGURE F-13. Weights of heat-exchanger cores for closed-cycle Brayton engines (helium, 300 lbf/in.²).

TABLE F-5. WEIGHTS OF CLOSED-CYCLE BRAYTON ENGINE HEAT EXCHANGERS

$\frac{\Delta p}{p}$ ϵ	0.03			0.05			0.07			0.09		
	0.95	0.90	0.85	0.95	0.90	0.85	0.95	0.90	0.85	0.95	0.90	0.85
hp/m		417		395			373			350		
sfc	0.310	0.339	0.368	0.320	0.350	0.380	0.330	0.363	0.396	0.342	0.378	0.412
W_{heater}	5.5			4.5			3.9			3.5		
W_{regen}	186.9	68.7	37.8	151.2	55.9	30.7	132.2	48.6	26.7	120.1	44.1	24.3
W_{cooler}	9.8			8.0			7.0			6.3		
W_{total}	202.2	84.0	53.1	163.7	68.4	43.2	143.1	59.5	37.6	129.9	53.9	34.1
$\frac{W_{\text{total}}}{\text{Power Output}}$	0.48	0.20	0.13	0.41	0.17	0.11	0.38	0.16	0.10	0.37	0.15	0.10

Assumptions:

Tube diameter	1/8 in.
Tube thickness	.0076 in.
Tube stress	5000 lbf/in. ²
Maximum pressure	600 lbf/in. ²
Density	0.3 lb/in. ³

The existing closed Brayton cycle engines have been built as a few heavy-duty utility power plants and a small number of space-type power plants having very low power levels. These units are not representative of the vehicular applications considered here. Recent paper studies have been made of closed Brayton cycle engines applied to ships and tracked vehicles (Refs. F-7, F-8, and F-9). The performance and weight figures from these studies are representative of current technology and will be used here for comparison purposes.

1. Limitations to Performance and Size of Closed Brayton Cycle Engines

The performance of closed Brayton cycle engines is strongly influenced by the level of turbine inlet temperature, but it is also affected by the turbomachinery efficiency, effectiveness of the regenerator, and the pressure losses in the various components.

The level of turbine inlet temperature is selected from consideration of material properties, fabrication techniques, and stress levels. Since the heat must be transferred to the working fluid in the Brayton cycle through the heater tubes, there will be "hot spots" in the heater tubes at temperatures higher than the turbine inlet temperature. The use of ceramic-tube heat exchangers will allow the turbine inlet temperatures to reach perhaps 2000-2300°F and higher. If metal tubes must be used in the heater, the turbine inlet temperature may be restricted to 1500°F.

The efficiency levels of compressors and turbines at the present time appear to be at their maximum levels. The designs of compressors and turbines are unlikely to be improved above the best of current practice.

Heat exchanger geometries developed for some gas-turbine applications are currently very compact, although further reduction in the sizes of flow passages would reduce the size and weight

of the heat exchangers in the engine. The heat transfer pressure loss correlations for compact heat exchangers have been established, and little improvement appears to be possible except through the reduction in the size of the flow passages.

The pressure level in the closed Brayton cycle has an important influence on the size and weight of the components, although performance remains substantially unchanged except at extremely high pressure. The sizes and weights of the turbomachinery and the heat exchangers are reduced by raising the pressure level in the cycle. Eventually, at extremely high pressure levels, the components become too small and difficult to manufacture. The highest acceptable pressure level for minimum component sizes and weights is a function of power output. In Ref. F-9 it is suggested that the optimum pressure level for 40,000-hp output is 580 psia, rising to 840 psia for 200,000-hp output.

The tip speed of the turbomachinery also has an influence on the size and weight of the machinery. Increases in tip speed generally result in a reduction in size and weight of the machines until stresses due to centrifugal forces become very high. Since centrifugal stress is the important parameter, the tip speed of turbomachines can be raised by reducing the density and raising the yield stress of the blade and disc materials. Strong, lightweight materials such as titanium may be utilized in compressors, while ceramics may be used in turbines. With working fluids of low molecular weight, such as helium, the Mach number problems associated with operation at high tip speed may be neglected because of the high velocity of sound in such working fluids.

2. Performance, Size, and Weight of Closed Brayton Cycle Engines

a. The Core Engine. The relationships between engine performance of closed-cycle Brayton engines may be predicted for a range of performance and design parameters. The most critical decisions are the choice of turbine inlet temperature and

pressure. In this study a temperature of 1620°F is selected for the turbine inlet. The compressor exit pressure levels are taken as 600 and 1200 lbf/in.² With these conditions the performance, size, and weight of core engines for the closed-cycle Brayton engine have been predicted. The size and weight estimates are for the compressor, turbine, regenerator, and cooler. The heat source, including the helium heater, is not considered here (i.e., it is not part of the "core engine") except for the assumption that the heater efficiency is 90%.

For the fixed turbine inlet temperature and two values of compressor exit pressure, the sfc is calculated for a range of regenerator effectivenesses and pressure drops. The weights and volumes of the heat exchangers and turbomachinery are predicted for each condition. The low sfc and high engine weight correspond to high regenerator effectiveness and low pressure drop. The predicted weight and volume of the turbomachinery is only about 1% of the core engine values at the low sfc values, rising to approximately 10% of the weight and volume at the highest sfc values. The results of the prediction are presented in Figs. F-14 and F-15.

Also presented in these figures are performance, weight, and volume values extracted from Refs. F-8 and F-9. The values from these references represent the most recent predictions for closed-cycle Brayton engine performance. In Ref. F-8 a turbine inlet temperature of 1750°F was assumed (ceramic heater tubes), while in Ref. F-9 the turbine inlet temperature was 1500°F. The weight/power of the core engines given in these references are higher than the predictions of this study, at equivalent sfc levels, while the volume/power given in Ref. F-8 is very close to the equivalent performance and size predicted here.

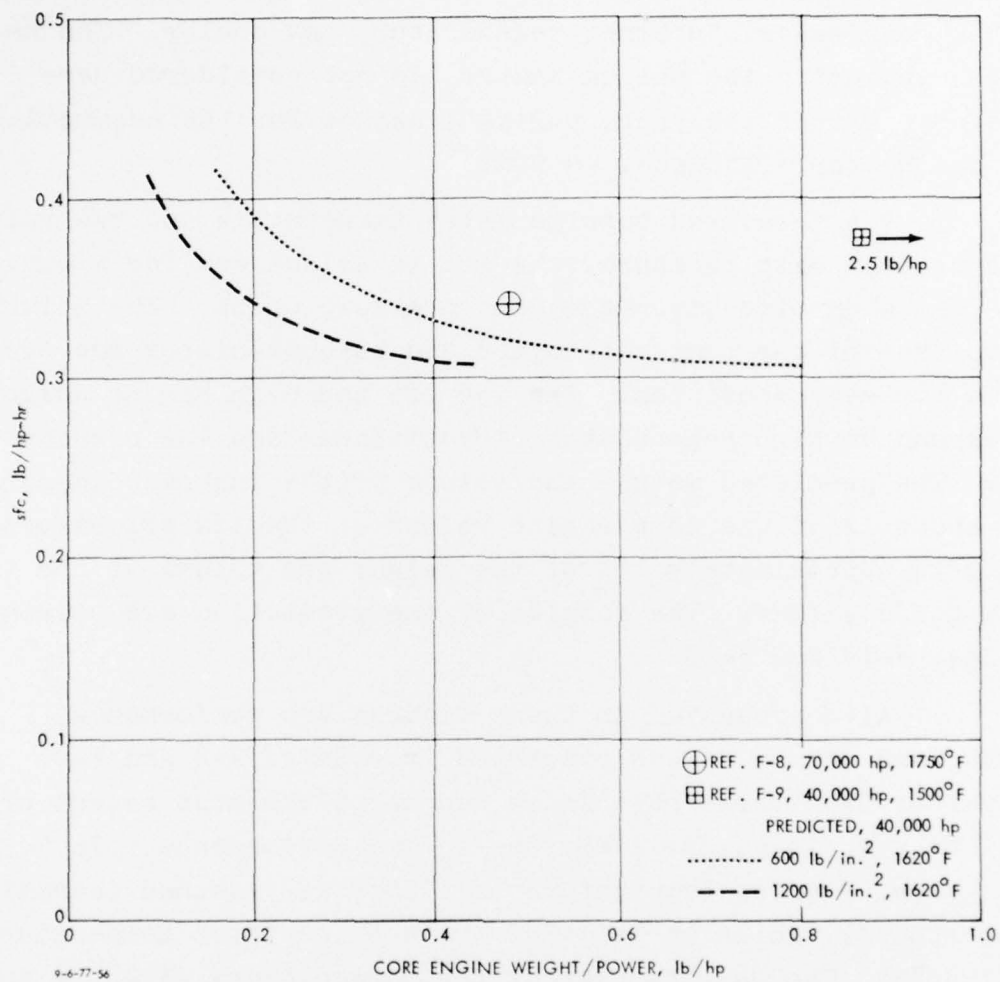


FIGURE F-14. Weight/power and sfc of core engines for closed-cycle Brayton engines.

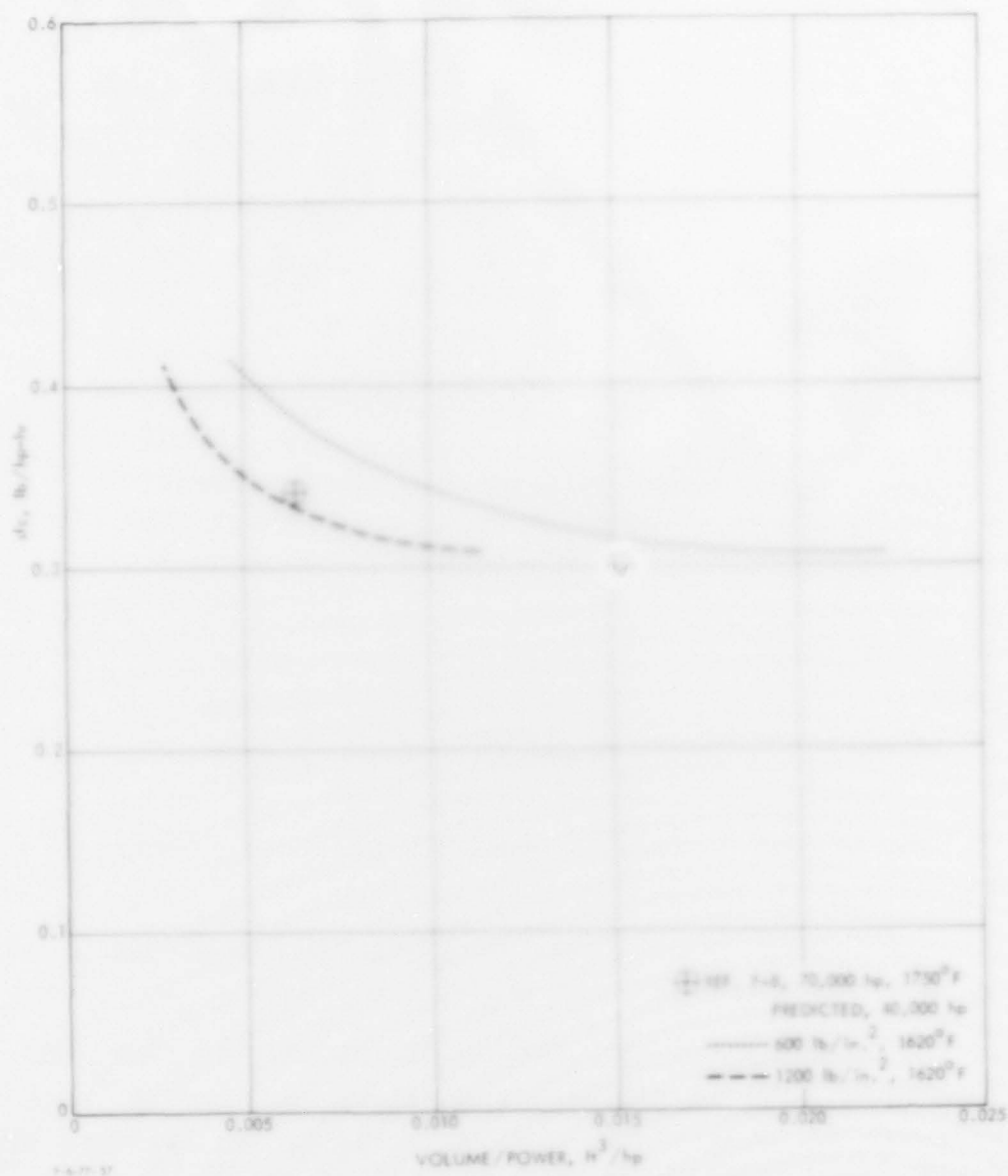


FIGURE F-15. Volume/power and sfc of core engines for closed-cycle Brayton engines.

b. The Heat Source. A compact heat source for the closed-cycle Brayton engine would likely have a turbocharged combustor with an air preheater. The weight/power and volume/power of the heat source is strongly dependent on the arrangement and tube sizes of the helium heater and the air preheater. If it is assumed that 1/8-in. internal-diameter tubes with wall thickness of 0.015 in. may be used for the helium heater and air preheater and that counterflow arrangements can be devised, the weights and volumes of the components of the heat source at the 40,000-hp level are as follows:

PREDICTED HEAT SOURCE WEIGHT AND VOLUME (40,000 hp)

	Weight/Power, lb/hp	Volume/Power, ft ³ /hp
Helium heater	0.020	0.0003
Air preheater	0.053	0.0008
Turbomachinery	0.007	0.0002
Combustor	0.003	0.0003
Total	0.083	0.0016

The volume of the combustor is based on a combustion intensity of 5×10^6 Btu/ft³-hr atmos.

The values of predicted weight/power and volume/power given in Ref. F-8 are 0.58 lb/hp and 0.011 ft³/hp.

c. The Complete Engine. The predicted weight/power and the volume/power for the complete engine were obtained by summing the values for the core engine and heat source. The results are presented in Figs. F-16 and F-17. The predicted weight/power and volume/power for the complete engine are lower than the values given in Ref. F-8; much of the predicted improvement is in the heat source.

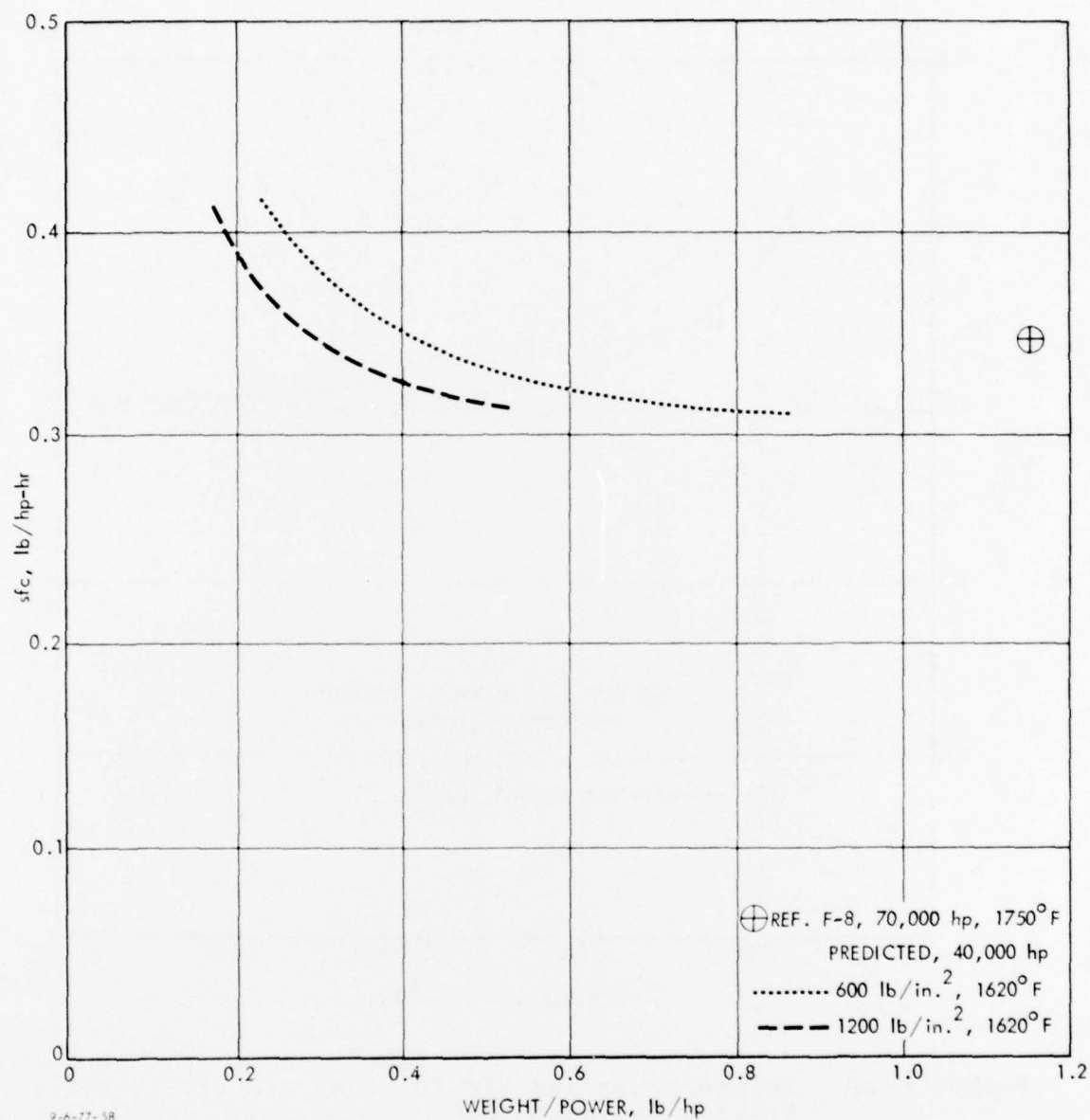


FIGURE F-16. Weight/power and sfc for complete closed-cycle Brayton engines.

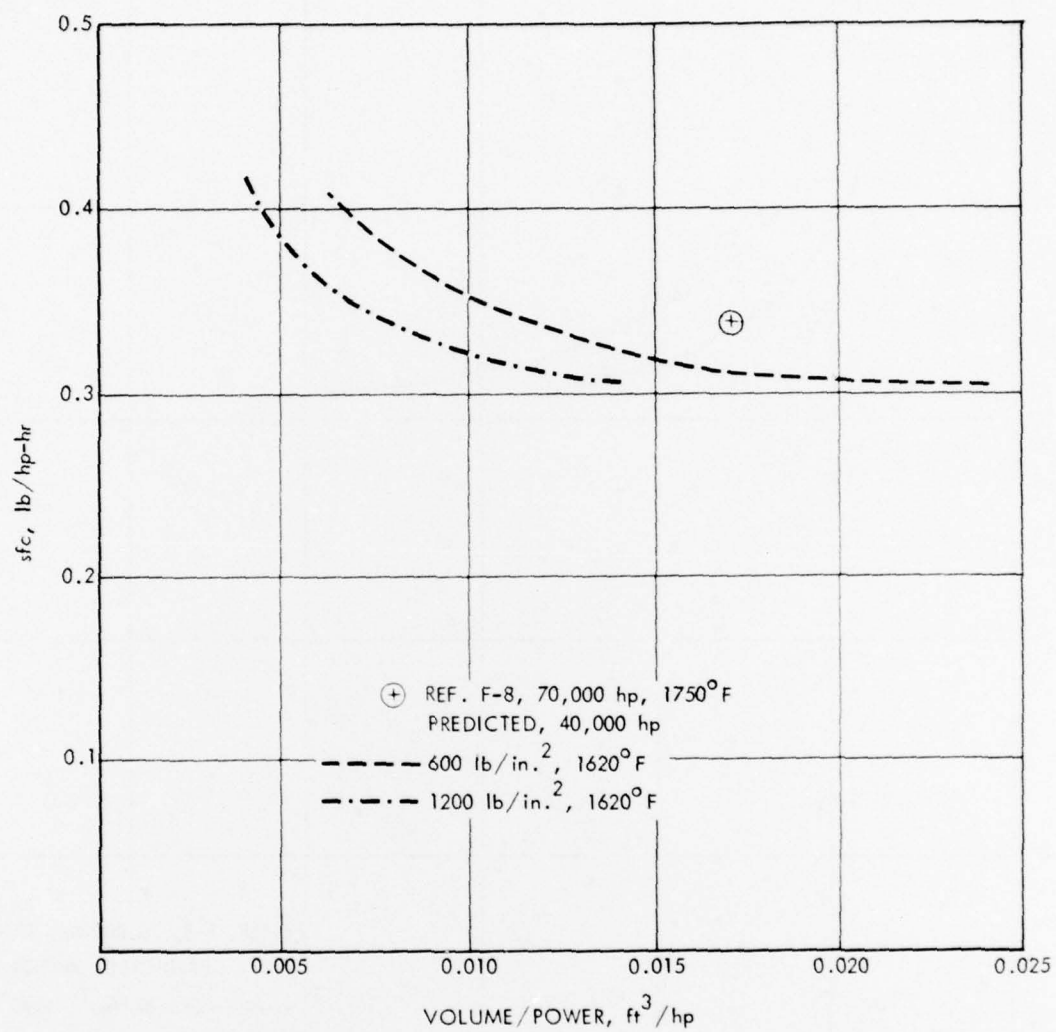


FIGURE F-17. Volume/power and sfc for complete closed-cycle Brayton engines.

G. RESEARCH AND DEVELOPMENT AREAS--THE CLOSED-CYCLE BRAYTON ENGINE

The most important research and development tasks are associated with the high-temperature heat exchangers. The helium heater is probably the most critical component as it has the highest metal (or ceramic) temperatures, and there is possible corrosion from the combustion products. The air preheater and the regenerator operate at somewhat lower temperatures than the helium heater, but they would be more highly rated than current units in any power-plant system.

The low-temperature heat exchangers would be within the current state of the art and would require little development.

The turbomachinery design methods for this application are well established and would not require a research effort. The use of ceramic materials for the turbine may be required at extremely high turbine inlet temperatures. However, the problem would be more severe in the helium heater, since the tubes would be at higher temperatures and would be in contact with combustion products.

High-pressure seals are required for the turbine and compressor to restrict the loss of helium. These are not a new development but may pose problems because of the sizes and rotational speeds of the units.

GLOSSARY, APPENDIX F

a	Amplification factor
A	Heat-transfer surface area
A_h	Blade cross-sectional area at hub
c	Blade chord
c_p	Specific heat at constant pressure of the working fluid
D	Inside diameter of heat-exchanger tubes
d_h	Hydraulic diameter of passages outside tubes in heat exchanger
D_m	Mean diameter
D_r	Turbine rim diameter
E	Young's modulus
f	Fundamental natural frequency, cycles/sec
g_o	Gravitational constant, 32.174 ft/sec ²
h	Convective heat-transfer coefficient
HV	Lower heating value of fuel
J	Conversion factor 778 ft-lb/Btu
k	Thermal conductivity of the working fluid
ℓ	Blade height
L	Length of heat exchanger tube
\dot{m}	Mass flow rate
\dot{m}_f	Fuel flow rate

N	Shaft rotational speed; or, number of heat-exchanger tubes
N_s	Number of stages in a turbomachine
Nu	Nusselt number, hd_h/k
p	Pressure of the working fluid
P	Power
P_{add}	Rate of heat addition to the working fluid in an actual cycle
$P_{add,id}$	Rate of heat addition to the working fluid in an ideal cycle
P_c	Power absorbed by a compressor stage
$P_{comp,id}$	Power absorbed by a compressor in an ideal cycle
P_i	Rate of energy transport associated with the working fluid, $\dot{m}c_p T_1$
P_{int}	Internal power transfer, the energy transfer rate to the working fluid before heat addition from the working fluid after heat addition
P_{it}	Total internal power transfer, $P_{int} + P_x$
$P_{loss,c}$	Equivalent power loss in the compressor; the difference between the actual power and that required for isentropic compression.
$P_{loss,E}$	Equivalent power loss associated with post-expansion pressure losses, Δp_E ; the reduction in expander power output due to these pressure losses.
$P_{loss,H}$	Equivalent power loss associated with pre-expansion pressure losses, Δp_H ; the additional compressor power required due to these losses.
$P_{loss,r}$	Additional rate of heat addition required, for a given maximum temperature, due to heat-exchanger ineffectiveness.

$P_{loss,t}$	Equivalent power loss in the expander; the difference between the power produced by isentropic expansion and the actual power produced.
P_o	Power output
Pr	Prandtl number, $C_p \mu / k$
$P_{RC,id}$	Total heat transfer rate, regenerator plus cooler, in an ideal cycle
P_{reg}	Heat transfer rate in the regenerator
$P_{reg,i}, P_{reg,id}$	Heat transfer rate in the regenerator in an ideal cycle
$P_{RH,id}$	Total heat-transfer rate, regenerator plus heater, in an ideal cycle
P_s	Power delivered by a turbine stage
P_{turb}	Power delivered by turbine
$P_{turb,i}$	Power delivered by turbine in an ideal cycle
P_x	Intermediate power transfer; the sum of the heat transfer rates in the heater and cooler
q	Dynamic pressure, $\rho u^2 / 2$
\dot{Q}_C	Heat transfer rate in cooler
\dot{Q}_H	Heat-transfer rate in heater
\dot{Q}_R	Heat-transfer rate in regenerator
r_D	Disc radius
Re	Reynolds number $\rho u d_h / \mu$
r_h	Hub radius
r_t	Tip radius
s	Entropy; or, blade spacing
S	Spacing between heat exchanger tubes
sfc	Specific fuel consumption, lb/hp-hr

s_m	Blade spacing at mean radius
t	Temperature; or, thickness of heat-exchanger tube
T	Temperature
t_c	Casing thickness
t_D	Minimum disc thickness
T	Temperature of working fluid
T_l	Minimum temperature of working fluid
u	Tangential speed; or, fluid velocity
u_D	Tangential speed of disc
u_m	Tangential blade speed at mean radius
u_t	Blade tip speed
V	Volume; average fluid velocity
V_x	Axial through-flow velocity
W_B	Weight of a single blade row, rotor or stator, compressor or turbine
W_c	Casing weight
W_{cooler}	Cooler weight
W_c	Compressor power
W_D	Disc weight
W_{heater}	Heater weight
W_R	Disc rim weight
W_{regen}	Regenerator weight
W_s	Total stage weight
W_{total}	Total heat exchanger weight
W_t	Turbine power

γ	Ratio of specific heats of the working fluid
Δh_o	Stagnation enthalpy change across a turbo-machinery stage
Δp_E	Pressure loss of the working fluid in the cooler and the hot side of the regenerator
Δp_H	Pressure loss of the working fluid in the heater and the cold side of the regenerator
ϵ	Heat-exchanger effectiveness
η	Cycle efficiency, (work output)/(heat input to the working fluid)
η_c	Compressor isentropic efficiency
η_h	Heater efficiency, (heat input to the working fluid)/(total heat input)
η_{id}	Thermodynamic efficiency of an ideal cycle
η_m	Mechanical efficiency
η_p	Polytropic efficiency
η_t	Turbine isentropic efficiency
λ	Hub/tip ratio, r_h/r_t
μ	Viscosity of the working fluid
π	Pressure ratio
ρ	Density of the working fluid
ρ_m	Material density
σ_B	Bending stress
σ_c	Casing stress; or, creep-rupture stress
σ_{CF}, σ_z	Centrifugal stress
σ_D	Disc stress
σ_s	Maximum steady stress level
σ_v	Vibratory stress

σ_y

Yield stress

ϕ

Flow coefficient, V_x/u_m

ψ

Stage loading coefficient, $\Delta h_o/u_m^2$

REFERENCES, APPENDIX F

- F-1. Proprietary communication.
- F-2. National Gas Turbine Establishment, NGTE Report M55.
- F-3. W.E. Trumpler and H.M. Owens, Turbine Blade Vibration and Strength, American Society of Mechanical Engineers Paper 53-A-98, 1953.
- F-4. R.E. Dundas, "Design of the Gas Turbine," in Gas-Turbine Engineering Handbook, Vol. 1, GT Publications, Stamford, Connecticut, 1972.
- F-5. V.L. La Valle and M.C. Huppert, Effects of Several Design Variables on Turbine Wheel Weight, National Advisory Committee on Aeronautics Technical Note 1814, 1949.
- F-6. S.F. Smith, "A Simple Correlation of Turbine Efficiency," Journal of the Royal Aeronautical Society, Vol. 69, July 1965.
- F-7. Garrett AiResearch Manufacturing Company of Arizona, Tracked Vehicle Gas Turbine Engine Combined Programs, Technical Report 12141, TACOM, Propulsion Systems Laboratory, March 1976.
- F-8. Garrett AiResearch Manufacturing Company of Arizona, A Feasibility Study on a Compact Lightweight Closed-Brayton System, Progress Report 31-2172 (R4) A, June 1977.
- F-9. United Technologies Research Center, Lightweight Propulsion Systems for Advanced Naval Ships, Applications Part 1-- System Studies, UTRC Report R-77-952566-5, May 1977.
- F-10. O. Zweifel, "The Spacing of Turbo-Machine Blading Especially with Large Deflection," The Brown Boveri Review, December 1945.